# MOLECULAR MECHANISMS OF ASSEMBLY AND LONG-TERM MAINTENANCE OF NEURONAL ARCHITECTURE

A Dissertation Presented

By

CASSANDRA R. BLANCHETTE

Submitted to the Faculty of the
University of Massachusetts Graduate School of Biomedical Sciences, Worcester
in partial fulfillment of the requirements for the degree of

DOCTOR OF PHILOSOPHY

MARCH 18$^{TH}$, 2016

NEUROBIOLOGY

MOLECULAR MECHANISMS OF ASSEMBLY AND
LONG-TERM MAINTENANCE OF NEURONAL ARCHITECTURE

A Dissertation Presented
By
CASSANDRA R. BLANCHETTE

This work was undertaken in the Graduate School of Biomedical Sciences
Program in Neuroscience

The signature of the Thesis Advisor signifies
validation of the Dissertation content

_____
Claire Bénard, Ph.D., Thesis Advisor

The signatures of the Dissertation Defense Committee signify
completion and approval as to style and content of the Dissertation

_____
Vivian Budnik, Ph.D., Member of the Committee

_____
Patrick Emery, Ph.D., Member of the Committee

_____
Hong-Sheng Li, Ph.D., Member of the Committee

_____
Maxwell Heiman, Ph.D., External Member of the Committee

The Signature of the Chair of the Committee signifies that the written dissertation meets
the requirements of the Dissertation Committee

_____
Michael Francis, Ph.D., Chair of Committee

The signature of the Dean of the Graduate School of Biomedical Science signifies
that the student has met all graduation requirements of the School.

_____
Anthony Carruthers, Ph.D.,
Dean of the Graduate School of Biomedical Sciences

March 18th, 2016

**ACKNOWLEDGEMENTS**

First I would like to thank my mentor, Claire, who has molded me into the scientist that I am today. Not only has she transformed me scientifically, but she has also helped me to become a more confident and assertive person through her positive and compassionate mentoring. She has provided me with unconditional support during all of the ups and downs of graduate school, and has always made me feel valued, appreciated, and understood. Claire has invested much of her time and energy to my training and provided me with many opportunities for scientific growth. She is genuine and puts her heart and soul into the people in her life, and I have been so fortunate to be a part of that.

I especially would like to thank Andrea, for everything she does to make our lab run smoothly, for her scientific rigor and support with my projects, and for being an admirable and compassionate friend. Paola, thank you for being a strong role model for me in lab and in life, for making me laugh, and for your help with my research. Thank you to my good friend Gillian not only for her assistance with my projects, but also for always being so thoughtful and encouraging. Devyn, it has been a joy getting to work with you in the lab, thank you for your positive energy and enthusiasm for science. I would also like to thank all other past and present members of the Bénard Lab, in particular Anagha Khandekar who went through all of graduate school with me side by side, Janine Recio who trained me during my rotation, Brother James Ritch, Avery Fisher, and Catherine Harwood.

I am thankful to all of the staff and faculty of the Neurobiology Department for making our department a one-of-a-kind place. Thank you to my past and present committee members, for all of their insights into my project and advice for my future, especially to my Dissertation Exam Committee members Vivian Budnik, Patrick Emery, Hong-Sheng Li, external examiner Maxwell Heiman, and committee chair Michael Francis.

I thank my parents and my brother who have always unconditionally supported me in any endeavor that I’ve undertaken. Thank you for always believing in me. I am so grateful for my best friend and future husband Joe, who has been by my side every step of the way. I would also like to thank the rest of my family and my friends for their encouragement and for being the most supportive and loving group of people anyone could ever wish for.

**ABSTRACT**

Nervous system function is closely tied to its structure, which ensures proper connectivity and neural activity. Neuronal architecture is assembled by a series of morphogenetic events, including the coordinated migrations of neurons and axons during development. Subsequently, the neuronal architecture established earlier must persist in the face of further growth, maturation of the nervous system, and the mechanical stress of body movements. In this work, we have shed light on the molecular mechanisms governing both the initial assembly of the nervous system and the long-term maintenance of neural circuits. In particular, we identified heparan sulfate proteoglycans (HSPGs) as regulators of neuronal migrations. Our discovery and analysis of viable mutations in the two subunits of the heparan sulfate co-polymerase reveals the importance of the coordinated and dynamic action of HSPGs in neuronal and axon guidance during development. Furthermore, we uncovered that the HSPG LON-2/glypican functions as a modulator of UNC-6/netrin signaling through interactions with the UNC-40/DCC receptor. During larval and adult life, molecules such as the protein SAX-7, homologous to mammalian L1CAM, function to protect the integrity of nervous system architecture. Indeed, loss of *sax-7* leads to progressive disorganization of neuronal architecture. Through a forward genetic screen, we identified LON-1 as a novel maintenance molecule that functions post-embryonically with SAX-7 to maintain the architecture of the nervous system. Together, our work highlights the importance of extracellular interactions to

modulate signaling events during the initial development of the nervous system, and to subsequently maintain neuronal architecture for the long-term.

## TABLE OF CONTENTS

## List of Tables

**List of Figures**

**List of Copyrighted Materials Produced by the Author**

Chapter III represents work previously published and is presented in accordance with copyright law.

Blanchette CR, Perrat PN, Thackeray A, Bénard CY (2015) Glypican Is a Modulator of Netrin-Mediated Axon Guidance. PLoS Biol 13(7): e1002183. doi: 10.1371/journal.pbio.1002183

**List of Symbols, Abbreviations, or Nomenclature**

GFP: Green fluorescent protein

GPI: Glycerophosphatidylinositide

HS: Heparan sulfate

HSPG: Heparan sulfate proteoglycan

NSA: Netrin synergizing activity

DTC: Distal tip cell

SfGFP: Superfolder GFP

CS: Chondroitin sulfate

CSPG: Chondroitin sulfate proteoglycan

GlcA: Glucuronic acid

GlcNAc: N-acetyl glucosamine

GalNAc: N-acetyl galactosamine

PCR: Polymerase chain reaction

L1CAM: L1 cell adhesion molecule

TGF-β: Transforming growth factor beta

FERM: 4.1 protein, ezrin, radixin, moesin

PDZ: Post-synaptic density protein (PSD95), *Drosophila* disc large tumor suppressor (Dlg1), and zonula occuldens-1 protein (zo-1)

CAP: Cysteine-rich secretory protein, antigen 5, and pathogenesis-related 1

EMS: Ethyl methanesulfonate

## Preface

The work presented in **Chapter II** represents unpublished work that is in preparation for publication.

**Blanchette CR**, Thackeray A, Perrat PN, Hekimi S, Bénard CY. Heparan sulfate proteoglycans are required for the guidance of migrations during development (in preparation).

The work presented in **Chapter III** is previously published.

**Blanchette CR**, Perrat PN, Thackeray A, Bénard CY (2015) Glypican Is a Modulator of Netrin-Mediated Axon Guidance. PLoS Biol 13(7): e1002183. doi: 10.1371/journal.pbio.1002183

The work presented in **Chapter IV** represents unpublished work that will be prepared for publication.

**Blanchette CR**, Oliver D, Thackeray A, Ritch J, Fisher A, Bénard CY. LON-1, a conserved CAP superfamily protein and TGF-β pathway target, functions with SAX-7/L1CAM to maintain nervous system architecture.

# Chapter I

# GENERAL INTRODUCTION

***Nervous system development***

Proper function of the nervous system is essential for life and dependent upon the execution of a series of exquisitely regulated spatial and temporal events that take place during embryonic and post-natal development. How such a complex system is generated has continued to be an intensively researched subject within the field of neurobiology. While our knowledge surrounding the stages of nervous system development and their corresponding molecular programs has greatly expanded, many basic biological questions remain to be answered concerning the formation of a functional nervous system.

Embryonic vertebrate nervous system development begins when the ectoderm is molecularly induced to give rise, in part, to neural tissue which goes on to become neurons or glial cells of the central and peripheral nervous system. Following this induction of neural tissue, patterning sets up the regional differences along the axes of the nervous system, and immature neurons migrate to their final positions, becoming fully differentiated neurons. Growth cones extend from neurons to guide axons across long distances to reach and innervate their targets to assemble neural circuits within the brain and the peripheral nervous system. Within neural circuits, neurons communicate with neurons and other cells through synaptic connections via dendrites and axons, which function to receive and transmit information, respectively. In addition to the

proliferations of neurons and glia during nervous system development, cell death and the elimination of synapses also occur.

***Axon guidance***

How particular growth cones can precisely and efficiently guide axons though a complex molecular environment, dynamically responding to specific cues while ignoring others, remains to be fully determined. Axons are often guided over long distances to reach their final target. During this process, neurons extend an actin-rich growth cone at the tip of their developing axon which integrates and responds to the molecular environment to precisely guide the axon to its appropriate target. Insight into this process first came from the observations of Ramón y Cajal, who described the existence of a growth cone as a “terminal lump, that we will call a growth cone, [that] sometimes displays fine short, spiny and divergent expansions” (Ramón y Cajal 1890a, Ramón y Cajal 1890b). He was the first to point out the precision with which growth cones guide axons to their targets, and proposed his “neurotropic hypothesis” that attractive chemical cues direct the guidance of neuronal processes (Ramón y Cajal 1892). Despite making these observations more than a century ago, they remarkably remain generally true today.

Axons are guided to their targets by short- and long-range attractants and repellents, as well as by contact-mediated attraction and repulsion (Tessier-

Lavigne & Goodman 1996). Attractants and repellents are sensed through receptors expressed on the growth cone at the tip of the growing axon, which upon transduction of these cues, responds with cytoskeletal rearrangements to affect axon guidance (reviewed by (O'Donnell et al 2009)). Research dedicated to the identification of the molecular cues that impact axon guidance identified four major classes of axon guidance molecules: netrins, semaphorins, ephrins, and slits (Chan et al 1996, Flanagan & Vanderhaeghen 1998, Ishii et al 1992, Kidd et al 1999, Kidd et al 1998a, Kolodkin et al 1993, Kolodkin et al 1992, Kolodkin & Tessier-Lavigne 2011, Seeger et al 1993). In addition to these molecules, morphogens, cell adhesion molecules, extracellular matrix molecules, and growth factors also play important roles in axon guidance events (Kolodkin & Tessier-Lavigne 2011, Raper & Mason 2010, Tessier-Lavigne & Goodman 1996). The work in this thesis on guidance investigates UNC-6/netrin and SLT-1/Slit-mediated guidance events and therefore these pathways will be described in more detail.

A screen for *Drosophila* mutants with CNS axon guidance defects led to the identification of the Slit signaling pathway through the isolation of mutants for the Slit receptor Robo (Seeger et al 1993). *robo* mutants isolated from the screen exhibited an increase in midline axon crossing events, due to its normal role in the repulsion of axons away from the midline (Seeger et al 1993). While Robo functions in the subset of axons that are not meant to cross the midline, Robo

also functions in axons that do cross the midline to ensure they only cross the midline once (Kidd et al 1998a). Following the identification of the Robo receptor as an immunoglobulin superfamily protein (Kidd et al 1998b), its secreted ligand Slit was also identified in *Drosophila* (Kidd et al 1999). Robo and Slit signaling pathway molecules were found to be highly conserved in *C. elegans* (Hao et al 2001, Zallen et al 1998) and in mammals (Brose et al 1999, Kidd et al 1998a, Li et al 1999) where they also function in repulsive midline axon guidance.

UNC-6/netrin was first molecularly cloned in *C. elegans* (Ishii et al 1992) after *unc-6* mutants were initially identified by their uncoordinated locomotion in a screen (Brenner 1974) and found to exhibit defects in circumferential and sensory axon guidance (Hedgecock et al 1990, Hedgecock et al 1985). UNC-6/netrin is a secreted laminin-like molecule and can function as either an attractive or a repulsive cue, depending on the receptors expressed in the developing growth cone (Chan et al 1996, Ishii et al 1992, Leung-Hagesteijn et al 1992). UNC-6/netrin signaling through the UNC-40/DCC receptor mediates attractive guidance towards netrin at the ventral midline, whereas UNC-6/netrin signaling through either the UNC-5/UNC5 receptor alone or the UNC-5/UNC5 and UNC-40/DCC receptors together mediates repulsive guidance away from netrin at the ventral midline (Chan et al 1996, Hedgecock et al 1990, Leung-Hagesteijn et al 1992). Both the UNC-5/UNC5 and UNC-40/DCC receptors are members of the immunoglobulin superfamily (Chan et al 1996, Leung-Hagesteijn

et al 1992) and these UNC-6/netrin pathway molecules were found to be highly conserved in flies and mammals where they also function to mediate attractive and repulsive guidance (Harris et al 1996, Hong et al 1999, Keino-Masu et al 1996, Keleman & Dickson 2001, Kennedy et al 1994, Kolodziej et al 1996, Leonardo et al 1997, Mitchell et al 1996, Serafini et al 1994).

Our understanding of axon guidance has been emerging over the past century in a step-wise fashion. After the initial hypothesis that axons were guided to their targets though chemical cues, this was shown to be true with in vitro studies where axons would turn towards or away from tissues expressing unidentified attractants or repellents, respectively. Genetic studies in model organisms have molecularly identified a number of guidance cues, receptors, and downstream effectors (Tessier-Lavigne & Goodman 1996). This brings us to a point where another layer of understanding is required to fully grasp how growth cones precisely and efficiently guide axons to their targets. Tackling the mechanisms that modulate the ligands and receptors of axon guidance pathways will likely provide the most insight into how a specific pathway is extracellularly regulated to guide axons, as cytoskeletal rearrangements downstream of multiple axon guidance pathways have been shown to converge onto the same molecules to alter growth cone mobility. For instance, both the UNC-6/netrin and SLT-1/slit signaling pathways have been shown to mediate cytoskeletal rearrangements through MIG-10/lamellipodin, CED-10/rac1, UNC-34/enabled, and UNC-

115/abLIM to guide the axon of the AVM neuron ventrally in *C. elegans* (Chang et al 2006, Gitai et al 2003, Quinn et al 2006, Quinn et al 2008, Yu et al 2002). Therefore, mechanisms that impart specificity onto the UNC-6/netrin and SLT-1/slit signaling pathways are likely to do so upstream of cytoskeletal rearrangements, either though regulation of the ligands, receptors, or both.

***C. elegans as a model to study nervous system development***

During *C. elegans* nervous system development 222 neurons are born embryonically, and 80 are born post-embryonically during the first and second larval stages in hermaphrodites (Sulston & Horvitz 1977, Sulston et al 1983, White et al 1986). These 302 neurons fall into 118 classes and form roughly 7000 synaptic connections (White et al 1986). Although most neurons are born close to their final positions, a handful of neurons in *C. elegans* undergo long-range migrations after their birth, including the CAN, HSN, and ALM neurons (Hedgecock et al 1987, Sulston et al 1983). Embryogenesis comprises the majority of neurodevelopmental events, including the guidance of axons into the nerve ring as well as the two largest nerve cords, the ventral and dorsal nerve cords, in addition to the assembly of neurons into multiple distinct ganglia in the head and tail.

The nematode *C. elegans* has proven to be an invaluable model organism with which to study the mechanisms of axon guidance during nervous system

development. Studies using the worm have pioneered our knowledge of the molecular pathways that guide axons. For example, the first chemotropic axon guidance molecule, UNC-6/netrin, was molecularly identified using *C. elegans* (Ishii et al 1992), prior to its identification in vertebrates (Serafini et al 1994). In addition, molecules identified in *C. elegans* have a high level of conservation to flies, mice, and humans. Therefore, mechanisms of axon guidance that we uncover using *C. elegans* are likely to be conserved as well.

There are many reasons why *C. elegans* is an ideal model organism for the study of nervous system development. *C. elegans* is an extremely genetically tractable model organism allowing for the fast identification of molecules important for nervous system development. For example, forward genetic screens can be carried out rapidly and whole-genome sequencing can be used to quickly identify causal genetic mutations (Doitsidou et al 2010, Minevich et al 2012, Zuryn et al 2010). Transgenic animals can quickly and easily be generated by microinjection (Mello & Fire 1995), which has a variety of experimental applications. One application is CRISPR, a new genome-editing technique (Jinek et al 2012) which functions efficiently in many organisms including *C. elegans* (Friedland et al 2013), and can be used to manipulate the genome, for example to engineer a mutation into the genome or to tag a gene of interest. Worms are easy to maintain and have a short life cycle, which means that experimental manipulations can be assessed quickly and repeated with large sample sizes in a

short time span. Specifically in regards to analysis of neurodevelopmental phenotypes for mutants of essential genes, RNAi knockdown by feeding can be performed specifically in subsets of neurons to circumvent lethality (Firnhaber & Hammarlund 2013).

Painstakingly detailed reconstructions have provided an abundance of information concerning developmental processes in *C. elegans*. The complete cell lineage has been reconstructed from electron micrographs (Kimble & Hirsh 1979, Sulston & Horvitz 1977, Sulston et al 1983) and appears to be largely invariant between animals. *C. elegans* is especially suited for neurodevelopmental studies, as its simple nervous system consists of just 302 neurons in the hermaphrodite, and it is the only model organism for which we have a complete neural wiring diagram detailing all of the connections of the nervous system (White et al 1986). Adult human brains are estimated to contain roughly 86 billion neuronal cells and 84 billion non-neuronal cells (Azevedo et al 2009), which creates a major obstacle in the study of reproducible cell and axon guidance events. Fortunately in *C. elegans*, cell and axon guidance can be easily studied at a single-cell resolution in intact, living animals on account of their transparent bodies and the ease of labeling their cells with fluorescent markers. This coupled with the knowledge of when every neuron is born, its final position, and its synaptic partners (Sulston et al 1983, White et al 1986) makes studies concerning cell and axon migrations particularly powerful in *C. elegans.*

***Postnatal challenges to the nervous system***

Assembling a functional nervous system is not an easy task. It requires a complex molecular interplay of spatially and temporally regulated factors sensed and integrated by developing cells to ensure proper assembly of critical connections. After the completion of these early neurodevelopmental events, the challenge of maintaining the structural and functional integrity of the nervous system begins. These initially established structures and features of the nervous system are not static, and instead undergo dynamic alterations even through adulthood. In the face of these changes, the embryonically established neuroanatomical structures must persist to maintain the integrity of the nervous system (Benard & Hobert 2009).

Postnatal growth, addition and elimination of neurons, glia, and synapses, myelination, and movement are examples of the challenges the prenatally established neuroanatomical structures face postnatally and through adulthood (Benard & Hobert 2009). Growth is not limited to an increase in height and body weight, but also a postnatal increase in the weight of the brain, roughly four-fold in the first several years after birth (Dekaban 1978, Dobbing & Sands 1973) which includes a 100% increase in volume in the first year alone (Knickmeyer et al 2008). Brain weight continues to increase roughly until the age of 19, and then begins to decline between the ages of 45 and 50, reaching its lowest around the age of 86 (Dekaban 1978). These changes in overall weight and volume likely

reflect the combined effect of a number of maturation events that occur in the brain during childhood, adolescence, and adulthood. For instance, myelination of axons is highly active during the first several years of life, and continues well into adulthood (Benes et al 1994, Holland et al 1986, Yakovlev & Lecours 1967), and this accounts for an overall increase in white matter through the age of 20 (Giedd et al 1999).

In addition to growth, the nervous system must also accommodate the proliferation and elimination of cells. Even in adulthood a small fraction of new neurons are born and migrate to specific regions of the human brain, namely the hippocampus (Eriksson et al 1998) and the olfactory bulb (Curtis et al 2007). In rodents these adult-born neurons become functionally integrated within existing circuits (Carleton et al 2003, van Praag et al 2002). Therefore these adult-born neurons create a challenge not only for the new neurons which must integrate into pre-existing circuits, but also for the neuronal structures that must accommodate the integration of new cells and processes. Programmed cell death occurs not only prenatally, but postnatally and into adulthood as well, eliminating glial cells and a small fraction of neurons (Buss et al 2006), therefore leaving the remaining cells with the task of adapting to the loss.

Density of synapses increases postnatally, to ultimately decline to reach the level observed in adulthood (reviewed in (Stiles & Jernigan 2010)), and overall

changes in synaptic density are a reflection of changes in timing of synaptic proliferation and elimination observed in different brain regions (reviewed in (Toga et al 2006)). For example, in the auditory cortex the maximum synaptic density is achieved by three months, and synaptic elimination continues until age 12 (Huttenlocher & Dabholkar 1997). Conversely, in the prefrontal cortex the highest density of synapses is observed at 15 months with elimination continuing into adolescence (Huttenlocher & Dabholkar 1997). Moreover, in the visual cortex maximum synaptic density is achieved by eight months and synaptic elimination occurs through the age of three (Huttenlocher et al 1982). Nervous systems must remain flexible in order to adapt to these changes, while simultaneously maintaining the stability necessary to preserve the integrity of preexisting structures and circuits essential for function.

Another challenge that the nervous system encounters on a daily basis is the mechanical stress of movement, especially on the peripheral nervous system (Benard & Hobert 2009). Physical stress theory proposes that physical stress leads to adaptive responses in tissues, including the nervous system (Mueller & Maluf 2002). Nerves experience mechanical stresses from normal conditions of posture and movement, and respond adaptively through elongation and displacement (reviewed in (Topp & Boyd 2006)). In extreme cases outside of normal daily movements, traumatic physical stress, especially to the central nervous system, cannot be tolerated. For example, repetitive concussive head

injuries in athletes and combat soldiers leads to neurodegeneration, indicating that the trauma resulting from the mechanical impact to the nervous system cannot be rectified over the long term (McKee et al 2009). Expanding our understanding of the basic mechanisms that function to maintain the integrity of the nervous system in the face of mechanical stress may provide insight into both the impacts of mechanical stress on normal physiological conditions as well as in the face of traumatic injury.

### *C. elegans as a model to study long-term maintenance of nervous system architecture*

In order to understand the basic mechanisms of how the integrity of the nervous system is maintained over time in the face of these challenges, we have turned to the model organism *C. elegans. C. elegans* also encounters many of the same challenges as mammalian nervous systems in the long-term preservation of nervous system integrity. For example, *C. elegans* also undergoes post-embryonic addition of new neurons. At hatch, *C. elegans* has 222 neurons, and 80 additional neurons are added postembryonically (Sulston & Horvitz 1977, Sulston et al 1983) and therefore are faced with the challenge of integrating within existing circuits. Additionally, worms also undergo a great deal of growth between hatch and adulthood that amounts to an approximately six-fold increase in length and 100-fold increase in volume (Benard & Hobert 2009, Knight et al 2002). Furthermore, the sinusoidal body waves of locomotion as well as

pharyngeal pumping are likely to exert mechanical stress on nervous system structures (Benard & Hobert 2009). Indeed, molecules have been identified that function to counteract the mechanical stress of locomotion and protect the architecture of the nervous system (Benard et al 2009, Benard et al 2006, Pocock et al 2008, Sasakura et al 2005).

*C. elegans* is an unparalleled model with which to ask how the structural and functional integrity of the nervous system is preserved in the face of maturational changes and physical stress. With the tools and information currently available, it would be highly challenging to address these questions in any other model. *C. elegans* has a simple nervous system which in the hermaphrodite consists of just 302 neurons. The entire neural wiring diagram has been solved for *C. elegans* and its neuroanatomy is largely invariable between animals (White et al 1986). It is the only model organism for which a complete neural wiring diagram exists. This allows for the observation of changes across genotypes and ages in positioning, organization, fasciculation, or other aspects of neuroanatomy that would generally be consistent among individual animals. In addition, this means that we have the information needed to know where specific neuronal cell bodies and axons are meant to be initially, and so we can compare this to their positioning in later stages in different genotypic backgrounds. This level of information is not available for any other model system.

*C. elegans* becomes a reproductively mature adult within three days and its mean life span is roughly three weeks. This short life cycle allows for the rapid study of post-embryonic and adult phenotypes, making *C. elegans* an ideal model for the study of changes to the nervous system over time. In addition, knockdown of gene function by RNAi can be started at any life stage, therefore allowing for the investigation of genes with post-embryonic functions while circumventing any developmental roles.

Perhaps the most compelling rationale for the use of *C. elegans* for studies on the long-term maintenance of nervous system architecture is that molecules with dedicated functions in the post-embryonic maintenance of nervous system architecture have been identified using *C. elegans* (Aurelio et al 2002, Barsi-Rhyne et al 2013, Benard et al 2009, Benard et al 2006, Bülow et al 2004, Cherra & Jin 2016, Johnson & Kramer 2012, Pocock et al 2008, Sasakura et al 2005, Shao et al 2013, Wang et al 2005, Woo et al 2008, Zallen et al 1999). One of the molecules critical for the long-term maintenance of neural architecture in *C. elegans* is SAX-7/L1CAM, which is homologous to vertebrate L1 cell adhesion molecule family members (Chen et al 2001, Pocock et al 2008, Sasakura et al 2005, Wang et al 2005). Roles for L1 family members in the postnatal nervous system have been shown through conditional ablation studies (Amor et al 2014, Kolata et al 2008, Kriebel et al 2011, Law et al 2003, Zonta et al 2011). In addition, rodent models lacking L1 family members exhibit an altered distribution

of neurons (Demyanenko et al 2004, Demyanenko et al 2001), though whether these defects are developmental or a result of a failure to maintain neuronal positioning remains to be determined.

Despite the identification of molecules that function to maintain the architecture of the nervous system, our mechanistic understanding of how these molecules carry out these functions remains limited. It is clear that mechanisms exist to preserve the long-term integrity of the nervous system in the face of challenges, and that *C. elegans* is an ideal model for this type of investigation. Research dedicated to understanding the mechanisms by which these molecules function will provide important insight into how the nervous system adopts the flexibility needed to accommodate to important maturational changes and physical stresses, while providing stability to early-developed structures integral to the structure and function of the nervous system.

# Chapter II

## Heparan sulfate proteoglycans are required for the guidance of migrations during development

Cassandra R. Blanchette[1], Andrea Thackeray[1], Paola N. Perrat[1],

Siegfried Hekimi[2], Claire Y. Bénard[1]

1. Department of Neurobiology, UMass Medical School

364 Plantation Street, Worcester, MA 01605, USA

2. Department of Biology, McGill University

1205 Dr Penfield Avenue, Montreal, QC H3A 1B1, Canada

Contribution summary: C.Y.B. and C.R.B. designed the experiments. C.Y.B., C.R.B., A.T, P.P., and S.H. carried out the experiments. C.Y.B. and C.R.B. wrote the manuscript.

**ABSTRACT**

The regulation of cell migrations is essential to animal development and physiology. Heparan sulphate proteoglycans (HSPGs) shape interactions between morphogens and guidance cues with their respective receptors to elicit appropriate cellular responses. Dysfunction of HSPG synthesis results in pleiotropic consequences, including tumorous growth. Human mutations in the genes EXT1 and EXT2 that encode the two subunits of the heparan sulphate (HS) copolymerase result in osteosarcomas called multiple exostoses. Analysis of mutations in the *Drosophila* HS copolymerase of the *tout-velu* family has uncovered key roles of HSPGs during morphogenesis. The use of the powerful *C. elegans* model for understanding HSPGs functions has been precluded, however, by the unavailability of viable mutations in the HS copolymerase genes. Here, we report our identification and analysis of viable mutations in the genes *rib-1* and *rib-2*, which encode the HS copolymerase. We show that these hypomorphic mutations of *rib-1* and *rib-2* severely reduce the levels of HS synthesis and lead to dramatic morphogenetic defects and abnormal cell and axonal migrations during the development of the nematode. We analyze the expression pattern of the HS copolymerase and find that it is very dynamic during embryonic and larval morphogenesis, while also being sustained in distinct tissues throughout life, consistent with both developmental and post-developmental roles for HSPGs. We analyze neuronal migrations and find that multiple HSPGs synthesized in the migrating neuron and neighboring cells

together contribute to regulate their guidance. Our findings establish a model to dissect the diverse and specific functions of HSPGs in *C. elegans* and uncover general principles of their roles in development and tissue homeostasis.

## INTRODUCTION

Cell migrations are a key feature of animal development and physiology. The orientation of migrating cells relies on molecular cues present in their extracellular environment to reach their targets. Many guidance factors and morphogens are regulated by heparan sulfate proteoglycans (HSPGs), which are cell-surface or extracellular proteins characterized by the attachment of heparan sulfate (HS) chains to their extracellular domain (Bernfield et al 1999). HSPGs interact with molecules at the cell surface and in the extracellular matrix via both their HS chains and core proteins, and are part of multiple signaling pathways, including of guidance cues (Slit, netrin) and morphogens (Hedgehog, FGF, Sonic Hedgehog, Wnts, and BMPs) (Bernfield et al 1999, Bishop et al 2007, Bülow & Hobert 2006). HSPGs function as co-factors, for instance to regulate the gradient formation of morphogens and to modulate the interactions between extracellular ligands and their receptors, playing crucial roles in morphogenesis, nervous system development, and physiology (Bülow & Hobert 2006, Lin 2004).

The HS chains of HSPGs are linear glycosaminoglycan polysaccharides composed of alternating repeats of D-glucuronic acid (GlcA) and N-

acetylglucosamine (GlcNAc) (reviewed in (Esko & Selleck 2002)). HS chain synthesis in the Golgi apparatus is initiated by the addition of a tetrasaccharide linker on specific Serine residues on the core protein. HS chains are then elongated by the HS copolymerase, which is a heterodimer composed of two glycosyltransferases of the EXT family. HS chains are subsequently chemically modified (e.g. by epimerases and sulfotransferases). Dysfunction of the biosynthesis of HS chains results in pleiotropic consequences across metazoans, including developmental defects and tumor growth. In humans, mutations in the genes EXT1 and EXT2, which encode the two subunits of the HS copolymerase, result in osteosarcomas called multiple exostoses (Cook et al 1993, Francannet et al 2001, Le Merrer et al 1994, Wu et al 1994, Wuyts & Van Hul 2000). In *Drosophila*, mutations in the HS copolymerase genes *tout-velu*, *brother of tout-velu* and *sister of tout-velu* lead to striking defects, including the loss of segment polarity and disruption of Hh diffusion (Bellaiche et al 1998, Han et al 2004, The et al 1999), and their analysis has yielded key insights into general principles of morphogenesis.

In *C. elegans*, the mutations of the HS copolymerase genes *rib-1* and *rib-2* available to date are embryonic lethal (Franks et al 2006, Kitagawa et al 2007, Morio et al 2003), which has restricted their analysis. The field has been limited to study these lethal alleles by examining homozygous mutant animals that are maternally rescued (M+/- Z-/-), which are virtually normal thanks to the

contribution of wild-type gene product from their heterozygous mothers (Edwards & Hammarlund 2014, Franks et al 2006, Morio et al 2003). RNAi has been used to knockdown the genes *rib-1* and *rib-2*, but the resulting phenotypes are weak at best (Edwards & Hammarlund 2014, Pedersen et al 2013), indicating low efficiency of the interference for these genes. Mutations in the enzymes that catalyze the initiation of the HS chains (production of the tetrasaccharide linker) are not specific for HS as they also catalyze the initiation of chondroitin sulfate (CS) chains, leading to phenotypic consequences that are the result of the combined loss of HSPGs and CSPGs. Mutations disrupting individual HSPG core proteins (e.g. *sdn-1*/syndecan, *lon-2*/glypican, *cle-1*/collagen type XVIII, and *unc-52*/perlecan) and HS modifying enzymes (e.g. the *hse-5* epimerase and the *hst-1, hst-2, hst-3.1, hst-3.2* and *hst-6* sulfotransferases) have been identified and studied, revealing specific roles of individual HSPGs and their chemical modifications during development, respectively (Ackley et al 2003, Blanchette et al 2015, Bülow et al 2002, Bülow & Hobert 2004, Bulow et al 2008, Diaz-Balzac et al 2014, Gysi et al 2013, Kinnunen et al 2005, Merz et al 2003, Pedersen et al 2013, Rhiner et al 2005). However, a general view of the function of heparan sulfate proteoglycans has not been available in this powerful model organism.

Here we report a *C. elegans* model of loss of function of the two subunits of the HS copolymerase genes. We identified viable mutations in each of the HS copolymerase genes *rib-1* and *rib-2*, which severely reduce HS levels and result

in dramatic morphogenetic defects and abnormal cell and axonal migrations. We find the HS copolymerase is expressed dynamically during development, as well as later in adulthood, consistent with HSPGs functioning in both morphogenesis and physiology. Our findings indicate that proper neuronal migration is ensured by the coordinated synthesis of HSPGs in the migrating neuron itself as well as in adjacent cells that secrete the extracellular matrix along which the growth cone extends. Our analysis highlights the functional importance of HSPGs and establishes a model for dissecting their roles during animal development and homeostasis.

## RESULTS

### Cell and axonal migrations are impaired in *mum-1/rib-1* and *mum-3/rib-2* mutants

In order to identify genes required for neural development, a genetic screen for maternal-effect mutants was carried out (Hekimi et al 1995). Mutations *qm32* and *qm46* were identified in this screen and define the genes *mum-1* and *mum-3,* respectively *(mum* stands for maternal-effect uncoordinated and morphologically abnormal). *mum-1* and *mum-3* mutants display very similar defects, which include severe uncoordination, defective egg-laying, and morphological abnormalities, as well as some embryonic and larval lethality (Hekimi et al 1995, Takagi et al 1997). As we report below, *mum-1(qm32)* and *mum-3(qm46)* are

loss-of-function alleles in the genes *rib-1* and *rib-2*, respectively, which encode the two subunits of the HSPG copolymerase. For clarity, we henceforth refer to *mum-1(qm32)* as *rib-1(qm32)*, and to *mum-3(qm46)* as *rib-2(qm46)*.

To characterize the underlying neuroanatomical defects of *rib-1(qm32)* and *rib-2(qm46)*, we built strains of these mutants carrying a number of integrated transgenes, which drive the expression of fluorescent proteins and allow the visualization of specific neurons (see **Table 2.1**). We examined the nervous system of *rib-1* and *rib-2* mutants with single-cell resolution and found that numerous neuronal migrations are affected by loss of function of *rib-1* or *rib-2* compared to wild type. For instance, we found that the CAN neuron, which migrates from the head region towards the midbody region in wild-type animals, was frequently positioned too anterior or too posterior in *rib-1* and *rib-2* mutants (**Fig. 2.1A**). Also, the HSN neuron that migrates from the tail region to the midbody region in the wild type is often located too posterior in *rib-1* and *rib-2* mutants (**Fig. 2.1B**). Moreover, the AVM neuron is frequently located in the posterior of the body in *rib-1* and *rib-2* mutants, instead of being anterior to the vulva (**Fig. 2.1C**). The penetrance and expressivity of these defects is similar in both *rib-1* and *rib-2* single mutants. Thus, loss of function of the genes *rib-1* or *rib-2* disrupts the guided migration of several neurons that undergo long-range migrations during development.

We also found that axonal projections are defective in *rib-1* and *rib-2* single mutants. For example, we observed that the axon of the interneuron PVQ, which projects into the ipsilateral fascicle of the ventral nerve cord in the wild type, frequently projects in the contralateral fascicle or even laterally in *rib-1* and *rib-2* mutants (**Fig. 2.1D**). Similarly, the axon of the motorneuron HSN, which projects ventrally and into the ipsilateral fascicle of the ventral nerve cord in the wild type, is misguided in *rib-1* and *rib-2* mutants as it projects into the contralateral fascicle or laterally in these mutants (**Fig. 2.1D**). Another example is the axon of the mechanosensory neuron AVM, which extends ventrally towards the ventral nerve cord in the wild type, but projects laterally in *rib-1* and *rib-2* mutants (**Fig. 2.1C**). The axons of cholinergic and GABAergic motorneurons are also misguided in *rib-1* and *rib-2* mutants: contrary to the wild type, where most motorneuron axons exit the ventral midline on the right side to migrate along on the right side of the worm's body wall, many motorneuron axons abnormally project to the left side in *rib-1* and *rib-2* mutants (**Fig. 2.1E**). Finally, the dorsal nerve cord, which is composed of several motor axons that run as a single fascicle in the wild type, is frequently defasciculated into several bundles in *rib-1* and *rib-2* mutants (**Fig. 2.1F**). It is worth nothing that the capacity to migrate is not lost in *rib-1* and *rib-2* mutants as soma and axons often overshoot their target. Rather, the guidance of migrations during development is disrupted by the loss of function of the genes *rib-1* and *rib-2*.

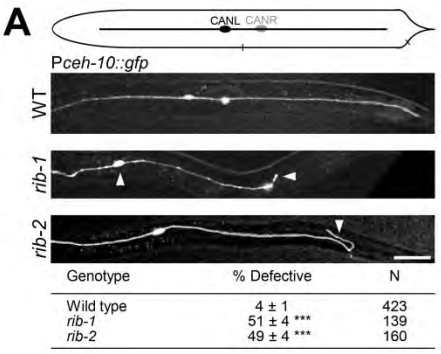


| Genotype | % Defective | N |
|---|---|---|
| Wild type | 4 ± 1 | 423 |
| *rib-1* | 51 ± 4 *** | 139 |
| *rib-2* | 49 ± 4 *** | 160 |

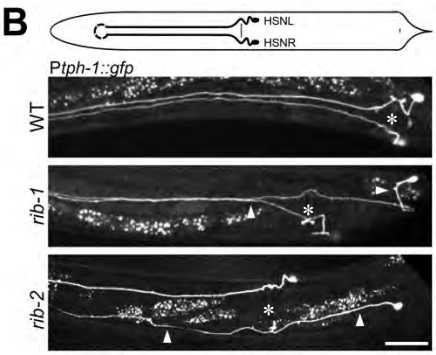


| Genotype | % Defective | N |
|---|---|---|
| Wild type | 11 ± 4 | 74 |
| *rib-1* | 100 *** | 55 |
| *rib-2* | 95 ± 2 *** | 74 |

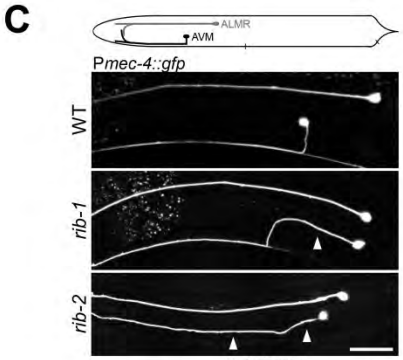


| Genotype | % Defective Soma + Axon | N |
|---|---|---|
| Wild type | 1 ± 1 | 139 |
| *rib-1* | 70 ± 4 *** | 124 |
| *rib-2* | 67 ± 4 *** | 159 |

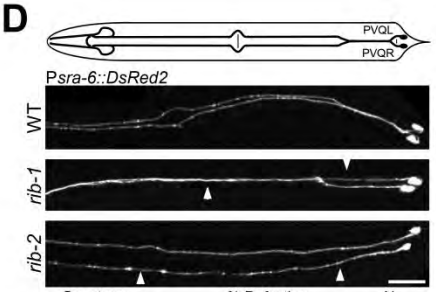


| Genotype | % Defective | N |
|---|---|---|
| Wild type | 6 ± 3 | 66 |
| *rib-1* | 91 ± 3 *** | 119 |
| *rib-2* | 79 ± 5 *** | 78 |

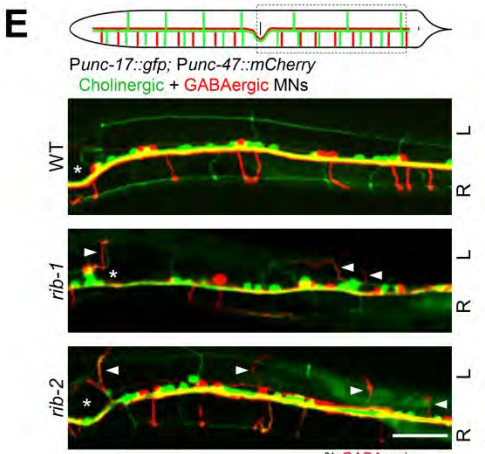


| | % >7 Cholinergic axons on the left | N | % GABAergic axons on the left | N |
|---|---|---|---|---|
| WT | 11 ± 3 | 89 | 21 ± 3 | 234 |
| *rib-1* | 91 ± 4 *** | 55 | 96 ± 3 *** | 54 |
| *rib-2* | 77 ± 4 *** | 99 | 95 ± 2 *** | 78 |

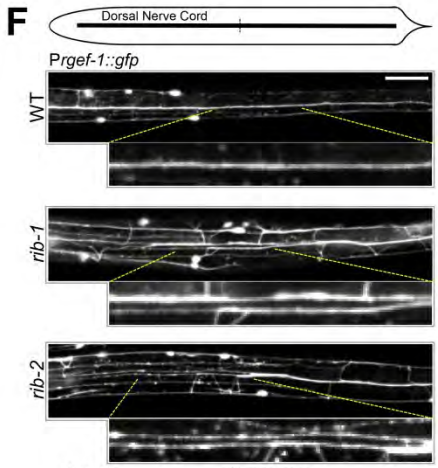


| Genotype | % Defective | N |
|---|---|---|
| Wild type | 2 ± 2 | 58 |
| *rib-1* | 91 ± 3 *** | 79 |
| *rib-2* | 93 ± 3 *** | 82 |

**Fig. 2.1. Neuronal migration defects in *mum-1/rib-1(qm32)* and *mum-3/rib-2(qm46)* mutants.**

**A.** Lateral views of animals expressing the transgene P*ceh-10::gfp* to visualize the CAN neurons (CANL and CANR). In the wild type, the soma of the CAN neuron is located laterally in the midbody region and its axon extends laterally along the antero-posterior axis. *mum-1/rib-1* and *mum-3/rib-2* mutants display defective CAN soma migration and are frequently observed in very anterior positions. In addition, the CAN axon in *mum-1/rib-1* and *mum-3/rib-2* mutants project in abnormal directions (arrowhead), or fail to extend fully in the posterior direction. The table indicates the sum of soma and axon defects of the CAN neurons (axon guidance was only scored in animals that had normal soma migration).

**B**. Ventral views of animals expressing the transgene P*tph-1::gfp* to visualize the HSN neurons (HSNL and HSNR). In wild type, the soma of HSN is located laterally just posterior to the vulva and its axon extends ventrally and projects along the ipsilateral side of the ventral nerve cord. *mum-1/rib-1* and *mum-3/rib-2* mutants display defective HSN soma positions and defective axons that extend laterally or project into the opposite side of the ventral nerve cord. The table indicates the sum of soma and axon defects of the HSN neurons (axon guidance was only scored in animals that had normal soma position). White asterisk denotes position of the vulva.

**C**. Lateral views of animals expressing the transgene P*mec-4::gfp* to visualize the AVM neuron. In the wild type, the AVM soma is located in the anterior midbody region and its axon projects ventrally to reach the ventral nerve cord and then extends anteriorly. *mum-1/rib-1* and *mum-3/rib-2* mutants display defective AVM soma (posterior to the vulva), as well as defective axons that project laterally instead of ventrally. The table indicates the sum of soma and axon defects of the AVM neuron (axon guidance was only scored in animals that had normal soma position).

**D**. Ventral views of animals expressing the transgene P*sra-6::DsRed2* to visualize the PVQ neurons (PVQL and PVQR). In the wild type, the axon of PVQ extends along the ipsilateral side of the ventral nerve cord. *mum-1/rib-1* and *mum-3/rib-2* mutants display defective PVQ axons, including axons that extend laterally or project into the opposite side of the ventral nerve cord.

**E.** Ventral views of animals expressing the transgenes P*unc-17::gfp* and P*unc-47::mCherry* to visualize the cholinergic (green) and GABAergic (red) motorneurons, respectively. The position of the vulva is indicated by an asterisk. In the wild type, most motorneuron axons extend along the right side of the animal, whereas on the left side only three cholinergic and no GABAergic axons extend in the area shown in the picture. *mum-1/rib-1* and *mum-3/rib-2* mutants display defective guidance of motorneuron axons of both cholinergic and GABAergic motorneuron axons, as more axons project along the left side of the animal compared to wild type (arrowheads).

**F**. Dorsal views of animals expressing the transgene P*rgef-1::gfp* to visualize the dorsal nerve cord. The dorsal nerve cord runs as one tight fascicle in the wild type. In *mum-1/rib-1* and *mum-3/rib-2* mutants, the dorsal nerve cord is frequently split into two or more fascicles. Indicated area is enlarged in insets.

Scale bars 20 μm. *** $P \leq 0.001$ (z-tests, P values were corrected by multiplying by the number of comparisons).

In a similar way, the migration of mesodermal cells, which share guidance mechanisms with neurons (Hedgecock et al 1990), is defective in *rib-1* and *rib-2* single mutants. For instance, the canals of the excretory cell (two anterior and two posterior canals) run laterally in the wild type but are frequently too short or extend along the ventral or dorsal aspect of the body in *rib-1* and *rib-2* mutants (**Fig. 2.2A**). Another example of misguided mesodermal cells in *rib-1* and *rib-2* mutants is that of the distal tip cell (DTC), whose path determines the shape of the gonad. In wild-type animals, the anterior DTC migrates anteriorly along the right side of the animal and the posterior DTC migrates posteriorly along the left side of the animal; then, the DTCs turn dorsally, and turn again to migrate towards the midbody region, resulting in the anterior arm of the gonad being on the right side of the animal and the posterior arm of the gonad being on the left side. In *rib-1* and *rib-2* mutants, the anterior arm of the gonad is often found on the left side of the animal and the posterior arm on the right side, and in some cases, both gonad arms can lie on the opposite side of the animal (**Fig. 2.2B**). Lastly, the excretory gland is also found in abnormal positions in *rib-1* and *rib-2* mutants (**Fig. 2.2C**). Thus, loss of function of the genes *rib-1* or *rib-2* disrupts the guidance of migrations of neuronal and mesodermal cells during development.

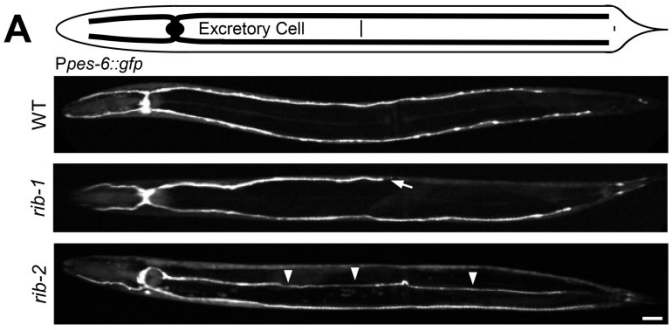


| Genotype | % Defective | N |
|---|---|---|
| Wild type | 1 ± 1 | 216 |
| *rib-1* | 57 ± 7 *** | 51 |
| *rib-2* | 59 ± 7 *** | 56 |

**B Gonad Arms**

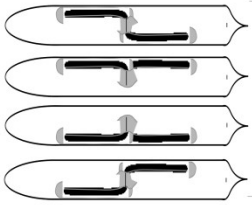

| Wild type | *rib-1* | *rib-2* | |
|---|---|---|---|
| 100 | 51 ± 6 | 52 ± 5 | % Phenotype |
| 0 | 42 ± 6 | 28 ± 5 | |
| 0 | 1 ± 1 | 1 ± 1 | |
| 0 | 6 ± 3 | 19 ± 4 | |
| *80* | *75* | *92* | *N* |

**C Excretory Glands**

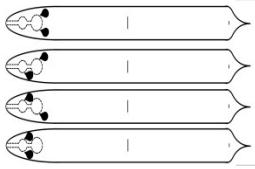

| Wild type | *rib-1* | *rib-2* | |
|---|---|---|---|
| 100 | 28 ± 5 | 58 ± 5 | % Phenotype |
| 0 | 57 ± 5 | 16 ± 4 | |
| 0 | 5 ± 2 | 9 ± 3 | |
| 0 | 10 ± 3 | 0 | |
| *70* | *89* | *98* | *N* |

**Fig. 2.2. Other migration defects in *mum-1/rib-1(qm32)* and *mum-3/rib-2(qm46)* mutants.**
**A**. Ventral views of animals expressing the transgene P*pes-6::gfp* to visualize the canals of the excretory cell. In the wild type, the excretory cell extends four lateral canals, two that are anteriorly-directed along the sides of the head and two that are posteriorly-directed along the sides of the body. *mum-1/rib-1* and *mum-3/rib-2* mutants display defective excretory canals that can be too short (arrows), or extend ventrally or dorsally instead of laterally (arrowheads). Scale bar, 10 μm. Asterisk denotes significant difference: *** $P \leq 0.001$ (z-tests, P values were corrected by multiplying by the number of comparisons).
**B**. Diagrams of the gonad arms (dorsal view). In the wild type, the anterior arm of the gonad is located on the right side of the animal, and the posterior arm is located on the left side. Gonad arms are abnormally positioned in *mum-1/rib-1* and *mum-3/rib-2* mutants, where one or both gonad arms can lie on the opposite side of the animal.
**C**. Diagrams of the excretory glands (dorsal view). In the wild type, the excretory glands are located just posterior of the terminal bulb of the pharynx. *mum-1/rib-1* and *mum-3/rib-2* mutants display abnormally located excretory glands, where one or both lie anterior of the terminal bulb.

## *mum-1(qm32)* and *mum-3(qm46)* are viable hypomorphic mutations of the genes *rib-1* and *rib-2* that encode the two subunits of the HSPG copolymerase

To gain insight into the molecular mechanisms that are disrupted in the *mum-1* and *mum-3* mutants, we determined the molecular identity of the mutations *qm32* and *qm46*. First, we narrowed down the genetic position of the *mum-1(qm32)* mutation by genetic mapping and assayed cosmids corresponding to the genetic position of *mum-1* for transformation rescue of the *mum-1(qm32)* mutants (**Fig. 2.3B**). We found that cosmid F12F6 fully rescued the *mum-1* mutants for larval development, uncoordination and egg laying defects (**Fig. 2.3A,B**). We tested PCR products corresponding to each of the genes located on this cosmid and found that a 9 kb PCR product containing the gene F12F6.3/*rib-1* fully rescued the *mum-1* mutants for larval development, uncoordination and egg-laying

defects (**Fig. 2.3A,B**). In addition, construct P*rib-1::rib-1(+)* completely rescued the axon guidance defects of AVM and PVQ in *mum-1* mutants (**Fig. 2.3C**). We verified the predicted gene structure by sequencing the cDNA clone yk187a9. We sequenced the genomic region of the gene *rib-1* in *mum-1(qm32)* mutants and found that the *qm32* molecular lesion is a T to A base pair change at position 39528 of cosmid F12F6, which converts the Stop codon of *rib-1* into a Lys residue (**Fig. 2.3B**). This mutation likely results in the translation of an open reading frame present in the 3'UTR, which would extend the protein RIB-1 by 114 aa residues, until the next in-frame Stop codon. The activity of the mutant RIB-1 protein in *rib-1(qm32)* is likely impaired by the presence of the abnormal extension or the instability of the translated protein. Stronger mutations of *rib-1*, namely deletion alleles *tm516* and *ok556*, result in complete embryonic lethality (Franks et al 2006, Kitagawa et al 2007). Thus, *qm32* is a viable hypomorphic mutation in the gene *rib-1* that encodes one of the two subunits of the HSPG copolymerase and is homologous to *Drosophila tout-velu* and mammalian EXT1 (**Fig. 2.3D**).

The second subunit of the *C. elegans* HSPG copolymerase is encoded by the gene *rib-2*. Given the phenotypic similarities between the *rib-1(qm32)* and *mum-3(qm46)* mutants and that the genetic position of *mum-3(qm46)* corresponds to a chromosomal interval containing the gene *rib-2*, we tested whether *mum-3(qm46)* was an allele of the gene *rib-2*. We tested the rescue of *mum-3(qm46)*

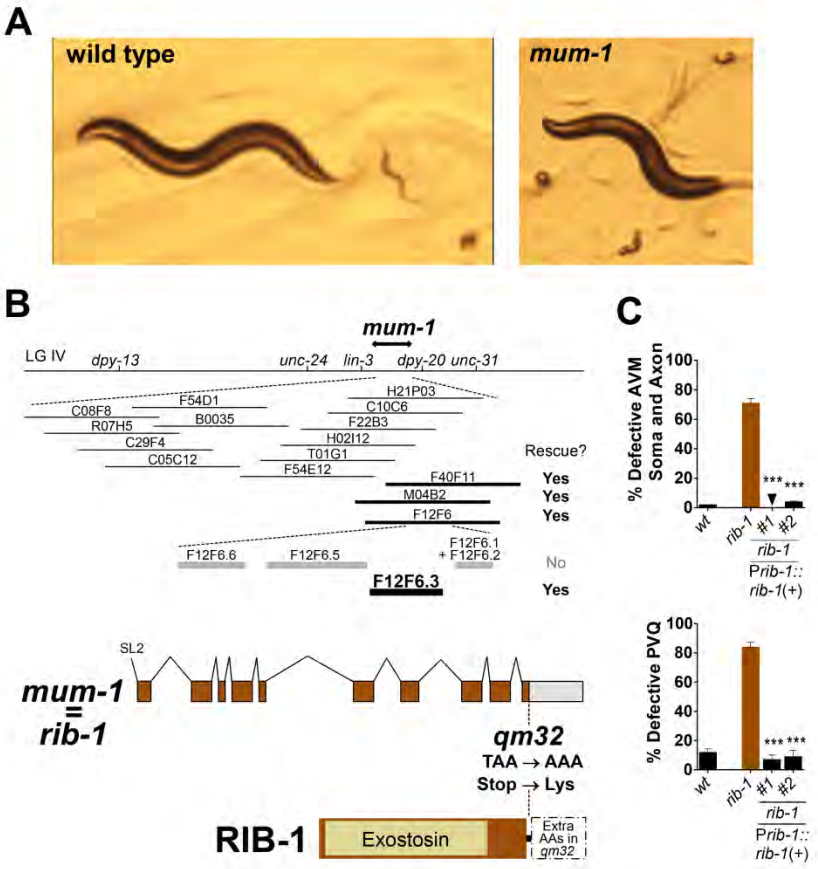
A
wild type
mum-1
B
mum-1
LG IV
dpy-13
unc-24
lin-3
dpy-20 unc-31
H21P03
C10C6
F54D1
C08F8
B0035
F22B3
R07H5
H02I12
C29F4
T01G1
C05C12
F54E12
Rescue?
F40F11
Yes
M04B2
Yes
F12F6
Yes
F12F6.6
F12F6.5
F12F6.1
+ F12F6.2
No
F12F6.3
Yes
SL2
mum-1
rib-1
qm32
TAA → AAA
Stop → Lys
RIB-1
Exostosin
Extra
AAs in
gm32
C
% Defective AVM
Soma and Axon
wt
rib-1
#1
#2
rib-1
Prib-1::
rib-1(+)
% Defective PVQ
wt
rib-1
#1
#2
rib-1
Prib-1::
rib-1(+)
D
Worm
Fly
Mouse
Human

**Fig. 2.3. *mum-1(qm32)* is a viable hypomorphic mutation of the gene *rib-1,* which encodes one of the two HS copolymerase subunits.**
**A.** Pictures of wild type and *mum-1/rib-1* mutant animals. Some of the *mum-1/rib-1* mutants die as embryos or misshapen larvae, but the majority reach adulthood and display morphological defects, as described in (Hekimi et al 1995).
**B.** Molecular identification of *mum-1(qm32). mum-1* was previously mapped between *dpy-13* and *unc-31* on linkage group I (Hekimi et al 1995). We narrowed down its genetic position by a combination of three-factor and two-factor mapping (results were *unc-24* 70/79 *mum-1* 9/79 *dpy-20*; 10 Dpy-20 non Mum-1/4320 F2s ; and *lin-3* 6/7 *mum-1* 1/7 *dpy*-20; which placed *mum-1* between *lin-3* and *dpy-20*, between 4.98 and 5.07 cM, according to the 95% confidence intervals). Cosmids (thin lines) and PCR products (thick lines) encompassing the gene *rib-1(+)* rescued the morphological and uncoordination defects of the *mum-1* mutants. *mum-1(qm32)* is a missense mutation at base 39528 of cosmid F12F6 and changes the Stop into a Lys codon, which leads to a putative extension of 114 amino acids until the first in frame Stop codon.
**C.** Rescue of the guidance defects of the neurons AVM and PVQ of *mum-1(qm32)* with DNA corresponding to the genomic region of *rib-1(+)* (plasmid P*rib-1::rib-1::Venus*). Error bars are standard error of the proportion. Asterisks denote significant difference: *** $P \leq 0.001$ (z-tests, P values were corrected by multiplying by the number of comparisons).
**D.** An alignment of the predicted amino acid sequences of *C. elegans* RIB-1 and its homologues from *D. melanogaster* (Ttv)*, M. musculus* (EXT1)*,* and *H. sapiens* (EXT1).

mutants by a 5.6 kb PCR product of the gene *rib-2(+)* and found that it fully rescued their larval development, locomotion, and egg laying (**Fig. 2.4A,B**). In addition, construct P*rib-2::rib-2(+)* completely rescued the axon guidance defects of AVM and PVQ in *mum-3* mutants (**Fig. 2.4C**). We verified the predicted gene structure by sequencing the cDNA clone yk3c1. We sequenced the genomic region of the gene *rib-2* in *mum-3(qm46)* mutants and found that the *qm46* molecular lesion is a G to A transition at position 4366 of cosmid K01G5. The *qm46* mutation results in an Arg to Gln amino acid substitution at residue 434, which is near the exostosin domain in the 814 amino acid long RIB-2 protein. A stronger mutation of *rib-2*, deletion allele *tm710*, results in complete embryonic

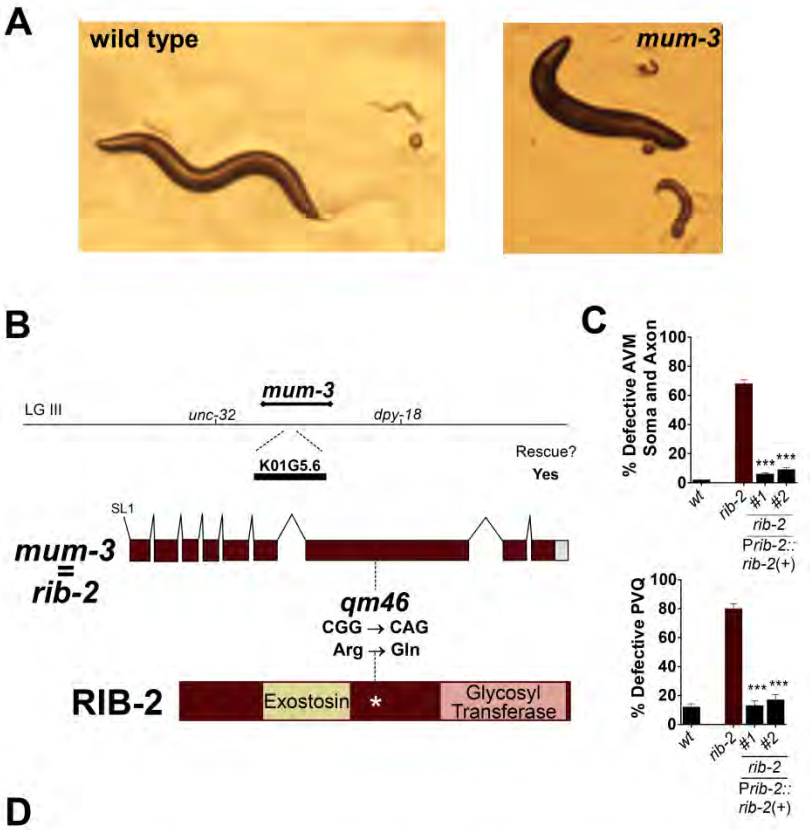
A
wild type
mum-3
B
LG III
unc-32
mum-3
dpy-18
K01G5.6
Rescue?
Yes
SL1
mum-3
rib-2
qm46
CGG → CAG
Arg → Gln
RIB-2
Exostosin
*
Glycosyl Transferase
C
% Defective AVM Soma and Axon
wt
rib-2
#1
#2
rib-2
Prib-2::rib-2(+)
% Defective PVQ
D
Worm
Fly
Mouse
Human

**Fig. 2.4. *mum-3(qm46)* is a viable hypomorphic mutation of the gene *rib-2,* which encodes the second HS copolymerase subunit.**
**A.** Pictures of wild type and *mum-3/rib-2* mutant worms. Some of the *mum-3/rib-2* mutants die as embryos or deformed larvae, but the majority reach adulthood and display morphological defects, as described in (Hekimi et al 1995).
**B.** Molecular identification of *mum-3*. *mum-3(qm46)* was previously mapped on linkage group III, between *unc-32* and *dpy-18* (Hekimi et al 1995), which includes the second HSPG copolymerase gene *rib-2*. A PCR product containing the genomic locus of *rib-2(+)* rescued the morphological and uncoordination defects of the *mum-3(qm46)* mutants. *mum-3(qm46)* is a missense mutation at base 4366 on cosmid K01G5 that changes an Arg to a Gln at residue 434.
**C.** Rescue of the guidance defects of the neurons AVM and PVQ of *mum-3(qm46)* with DNA containing the genomic region of *rib-2(+)* (PCR product P*rib-2::rib-2*). Error bars are standard error of the proportion. Asterisks denote significant difference: *** $P \leq 0.001$ (z-tests, P values were corrected by multiplying by the number of comparisons).
**D.** An alignment of the predicted amino acid sequence of *C. elegans* RIB-2 and its homologues from *D. melanogaster* (Botv), *M. musculus* (EXT2), and *H. sapiens* (EXT2).

lethality (Franks et al 2006). Thus, *qm46* is a viable hypomorphic mutation in the gene *rib-2* that encodes the second subunit of the HSPG copolymerase and is homologous to *Drosophila brother of tout-velu* and mammalian EXT2 and EXTL3 family members (**Fig. 2.4D**).

### HS levels are impaired in *rib-1(qm32)* and *rib-2(qm46)* mutants

The genes *rib-1* and *rib-2* encode the two subunits of the *C. elegans* HS copolymerase that synthesizes HS chains onto core proteins to generate HSPGs (**Fig. 2.5A**; (Kitagawa et al 2007)). HS chains are composed of alternating glucuronic acid and N-acetylglucosamine residues. The first step of HS chain biosynthesis is the addition of a tetrasaccharide linker onto specific Ser residues of the core protein. Next, proteins homologous to RIB-2, like mammalian EXTL3

and *Drosophila sister of tout-velu* (Sotv), catalyze the addition of the initial N-acetylglucosamine residue onto the tetrasaccharide linker (Kitagawa et al 2001). Subsequently, proteins homologous to RIB-1 and RIB-2 together, like mammalian EXT1 and EXT2 or *Drosophila tout-velu* (Ttv) and *brother of tout-velu* (Botv), function as a complex to polymerize HS chains by adding disaccharide units of glucuronic acid and N-acetylglucosamine (Kitagawa et al 2007). To directly determine the impact of the mutations *rib-1(qm32)* and *rib-2(qm46)* on HS biosynthesis, we probed for total HS content by western blot analysis. We extracted proteins from wild-type (N2) animals, *rib-1(qm32)* and *rib-2(qm46)* single mutants, as well as transgenic *rib-1(qm32)* animals expressing *rib-1(+)* and transgenic *rib-2(qm46)* animals expressing *rib-2(+)*, which rescue their developmental defects. We treated the extracts with heparinases I and III, and performed western blot analysis using an antibody that specifically recognizes heparinase-digested HS chains (3G10, (David et al 1992)). As expected, no signal was detected in untreated control samples (**Fig. 2.5B**). We found that the total HS content was severely reduced in the *rib-1(qm32)* and the *rib-2(qm46)* mutants compared to the wild type (**Fig. 2.5B**). Providing wild-type transgenic copies of *rib-1* or *rib-2* rescued HS biosynthesis, confirming that loss of the genes *rib-1* or *rib-2* leads to the disruption of HS biosynthesis in the *qm32* and *qm46* mutants (**Fig. 2.5B**). The partial rescue of HS levels is likely due to the transgenic strains in fact being a mixture of rescued transgenic animals as well as non-rescued non-transgenic animals, as the strains were grown for several

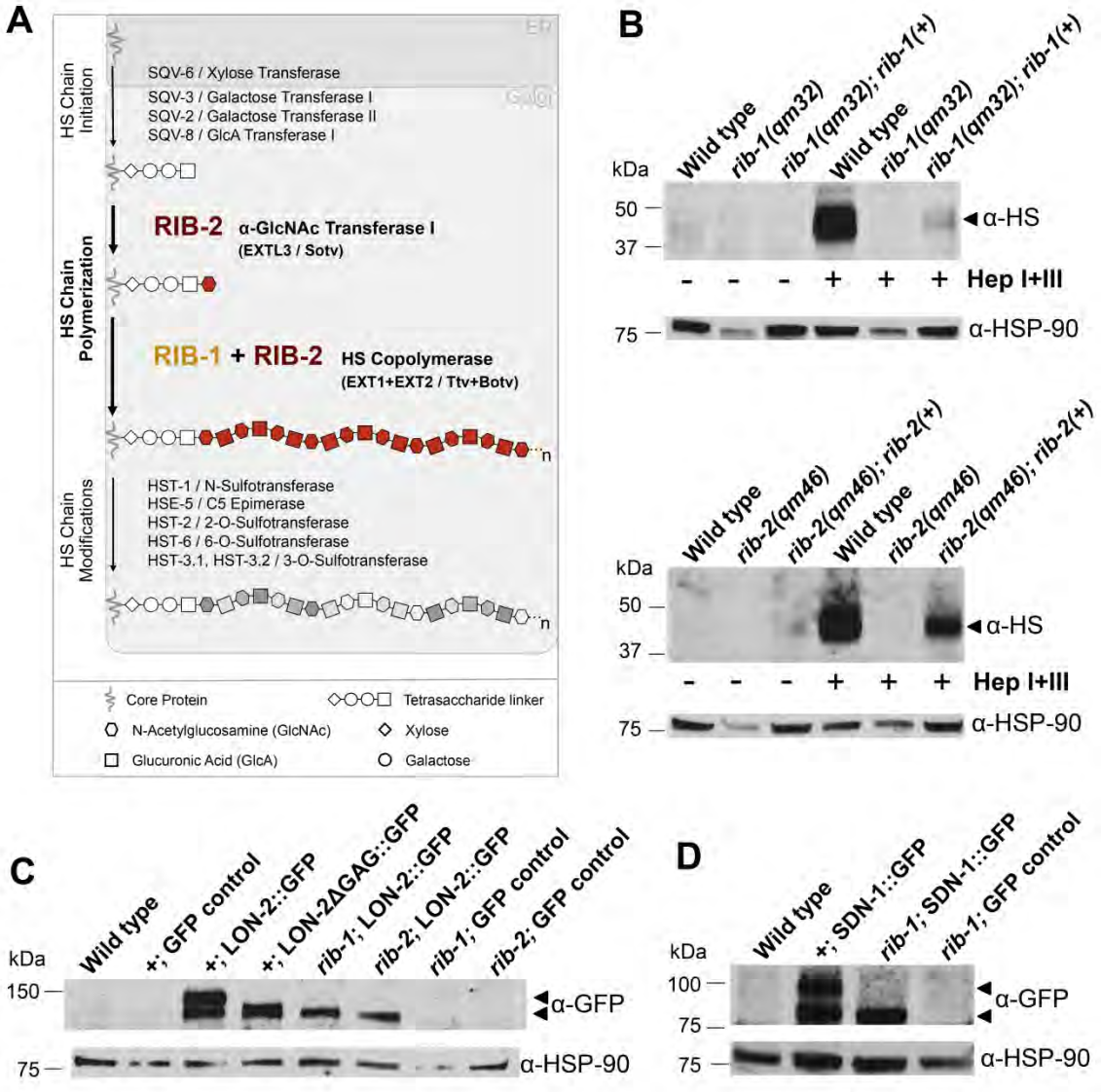
A
HS Chain Initiation
HS Chain Polymerization
HS Chain Modifications
ER
Golgi
SQV-6 / Xylose Transferase
SQV-3 / Galactose Transferase I
SQV-2 / Galactose Transferase II
SQV-8 / GlcA Transferase I
RIB-2 α-GlcNAc Transferase I
(EXTL3 / Sotv)
RIB-1 + RIB-2 HS Copolymerase
(EXT1+EXT2 / Ttv+Botv)
HST-1 / N-Sulfotransferase
HSE-5 / C5 Epimerase
HST-2 / 2-O-Sulfotransferase
HST-6 / 6-O-Sulfotransferase
HST-3.1, HST-3.2 / 3-O-Sulfotransferase
Core Protein
Tetrasaccharide linker
N-Acetylglucosamine (GlcNAc)
Xylose
Glucuronic Acid (GlcA)
Galactose
B
kDa
Wild type
rib-1(qm32)
rib-1(qm32); rib-1(+)
rib-1(qm32); rib-1(+)
50
37
α-HS
Hep I+III
75
α-HSP-90
rib-2(qm46)
rib-2(qm46); rib-2(+)
rib-2(qm46); rib-2(+)
C
Wild type
+; GFP control
+; LON-2::GFP
+; LON-2ΔGAG::GFP
rib-1; LON-2::GFP
rib-2; LON-2::GFP
rib-1; GFP control
rib-2; GFP control
150
α-GFP
α-HSP-90
D
Wild type
+; SDN-1::GFP
rib-1; SDN-1::GFP
rib-1; GFP control
100

**Fig. 2.5. Loss of function of the genes *rib-1* and *rib-2* impairs HS synthesis.**
**A.** Schematic representation of the biochemical synthesis of HS chains onto HSPG core proteins in the Golgi. HS chain synthesis starts by the addition of a tetrasaccharide linker (xylose-galactose-galactose-glucuronic acid) onto specific Ser residues on the core proteins to serve as a primer for HS polysaccharide growth. RIB-1 and RIB-2, homologous to the exostosin (EXT) proteins, catalyze the extension of HS chains, which are composed of repeating glucuronic acid (square) and N-acetylglucosamine (hexagon) residues. RIB-2, like mammalian EXTL3 and *Drosophila* Sotv, catalyzes the first step with the addition of the first N-acetylglucosamine onto the tetrasaccharide linker on HSPG core proteins. Then, RIB-1 and RIB-2 together, like mammalian EXT1 and EXT2, and *Drosophila* Ttv and Botv, function as a heterodimer to extend the HS chains.
**B.** Western blot analysis of HS chains in *rib-1(qm32)* mutants (top) and in *rib-2(qm46)* mutants (bottom). HS chains were detected with antibodies specific for HS epitope 3G10, which is detectable after cleavage by heparinase. For the three left lanes, protein extracts were not heparinase treated (control, indicated by "-"), and as expected no HS signal is detected. For the three right lanes, protein extracts were treated with heparinases I and III (Hep I+III, indicated by "+"). The HS signal is severely reduced in the *rib-1(qm32)* and the *rib-2(qm46)* mutants compared to wild type (N2), indicating that HS chain synthesis is strongly affected in *rib-1* and *rib-2* mutants. The HS signal is partially rescued in *rib-1* mutants expressing the transgene P*rib-1::rib-1(+)* and *rib-2* mutants expressing the transgene P*rib-2::rib-2(+)*. Therefore, HS biosynthesis is disrupted in the *rib-1(qm32)* and the *rib-2(qm46)* mutants, and their developmental and biochemical phenotypes can be rescued by reintroducing wild-type *rib-1(+)* and *rib-2(+)*, respectively.
**C**. Western blot analysis of LON-2::GFP in the *rib-1(qm32)* and *rib-2(qm46)* mutants. The anti-GFP antibody detects high molecular weight bands in extracts of transgenic animals expressing LON-2::GFP; as controls, these high molecular weight bands are absent in wild type N2 and in three GFP controls that do not express LON-2::GFP (*lqIs4*, *rib-1;lqIs4,* and *rib-2;lqIs4*). In transgenic animals expressing a mutant version of LON-2 lacking the three HS attachment sites (LON-2ΔGAG::GFP; Gumienny & Taneja-Bageshwar, 2012), the detected band is smaller than LON-2::GFP. Similarly, the band detected in extracts of the *rib-1* and *rib-2* mutants expressing LON-2::GFP is smaller, indicating that the HS chains of glypican/LON-2 are affected in *rib-1* and *rib-2* mutants.
**D.** Western blot analysis of SDN-1::GFP (Rhiner et al., 2005) in the *rib-1(qm32)* mutants. The anti-GFP antibody detects high molecular weight bands in extracts of transgenic animals expressing SDN-1::GFP; as controls, these high molecular weight bands are absent in the wild type N2 or the GFP control *rib-1; lqIs4*. In extracts of *rib-1* mutants expressing SDN-1::GFP, the band detected is smaller, indicating that the HS chains of syndecan/SDN-1 are affected in *rib-1* mutants.
α-HSP-90 was used as a loading control.

generations and the extrachromosomal array carrying the transgene is lost during cell divisions. Nevertheless, our results indicate that the alleles of *rib-1(qm32)* and *rib-2(qm46)* strongly disrupt HS chain synthesis.

Having examined the impact of *rib-1* or *rib-2* function on global HS levels, we tested how two distinct HSPGs, namely LON-2/glypican and SDN-1/syndecan, are affected in *rib-1(qm32)* and *rib-2(qm46)* single mutants. To detect LON-2/glypican, we expressed LON-2 tagged with GFP (using transgene LON-2::GFP, (Gumienny et al 2007)) in wild type (N2), *rib-1(qm32)*, and *rib-2(qm46)* mutant backgrounds, and carried out western blot analysis with anti-GFP antibodies. Whereas two high molecular weight bands corresponding to LON-2::GFP were detected in wild-type lysates, only one of the bands is detected in lysates of *rib-1* and *rib-2* mutants (**Fig. 2.5C**), indicating that HS synthesis onto LON-2/glypican is affected by the loss of function of *rib-1* or *rib-2*. In support of this, we found that wild-type worms expressing a mutant version of LON-2 in which the HS attachment sites are mutated (LON-2ΔGAG::GFP, (Taneja-Bageshwar & Gumienny 2012)) also produced only one high molecular weight band similar to the migration of LON-2::GFP in the *rib-1* and *rib-2* mutants (**Fig. 2.5C**). To detect the HSPG SDN-1/syndecan, we expressed SDN-1/syndecan tagged with GFP (SDN-1::GFP, (Rhiner et al 2005)) in wild-type (N2) and *rib-1* mutant worms, and probed for GFP in lysates of these worms. In wild-type lysates, we detected two high molecular weight bands corresponding to SDN-

1::GFP, but detected a single band in lysates of *rib-1* mutants (**Fig. 2.5D**), indicating that loss of *rib-1* impairs HS synthesis onto SDN-1/syndecan. Our results show that the mutants *rib-1(qm32)* and *rib-2(qm46)* drastically reduce the HS content and affect the biosynthesis of HSPGs.

**The HS copolymerase is dynamically expressed during development**

To gain insight into the roles of HSPGs during development, we determined the expression pattern of the HS copolymerase. We constructed expression reporters for the genes *rib-1* and *rib-2*. First, we designed a transcriptional fusion (P*rib-1::gfp*) between the upstream regulatory region of *rib-1* and the green fluorescent protein gene (*gfp*). Since *rib-1* is the second gene in an operon of two genes (Blumenthal et al 2002), we included the region upstream of the first gene in the operon, as well as the intergenic region of the operon that lies immediately upstream of *rib-1* (see Materials and Methods). Second, we constructed a translational fusion (P*rib-1::rib-1::venus*) using the same upstream regulatory region as for P*rib-1::gfp* (see Materials and Methods) and fusing the coding region of *rib-1* with the gene *venus* (a translational fusion of *rib-1* with *gfp* gave no detectable expression; *venus* encodes a variant of *gfp* that fluoresces in acidic cellular environments (Nagai et al 2002)). We generated at least five transgenic lines for each of these two *rib-1* reporters and examined transgenic animals by fluorescence microscopy. We observed that GFP fills the cytoplasm of cells expressing the transcriptional fusion P*rib-1::gfp*, as expected, and that VENUS

has a punctate cytoplasmic pattern in cells expressing the translational fusion P*rib-1::rib-1::venus*, consistent with the HS copolymerase being localized to the Golgi apparatus (**Fig. 2.6A**). Moreover, we found that both the transcriptional and the translational fusions have a very similar spatial and temporal expression pattern during development: expression was visible in neurons, some hypodermal cells, pharynx, and muscles of the digestive system and reproductive tissues (**Fig. 2.6A**). Importantly, we found that the translational fusion P*rib-1::rib-1::venus* is functional, as it fully rescued the defective locomotion, egg-laying, morphology, and axon guidance of *rib-1(qm32)* mutants, indicating that the observed expression pattern of the translational fusion, and thus also of the transcriptional fusion, is functionally relevant and largely reflects the sites of endogenous expression of the gene *rib-1*.

Since the transcriptional and translational fusions for *rib-1* have similar expression patterns, and P*rib-1::gfp* expresses at higher levels and readily allows the identification of expressing cells, we characterized the expression pattern of P*rib-1::gfp* in more detail. One salient feature of the expression pattern of *rib-1* is that it is very dynamic in hypodermal cells during development. During embryogenesis, P*rib-1::gfp* was detected along the entire layer of hypodermoblasts that surrounds the gastrulating embryo at about 200 minutes after fertilization (at this stage, numerous more interiorly located cells, likely mesodermal cells, also expressed P*rib-1::gfp*). By the early comma stage of

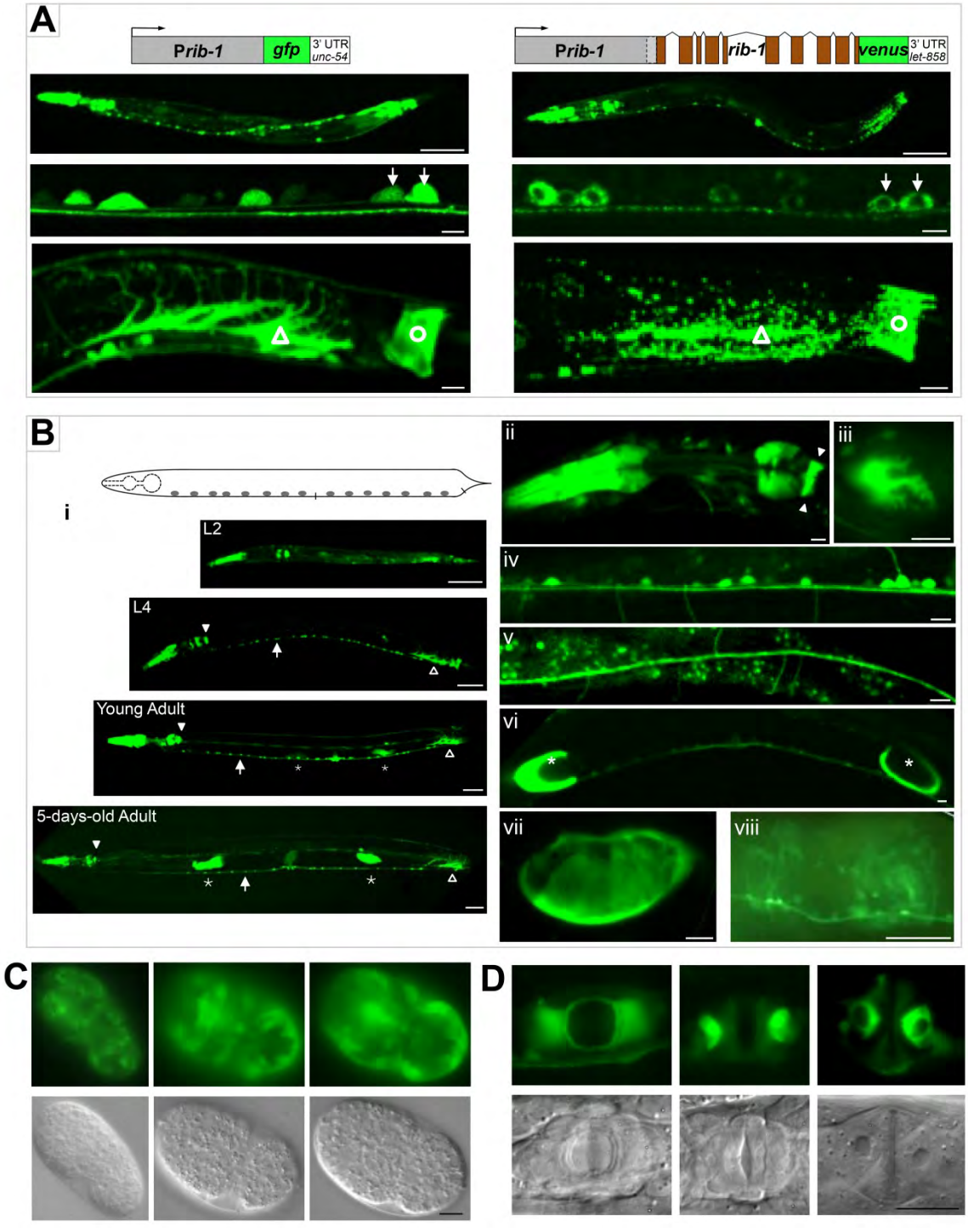
A
Prib-1
gfp
3' UTR unc-54
Prib-1
rib-1
venus
3' UTR let-858
B
i
L2
L4
Young Adult
5-days-old Adult
ii
iii
iv
v
vi
vii
viii
C
D

**Fig. 2.6. Dynamic expression of the HS copolymerase during development.**
**A.** A transcriptional reporter and a functional translational reporter for the gene *rib-1*, P*rib-1::gfp* and P*rib*-1::*rib-1*::*venus*, respectively, display similar expression patterns. Expression of *rib-1* is observed in numerous cell types, including in the pharynx, hypodermal cells, neurons (arrows), the enteric muscle (triangle) and the anal depressor (circle). The RIB-1::Venus signal is punctate, consistent with a Golgi localization. Scale bars: 50 µm in top panels of entire worms, and 5 µm in lower panels.
**B.** Larval and adult expression of *rib-1*. (**i**) Throughout larval and adult stages, the expression of P*rib-1::gfp* is observed in the pharynx, including in the pharyngeal-intestinal valve (**ii**, closed arrowhead) and muscles of the anterior and terminal pharyngeal bulbs (**iii**, pharyngeal muscle pm6); in the enteric muscle (open arrowhead, see **a**); in the ventral nerve cord (arrows, **iv**, see **a**); and the dorsal nerve cord (**v**). P*rib-1::gfp* expression in spermathecae (asterisks, **vi**, seen enlarged by an oocyte in **vii**) and in uterine muscles (**viii**) is first detected in adults, initially at very low levels, and becoming increasingly stronger as the reproductive phase progresses. Scale bars, 50 µm in panels of entire worms, and 5 µm in the rest of the panels.
**C**. Embryonic expression of *rib-1*. Views of comma stage embryos in GFP epifluorescence and DIC. The transcriptional reporter P*rib-1::gfp* is predominantly expressed in lateral and ventral epidermal cells that undergo major morphogenetic movements during dorsal intercalation and ventral enclosure of the embryo. Scale bar, 5 µm.
**D.** *rib-1* is expressed during vulva development. Views of the developing vulva in fourth larval stage animals by GFP and DIC epifluorescence. P*rib-1::gfp* is expressed in epidermal cells of the developing vulva at a time when these cells undergo major rearrangements. Scale bar, 10 µm.

embryogenesis, P*rib-1::gfp* was expressed at high levels in hypodermal cells of the elongating embryo (**Fig. 2.6C**), including in hypodermal cells that extend ventrally during ventral closure and in the two rows of dorsal hypodermal cells undergoing dorsal intercalation. Subsequent to these embryonic morphogenetic events, expression of P*rib-1::gfp* in body wall hypodermal cells was no longer visible during larval and adult stages, except for seam cells undergoing fusion during larval development. During vulva development, however, hypodermal cells that compose the developing vulva, including the utse, strongly expressed P*rib-1::gfp* (**Fig. 2.6D**). At first, a very low expression level was detected in vulval cells

of late L3 larvae, then expression became strong in these cells in L4 larvae and young adults that had just molted, and finally expression ended in adults. These dynamic expression patterns in cells undergoing dramatic changes during morphogenesis suggest that HSPGs play important and acute roles during development.

The nervous and digestive systems express P*rib-1::gfp* stably and continuously from embryogenesis into larval stages and throughout adulthood. Strong and sustained expression was seen in motorneurons, interneurons, sensory neurons (including AVM), neurons in the head and tail ganglia, with the GFP signal filling axons running along the ventral and dorsal nerve cords, the commissures, and sublaterals. Neurons of the ventral nerve cord and of the head ganglia were observed expressing P*rib-1::gfp* already in 1.5-, 2-, and 3-fold embryos, and expression persisted well into adulthood (**Fig. 2.6A,B**). Strong expression of P*rib-1::gfp* was also observed in the pharynx from the 2-fold stage of embryogenesis onwards and remained strong even in adults (procorpus, metacorpus, terminal bulb, grinder, and pharyngeal-intestinal valve). The anal depressor, the anal sphincter, and the two enteric muscles also strongly expressed P*rib-1::gfp* throughout life. The continued expression of *rib-1* in the nervous and digestive systems indicates that HSPGs not only play developmental roles in these cell types, but also have post-developmental roles in a variety of cellular contexts.

Another set of cells initiated expression of *rib-1* only during the adult reproductive phase: P*rib-1::gfp* first became detectable in the spermathecae in young adults and accumulated at very high levels in adults during the peak of fertilization and embryo production (**Fig. 2.6B**). Also, the uterine muscles expressed P*rib-1::gfp* only in reproducing adults and the signal became strongest around day three of adulthood (**Fig. 2.6B**). The observation that the HS copolymerase is expressed in cells of reproductive tissues coinciding with the time of active reproduction further indicates that the synthesis of HSPGs is required in diverse post-developmental contexts.

We also constructed transcriptional and translational reporters for *rib*-2, the second gene encoding the HS copolymerase. Despite numerous attempts, the detected expression level was extremely weak in transgenic worms carrying these constructs. We could nonetheless observe diffuse P*rib-2::gfp* expression in comma-stage embryos, as well as in neurons, the pharynx, seam cells, and the developing vulva at later developmental stages. Thus, the expression pattern of *rib-2* appears to overlap with that of *rib-1*, consistent with the notion that these genes encode proteins that function together as the HS copolymerase complex.

**Synthesis of HSPGs in multiple cell types contributes to axon guidance**

A prominent site of expression of the HS copolymerase is the nervous system, including at times of axon migrations during embryonic and larval development

(**Fig. 2.6**), and disruption of the HS copolymerase leads to numerous defects of axon guidance (**Fig. 2.1**). To determine which cells produce HSPGs required for axon guidance, we provided wild-type copies of *rib-1(+)* in subsets of cells to *rib-1* mutants and assessed whether the axon guidance defects of the PVQ neurons could be rescued. The axon of PVQ extends along the ventral nerve cord during embryogenesis, following the path of other axons, and is in proximity with the hypodermis and body wall muscles. We built several constructs to express *rib-1(+)* in neurons including PVQ (using the heterologous promoter P*rgef-1*), in hypodermis (using the heterologous promoter P*dpy-7*), or in body wall muscles (using the heterologous promoter P*myo-3*). We generated transgenic *rib-1(qm32)* worms expressing *rib-1(+)* in these tissues and analyzed PVQ axon guidance. As a control, expression of *rib-1(+)* under its own promoter completely rescued the guidance defects of the PVQ axon (**Fig. 2.7A**). Targeted expression of *rib-1(+)* only in neurons, only in hypodermis, or only in body wall muscles did not rescue the PVQ axon guidance defects of *rib-1* mutants. However, co-expression of *rib-1(+)* in the hypodermis, neurons, and body wall muscles led to rescue of the PVQ guidance defects (**Fig. 2.7A**), suggesting that HSPGs from distinct cell types together contribute to properly guide the PVQ axon. The rescue of the PVQ axon was strong but incomplete, possibly due to the expression level or timing of *rib-1* under these heterologous promoters being inappropriate. Nonetheless, expressing *rib-1* simultaneously in these three tissues significantly rescued the

PVQ defects, indicating a functional requirement for HSPGs in several cell types to regulate the guidance of the PVQ axon.

We next analyzed the spatial requirements for HS biosynthesis in the context of another migrating axon, that of the mechanosensory neuron AVM. During the first larval stage, the AVM axon pioneers its own ventral migration through a basement membrane along the body wall, sandwiched between the hypodermis and the body wall muscles. We expressed *rib-1(+)* in the hypodermis (using the heterologous promoter P*dpy-7*), in body wall muscles (using the heterologous promoter P*myo-3*), or in the neuron AVM itself (using the heterologous promoter P*mec-7)* in *rib-1(qm32)* mutants, and analyzed AVM axon guidance. As a control, expression of *rib-1(+)* under its own promoter completely rescued the guidance defects of the AVM axon (**Fig. 2.7B**). We found that the AVM axon guidance defects of *rib-1* mutants were rescued by expression of *rib-1(+)* in the neuron AVM itself, or by expression of *rib-1(+)* from the hypodermis (**Fig. 2.7B**). These results suggest that HSPGs produced both in the AVM neuron itself and in the hypodermis crucially impact the guidance of the axon of AVM. Taken together, our results support the notion that HSPGs synthesized in distinct cell types contribute to guided axonal migrations during development.

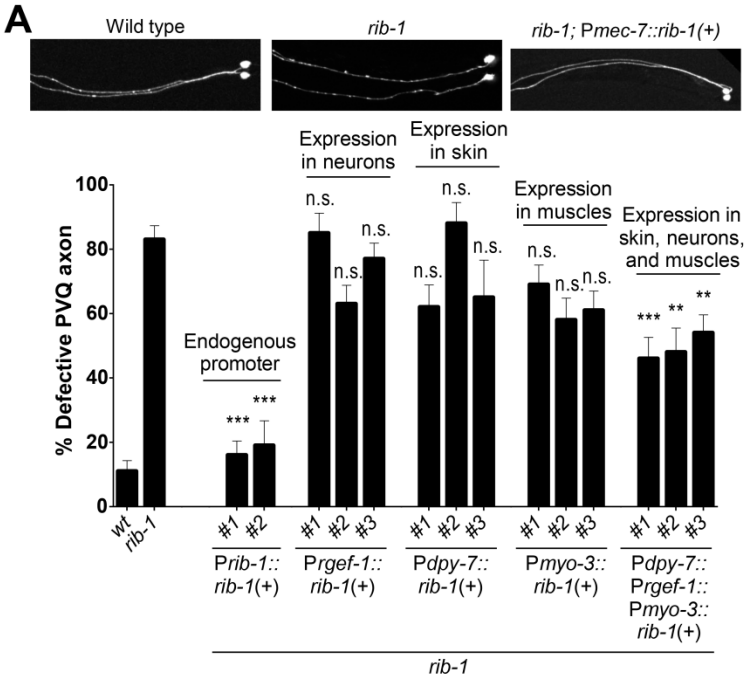
A
Wild type
rib-1
rib-1; Pmec-7::rib-1(+)
% Defective PVQ axon
Endogenous promoter
Expression in neurons
Expression in skin
Expression in muscles
Expression in skin, neurons, and muscles
n.s.
***
**
wt
rib-1
#1
#2
#3
Prib-1:: rib-1(+)
Prgef-1:: rib-1(+)
Pdpy-7:: rib-1(+)
Pmyo-3:: rib-1(+)
Pdpy-7:: Prgef-1:: Pmyo-3:: rib-1(+)
rib-1

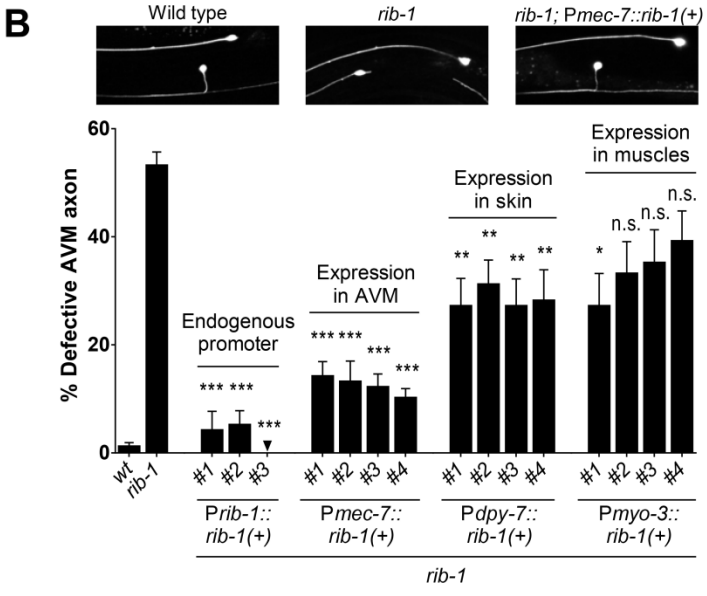
B
Wild type
rib-1
rib-1; Pmec-7::rib-1(+)
% Defective AVM axon
Endogenous promoter
Expression in AVM
Expression in skin
Expression in muscles
n.s.
*
**
***
wt
rib-1
#1
#2
#3
#4
Prib-1:: rib-1(+)
Pmec-7:: rib-1(+)
Pdpy-7:: rib-1(+)
Pmyo-3:: rib-1(+)
rib-1

**Fig. 2.7. HS chain synthesis in multiple cell types contributes to axon guidance.**
**A.** The defects in the guidance of the PVQ axons in *rib-1(qm32)* mutants are rescued by the combined expression of *rib-1*(+) in the hypodermis (under the heterologous promoter P*dpy-7)*, neurons (under the heterologous promoter P*rgef-1)*, and muscles (under the heterologous promoter P*myo-3)*.
**B**. The defects in the guidance of the AVM axon in *rib-1(qm32)* mutants are rescued by expression of *rib-1(+)* in the migrating neuron itself (under the heterologous promoter P*mec-7*) or by expression in the hypodermis (under the control of the heterologous promoter P*dpy-7*). Error bars are standard error of the proportion. Asterisks denote significant difference: *** $P \leq 0.001$, ** $P \leq 0.01$, * $P \leq 0.05$ (z-tests, P values were corrected by multiplying by the number of comparisons). ns, not significant.

## HS chain synthesis is required for *unc-6*/netrin- and *slt-1*/Slit-mediated axon guidance

To gain understanding of the role of HSPGs during neural development, we analyzed the requirements of HS chain synthesis for *unc-6*/netrin- or *slt-1*/Slit-mediated axon guidance. For this, we focused on the guidance of the axon AVM **(Fig. 2.8A)**, which has been extensively studied and is known to be guided by two complementary and highly conserved guidance pathways: attraction towards ventral UNC-6/netrin through its receptor UNC-40/DCC and repulsion away from dorsal SLT-1/Slit through its receptor SAX-3/Robo (**Fig. 2.8B**) (Chan et al 1996, Hao et al 2001, Hedgecock et al 1990, Hedgecock et al 1987, Ishii et al 1992, Leung-Hagesteijn et al 1992, Zallen et al 1998). *rib-1* and *rib-2* mutants are defective in AVM axon guidance (**Fig. 2.1C**), suggesting the loss of HS chain synthesis may be affecting *unc-6*/netrin signaling, *slt-1*/Slit signaling, or both.

Disrupting HS chain synthesis is expected to impact all HSPGs. Therefore, if the

HS chains contribute significantly to axon guidance by both signaling pathways, then the defects of both *unc-6*/netrin and *slt-1*/Slit single mutants would be enhanced by loss of function of *rib-1* or *rib-2*. We constructed several double mutant strains and indeed found that the two double mutants *rib-1;unc-6* and *rib-2;unc-6*, as well as the two double mutants *rib-1;slt-1* and *rib-2;slt-1*, have stronger AVM axon guidance defects than the respective single mutants (**Fig. 2.8B**). Mutation of *rib-1* or *rib-2* also enhanced AVM guidance defects in P*myo-3::slt-1* animals (Yu et al 2002) in which *slt-1* is misexpressed from all body wall muscles (**Fig. 2.8B**). Given that the two key forces guiding the AVM axon are *unc-6*/netrin and *slt-1*/Slit, our observations support the model that HS chain synthesis plays a critical role in both *unc-6*/netrin- and *slt-1*/Slit- guidance pathways.

To directly test the functional importance of the HS chain synthesis on *unc-6*/netrin signaling, we used a netrin-dependent gain-of-function approach in the PVM axon. Similar to AVM, the axon of the neuron PVM is attracted ventrally towards secreted UNC-6/netrin via the UNC-40/DCC receptor. However, misexpression of a second receptor for UNC-6/netrin that mediates repulsive guidance, namely UNC-5/UNC5, using the transgene P*mec-7::unc-5* ((Hamelin et al 1993), **Fig. 2.8C**), results in the abnormal extension of the PVM axon to the dorsal side of the animal that is *unc-6*/netrin- and *unc-40*/DCC-dependent.

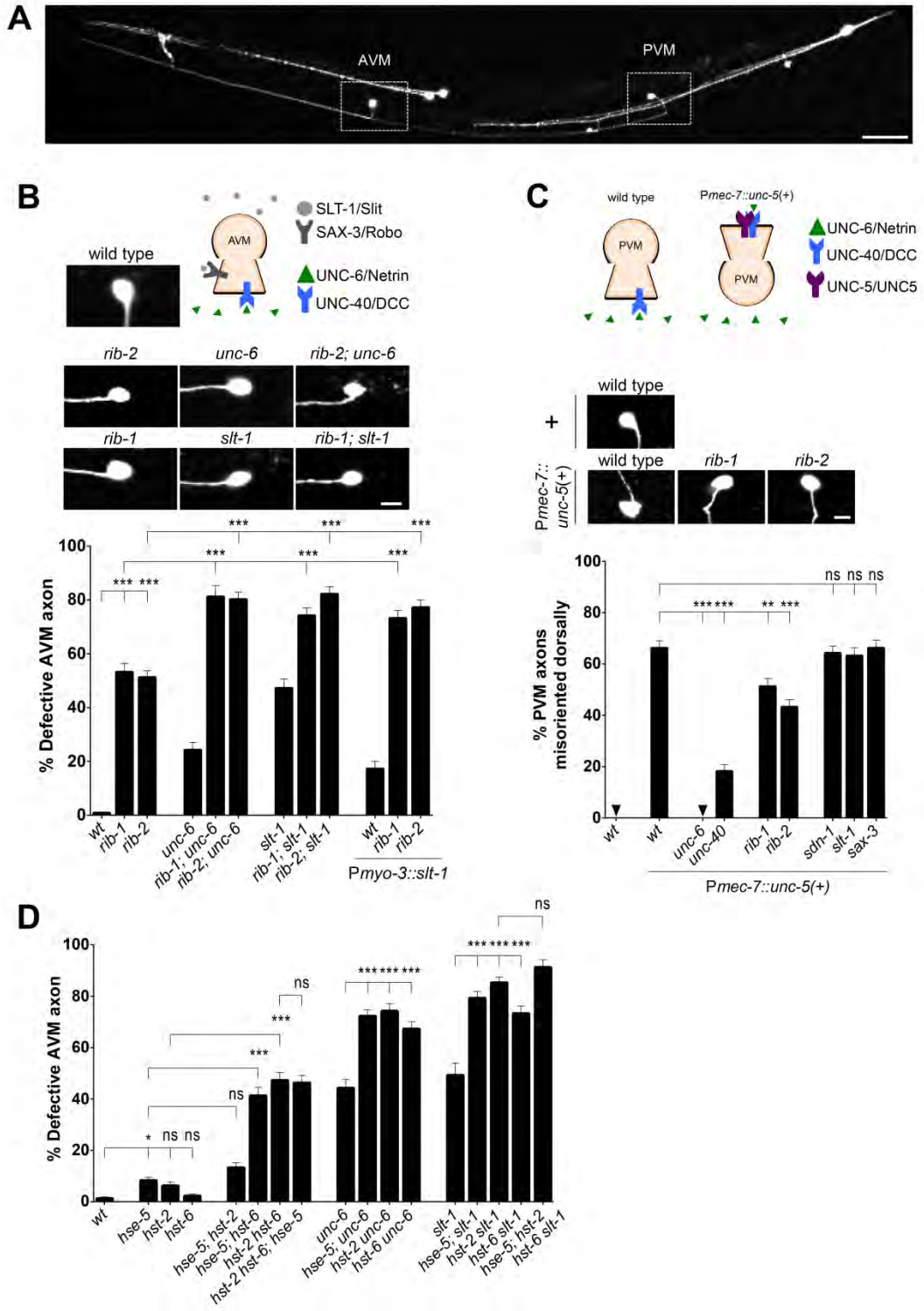
A
AVM
PVM
B
wild type
SLT-1/Slit
SAX-3/Robo
UNC-6/Netrin
UNC-40/DCC
rib-2
unc-6
rib-2; unc-6
rib-1
slt-1
rib-1; slt-1
% Defective AVM axon
wt
rib-1
rib-2
unc-6
rib-1; unc-6
rib-2; unc-6
slt-1
rib-1; slt-1
rib-2; slt-1
Pmyo-3::slt-1
C
wild type
Pmec-7::unc-5(+)
UNC-6/Netrin
UNC-40/DCC
UNC-5/UNC5
% PVM axons misoriented dorsally
unc-40
sdn-1
sax-3
Pmec-7::unc-5(+)
D
% Defective AVM axon
hse-5
hst-2
hst-6
hse-5; hst-2
hse-5; hst-6
hst-2 hst-6
hst-2 hst-6; hse-5
unc-6
hse-5; unc-6
hst-2 unc-6
hst-6 unc-6
slt-1
hse-5; slt-1
hst-2 slt-1
hst-6 slt-1
hse-5; hst-2
hst-6 slt-1
ns

**Fig. 2.8. *unc-6*/netrin and *slt-1*/Slit signaling pathways require functional HS chains to guide axons during development.**
**A.** We visualized the morphology of the AVM and PVM axons using the transgene P*mec-4::gfp*. Scale bar, 50 µm.
**B**. During the first larval stage of wild-type *C. elegans*, the pioneer neuron AVM extends ventrally along the body wall until it reaches the ventral nerve cord. Its migration results from the combined attractive response to UNC-6/netrin (secreted at the ventral midline) via the UNC-40/DCC receptor and the repulsive response to SLT-1/Slit (secreted by the dorsal muscles) via its SAX-3/Robo receptor. Mutations *rib-1(qm32)* or *rib-2(qm46)* enhance the AVM guidance defects of animals where *slt-1*/Slit signaling is disrupted, either in mutants for *slt-1*/Slit or in animals misexpressing *slt-1* in all body wall muscles (using a P*myo-3::slt-1* transgene). Mutation of *rib-1* or *rib-2* also enhances the AVM axon guidance defects of *unc-6*/netrin mutants. That AVM guidance defects of mutants in both key guidance pathways, *slt-1* and *unc-6*, are enhanced by loss of *rib-1* or *rib-2* suggests that HS chains function in both the *slt-1*/Slit- and the *unc-6*/netrin-mediated pathways. Scale bar, 5 µm.
**C.** *unc-6*/netrin signaling via the *unc-5*/UNC5 receptor requires functional HS chains. The pioneer axon of PVM normally migrates ventrally; however, upon misexpression of *unc-5*/UNC5 in PVM using the transgene P*mec-7::unc-5*, the axon of PVM projects dorsally in an *unc-6*/netrin- and *unc-40*/DCC-dependent manner. Loss of function of *rib-1* or *rib-2* partially suppresses this forced dorsal migration, indicating that *unc-6*/netrin signaling depends on functional HS chains. Scale bar, 5 µm.
**D.** HS modifying enzymes function in the *unc-6*/netrin- and *slt-1*/Slit mediated-guidance of the AVM axon. Loss of HS modifying enzymes including the epimerase *hse-5* and the sulfotransferases *hst-2* and *hst-6* enhance the AVM guidance defects of *unc-6*/netrin and *slt-1*/Slit mutants, indicating that proper modifications of the heparan sulfate chains are important in guiding AVM through the *unc-6*/netrin and *slt-1*/Slit pathways.
Error bars are standard error of the proportion. Asterisks denote significant difference: *** $P \leq 0.001$, ** $P \leq 0.01$, * $P \leq 0.05$ (z-tests, P values were corrected by multiplying by the number of comparisons). ns, not significant

Dorsal extension of the PVM axon never occurs in the wild type or mutants for the *unc-6*/netrin or *slt-1*/Slit signaling pathways (**Fig. 2.8C**). The AVM axon also extends dorsally upon misexpression of *unc-5*; however the axons of AVM and neighboring ALMR cannot be reliably distinguished in P*mec-7::unc-5* transgenic animals. We built strains mutant for *rib-1* or *rib-2* that carry the transgene P*mec-7::unc-5* (Hamelin et al 1993) to misexpress *unc-5* in PVM. If loss of *rib-1* and *rib-2* functionally disrupts *unc-6*/netrin signaling, we would expect to see a decrease

in the *unc-5*-mediated dorsal migration of PVM. We found that loss of function of *rib-1* and *rib-2* significantly suppressed the *unc-6/*netrin-dependent *unc-5*-mediated dorsal migration of PVM (**Fig. 2.8C**), indicating that *unc-6*/netrin signaling requires HS chains. This suppression of the dorsal extension of the PVM axon by mutations in *rib-1* and *rib-2* is specific as loss of function of other genes such as *sdn-1*/syndecan, *slt-1*/Slit and *sax-3*/Robo, could not suppress these abnormal dorsal extensions (**Fig. 2.8C**). Taken together, our findings suggest a requirement for HS chains synthesis in regulating *unc-6*/netrin- and *slt-1*/Slit-mediated axon guidance.

**Modifications of the HS chains are required for *unc-6/*netrin and *slt-1/*Slit mediated axon guidance**

Our results indicate that the biosynthesis of HS chains onto core proteins is required for axon guidance mediated by *unc-6/*netrin and *slt-1*/Slit signaling. Once synthesized by the HS copolymerase, HS chains become extensively modified by epimerases and sulfotransferases (reviewed in (Bülow & Hobert 2006)). In *C. elegans*, key modifying enzymes have been studied, including the glucuronyl C5-epimerase encoded by the gene *hse-5*, the 2O-sulfotransferase encoded by the gene *hst-2*, and the 6O-sulfotransferase encoded by the gene *hst-6* (Bülow et al 2002, Bülow & Hobert 2004, Bulow et al 2008, Kinnunen et al 2005, Townley & Bulow 2011). These HS modifying enzymes are required for axon guidance as mutations disrupting their function impair axon guidance

(Bülow et al 2002, Bülow & Hobert 2004, Bülow & Hobert 2006, Bulow et al 2008, Kinnunen et al 2005), but their specific roles in *unc-6/*netrin- and *slt-1/*Slit-mediated guidance of AVM is unclear. To determine the functional importance of specific HS modifications in *unc-6/*netrin- and *slt-1/*Slit-mediated AVM axon guidance, we first analyzed single, double, and triple mutants of the genes coding for the HS modifying enzymes *hse-5*, *hst-2* and *hst-6*, and found that loss of each single modifying enzyme led to minimal AVM axon guidance defects (**Fig. 2.8D**). However, the double mutants *hse-5; hst-6* and *hst-2 hst-6*, in which the 6O-sulfotransferase and either the 2O-sulfotransferase or the C5-epimerase are mutant, display significant AVM guidance defects (**Fig. 2.8D**). The defects of these two double mutants are not further enhanced by the loss of the third key HS modifying enzyme in the triple mutant *hse-5; hst-2 hst-6* (**Fig. 2.8D**). These observations indicate some level of compensation between the HS chain modifying enzymes and suggest that combinations of modifications on the HS chains impact *unc-6/*netrin- and *slt-1/*Slit-mediated AVM axon guidance. Next, we analyzed AVM ventral axon guidance in double mutant animals lacking one of the HS modifying enzymes encoded by *hse-5*, *hst-2*, and *hst*-6 as well as lacking *unc-6/*netrin or *slt-1/*Slit. We found that loss of function of any of the HS modifying enzymes *hse-5, hst-2,* or *hst-6* enhanced the AVM guidance defects of null mutants for *unc-6*/netrin. Similarly, loss of function of any of the HS modifying enzymes *hse-5, hst-2,* or *hst-6* enhanced the AVM guidance defects of presumptive null mutants for *slt*-1/Slit (**Fig. 2.8D**, ((Hao et al 2001)). These

results suggest that the sulfations and epimerizations of HS chains carried out by the enzymes encoded by *hse-5*, *hst-2*, or *hst-6* are important for both *unc-6/*netrin- and *slt-1/*Slit-mediated signaling in AVM axon guidance. Thus, not only is the polymerization of the HS chains on core proteins required for axon guidance during nervous system development, but also the subsequent modifications, as has been observed in other neurodevelopmental contexts (Bülow & Hobert 2006). These observations confirm the importance of HSPGs for neural development.

## DISCUSSION

Animal development and tissue homeostasis rely on the regulation of molecules that instruct cellular responses. HSPGs regulate morphogens and guidance cues in the extracellular environment, but their mechanisms of action are still not understood, including how several HSPGs may together coordinate cellular responses. Here, we identify previously unavailable viable hypomorphic mutations for the genes *rib-1* and *rib-2*, which encode the HS copolymerase of *C. elegans*. These mutations severely reduce HS biosynthesis and disrupt morphogenesis and nervous system development. We show that the action of HSPGs from various tissues contributes to the guidance of cellular migrations during development.

**Viable mutations of the HS copolymerase in *C. elegans***

The human EXT genes, namely EXT1, EXT2, EXTL1, EXTL2 and EXTL3, are members of the hereditary multiple exostoses gene family of tumor suppressors and are glycosyltransferases required for the biosynthesis of HS (reviewed in (Busse-Wicher et al 2014, Sugahara & Kitagawa 2000)). Only two genes in the *C. elegans* genome, *rib-1* and *rib*-2, have recognizable homology to the mammalian EXT genes. Together, the RIB-1 and RIB-2 proteins form a functional heterodimer that catalyzes the elongation of HS chains. RIB-2 protein has alpha1,4-N-acetylglucosaminyltransferase activity involved in both the initiation and elongation steps of heparan sulfate biosynthesis, as it displays GlcNAc transferase I and II activities (Kitagawa et al 2001, Morio et al 2003), and RIB-1 and RIB-2 together have glycosyltransferase activity and catalyze the polymerization of HS chains (Kitagawa et al 2007).

Through a forward genetic screen for mutants defective in nervous system development, we have identified viable partial loss-of-function mutations of the HS copolymerase in *C. elegans*. Each of the single mutants, *rib-1(qm32)* and *rib-2(qm46)*, displays severe mutant phenotypes, indicating that the genes *rib-1* and *rib-2* are not redundant, as their encoded products cannot substitute for each other, consistent with their specific biochemical roles in HS chain initiation and elongation. The point mutations *rib-1(qm32)* and *rib-2(qm46)* profoundly disrupt the function of these genes; we find that the global HS levels are severely

reduced in the viable single mutants, and that high molecular species of glypican/LON-2 and syndecan/SDN-1 are absent in homozygous populations of these viable mutants. Our results indicate that as predicted by sequence homology, the functions of RIB-1 and RIB-2 are indeed required for HS biosynthesis in *C. elegans*, consistent with the biochemical demonstration of the enzymatic activities of RIB-1 and RIB-2 and the observation that HS levels are decreased in maternally rescued null lethal mutants of *rib-1* and *rib-2* (Kitagawa et al 2007, Morio et al 2003).

Despite the severe reduction in HSPGs in the *rib-1(qm32)* and *rib-2(qm46)* single mutants, it appears that residual HS copolymerase activity allows for viability. Approximately a third of the *rib-1(qm32)* and *rib-2(qm46)* animals are able to complete development and become fertile adults. In contrast, previously isolated deletion alleles that completely abolish the function of *rib-1*or *rib-2* are embryonic lethal (Franks et al 2006, Kitagawa et al 2007, Morio et al 2003), which precluded their detailed analysis. Therefore, *rib-1(qm32)* and *rib-2(qm46)* are hypomorphic mutations and it is possible that HS copolymerase dimers composed of one mutant protein and one wild-type protein in the single mutants (e.g. mutant RIB-1 and wild-type RIB-2) may be stabilized by the presence of one normal protein in the complex. Consistent with this notion, simultaneous disruption of both the *rib-1* and *rib-2* genes in double hypomorphic mutants *rib-1(qm32); rib-2(qm46)*, drastically impairs HS copolymerase and leads to early embryonic lethality.

In support of the possibility that in single mutants the HS copolymerase may be stabilized by one of the two subunits being wild type, the hypomorphic mutants *rib-1(qm32)* or *rib-2(qm46)* are completely maternally rescued (Hekimi et al 1995), whereas null mutants are incompletely maternally rescued (Kitagawa et al 2007, Morio et al 2003). *rib-1(qm32)* or *rib-2(qm46)* single hypomorphic mutant animals of the first homozygous mutant generation ($m^{+/-}$ $z^{-/-}$) are phenotypically indistinguishable from the wild type throughout life when their mother was heterozygous for the mutation (Hekimi et al 1995). In contrast, for *rib-1* or *rib-2* null alleles, animals of the first homozygous mutant generation ($m^{+/-}$ $z^{-/-}$) are maternally rescued only to the extent that the animals survive and become adults, but display abnormal locomotion and egg laying, becoming filled with dead embryos of the next homozygous generation (Kitagawa et al 2007, Morio et al 2003). The maternal rescue effect is also incomplete in the double hypomorphic *rib-1(qm32); rib-2(qm46)* mutants, as the first generation of double homozygous animals ($m^{+/-}$ $z^{-/-}$) are severely egg-laying defective and become bloated with dead embryos. Thus, it appears that maternal product deposited in the oocyte is sufficient to support HS copolymerase activity and allow development to unfold normally in single *rib-1(qm32)* and *rib-2(qm46)* hypomorphic mutants, but insufficient for single null mutants. These observations highlight the importance of HS copolymerase activity, and therefore HSPGs, for the earlier stages of development as well as later in life. These observations

indicate that *rib-1(qm32)* and *rib-2(qm46)*, while severe loss-of-function alleles, are hypomorphic, and their viability offers the opportunity to study the functional requirements of HSPGs throughout development.

RIB-1 and RIB-2 are not expected to affect the biosynthesis of glycosaminoglycans other than HS. In *C. elegans*, both heparan sulfate and chondroitin sulfate (CS) have been detected (not hyaluronate, nor dermatan sulfate; (Toyoda et al 2000, Yamada et al 1999)). Like HS, CS chains are covalently linked to the polypeptide at serine residues through a tetrasaccharide linker. However, the initiation and elongation of the chains of HS and CS are carried out by different enzymes. In the case of CS, a polymer of alternating GlcA (glucuronic acid) and N-acetyl galactosamine (GalNAc) residues is synthesized, which is catalyzed by a bifunctional glycosyltransferase encoded by the *sqv-5* gene (Hwang et al 2003b). Furthermore, enzymes transporting and synthesizing precursors of HS and CS include a UDP-glucose dehydrogenase, UDP-glucuronic acid decarboxylase, and nucleotide-sugar transporter, encoded by the genes *sqv-4, sqv-1* and *sqv-7*, respectively (Hwang & Horvitz 2002a, Hwang & Horvitz 2002b). Mutations in these genes cause more severe phenotypes than mutations of *rib-1* and *rib-2* because synthesis of both types of proteoglycans, HSPGs and chondroitin sulfate proteoglycans (CSPGs), are affected. Interestingly, mutations in these *sqv* genes all display maternal effect, consistent with proteoglycans playing crucial roles from the earliest stages of development.

Mutations in other proteoglycan biosynthesis enzymes also display maternal effect (Hwang et al 2003a, Mizuguchi et al 2003). In contrast, null mutations of *hst-1, hst-6,* and *hse-5* that affect specific modifications of the HS chains (epimerizations, sulfations) are less severe and viable (Bülow & Hobert 2004), as they affect later steps in the HSPG production. Thus, *rib-1(qm32)* and *rib-2(qm46)* mutations allow for the study of the impact of a global and specific disruption of HSPG biosynthesis in the context of live animals.

**HSPGs required for morphogenesis and cell migrations**

Disruption of HS chain synthesis by the *rib-1(qm32)* and *rib-2(qm46)* mutations leads to pleiotropic phenotypic consequences, including abnormal morphogenesis during embryonic and larval development, where embryos and larvae can be misshapen, with concomitant lethality. Among escapers that reach adulthood, locomotion and egg-laying behaviors are defective, and the underlying neuroanatomy is highly abnormal. Whereas we detected no defects in neuron identity, the migrations of numerous neurons and their axons are misguided, including migrations that occur during embryonic and post-embryonic development, as well as along both body axes (antero-posterior and dorso-ventral). It is worth nothing that the motility *per se* of migrating cells is not lost in *rib-1* and *rib-2* mutants as soma and axons often overshoot their targets. Rather, the guidance of migrations during development is disrupted by the loss of function of the genes *rib-1* and *rib-2*.

The numerous and penetrant defects of neuronal migrations observed in *rib-1(qm32)* and *rib-2(qm46)* mutants suggest that disruption of HSPG biosynthesis impacts numerous guidance pathways. In particular, our analysis of the guidance of the AVM pioneer neuron reveals that HS chains are required for *unc-6*/netrin- and *slt-1*/Slit-mediated axon guidance. HS has been shown *in vitro* to be required for netrin- and slit-mediated axon guidance using mouse neuronal explant assays (Matsumoto et al 2007, Ogata-Iwao et al 2011). As HS chains are attached to HSPGs, this result suggests that specific HSPGs are required for *unc-6*/netrin- and *slt-1*/Slit-mediated axon guidance. Indeed, *sdn-1/*syndecan has documented roles in the *slt-1/*Slit pathway in worms and flies (Blanchette et al 2015, Johnson et al 2004, Rhiner et al 2005, Steigemann et al 2004), though it has not been directly tested whether in these contexts the HS chains on SDN-1/syndecan are required for its function. Our work, along with the *in vitro* mouse neuronal explant assays (Matsumoto et al 2007, Ogata-Iwao et al 2011) suggests that the HS chains on SDN-1/syndecan may play an important role in *slt-1*/Slit-mediated axon guidance. We have also found that HS chains are important for *in vivo unc-6/*netrin-mediated axon guidance, suggesting that a specific HSPG functions in *unc-6/*netrin-mediated axon guidance. Recent work from our lab has shown that *lon-2/*glypican functions in *unc-6/*netrin-mediated guidance, though we found that this function was independent of the HS chains on LON-2/glypican (Blanchette et al 2015). This suggests the possibility that another HSPG could interact with the *unc-6/*netrin signaling pathway to mediate axon guidance in a HS-dependent

manner. Alternatively, this result suggests that possibly the HS chains on LON-2/glypican serve a role that we did not detect with our previous studies, for example in trafficking LON-2/glypican molecules to the membrane or in regulating the stability of LON-2/glypican.

**HSPGs are expressed and function from multiple tissues throughout development**

Given that HSPGs decorate most cells in metazoans and are implicated in numerous cellular processes at the cell surface, including cell-matrix, cell-cell, and ligand-receptor interactions, the HS copolymerase could be expected to be expressed ubiquitously. We indeed found that the HS copolymerase is broadly expressed, as functional reporter *rib-1::gfp* was detected in virtually all cell types at some point during development. Interestingly, the expression pattern of the HS copolymerase is dynamic, as the levels differed across tissues and at different stages of development. Expression was strong and transient in hypodermal cells of the embryo, the larva, and the developing vulva, likely reflecting the developmental needs of cells that undergo complex shape changes and/or migration during morphogenesis. It is possible that hypodermal cells, which secrete a basement membrane along which cells migrate, express the HS copolymerase at high levels. Also, cells that migrate during development may dynamically regulate the HSPGs at their surface to alter their adhesion

properties, reflected in the HS copolymerase expression peaking at times of migration.

In addition to this dynamic expression pattern, the HS copolymerase is continuously expressed throughout the life of the animal in a number of structures, including the pharynx, the pharyngeal-intestinal valve, the anal depressor, sphincter, and enteric muscles, as well as the nervous system. These are morphologically complex cells and are under continuous mechanical stress throughout larval and adult life; for instance, the pharynx is constantly pumping bacteria exerting pressure on the pharynx itself and the pharyngeal-intestinal valve; the enteric muscles, the anal depressor, the sphincter, all contract to expel the worm's waste; and the relatively long axons of neurons within the nerve cords are constantly subjected to being stretched as the animal moves. Other cell types accumulate increasing levels of HS copolymerase in reproducing adults, such as the spermatheca, which stretches to welcome oocytes to be fertilized and contracts to expel the zygotes, and the uterine muscles, which contract to lay embryos. Our observations point to a role for HSPGs in maintaining the integrity of tissues, possibly by regulating the attachment of cells that undergo considerable mechanical stress from repeated body contractions, and thus contribute to tissue homeostasis.

We analyzed the spatial requirements for the HS copolymerase by focusing on two specific migrating neurons, namely the embryonically migrating PVQ axon and the AVM axon that extends during the first larval stage. In both cases we found that combined expression of *rib-1* from several cell types was necessary to restore a more complete function during development. For the guidance of the migrating PVQ axon, the combined expression of the HS copolymerase in the hypodermis, neurons, and body wall muscles was able to rescue PVQ axon guidance defects, while single tissue expression of *rib-1* was not sufficient. This observation indicates that combined expression of HSPGs from multiple tissues is required to properly pattern the ventral midline. Distinct HSPGs from specific tissues may contribute to properly guide the PVQ axons at the ventral midline (**Fig. 2.9A**). Interestingly, the combined loss of two HSPGs, a glypican and a syndecan, in the double mutant *lon-2 sdn-1* leads to a similar penetrance of defects in PVQ guidance as *rib-1(qm32)* and *rib-2(qm46)* mutants (Diaz-Balzac et al 2014), suggesting that the PVQ axon guidance defects observed in *rib-1* and *rib-2* mutants may reflect the disruption of the glypican/LON-2 in the hypodermis and syndecan/SDN-1 in the PVQ neurons specifically. Consistent with this, glypican/*lon-2* has been found to function non-cell autonomously from the hypodermis to guide the axon of AVM (Blanchette et al 2015), and syndecan/*sdn-1* has been shown to function cell autonomously in the migrating neuron in a variety of contexts, such as to guide the AVM axon (Blanchette et al 2015), HSN soma, ALM soma, and PVQ axons (Rhiner et al 2005).

Furthermore, PVQ axon guidance likely requires that the specific HSPGs contributing to its guidance be not only synthesized but also modified, as the combined loss of HS modifying enzymes leads to PVQ axon guidance defects. Indeed, loss of the C5-epimerase *hse-5* and the 6-O-sulfotransferase *hst-6* in *hse-5; hst-6* double mutants, or loss of the 2-O-sulfotransferase *hst-2* in double mutants *hst-2 hst-6* leads to a similar penetrance of PVQ axon guidance defects as *rib-1* and *rib-2* mutants (Bülow & Hobert 2004). Together, it appears that the coordinated action of specific modified HS chains synthesized in different tissues onto distinct core proteins function to properly guide the PVQ axons at the ventral midline.

Similarly, the defective guidance of the axon of the AVM neuron is strongly rescued by expression of the HS copolymerase in the AVM neuron itself, but expression in the underlying hypodermis also contributes to normal AVM development. In this case too, possible HSPGs functioning to guide AVM may be syndecan/*sdn-1* in AVM and *lon-2*/glypican in the hypodermis (**Fig. 2.9B)**, as previously identified by analysis of core protein mutants (Blanchette et al 2015).

Our studies uncovered viable mutations in each of the two subunits of the HS copolymerase in *C. elegans*, which severely disrupt HS biosynthesis and lead to profound developmental defects. Given the evolutionary conservation of the guidance cues and signaling pathways and of HSPGs, analysis of HS

copolymerase in C. elegans is likely to provide insights into the coordinated roles of HSPGs in mammals as well. Our findings provide a model to to dissect the functions of HSPGs in *C. elegans* and uncover general principles of their roles in development and tissue homeostasis.

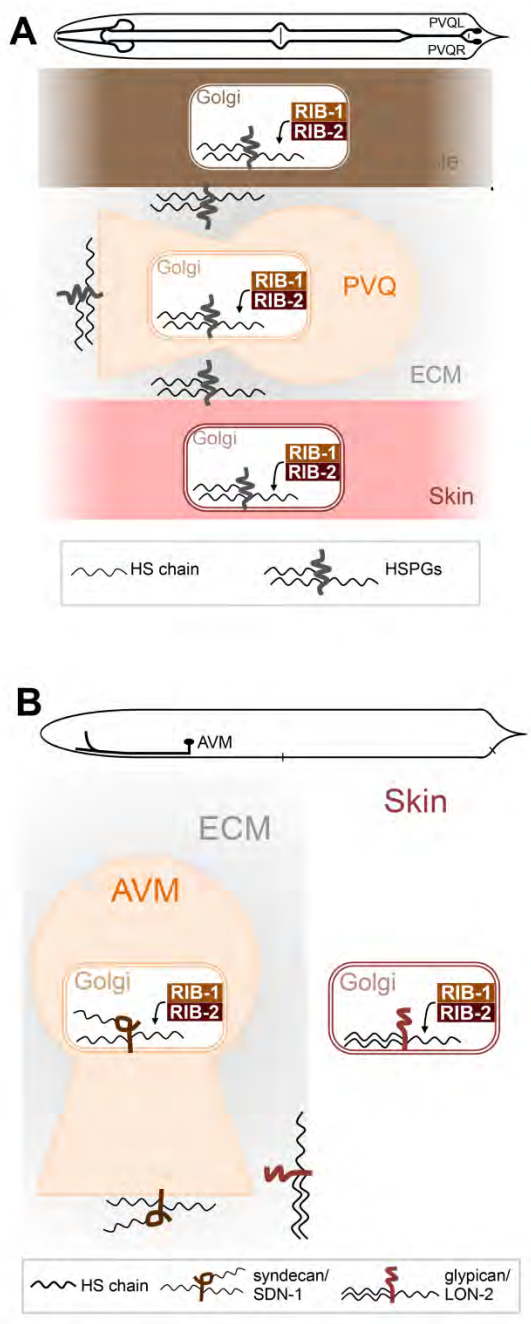


**Fig. 2.9. A model for the role of HSPGs in the guidance of PVQ and AVM axons.**
**A.** The PVQ axons extend along the ventral nerve cord, following preceding pioneer axons. PVQ axons are in contact with the extracellular matrix and in close proximity to muscles and hypodermis (skin). For proper guidance of the PVQ axons, combined HS function from the muscles, skin, and neurons is required, suggesting that multiple HSPGs coordinate the guidance of the PVQ axon.
**B.** The ventral axon guidance of AVM requires HS function from the migrating neuron itself, or from the skin, and HS chains are required for both *unc-6*/netrin and *slt-1*/Slit guidance systems. Taken together, AVM is guided by a HSPG functioning from AVM, likely *sdn-1*/syndecan, and a HSPG functioning from the skin, likely *lon-2*/glypican (Blanchette et al 2015).

## MATERIALS AND METHODS

### Nematode strains and genetics

Nematode cultures were maintained at 20$^{o}$C on NGM plates seeded with OP50 bacteria as described (Brenner 1974). *mum-1(qm32)* and *mum-3(qm46)* alleles were outcrossed 5 times before building strains with reporters. Strains were constructed using standard genetic procedures and are listed in **Table 2.1** with allele details listed in **Table 2.2**. When needed, genotypes were confirmed by genotyping PCR or sequencing, using primers listed in **Table 2.3**.

### Observations of cell and axon guidance

Guidance of cells and axons was examined in L4 larvae and adult animals using specific reporters. Animals were mounted on agarose pads, anaesthetized with 100 mM sodium azide, and examined under a Zeiss Axio Scope.A1 or a Zeiss Axioskop 2 Plus.

*CAN soma and axon*: CAN was examined using the reporter *lqIs4*. Axons were scored as defective when they were located away from the lateral aspect of the animal, either ventrally or dorsally, when they failed to extend fully, or exhibited branching. Cell bodies were scored as defective for migration when they were located anterior to the midpoint between the pharynx and the vulva (the wild-type CAN soma position near the vulva). CAN soma was virtually never found posterior to the vulva.

*PVQ axon*: PVQ was examined using the reporter *hdIs29.* Animals were scored as defective when axons projected laterally, fasciculated inappropriately, or failed to extend fully.

*AVM axon and AVM axon and soma:* AVM neurons were examined in L4 larvae and adult animals using the reporter *zdIs5*. Worms were counted as having an AVM soma migration defect when it was located posterior to the vulva. Animals with the cell body of AVM posterior to the vulva (cell migration defect) were excluded from axon guidance analysis, but included in **Fig. 2.1C** for % Defective soma and axon. Worms were counted as mutant for AVM ventral axon guidance if: **a)** AVM failed to send an axon ventrally and instead projected laterally to the anterior; or **b)** the AVM axon projected laterally, in the anterior or the posterior direction, for at least ~15 µm (>3 AVM cell body diameters) before projecting to the ventral side. When the angle between the initial anterior/posterior axon projection and the ventral axon projection was >45°, it was counted as mutant; thus, AVM axons with a slight curve in their ventral trajectory were not considered defective.

*PVM axon:* Axons of neurons PVM were examined in L4 larvae and adult animals using the reporter *zdIs5*. Worms were counted as having their PVM axon misoriented dorsally if the axon of PVM was projecting to the dorsal side of the animal. The vulva was used as a reference for the ventral side. Worms carrying the transgene *evIs25* (P*mec-4::unc-5*) whose *zdIs5* labeled neurons were too misplaced to be reliably identified were excluded from the analysis.

*HSN soma and axon*: HSN was examined using the reporter *zdIs13* in young adult animals. Animals were scored as defective for HSN axon guidance when axons projected laterally, posteriorly, fasciculated inappropriately, or failed to extend fully. Cell bodies were scored as defective for migration when they were either anterior to the vulva, or more posterior than the midpoint between the vulva and the tail.

*Motor neuron commissures:* Cholinergic and GABAergic motor neurons were examined using the reporters *ufIs34* and *vsIs48*, respectively. *Cholinergic*: In wild-type animals, only seven cholinergic motor neurons (DA3, DB4, DA4, DB5, DA5, DA6, DA7) have left-handed commissures between the terminal bulb of the pharynx and the anal depressor. Animals were scored as defective when more than seven cholinergic motor neuron commissures were on the left side of the animal between the posterior end of the terminal bulb of the pharynx and the anal depressor. *GABAergic*: Only the commissures of motor neuron DD1 and VD2 are left-handed in wild-type animals. Animals were scored as defective when additional GABAergic commissures were present on the left side of the animal.

*Dorsal cord:* The dorsal nerve cord was examined using the reporter *evIs111.* Animals were scored as having a defasciculated dorsal nerve cord when the cord was split into two or more bundles for any length of the dorsal nerve cord, instead of running as a single tight bundle as seen in the wild type.

*Excretory canals*: Excretory canals were examined using reporter *bgIs312.* Wild-type animals exhibit four lateral canals, two projecting anteriorly in the head and

two projecting posteriorly along the length of the body. Animals were scored as defective when a canal was located in an abnormal position (including when an anterior canal extended posteriorly, or a posterior canal extended anteriorly, or a canal laid ventrally or dorsally instead of laterally), when canals were too short (i.e., a posterior canal did not extend beyond the vulva), or when an abnormal number of canals was present.

*Distal tip cell guidance analysis:* The path of migration of the distal tip cells (DTC) brings about the shape of the mature gonad arms. In the wild type, the DTC migrates away from the vulva location along the antero-posterior axis of the animal. The DTC then turns dorsally to reach the dorsal side of the animal. Once the DTC reaches the dorsal aspect, it migrates back towards the vulva along the antero-posterior axis of the animal. To infer the path of DTC migration, gonad arms were examined in late L4 and young adult animals using DIC microscopy. Animals were counted as having abnormal gonad arms when a) the anterior gonad arm was on the left side instead of being on the right side; b) the posterior gonad arm was located on the right side instead of the left side; c) the distal portion of a gonad arm was located ventrally instead of dorsally; d) the proximal portion of the gonad arm was located dorsally instead of ventrally; or e) the proximal gonad arm was too short, resulting from a premature turn of the DTC towards the dorsal side.

*Excretory glands*: Excretory glands were examined in larvae using DIC microscopy. Animals were counted as having abnormally located excretory

glands when they were anterior of the pharyngeal terminal bulb (excretory glands are located just posterior of the pharyngeal terminal bulb in wild-type animals).

**Genetic mapping of *mum-1/rib-1***

For mapping *mum-1*, a three-point mapping experiment was carried out by picking Unc-non-Dpy and Dpy-non-Unc recombinants from heterozygous mothers of the genotype *mum-1/unc-24 dpy-20*, and the presence of *mum-1* was assessed among the progeny of the homozygosed recombinants. Two-point mapping was carried out by picking Dpy worms from *mum-1 dpy-20/++* heterozygous mothers, and the presence of *mum-1* was assessed in the next generation. Also, Lin-non-Dpy recombinants were picked from heterozygous *mum-1/lin-3 dpy-20*.

**Microinjections and transgenic animals**

As the *rib-1 and rib-2* mutants are severely morphologically abnormal, cosmids, constructs, and PCR products were injected into strains carrying the *mum-1/rib-1* or *mum-3/rib-2* mutations in a heterozygous state, balanced by flanking visible markers. For *rib-1*, we used *rib-1(qm32)/unc-24(e138) dpy-20(e1282ts)* and for *rib-2*, we used *rib-2(qm46)/unc-32(e189) dpy-18(e364)* (see **Table 2.1**). Transgenic F1s were isolated and lines homozygous for *rib-1* or *rib-2* were established.

Transgenic animals were generated by standard microinjection techniques (Mello & Fire 1995). Each construct or PCR amplicon was injected at 5 to 25 ng/µl with one or two coinjection markers which included pRF4-*rol-6(su1006d)* (100 - 150 ng/µL), P*ttx-3*::*mCherry* (50 ng/µl), P*ceh-22*::*gfp* (50 ng/µL), pCB101.1 P*rgef-1*::*DsRed2* (50 ng/µL) , and P*unc-122*::*rfp* (50 ng/µL). pBSK+ (90-100 ng/µL) used to increase total DNA concentration if needed. For coinjection markers used for each rescued transgenic line, see **Table 2.1**.

**Rescue and expression constructs**

The gene *rib-1*/F12F6.3 is downstream of the gene *srgp-1*/F12F6.5 in an operon of two genes. The nearest gene upstream of the operon is transcribed in the opposite direction. The genomic region between the operon of *srgp-1* and *rib-1*, and the upstream neighboring gene is 4352 bp, corresponding to coordinates 22290 – 26642 on cosmid F12F6.

**P*rib-1::rib-1* (PCR product):** A PCR product containing bases 34593 – 39595 of cosmid F12F6 of the *rib-1* locus was amplified with *Pfu* polymerase.

**P*rib-2::rib-2* (PCR product):** A PCR product containing bases 581 to 6196 of cosmid K01G5 of the *rib-2* locus was amplified with Phusion polymerase.

**P*rib-1*::*gfp* (pCB78):** A PCR generated piece containing bases 23701 to 26662 of cosmid F12F6 corresponding to the promoter region of the *rib-1* operon, as well as the initial 7 codons of *srgp-1*, was cloned upstream of *gfp* in the pPD95.77 vector using enzymes *Pst*I and *Xba*I.

**P*rib-1::rib-1::Venus* (pCB221):** The *rib-1* promoter region containing bases 23701 – 26580 of cosmid F12F6 was PCR amplified and cloned upstream of *gfp* in the pPD95.77 vector using enzymes *Sph*I and *Pst*I. A PCR generated piece containing bases 34452 - 39527 of cosmid F12F6 corresponding to the intergenic sequence between the genes *rib-1* and *srgp-1*, as well as the *rib-1* coding sequence, was cloned downstream of the *rib-1* promoter and upstream of *gfp* using enzymes *Pst*I and *Avr*II. Then, *gfp* was replaced with a PCR amplified *Venus* and cloned in frame with *rib-1* using enzymes *Msc*I and *Apa*I.

**P*dpy-7::rib-1* cDNA (pCB186):** The *rib-1* cDNA was amplified from yk1228g12 and ligated into a P*dpy-7* vector with a pPD95.75 backbone using enzymes *Xma*I – *Nco*I.

**P*myo-3::rib-1* cDNA (pCB196):** A P*myo-3 Hind*III – *Xba*I fragment was ligated upstream of the *rib-1* cDNA in a pCB186 *Hind*III – *Xba*I fragment in place of P*dpy-7*.

**P*mec-7::rib-1* cDNA (pCB204):** The *rib-1* cDNA was amplified from yk1228g12 and cloned into the pPD96.41 vector using enzymes *Age*I – *Bgl*II.

**P*rib-1::rib-1* cDNA (pCB225):** The *rib-1* cDNA was ligated downstream of the *rib-1* promoter (bases 23,701 to 26,580 of cosmid F12F6) using enzymes *Xma*I – *Apa*I in the pPD95.77 backbone.

**P*rgef-1::rib-1* cDNA (pCB199):** The *rib-1* cDNA was ligated downstream of P*rgef-1* in place of DsRed2 using enzymes *Xma*I – *Apa*I in the pCB101.1 vector.

All inserts of finalized clones were verified by sequencing.

**Molecular analysis of *mum-1/rib-1* and *mum-3/rib-2* mutant alleles**

The genomic regions of *mum-1/rib-1* and *mum-3/rib-2* were PCR amplified using *Pfu* polymerase and sequenced on two independent PCR products amplified from genomic DNA of *qm32* and *qm46*, respectively, using primers to cover the entire genomic region. Primers listed in **Table 2.3** sequence over the mutation in each of the two mutants.

**Western blot analysis of SDN-1::GFP expressed in worms**

Mixed-stage wild type (N2), SDN-1::GFP (*opIs171*), *rib-1*; SDN::GFP (*rib-1; opIs171*) and *rib-1* GFP control (*rib-1; lqIs4*) worms were collected from plates devoid of bacteria in buffer and protease inhibitors (Roche). Worm pellets were subjected to repeated freeze-thaw cycles. Protein concentration was measured using the Pierce 660 nm Protein Assay on a Nanodrop. 80 µg of samples mixed with 2x Laemmli sample buffer (Bio-Rad) were frozen in liquid nitrogen, then boiled, separated by SDS-PAGE on a 4-20% Mini-Protean TGX gel (Bio-Rad), and transferred to PVDF membrane. Membranes were incubated in 1:3000 anti-GFP primary antibody (Millipore #AB3080) and 1:9000 goat anti-rabbit HRP secondary antibody (Bio-Rad #166-2408EDU). For the loading control, membranes were incubated in 1:5000 anti-HSP90 antibody (CST #4874) and 1:10000 goat anti-rabbit HRP secondary antibody (Bio-Rad #166-2408EDU).

Signal was revealed using Clarity Western ECL Substrate (Bio-Rad), and imaged using film (LabScientific).

**Western blot analysis of LON-2::GFP and LON-2ΔGAG::GFP expressed in worms**

Mixed-stage wild type (N2), GFP control (*lqIs4*), LON-2::GFP (TLG257), LON-2ΔGAG::GFP (TLG199), *rib-1;* LON-2::GFP (VQ525), *rib-2;* LON-2::GFP (VQ528), *rib-1* GFP control (*rib-1; lqIs4*) and *rib-2* GFP control (*rib-2; lqIs4)* worms were collected from plates devoid of bacteria in buffer and protease inhibitors (Roche), mixed with 2x Laemmli sample buffer (Bio-Rad), and frozen in liquid nitrogen. Samples were boiled and spun down, separated by SDS-PAGE on a 4-20% Mini-Protean TGX gel (Bio-Rad), and transferred to PVDF membrane. Membranes were incubated in 1:3000 anti-GFP primary antibody (Millipore #AB3080) and 1:9000 goat anti-rabbit HRP secondary antibody (Bio-Rad #166-2408EDU). For the loading control, membranes were incubated in 1:5000 anti-HSP90 antibody (CST #4874) and 1:10000 goat anti-rabbit HRP secondary antibody (Bio-Rad #166-2408EDU). Signal was revealed using Clarity Western ECL Substrate (Bio-Rad), and imaged using film (LabScientific).

**Analysis of HS levels by western blot in worms**

**Protein extraction:** Mixed-stage worms from plates devoid of bacteria were collected in 50 mM Tris buffer and protease inhibitors (Roche # 11697498001),

and frozen in liquid nitrogen. Worm pellets were subjected to repeated freeze-thaw cycles and protein concentration was measured using the 660 nm Protein Assay (Pierce # 22660) on a Nanodrop.

**Detection of HS:** 80 µg of protein suspended in buffer and protease inhibitors (Roche) were used per sample. Undigested controls were treated exactly like the digested samples, except for the heparinase I and III enzyme treatment. To the digested samples, 10 mU of heparinase I and III enzyme (Sigma-Aldrich # H3917) was added. All samples were incubated at 37°C for 3 hours. 2x Laemmli sample buffer (Bio-Rad) was added and samples were frozen in liquid nitrogen. Samples were boiled, separated by SDS-PAGE on a 4-20% Mini-Protean TGX gel (Bio-Rad), and transferred to PVDF membrane. Membranes were incubated in 1:200 anti-Δ-Heparan Sulfate (3G10 epitope) primary antibody (Amsbio #370260-1) and 1:10000 horse anti-mouse HRP secondary antibody (Vector Labs #PI-2000). For the loading control, membranes were incubated in 1:5000 anti-HSP90 antibody (CST #4874) and 1:9000 goat anti-rabbit HRP secondary antibody (Bio-Rad #166-2408EDU). Signal was revealed using Clarity Western ECL Substrate (Bio-Rad), and imaged using film (LabScientific).

**ACKNOWLEDGEMENTS**

We are deeply grateful to Vivian Budnik, Mark Alkema, Carlos Lois, and Michael Francis for insightful discussions. We thank Catherine Harwood, Avery Fisher, Mark Broadwin, and Melissa Carroll for assistance with building strains. We thank Dr. A. Fire and Dr. Y. Kohara for clones, Wormbase, and the CGC funded by NIH Office of Research Infrastructure Programs (P40 OD010440) for strains. We thank David Hall for help in identifying pm6. We thank R. Pocock and C. Nehammer for HS western blot protocols. This work was supported by an R01 grant AG041870-01A1 from the NIH to C.Y.B..

## TABLES

### Table 2.1 Strains used in this study

| Strain | Genotype | Transgene | Reference |
|---|---|---|---|
| N2 | | | *(Brenner 1974)* |
| LE311 | *lqIs4 III* | P*ceh-10::gfp* | *(Tsalik et al 2003)* |
| | *hdIs29 V* | P*odr-2::cfp;* P*sra-6::DsRed2* | *(Schmitz et al 2008)* |
| MT4005 | *zdIs5 I* | P*mec-4::gfp; lin-15(+)* | *(Clark & Chiu 2003)* |
| SK4013 | *zdIs13 IV* | P*tph-1::gfp* | *(Clark & Chiu 2003)* |
| VQ84 | *vsIs48 X; ufIs34* | P*unc-17::gfp;* P*unc-47::mCherry* | *(Chase et al 2004, Petrash et al 2013)* |
| NW1229 | *evIs111 III* | P*rgef-1::gfp; dpy-20(+)* | *(Altun-Gultekin et al 2001)* |
| OH1360 | *bgIs312* | P*pes-6::gfp* | *(Berry et al 2003)* |
| ***rib-1* and *rib-2* alone and with AVM guidance factors** | | | |
| VQ344 | *rib-1(qm32) IV; lqIs4 III* | | *This study* |
| VQ355 | *rib-2(qm46) III; lqIs4 III* | | *This study* |
| VQ196 | *rib-1(qm32) IV; hdIs29 V* | | *This study* |
| VQ212 | *rib-2(qm46) III; hdIs29 V* | | *This study* |
| VQ252 | *rib-1(qm32) IV; zdIs5 I* | | *This study* |
| VQ200 | *rib-2(qm46) III; zdIs5 I* | | *This study* |
| VQ661 | *rib-1(qm32 ) zdIs13 IV* | | *This study* |
| VQ402 | *rib-2(qm46 )III; zdIs13 IV* | | *This study* |
| VQ202 | *rib-1(qm32) IV; vsIs48; ufIs34* | | *This study* |
| VQ208 | *rib-2(qm46) III; vsIs48; ufIs34* | | *This study* |
| VQ209 | *rib-1(qm32) IV; evIs111 III* | | *This study* |
| VQ213 | *rib-2(qm46) evIs111 III* | | *This study* |
| VQ342 | *rib-1(qm32) IV; bgIs312* | | *This study* |
| VQ343 | *rib-2(qm46) III; bgIs312* | | *This study* |
| VQ230 | *rib-1(qm32)/unc-24(e138) dpy-20(e1282ts) IV; hdIs29 V* | | *This study* |
| VQ265 | *rib-1(qm32)/unc-24(e138) dyp-20(e1282ts) IV; zdIs5 I* | | *This study* |
| VQ465 | *rib-1(qm32) IV; unc-6(e78) X; zdIs5 I* | | *This study* |
| VQ449 | *rib-2(qm46) IV; unc-6(e78) X; zdIs5 I* | | *This study* |
| VQ405 | *rib-1(qm32) IV; slt-1(eh15) X; zdIs5 I* | | *This study* |
| VQ404 | *rib-2(qm46) IV; slt-1(eh15) X; zdIs5 I* | | *This study* |
| VQ443 | *rib-1(qm32) IV; kyIs209 X; zdIs5 I* | | *This study* |
| VQ456 | *rib-2(qm46) IV; kyIs209 X; zdIs5 I* | | *This study* |
| **HS-modifying enzymes and AVM axon guidance factors** | | | |

| | | | |
|---|---|---|---|
| VQ551 | *hse-5(tm472) III; zdIs5 I* | | *This study* |
| VQ547 | *hst-2(ok595) X; zdIs5 I* | | *This study* |
| VQ546 | *hst-6(ok273) X; zdIs5 I* | | *This study* |
| VQ569 | *hse-5(tm472) III; hst-2(ok595) X; zdIs5 I* | | *This study* |
| VQ560 | *hse-5(tm472) III; hst-6(ok273) X; zdIs5 I* | | *This study* |
| VQ571 | *hst-2(ok595) hst-6(ok273) X; zdIs5 I* | | *This study* |
| VQ599 | *hst-2(ok595) hst-6(ok273) X; hse-5(tm472) III; zdIs5 I* | | *This study* |
| VQ395 | *unc-6(e78) X; zdIs5 I* | | *(Blanchette et al 2015)* |
| VQ577 | *hse-5(tm472) III; unc-6(ev400) X; zdIs5 I* | | *This study* |
| VQ573 | *hst-2(ok595) unc-6(ev400) X; zdIs5 I* | | *This study* |
| VQ579 | *hst-6(ok273) unc-6(ev400) X; zdIs5 I* | | *This study* |
| VQ401 | *slt-1(eh15) X; zdIs5 I* | | *(Blanchette et al 2015)* |
| VQ427 | *kyIs209 X; zdIs5 I* | | *(Blanchette et al 2015)* |
| VQ602 | *hse-5(tm472) III; slt-1(eh15) X; zdIs5 I* | | *This study* |
| VQ604 | *hst-2(ok595) slt-1(eh15) X; zdIs5 I* | | *This study* |
| VQ606 | *hst-6(ok273) slt-1(eh15) X; zdIs5 I* | | *This study* |
| VQ616 | *hse-5(tm472) III; hst-2(ok595) hst-6(ok273) slt-1(eh15)X; zdIs5 I* | | *This study* |
| **LON-2::GFP and SDN-1::GFP strains** | | | |
| WS3404 | *opIs171* | P*sdn-1::sdn-1::gfp; lin-15(+)* | *(Rhiner et al 2005)* |
| VQ450 | *rib-1(qm32) IV; opIs171* | P*sdn-1::sdn-1::gfp; lin-15(+)* | *This study* |
| TLG257 | *lon-2(e678) X; texEx164* | Plasmid HW483 (P*lon-2::lon-2::gfp),* P*ttx-3::mCherry* | *(Taneja-Bageshwar & Gumienny 2012)* |
| TLG199 | *lon-2(e678) X; texEx144* | pSBL3SG006 (P*lon-2::*LON-2ΔGAG::*gfp*), P*ttx-3::mCherry* | *(Taneja-Bageshwar & Gumienny 2012)* |
| VQ525 | *rib-1(qm32) IV; texEx164* | Plasmid HW483 (P*lon-2::lon-2::gfp),* P*ttx-3::mCherry* | *This study* |
| VQ528 | *rib-2(qm46) III; texEx144* | Plasmid HW483 (P*lon-2::lon-2::gfp),* P*ttx-3::mCherry* | *This study* |
| **Transgenic Lines** | | | |
| VQ370 | *rib-1(qm32) IV; zdIs5 I; qvEx80* | pCB221 (P*rib-1::rib-1::Venus*), P*ttx-3::mCherry*, pRF4. Line #1 | *This study* |
| VQ684 | *rib-1(qm32) IV; zdIs5 I; qvEx148* | pCB221 (P*rib-1::rib-1::Venus*), P*ttx-3::mCherry*, pRF4. Line #2 | *This study* |
| VQ502 | *rib-2(qm46) III; zdIs5 I; qmEx329* | PCR product of bases 604..6196 of cosmid K01G5, pRF4. Line #1 | *This study* |
| VQ503 | *rib-2(qm46) III; zdIs5 I; qmEx330* | PCR product of bases 604..6196 of cosmid K01G5, pRF4. Line #2 | *This study* |
| VQ381 | *rib-1(qm32) IV; hdIs29 V; qvEx86* | pCB221 (P*rib-1::rib-1 ::Venus*), P*ttx-3::mCherry*, pRF4. Line #1 | *This study* |

| | | | |
|---|---|---|---|
| VQ673 | *rib-1(qm32) IV; hdIs29 V; qvEx140* | pCB221 (P*rib-1::rib-1::Venus*), P*ttx-3::mCherry*, pRF4. Line #2 | *This study* |
| VQ504 | *rib-2(qm46) III; hdIs29 V; qmEx329* | PCR product of bases 604…6196 of cosmid K01G5, pRF4. Line #1 | *This study* |
| VQ505 | *rib-2(qm46) III; hdIs29 V; qmEx330* | PCR product of bases 604…6196 of cosmid K01G5, pRF4. Line #2 | *This study* |
| VQ663 | *rib-1(qm32) IV; zdIs5 I; qvEx131* | pCB225 (P*rib-1::rib-1*), P*ttx-3::mCherry,* pRF4. Line #1 | *This study* |
| VQ376 | *rib-1(qm32) IV; zdIs5 I; qvEx81* | pCB225 (P*rib-1::rib-1*), P*ttx-3::mCherry,* pRF4. Line #2 | *This study* |
| VQ664 | *rib-1(qm32) IV; zdIs5 I; qvEx132* | pCB225 (P*rib-1::rib-1*), P*ttx-3::mCherry,* pRF4. Line #3 | *This study* |
| VQ665 | *rib-1(qm32) IV; zdIs5 I; qvEx133* | pCB204 (P*mec-7::rib-1*), P*ceh-22::gfp,* pRF4. Line #1 | *This study* |
| VQ334 | *rib-1(qm32) IV; zdIs5 I; qvEx85* | pCB204 (P*mec-7::rib-1*), P*ceh-22::gfp,* pRF4. Line #2 | *This study* |
| VQ508 | *rib-1(qm32) IV; zdIs5 I; qvEx101* | pCB204 (P*mec-7::rib-1*), pRF4, P*rgef-1*::*DsRed2*. Line #3 | *This study* |
| VQ509 | *rib-1(qm32) IV; zdIs5 I; qvEx102* | pCB204 (P*mec-7::rib-1*), pRF4, P*rgef-1*::*DsRed2*. Line #4 | *This study* |
| VQ667 | *rib-1(qm32) IV; zdIs5 I; qvEx134* | pCB196 (P*myo-3::rib-1*), P*ttx-3::mCherry*, pRF4. Line #1 | *This study* |
| VQ666 | *rib-1(qm32) IV; zdIs5 I; qvEx141* | pCB196 (P*myo-3::rib-1*), P*ttx-3::mCherry*, pRF4. Line #2 | *This study* |
| VQ668 | *rib-1(qm32) IV; zdIs5 I; qvEx135* | pCB196 (P*myo-3::rib-1*), P*ttx-3::mCherry*, pRF4. Line #3 | *This study* |
| VQ487 | *rib-1(qm32) IV; zdIs5 I; qvEx94* | pCB196 (P*myo-3::rib-1*), P*ttx-3::mCherry*, pRF4. Line #4 | *This study* |
| VQ488 | *rib-1(qm32) IV; zdIs5 I; qvEx95* | pCB186 (P*dpy-7::rib-1*), P*ttx-3::mCherry,* pRF4. Line #1 | *This study* |
| VQ669 | *rib-1(qm32) IV; zdIs5 I; qvEx136* | pCB186 (P*dpy-7::rib-1*), P*ttx-3::mCherry,* pRF4. Line #2 | *This study* |
| VQ670 | *rib-1(qm32) IV; zdIs5 I; qvEx137* | pCB186 (P*dpy-7::rib-1*), P*ttx-3::mCherry,* pRF4. Line #3 | *This study* |
| VQ672 | *rib-1(qm32) IV; zdIs5 I; qvEx139* | pCB186 (P*dpy-7::rib-1*), P*ttx-3::mCherry,* pRF4. Line #4 | *This study* |
| VQ391 | +; *qvEx90* | pCB78 (P*rib-1::gfp*), pRF4. Line #1 | *This study* |
| VQ204 | +; *qvEx36* | pCB78 (P*rib-1::gfp*), P*ttx-3::mCherry*, pBSK+. Line #2 | *This study* |
| VQ205 | +; *qvEx37* | pCB78 (P*rib-1::gfp*), P*ttx-3::mCherry*, pBSK+. Line #3 | *This study* |
| VQ356 | +; *qvEx79* | pCB221 (P*rib-1::rib-1 ::Venus*), pRF4, P*unc-122::rfp.* Line #1 | *This study* |
| VQ379 | +; *qvEx84* | pCB221 (P*rib-1::rib-1 ::Venus*), pRF4. Line #2 | *This study* |
| VQ694 | *rib-1(qm32) IV; hdIs29 V; qvEx153* | pCB199 (P*rgef-1::rib-1*), P*ttx-3::mCherry*, pRF4. Line #1 | *This study* |
| VQ695 | *rib-1(qm32) IV; hdIs29 V; qvEx154* | pCB199 (P*rgef-1::rib-1*), P*ttx-3::mCherry*, pRF4. Line #2 | *This study* |
| VQ696 | *rib-1(qm32) IV; hdIs29 V; qvEx155* | pCB199 (P*rgef-1::rib-1*), P*ttx-3::mCherry*, pRF4. Line #3 | *This study* |

| | | | |
|---|---|---|---|
| VQ253 | *rib-1(qm32) IV; hdIs29 V; qvEx43* | pCB186 (P*dpy-7::rib-1*), P*ttx-3::mCherry*, pRF4. Line #1 | *This study* |
| VQ698 | *rib-1(qm32) IV; hdIs29 V; qvEx157* | pCB186 (P*dpy-7::rib-1*), P*ttx-3::mCherry*, pRF4. Line #2 | *This study* |
| VQ699 | *rib-1(qm32) IV; hdIs29 V; qvEx158* | pCB186 (P*dpy-7::rib-1*), P*ttx-3::mCherry*, pRF4. Line #3 | *This study* |
| VQ260 | *rib-1(qm32) IV; hdIs29 V; qvEx47* | pCB196 (P*myo-3::rib-1*), P*ttx-3::mCherry*, pRF4. Line #1 | *This study* |
| VQ261 | *rib-1(qm32) IV; hdIs29 V; qvEx48* | pCB196 (P*myo-3::rib-1*), P*ttx-3::mCherry*, pRF4. Line #2 | *This study* |
| VQ702 | *rib-1(qm32) IV; hdIs29 V; qvEx161* | pCB196 (P*myo-3::rib-1*), P*ttx-3::mCherry*, pRF4. Line #3 | *This study* |
| VQ703 | *rib-1(qm32) IV; hdIs29 V; qvEx162* | pCB199 (P*rgef-1::rib-1*), pCB186 (P*dpy-7::rib-1*), pCB196 (P*myo-3::rib-1*), P*ttx-3::mCherry*, pRF4. Line #1 | *This study* |
| VQ704 | *rib-1(qm32) IV; hdIs29 V; qvEx163* | pCB199 (P*rgef-1::rib-1*), pCB186 (P*dpy-7::rib-1*), pCB196 (P*myo-3::rib-1*), P*ttx-3::mCherry*, pRF4. Line #2 | *This study* |
| VQ705 | *rib-1(qm32) IV; hdIs29 V; qvEx164* | pCB199 (P*rgef-1::rib-1*), pCB186 (P*dpy-7::rib-1*), pCB196 (P*myo-3::rib-1*), P*ttx-3::mCherry*, pRF4. Line #3 | *This study* |
| ***evIs25* strains and controls** | | | |
| VQ396 | *unc-6(ev400) X; zdIs5 I* | | *(Blanchette et al 2015)* |
| VQ470 | *unc-40(e271) zdIs5 I* | | *(Blanchette et al 2015)* |
| VQ473 | *sax-3(k123) X; zdIs5 I* | | *(Blanchette et al 2015)* |
| VQ423 | *sdn-1(zh20) X; zdIs5 I* | | *(Blanchette et al 2015)* |
| VQ536 | *evIs25 X; zdIs5 I* | | *(Blanchette et al 2015)* |
| VQ538 | *unc-6(ev400) evIs25 X; zdIs5 I* | | *(Blanchette et al 2015)* |
| VQ540 | *unc-40(e271) zdIs5 I; evIs25 X* | | *(Blanchette et al 2015)* |
| VQ556 | *slt-1(eh15) evIs25 X*; *zdIs5 I* | | *(Blanchette et al 2015)* |
| VQ557 | *sax-3(ky123) evIs25 X*; *zdIs5 I* | | *(Blanchette et al 2015)* |
| VQ572 | *sdn-1(zh20) evIs25 X; zdIs5 I* | | *(Blanchette et al 2015)* |
| VQ554 | *rib-1(qm32) IV; evIs25 X; zdIs5 I* | | *This study* |
| VQ539 | *rib-2(qm46) III; evIs25 X; zdIs5 I* | | *This study* |

## Table 2.2 Mutant alleles used in this study

| Gene | Allele | Nature of allele | Reference |
|---|---|---|---|
| ***rib-1*** | *qm32* | Stop codon converted into a Lys codon, likely extending the open reading frame into the 3'UTR | This study |
| ***rib-2*** | *qm46* | Arg to Gln amino acid substitution at residue 434 | This study |
| ***hse-5*** | *tm472* | 1249 bp deletion and addition of an adenosine, which deletes most of exons 4 – 7 and generates a frame shift after exon 4 | (Bülow & Hobert 2004) |
| ***hst-2*** | *ok595* | 1336 bp deletion, deleting from exon 4 to part of exon 7 | (Bülow & Hobert 2004) |
| ***hst-6*** | *ok273* | 1064 bp deletion, with the addition of nucleotides CTTT, which deletes exons 4 and 5 and generates a frameshift after exon 3 | (Bülow & Hobert 2004) |
| ***unc-6*** | *ev400* | Early stop Q78*. Null. | (Wadsworth et al 1996) |
| ***unc-6*** | *e78* | C410Y. Partial loss of function. | (Lim & Wadsworth 2002) |
| ***slt-1*** | *eh15* | Duplication and deletions. First copy contains a 1900 bp deletion. Both duplicated copies have a 100 bp deletion. First copy produces no mRNA while second copy produces mRNA with a frameshift. | (Hao et al 2001) |
| ***unc-40*** | *e271* | Early stop R824*. Null. | (Stavoe et al 2012) |
| ***sax-3*** | *ky123* | Deletion of signal peptide and first exon. | (Zallen et al 1998) |
| ***sdn-1*** | *zh20* | 1258 bp deletion. | (Rhiner et al 2005) |

**Table 2.3 Primers used for strain building**

| Gene | Primer | Sequence | PCR product (bp) |
|---|---|---|---|
| ***rib-1(qm32)* sequencing** | | | |
| | oCB1026 | gggtgcgtaaggagatgagg | 456 |
| | oCB1027 | ggcaaccagccatcacagcc | |
| ***rib-2(qm46)* sequencing** | | | |
| | oCB1028 | caacttatcggatcttcaacc | 437 |
| | oCB1029 | ttccagcggtccaaggagg | |
| ***slt-1(eh15)*** | | | |
| Mutant specific | oCB919 | tatgacgtgttccggaaacc | 467 |
| | oCB920 | atttctctaatacgggtagc | |
| Wild-type specific | oCB922 | tctcaattctaacatccatgtc | 339 |
| | oCB920 | atttctctaatacgggtagc | |
| ***sax-3(ky123)*** | | | |
| Mutant specific | oCB1038 | agaatgtggctctctagtcc | ~330 |
| | oCB1039 | tcgtttccgcgcattcagtc | |
| Wild-type specific | oCB1038 | agaatgtggctctctagtcc | 527 |
| | oCB1042 | agcttcggattactgcttgc | |
| ***sdn-1(zh20)*** | | | |
| Mutant specific | oCB837 | aaagagatgccggtcaggtg | 410 |
| | oCB842 | aatggacgggatgagtgtcc | |
| Wild-type specific | oCB837 | aaagagatgccggtcaggtg | 293 |
| | oCB876 | cttcagattcgagcctgctttgc | |
| ***evIs25:* Detection of insertion P*mec-7::unc-5*** | | | |
| | oCB933 | ttgtcagtcgagcctcaagg | ~631 |
| | oCB966 | tccactgtctgataatctgg | |
| ***kyIs209:* Detection of insertion P*myo-3::slt-1*** | | | |
| | oCB945 | tcattcgggatattttgtgg | 592 |
| | oCB950 | aagaagaagcatgcttctgg | |
| ***hse-5(tm472)*** | | | |
| Mutant specific | oCB1055 | atcgtgtacgatgtgtcagc | 546 |
| | oCB1056 | attcgcctcatacggtttcc | |
| Wild-type specific | oCB1055 | atcgtgtacgatgtgtcagc | 779 |
| | oCB1057 | aactttctctcggcaattg | |
| ***hst-2(ok595)*** | | | |
| Mutant specific | oCB1052 | tattacaacatggacggagc | 692 |
| | oCB1054 | aacattatgcgcatgaacgc | |
| Wild-type specific | oCB1052 | tattacaacatggacggagc | 486 |
| | oCB1053 | ttagcagtgattcaattacg | |
| ***hst-6(ok273)*** | | | |
| Mutant specific | oCB1049 | ttagacgtggctgttctcac | 723 |
| | oCB1051 | tgtgagtctgttaagggtgg | |
| Wild-type specific | oCB1049 | ttagacgtggctgttctcac | 804 |
| | oCB1212 | agaaatgttgtgtagaagtag | |

# Chapter III

# Glypican is a modulator of netrin-mediated axon guidance

Cassandra R. Blanchette, Paola N. Perrat, Andrea Thackeray, Claire Y. Bénard*

Department of Neurobiology, UMass Medical School

364 Plantation Street, Worcester, MA 01605, USA

**Contribution Summary**

C.R.B., P.P., A.T and C.Y.B. designed and carried out the experiments. C.R.B., P.P. and C.Y.B. co-wrote the manuscript.

This chapter represents work previously published and is presented in accordance with copyright law.

Blanchette CR, Perrat PN, Thackeray A, Bénard CY (2015) Glypican Is a Modulator of Netrin-Mediated Axon Guidance. PLoS Biol 13(7): e1002183. doi: 10.1371/journal.pbio.1002183

**ABSTRACT**

Netrin is a key axon guidance cue that orients axon growth during neural circuit formation. However, the mechanisms regulating netrin and its receptors in the extracellular milieu are largely unknown. Here we demonstrate that in *C. elegans,* LON-2/glypican, a heparan sulfate proteoglycan, modulates UNC-6/netrin signaling, and may do this through interactions with the UNC-40/DCC receptor. We show that developing axons misorient in the absence of LON-2/glypican when the SLT-1/slit guidance pathway is compromised, and that LON-2/glypican functions in both the attractive and repulsive UNC-6/netrin pathways. We find that the core LON-2/glypican protein, lacking its heparan sulfate chains, and secreted forms of LON-2/glypican, are functional in axon guidance. We also find that LON-2/glypican functions from the epidermal substrate cells to guide axons, and provide evidence that LON-2/glypican associates with UNC-40/DCC receptor-expressing cells. We propose that LON-2/glypican acts as a modulator of UNC-40/DCC-mediated guidance to fine-tune axonal responses to UNC-6/netrin signals during migration.

**INTRODUCTION**

Directed migrations of developing axons are essential for the proper wiring of the nervous system. A host of guidance cues and their receptors instruct axon guidance decisions. However, how these cues and the growth cone's responses to them are spatially and temporally regulated *in vivo* remains largely unknown.

Answering this question is central to our understanding of how growing axons navigate in complex environments to reach their targets during development and regeneration.

UNC-6/netrin is a highly conserved secreted guidance cue with structural similarity to the extracellular matrix protein laminin (Ishii et al 1992, Kennedy et al 1994, Serafini et al 1994). UNC-6/netrin directs attractive guidance through receptors of the UNC-40/DCC family, and repulsive guidance through both UNC-40/DCC and UNC-5/UNC5 receptors (Chan et al 1996, Hedgecock et al 1990, Leung-Hagesteijn et al 1992). Notably, whereas netrin receptors and downstream transduction pathways have been well characterized, how netrin signals are regulated extracellularly remains largely unknown. UNC-6/netrin was identified through genetic analysis in *C. elegans* (Ishii et al 1992), and biochemically purified and cloned from vertebrate embryos (Serafini et al 1994). A second biochemical component that synergized with netrin to elicit axon outgrowth was termed “netrin synergizing activity” (NSA) (Kennedy et al 1994) and remains unidentified. Vertebrate netrin-1 and its receptor DCC can bind heparin, a fully sulfated version of heparan sulfate (HS), *in vitro* (Bennett et al 1997, Geisbrecht et al 2003, Kennedy et al 1994), and a general disruption of HS chain synthesis is detrimental to netrin-1-mediated axon outgrowth *in vitro* (Matsumoto et al 2007, Ogata-Iwao et al 2011). While heparan sulfate proteoglycans (HSPGs) might be intriguing candidates for NSA, it is not yet

known whether a specific HSPG is required for netrin signaling, nor how interactions with HSPGs might regulate netrin signals to direct axons during nervous system development.

We addressed these questions using the nematode *Caenorhabditis elegans,* which has been instrumental for discovering major conserved axon guidance pathways. During larval development, the axon of the mechanosensory neuron AVM migrates ventrally as its growth cone integrates signals from two complementary guidance cues (**Fig. 3.1a**) (Chan et al 1996, Hao et al 2001, Hedgecock et al 1990, Hedgecock et al 1987, Ishii et al 1992, Leung-Hagesteijn et al 1992, Zallen et al 1998): (1) UNC-6/netrin is secreted at the ventral midline and attracts the growth cone ventrally via the receptor UNC-40/DCC (Chan et al 1996, Wadsworth et al 1996), and (2) SLT-1/Slit is secreted by the dorsal muscles and repels the growth cone away from the dorsal side via the receptor SAX-3/Robo (Hao et al 2001, Zallen et al 1998). Animals null for the guidance cues *unc-6*/netrin or *slt-1*/Slit exhibit partial AVM ventral axon guidance defects, and loss of both cues in *unc-6 slt-1* double mutants results in fully penetrant guidance defects ((Hao et al 2001), **Fig. 3.2**). AVM axons defective in guidance fail to extend ventrally and instead migrate laterally in the anterior direction (**Fig. 3.1**). In this study, we use the AVM axon as a model to elucidate mechanisms that regulate UNC-6/netrin signaling.

Here we provide a missing link in understanding the modulation of UNC-6/netrin signaling in the extracellular milieu. We demonstrate that LON-2/glypican, a HSPG secreted from epidermal cells, acts as a modulator of the UNC-6/netrin signaling pathways to guide migrating cells and axons. We show that LON-2/glypican modulates UNC-6/netrin signaling in both attractive guidance mediated by the UNC-40/DCC receptor, and repulsive guidance mediated by the UNC-40/DCC and UNC-5/UNC5 receptors. We provide evidence that LON-2/glypican associates with UNC-40/DCC-receptor-expressing cells. We show that the N-terminal globular region of LON-2/glypican, lacking the three HS chain attachment sites, is functional in UNC-6/netrin-mediated guidance. Our studies unravel a novel mechanism by which LON-2/glypican is produced by substrate epidermal cells and released from the membrane to likely associate with UNC-40/DCC-expressing neurons, enabling the modulation of their responses to UNC-6/netrin during axon migrations.

## RESULTS

### *lon-2*/glypican and *sdn-1*/syndecan cooperate to guide *unc-6*/netrin- and *slt-1*/Slit-mediated axon migration

To address whether a specific HSPG interacts with the netrin signaling system to guide axons, we first examined axon guidance in mutants lacking core HSPGs.

HSPGs are composed of a core protein with covalently attached long unbranched heparan sulfate (HS) chains (Bülow & Hobert 2006). HSPGs can be associated with the plasma membrane through either a transmembrane domain (e.g., syndecans) or a glycerophosphatidylinositide (GPI)-anchor (e.g., glypicans), or be secreted into the extracellular milieu (e.g., perlecans, agrins). We examined the axon morphology of AVM in single, double, and triple mutants for several core HSPG proteins (see **Table 3.1** for alleles). These included the sole *C. elegans* syndecan (*sdn-1*), the two glypicans (*lon-2, gpn-1)*, perlecan (*unc-52)*, and agrin (*agr-1*). We found that the mild AVM axon guidance defects of *sdn-1*/syndecan mutants, including a null, (Rhiner et al 2005) were enhanced by the complete loss of *lon*-2/glypican in double mutants *lon-2 sdn-1* (**Fig. 3.1b**), revealing a role for *lon-2*/glypican in AVM axon guidance. Similarly, loss of *lon-2/*glypican enhances *sdn-1/*syndecan mutants in motorneuron guidance (Gysi et al 2013). Although the *C. elegans* genome encodes two glypicans, loss of function of the second glypican, *gpn-1,* using two likely null mutant alleles (see **Fig. 3.3**), did not enhance the defects of *lon-2*/glypican or *sdn-1*/syndecan null mutants, in double or triple mutants (**Fig. 3.1b**). Moreover, we did not observe abnormal phenotypes in the single mutants for *agr-1*/agrin or *unc-52/*perlecan. These observations highlight the specificity of *lon-2*/glypican function in this axon guidance process, and raise the possibility that *lon-2*/glypican might be a component of the pathways guiding the AVM axon towards the ventral midline.

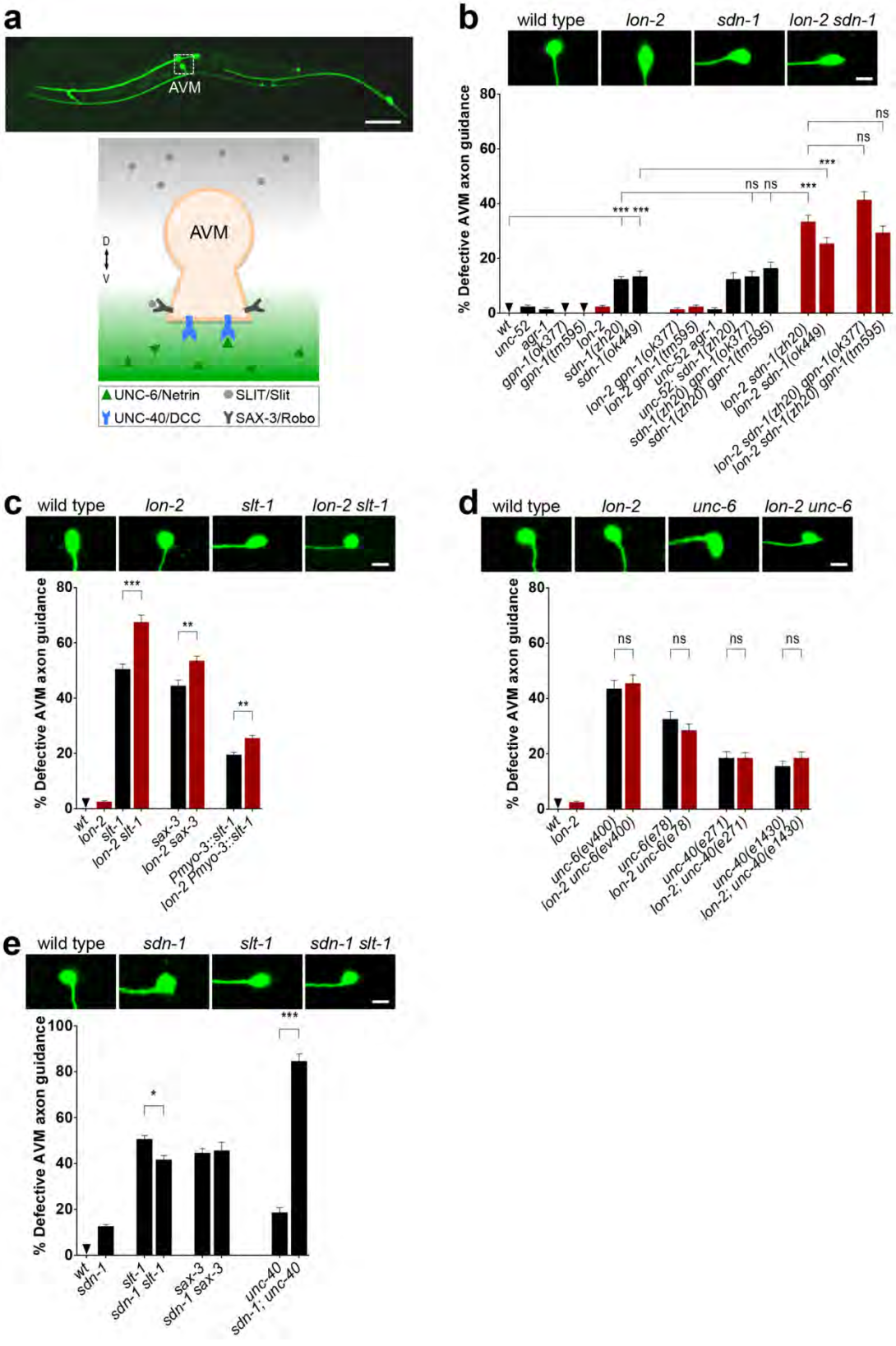
a
AVM
AVM
D
V
UNC-6/Netrin
SLIT/Slit
UNC-40/DCC
SAX-3/Robo
b
wild type
lon-2
sdn-1
lon-2 sdn-1
% Defective AVM axon guidance
wt
unc-52
agr-1
gpn-1(ok377)
gpn-1(tm595)
lon-2
sdn-1(zh20)
sdn-1(ok449)
lon-2 gpn-1(ok377)
lon-2 gpn-1(tm595)
unc-52 agr-1
unc-52; sdn-1(zh20)
sdn-1(zh20) gpn-1(ok377)
sdn-1(zh20) gpn-1(tm595)
lon-2 sdn-1(zh20)
lon-2 sdn-1(ok449)
lon-2 sdn-1(zh20) gpn-1(ok377)
lon-2 sdn-1(zh20) gpn-1(tm595)
c
wild type
lon-2
slt-1
lon-2 slt-1
% Defective AVM axon guidance
wt
lon-2
slt-1
lon-2 slt-1
sax-3
lon-2 sax-3
Pmyo-3::slt-1
lon-2 Pmyo-3::slt-1
d
wild type
lon-2
unc-6
lon-2 unc-6
% Defective AVM axon guidance
wt
lon-2
unc-6(ev400)
lon-2 unc-6(ev400)
unc-6(e78)
lon-2 unc-6(e78)
unc-40(e271)
lon-2; unc-40(e271)
unc-40(e1430)
lon-2; unc-40(e1430)
e
wild type
sdn-1
slt-1
sdn-1 slt-1
% Defective AVM axon guidance
wt
sdn-1
slt-1
sdn-1 slt-1
sax-3
sdn-1 sax-3
unc-40
sdn-1; unc-40

**Figure 3.1. *lon-2*/glypican functions in the attractive *unc-6*/netrin guidance pathway.** **(a)** During the first larval stage of *C. elegans*, the pioneer neuron AVM extends ventrally along the body wall until it reaches the ventral nerve cord. Its migration results from the combined attractive response to UNC-6/netrin (secreted at the ventral midline) via the UNC-40/DCC receptor, and the repulsive response to SLT-1/Slit (secreted by the dorsal muscles) via its SAX-3/Robo receptor. We visualized the morphology of the AVM axon using the transgene P*mec-4::gfp*. **(b)** The heparan sulfate proteoglycans *lon-2*/glypican and *sdn-1*/syndecan cooperate to guide the axon of AVM, as their simultaneous loss enhances guidance defects. The role of *lon-2*/glypican in axon guidance is specific as the loss of *lon-2*/glypican, but not the loss of the other *C. elegans* glypican, *gpn-1*, enhances the defects of *sdn-1*/syndecan mutants. **(c)** Complete loss of *lon-2*/glypican enhances the axon guidance defects resulting from disrupted *slt-1*/Slit signaling in mutants for *slt-1*/Slit or its receptor *sax-3*/Robo, as well as in animals misexpressing *slt-1* in all body wall muscles (using a P*myo-3::slt-1* transgene). Data for wild type and *lon-2* are the same as in **(b)**. **(d)** Complete loss of *lon-2*/glypican does not enhance the AVM guidance defects of *unc-6*/netrin mutants, nor of mutants for its receptor *unc-40*/DCC, suggesting that *lon-2*/glypican functions in the same genetic pathway as *unc-6*/netrin. Data for wild type, and *lon-2* are the same as in **(b)**. **(e)** Loss of *sdn-1*/syndecan function does not enhance the defects of *slt-1*/Slit or sax-3/Robo mutants, but enhances the defects of *unc*-40/DCC mutants. Data for wild type, *sdn-1, slt-1, sax-3,* and *unc-40* same as in (b-d). Error bars are standard error of the proportion. Asterisks denote significant difference: *** $P \leq 0.001$,** $P \leq 0.01$, and * $P \leq 0.05$ (z-tests, P values were corrected by multiplying by the number of comparisons). ns, not significant.

## *lon-2*/glypican acts in the attractive and repulsive *unc-6*/netrin guidance pathways

Considering that AVM axon guidance occurs via the *unc-6/*netrin and *slt-1/*Slit pathways, mutations in genes such as *lon-2/*glypican and *sdn-1/*syndecan that affect AVM axon guidance may point towards interactions with either of these two guidance systems. Since the AVM axon guidance defects in *lon-2 sdn-1* double mutants are qualitatively similar to those of mutants lacking *unc-6*/netrin or *slt-1*/Slit, we determined how *lon-2*/glypican and *sdn-1*/syndecan impact *unc-6*/netrin and *slt-1*/Slit signaling. In animals that completely lack *slt*-1/Slit function, the complete loss of a gene functioning independently of *slt*-1/Slit is expected to enhance the AVM guidance defects, such as in the double null mutants *unc-*

*6/*netrin *slt-1*/Slit (see **Fig. 3.2**). We tested the interactions of *lon-2*/glypican with the *slt-1*/Slit pathway in AVM axon guidance, and found that the complete loss of

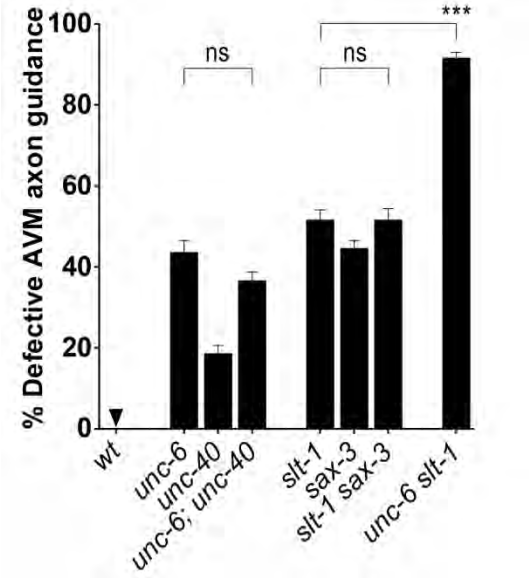


**Figure 3.2. Ventral guidance of the AVM axon.** Mutations in *unc-6*/netrin and *slt-1*/slit pathways result in partially redundant defects, as previously established by the Culotti and Bargmann labs (Hao et al 2001). Mutants displayed here never exhibit a dorsally migrated AVM axon. Error bars are standard error of the proportion. Asterisks denote significant difference: *** $P \leq 0.001$ (z-tests, P values were corrected by multiplying by the number of comparisons). ns, not significant.

*lon-2*/glypican enhanced a presumptive null allele of *slt-1*/Slit in *lon-2 slt-1* double mutants (**Fig. 3.1c**), suggesting that *lon-2*/glypican functions in a pathway separate from *slt-1*/Slit. Loss of *lon-2*/glypican also enhanced guidance defects when signaling through *sax-3*/Robo, the *slt-1*/Slit receptor, was disrupted in *lon-2 sax-3* double null mutants, providing further evidence that *lon-2*/glypican functions in a pathway separate from that of *slt-1*/Slit (**Fig. 3.1c**). As an additional method to investigate the impact of lacking *lon-2*/glypican function when *slt-1*/Slit signaling is perturbed, we used a transgene that ectopically expresses *slt-1*/Slit from both ventral and dorsal body wall muscles (using P*myo-3::slt-1*), and

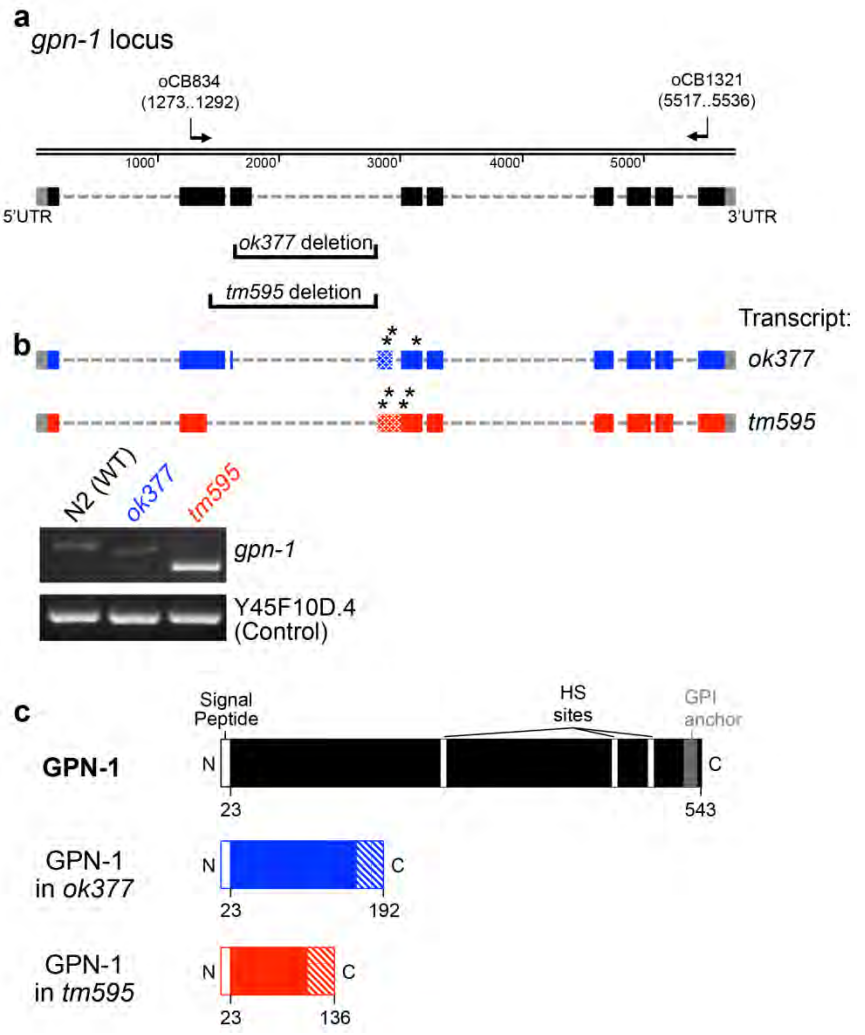


**Figure 3.3. *gpn-1(ok377)* and *gpn-1(tm595)* are likely null alleles.** (a) *gpn-1(ok377)* and *gpn-1(tm595)* are deletions (brackets) in the *gpn-1* locus. (b) RT-PCR using primers oCB834 and oCB1321 yields truncated products in *gpn-1(ok377)* and *gpn-1(tm595)*. Y45F10D.4 is a housekeeping gene used as an RT-PCR control (Hoogewijs et al 2008). Sequencing of the *gpn-1* RT-PCR products for *ok377* (blue) reveals that the transcript lacks most of exon 3 and has several in-frame Stop codons (*), as intronic sequence (hatch pattern) gets incorporated into the mature transcript. Sequencing of the *gpn-1* RT-PCR product for *tm595* (red) reveals that the transcript lacks exons 2 and 3, and has several in-frame Stop codons (*), as intronic sequence (hatch pattern) gets incorporated into the mature transcript. No alternatively spliced products were detected in the mutants *ok377* and *tm595*. (c) *gpn-1(ok377)* and *gpn-1(tm595)* are strong loss-of-function mutations, likely nulls, in which, at most, small truncated proteins would get produced.

misguides the axon of AVM (Yu et al 2002). Loss of *lon-2*/glypican enhanced the defects caused by *slt-1*/Slit misexpression (**Fig. 3.1c**), consistent with the above findings that *lon-2*/glypican mediates its axon guidance effects independently of *slt-1*/Slit.

The *unc-6*/netrin pathway functions independently of *slt-1*/Slit to guide AVM. To address whether *lon-2*/glypican functions in the *unc-6*/netrin axon guidance pathway, we examined the AVM axon in double mutants of *lon-2*/glypican and *unc-6*/netrin. In animals that completely lack *unc-6/*netrin function, the complete loss of a gene functioning in the same *unc-6/*netrin pathway is expected to not enhance the AVM guidance defects, such as in the double null mutants *unc-6*; *unc-40* (see **Fig. 3.2**). We found that the complete loss of *lon-2*/glypican did not enhance the guidance defects displayed by *unc-6*/netrin null mutants *ev400* (**Fig. 3.1d**). Given that loss of *lon-2* enhances the defects of other guidance mutants (see doubles with *sdn-1, slt-1, sax-3,* P*myo-3::slt-1,* in **Fig. 3.1b,c** and *sqv-5* in **Fig. 3.4**), the lack of enhancement when combined with the *unc-6* null mutation suggests that *lon-2*/glypican functions in the same pathway as *unc-6*/netrin.

Consistent with this idea, we also found that complete loss of *lon-2*/glypican did not enhance the AVM guidance defects of two null mutant alleles of the netrin receptor *unc-40*/DCC in the double mutants *unc-40; lon-2* (**Fig. 3.1d**), suggesting that *lon-2*/glypican functions in the same pathway as *unc-40*/DCC in AVM ventral

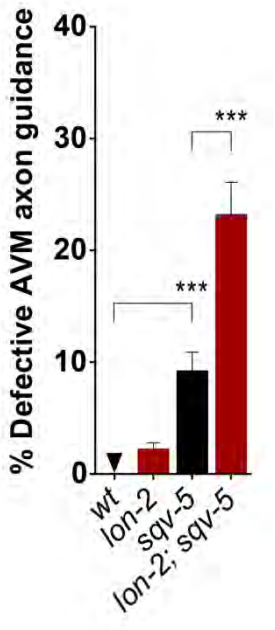


**Figure 3.4. Loss of *lon-2* enhances AVM guidance defects of *sqv-5*.** Loss of function of *sqv-5*, the gene coding for the chondroitin sulfate polymerase (Hwang et al., 2003), leads to defective AVM ventral axon guidance, which is significantly enhanced by loss of *lon-2* function. Error bars are standard error of the proportion. Asterisks denote significance: *** $P \leq 0.001$ (z-tests, P values were corrected by multiplying by the number of comparisons). (see also Table 3.6).

guidance. These observations raise the interesting possibility that *lon-2*/glypican may be the HSPG dedicated to modulate *unc-6*/netrin signaling through *unc-40/*DCC during axon guidance.

Since *lon-2*/glypican functions independently of *slt-1*/Slit (**Fig. 3.1c**) and partly separate from *sdn-1*/syndecan (**Fig. 3.1b**), we tested whether *sdn-1*/syndecan and *slt-1*/Slit function together to guide the axon of AVM. We found that defects in *slt-1 sdn-1* double null mutants were not enhanced compared to the single mutants (**Fig. 3.1e**), consistent with findings in *Drosophila* (Johnson et al 2004, Steigemann et al 2004) and *C. elegans* (Rhiner et al 2005). We also found that double null mutants for *sdn-1*/syndecan and the s*lt-1*/Slit receptor *sax-3*/Robo were not enhanced compared to the single mutants (**Fig. 3.1e**). Our results

support the notion that *sdn-1*/syndecan acts in the same genetic pathway as *slt-1*/Slit to guide AVM. Consistent with this, we found that the double null mutants for *sdn-1*/syndecan and the netrin receptor *unc-40*/DCC were enhanced, indicating that *sdn-1*/syndecan functions in a pathway separate from *unc-6*/netrin. The analysis of axon guidance in double mutants of *unc-6*/netrin and *sdn-1*/syndecan was precluded by their lethality (data not shown). Our results are consistent with the notion that *unc-6*/netrin and *sdn-1*/syndecan act in different pathways of axon guidance.

In addition to *unc-6*/netrin acting as an attractive cue for cells expressing the *unc-40*/DCC receptor in ventral guidance, *unc-6*/netrin also acts as a repulsive cue for cells expressing both the *unc-5*/UNC5 and *unc-40*/DCC receptors, which together mediate dorsal guidance away from *unc-6*/netrin (Chan et al 1996, Hedgecock et al 1990, Leung-Hagesteijn et al 1992). To address whether *lon-2*/glypican functions in *unc-6*/netrin-mediated repulsive guidance as well, we examined the dorsal migration of the distal tip cells (DTCs) and of the GABAergic motorneuron axons (Hedgecock et al 1990, Hedgecock et al 1987). We found that *lon-2*/glypican single null mutants are defective in dorsal DTC migrations

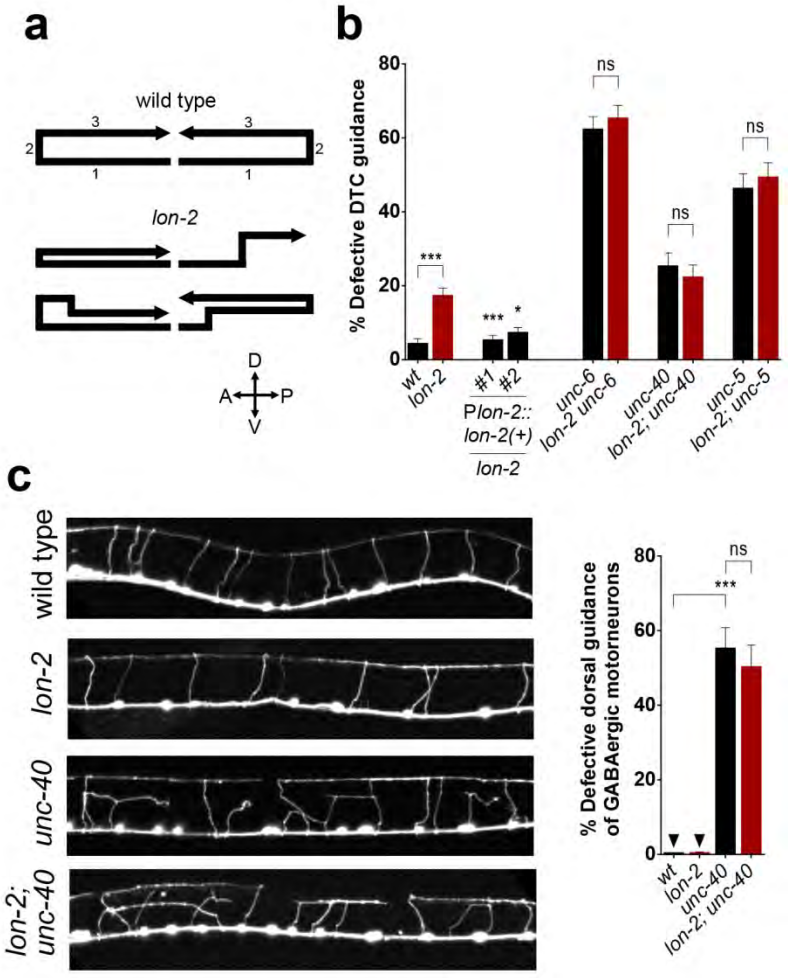
a
wild type
3
3
2
2
1
1
lon-2
D
A
P
V
b
% Defective DTC guidance
80
60
40
20
0
***
***
*
ns
ns
ns
wt
lon-2
#1
#2
Plon-2::
lon-2(+)
lon-2
unc-6
lon-2 unc-6
unc-40
lon-2; unc-40
unc-5
lon-2; unc-5
c
wild type
lon-2
unc-40
lon-2;
unc-40
% Defective dorsal guidance
of GABAergic motorneurons
80
60
40
20
0
***
ns
wt
lon-2
unc-40
lon-2; unc-40

**Figure 3.5. *lon-2*/glypican functions in the repulsive *unc-6*/netrin guidance pathway. (a)** Schematics of the migration path of the DTCs in the wild type, and examples of defective DTC migration in *lon-2*/glypican mutants (the anterior and the posterior DTCs exhibit similar defects). In wild-type animals, the DTCs migrate away from the vulva along the antero-posterior axis (1), then turn dorsally (2), and turn again to migrate towards the midbody region (3). Loss of *lon-2*/glypican leads to defective DTC guidance, including a failure to migrate dorsally, premature dorsal turning, or a failure to remain dorsal. **(b)** Quantification of the DTC migration defects in *lon-2*/glypican mutants and rescue by *lon-2(+)* (see **Table 3.7**). For each transgenic line, transgenic animals were compared to non-transgenic sibling controls. Complete loss of *lon-2*/glypican does not enhance the defects of the *unc-6*/netrin null mutants, nor of the null mutants for *unc-5*/UNC5 and *unc-40*/DCC, suggesting that *lon-2*/glypican functions in the same guidance pathway as *unc-5*/UNC5, *unc-40*/DCC and *unc-6*/netrin (see **Table 3.2)**. **(c)** The axons of the GABAergic motorneurons project dorsally from the ventral midline towards the dorsal nerve cord. *unc-6*/netrin, *unc*-5/UNC5, and unc-*40*/DCC are required for this dorsal guidance of GABAergic axons. Complete loss of *lon-2*/glypican does not enhance the partially penetrant defects of *unc-40*/DCC null mutants, suggesting that *lon-2*/glypican functions in the same pathway as *unc-40*/DCC and *unc-6*/netrin to guide axons dorsally (see **Table 3.3**). Error bars are standard error of the proportion. Asterisks denote significant difference: *** $P \leq 0.001$ and * $P \leq 0.05$ (z-tests, P values were corrected by multiplying by the number of comparisons). ns, not significant.

(**Fig. 3.5a,b**), and that the complete loss of *lon-2*/glypican did not enhance the dorsal DTC migration defects of *unc-6*/netrin, *unc-40*/DCC or *unc*-5/UNC5 null mutants (**Fig. 3.5b, Table 3.2**), indicating that *lon-2*/glypican functions in the *unc-6*/netrin-repulsive-guidance pathway as well. Similarly, complete loss of *lon-2*/glypican did not enhance the defects of *unc-40*/DCC mutants in the dorsal guidance of motorneuron axons (**Fig. 3.5c, Table 3.3**). Given that loss of *lon-2*/glypican enhances the motorneuron axon guidance defects of *sdn-1* mutants as shown in (Gysi et al 2013), *lon-2/*glypican plays a role in the dorsal guidance of motorneuron axons. The lack of enhancement of the defects in the dorsal guidance of motorneuron axons of *unc-40*/DCC mutants by loss of *lon-2*/glypican further supports that *lon-2*/glypican functions in the *unc-6*/netrin pathway

mediating dorsal guidance. Thus, *lon-2*/glypican may modulate *unc-6*/netrin signaling not only during attractive guidance, but also during repulsive guidance.

**_unc-6_/netrin signaling via the _unc-5_/UNC5 receptor requires _lon-2_/glypican**

To complement the above loss-of-function approach, we next used a gain-of-function strategy to test the model that *lon-2*/glypican functions in the *unc-6*/netrin signaling pathway. We focused on the axon of the PVM neuron instead of AVM, because it could reliably be identified (AVM cannot be distinguished from ALMR in these experiments). In wild-type animals, PVM, like AVM, expresses the receptor *unc-40*/DCC and its axon grows ventrally towards *unc-6*/netrin (**Fig. 3.6a**). In mutants lacking *unc-6*/netrin signaling, PVM axons that fail to extend

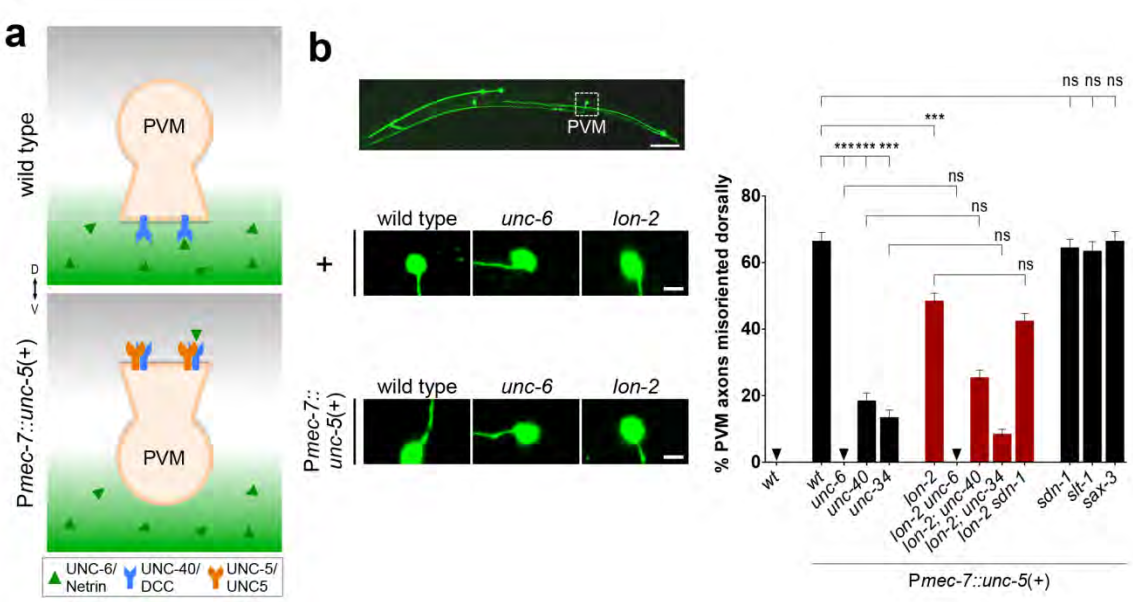

**Figure 3.6. *unc-6*/netrin signaling via the *unc-5*/UNC5 receptor requires *lon-2*/glypican.** **(a)** The axon of PVM normally migrates ventrally in the wild type, but it can be forced to migrate dorsally by misexpressing the repulsive receptor *unc-5*/UNC5. We quantified PVM since AVM could not be reliably identified (both AVM and neighboring ALMR axons project dorsally in P*mec-7::unc-5* transgenic animals.) **(b)** Upon misexpression of *unc-5*/UNC5 in PVM, using the transgene P*mec-7::unc-5*, the axon of PVM projects dorsally in an *unc-6*/netrin-, *unc-40*/DCC-, and *unc-34*/enabled-dependent manner. Loss of *lon-2*/glypican partially suppresses this forced dorsal migration, indicating that *unc-6*/netrin signaling depends on *lon-2*/glypican. Scale bar, 5 μm. Error bars are standard error of the proportion. Asterisks denote significant difference: *** $P \leq 0.001$ (z-tests, P values were corrected by multiplying by the number of comparisons). ns, not significant. (see **Table 3.4**). Wild type (without *evIs25*) is the same as in Fig. 3.1b).

ventrally, instead extend anteriorly (never dorsally, see **Table 3.4**). The PVM axon normally does not express the receptor *unc-5*/UNC5 that mediates repulsive guidance away from ventral *unc-6*/netrin (Leung-Hagesteijn et al 1992), but misexpression of the receptor *unc-5*/UNC5 (using transgene P*mec-7::unc-5* (Hamelin et al 1993)) in PVM forces its axon to extend dorsally in an *unc-6*/netrin- and *unc-40/*DCC-dependent manner (Hamelin et al 1993), **Fig. 3.6a,b**). We used this *unc-6*/netrin-dependent *unc-5*/UNC5-mediated abnormal dorsal migration to further investigate the function of *lon-2*/glypican in netrin signaling. By analyzing *lon-2*/glypican mutants carrying P*mec-7::unc-5*, we found that compete loss of *lon-2*/glypican function significantly suppressed the *unc-6*/netrin-dependent *unc-5*-mediated abnormal dorsal migration of the PVM axon, indicating that *unc-6*/netrin signaling is *lon-2*/glypican-dependent (**Fig. 3.6b**). In contrast, the complete loss of *sdn-1*/syndecan, of *slt-1*/Slit, or of *sax-3*/Robo function did not suppress these PVM abnormal dorsal migrations (**Fig. 3.6b,** see **Table 3.4**), highlighting the specificity of *lon-2*/glypican action on *unc-6*/netrin

signaling. As expected, *lon-2 sdn-1* double mutants lacking both *lon-2*/glypican and *sdn-1*/syndecan and expressing *unc*-5/UNC5 in PVM did not further suppress the abnormal *unc-5/*UNC-5-mediated dorsal migration of PVM as compared to *lon-2* single mutants, further supporting the specificity of *lon-2*/glypican on *unc-6*/netrin signaling.

To investigate whether *lon-2/*glypican functions in the same genetic pathway as known downstream mediators of *unc-6/*netrin signaling, we tested for genetic interactions between *lon-2*/glypican and *unc-34*/enabled. *unc-34*/enabled is a regulator of actin polymerization for axonal filopodia outgrowth (Chang et al 2006, Fleming et al 2010, Gertler et al 1995, Gertler et al 1990, Gitai et al 2003, Yu et al 2002), and its role in both *unc-6/*netrin and *slt-1*/*S*lit guidance pathways renders the analysis of genetic interactions in the context of normal AVM axon guidance challenging. Therefore, we used the *unc-6*/netrin-specific gain-of-function approach as above, where the dorsal migration of the PVM axon upon ectopic expression of *unc-5*/UNC5 is *unc-34*/enabled-dependent ((Colavita & Culotti 1998, Hamelin et al 1993); **Fig. 3.6b**). We asked whether loss of *lon-2*/glypican could enhance the extent of suppression of PVM dorsal migration induced by loss of *unc-34*/enabled. We found that the PVM dorsal migration was suppressed to the same degree in the double null mutants *lon-2; unc-34* and the single mutant *unc-34*/enabled upon expression of *unc-5*/UNC5 in PVM (P*mec-*

*7::unc-5*, **Fig. 3.6b**). These results support that *lon-2*/glypican functions with *unc-6*/netrin and *unc-34*/enabled during axon guidance.

**Epidermal *lon-2*/glypican functions in axon guidance**

The AVM growth cone extends along a basement membrane, located between the epidermis, referred to as hypodermis, and body wall muscles (Hedgecock et al 1987). *lon-2*/glypican is expressed in the hypodermis and the intestine (Gumienny et al 2007). We asked in which cell type *lon-2*/glypican needs to be produced to guide AVM. We found that wild-type *lon-2(+)* transgenes expressed under the heterologous epidermal promoters P*dpy-7* and P*elt-3* (that drive expression in the hypodermis underlying the AVM growth cone, hyp7), rescued *lon-2 slt-1* double mutants back to *slt-1* single mutant levels, as efficiently as when expressed under the endogenous promoter P*lon-2* (**Fig. 3.7a**, **Table 3.5**). Rescue was not observed when we expressed *lon-2*/glypican in other epidermal cells (seam cells, P*grd-10*), in the migrating neuron itself (P*mec-7*), in the intestine (P*elt-2*), or in body wall muscles (P*myo-3*) (**Fig. 3.7a, Table 3.5**). Our results suggest that *lon-2*/glypican is produced by the hypodermis underlying the growth cone of AVM to function in axon guidance.

***sdn-1*/syndecan functions cell autonomously**

We found that expressing wild-type copies of *sdn-1(+)* in the AVM neuron (using the heterologous promoter P*mec-7*) rescued axon defects of *lon-2 sdn-1* double

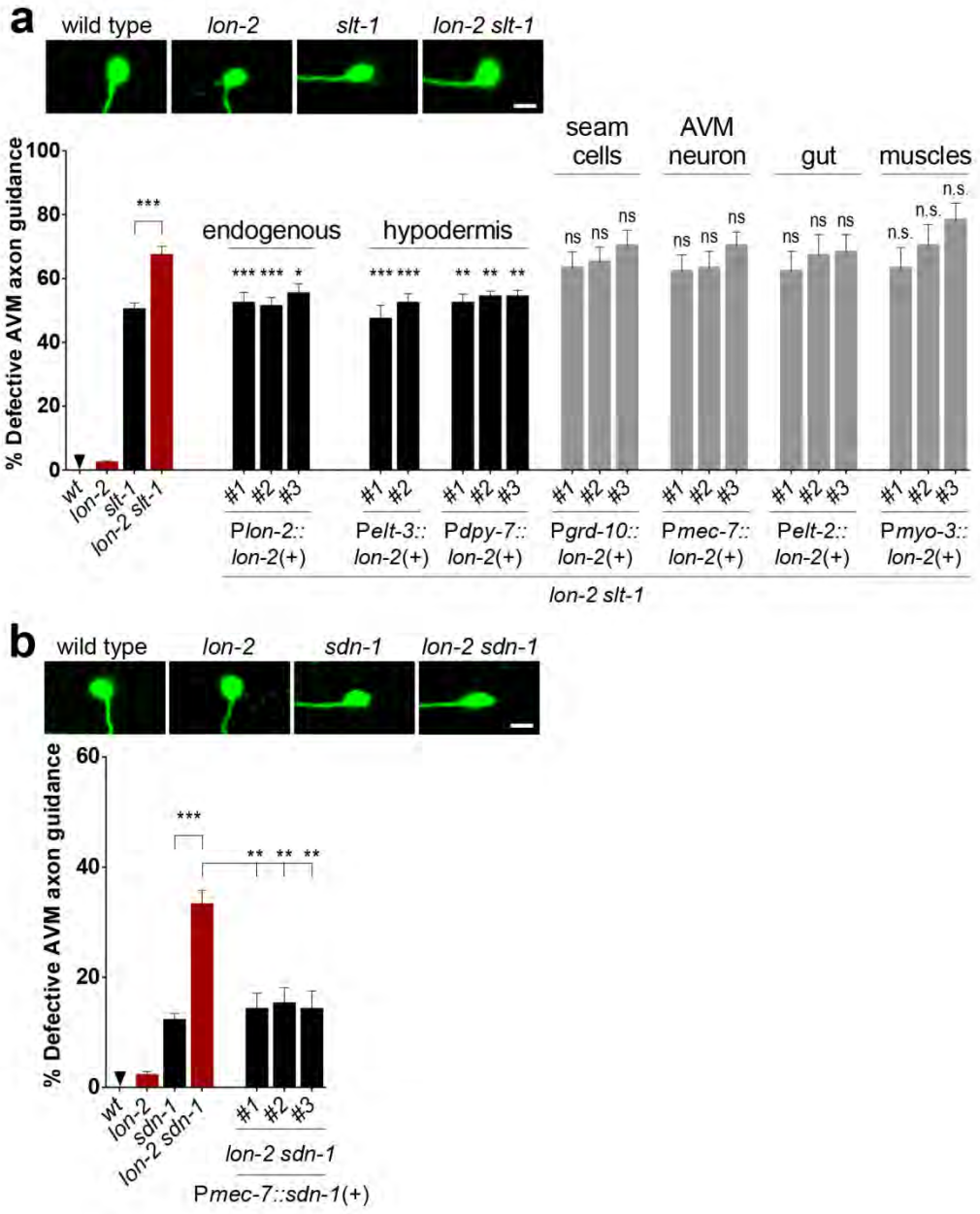
a
wild type
lon-2
slt-1
lon-2 slt-1
% Defective AVM axon guidance
seam cells
AVM neuron
gut
muscles
endogenous
hypodermis
wt
lon-2
slt-1
lon-2 slt-1
Plon-2:: lon-2(+)
Pelt-3:: lon-2(+)
Pdpy-7:: lon-2(+)
Pgrd-10:: lon-2(+)
Pmec-7:: lon-2(+)
Pelt-2:: lon-2(+)
Pmyo-3:: lon-2(+)
lon-2 slt-1
b
wild type
lon-2
sdn-1
lon-2 sdn-1
% Defective AVM axon guidance
wt
lon-2
sdn-1
lon-2 sdn-1
lon-2 sdn-1
Pmec-7::sdn-1(+)

**Figure 3.7. *lon-2*/glypican functions in the epidermal cells underlying the developing axon. (a)** Epidermal expression of *lon-2*/glypican is sufficient for function. Providing wild-type *lon-2(+)* in the hypodermis (under the heterologous hypodermal promoters P*dpy-7* and P*elt-3*) rescues the function of *lon-2* in the double mutants *lon-2 slt-1*, as it brings the defects down to the level of *slt-1* single mutants. In contrast, expression of *lon-2*(+) in other epidermal cells (seam cells), the migrating neuron AVM, the intestine, or the body wall muscles, fails to rescue the function of *lon-2*. For each rescued transgenic line, transgenic animals were compared to non-transgenic sibling controls (see **Tables 3.6 and 3.5**). Data for wild type, *lon-2, slt-1,* and *lon-2 slt-1* are the same as in Fig. 3.1b,c. **(b)** Expression of *sdn-1*/syndecan in the migrating neuron is sufficient for function. Providing wild-type copies of *sdn-1(+)* in AVM (expressed under the heterologous promoter P*mec*-7) rescues the axon guidance function of *sdn-1* in a *lon-2 sdn-1* double mutant. We assayed rescue of *sdn-1* function using the double mutant *lon-2 sdn-1* since it is easier to rescue defects that are 33% penetrant (as in the double *lon-2(e678) sdn-1(zh20)*) than to rescue defects that are 12% penetrant (as in the single mutant *sdn-1(zh20)*). For each transgenic line, transgenic animals were compared to non-transgenic sibling controls (see **Table 3.6**). Data for wild type*, lon-2, sdn-1,* and *lon-2 sdn-1* the same as in Fig. 3.1b-d**.** Scale bar, 5 μm. Error bars are standard error of the proportion. Asterisks denote significant difference: *** $P \leq 0.001$, ** $P \leq 0.01$ and * $P \leq 0.05$ (z-tests, P values were corrected by multiplying by the number of comparisons). ns, not significant.

mutants (**Fig. 3.7b, Table 3.6**). Accordingly, our examination of a transgene reporting *sdn-1*/syndecan expression (*sdn-1::gfp* ((Rhiner et al 2005)) revealed that *sdn-1*/syndecan is indeed expressed in the AVM neuron (**Fig. 3.8**), at the time of its ventral migration during the first larval stage. Thus, *sdn-1*/syndecan appears to function in the migrating neuron in the *slt-1*/Slit-*sax-3*/Robo guidance pathway, whereas *lon-2*/glypican appears to function non-autonomously, as it is produced by the hypodermis underlying the migrating neuron to modulate the *unc-6*/netrin guidance pathway. Consistent with this, we found that *sdn-1(+)*

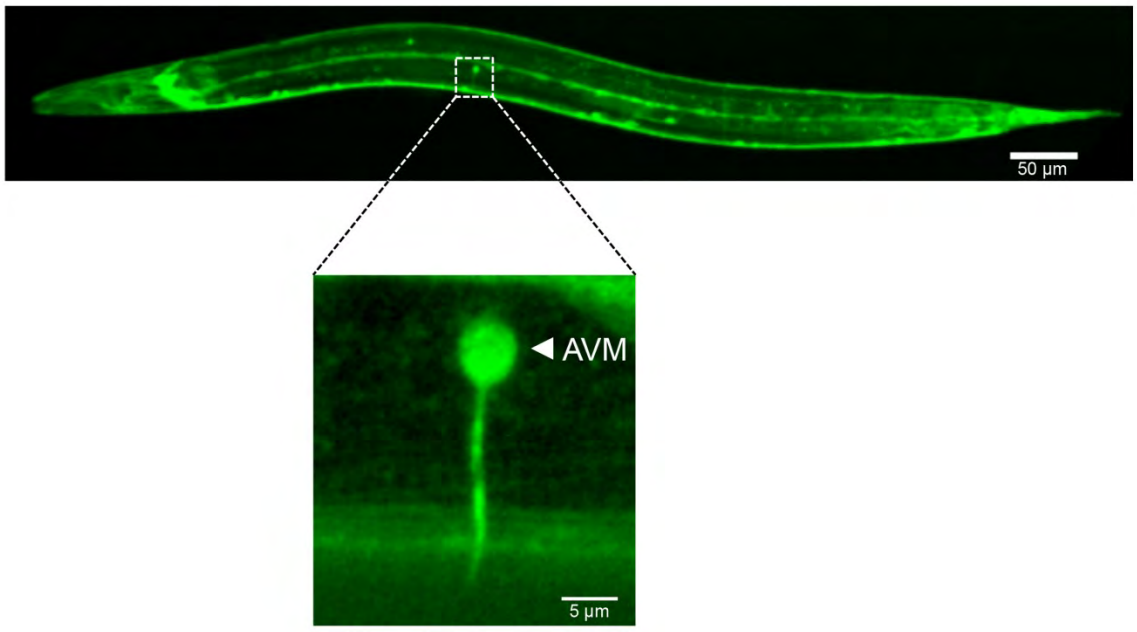


**Figure 3.8. SDN-1::GFP expression in the neuron AVM.** Using the translational fusion *sdn-1::gfp (opIs171)*, we found that SDN-1::GFP is expressed in hypodermal cells and neurons, as previously reported (Rhiner et al 2005). Importantly, we observed expression in the AVM neuron, including during the L1 stage, when the AVM growth cone migrates ventrally. This expression pattern is consistent with our finding that *sdn-1*/syndecan expression in AVM (P*mec-7::sdn-1*) rescues the defects of *sdn-1* mutants (Fig. 3.7c), supporting a cell-autonomous role for *sdn-1*/syndecan in AVM.

cannot replace the function of *lon-2*/glypican; expressing *sdn-1*/syndecan in either the cells that normally express *lon-2*/glypican (using P*lon-2::sdn-1*) or the migrating neuron itself (P*mec-7::sdn-1*) did not rescue the loss of *lon-2*/glypican **(Fig. 3.9)**, supporting that *lon-2*/glypican and *sdn-1*/syndecan have specific roles in axon guidance.

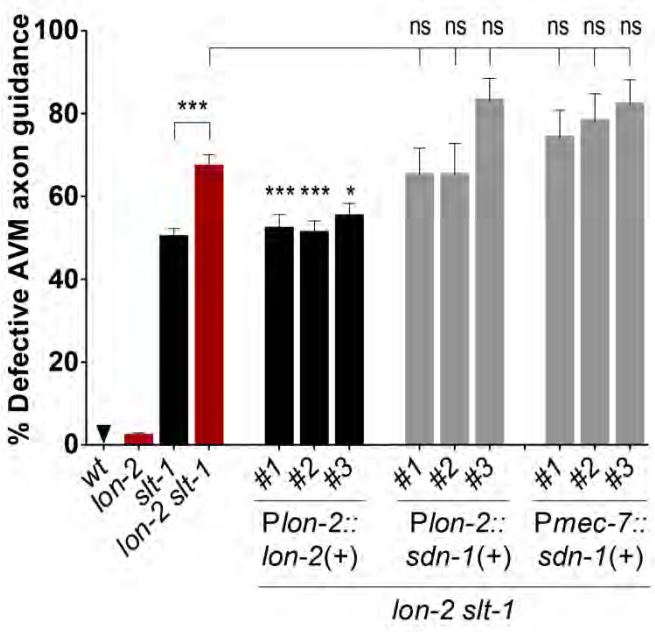


**Figure 3.9. *lon*-2/glypican cannot be replaced by *sdn-1*/syndecan.** *lon-2 slt-1* double mutants exhibit enhanced AVM guidance defects as compared to *slt-1* single mutants. The defects of the double mutants can be rescued back down to *slt-1* single mutant levels with expression of wild-type P*lon-2::lon-2*(+). In contrast, expression of *sdn-1(+)* where *lon-2*/glypican is normally expressed (using the P*lon-2* promoter) or in the AVM neuron (using the heterologous promoter P*mec-7*), cannot rescue the axon guidance defects of *lon-2 slt-1* double mutants. Data for wild type, *lon-2, slt-1, lon-2 slt-1,* and P*lon-2::lon-2* in *lon-2 slt-1* are as in Fig. 3.1b-c, and Fig. 3.7a. *** $P \leq 0.001$, * $P \leq 0.05$. (z-tests, P values were corrected by multiplying by the number of comparisons) (see Tables 3.6 and 3.5).

## LON-2/glypican lacking its heparan sulfate chain attachment sites functions in axon guidance

Glypicans are composed of a core protein moiety with covalently linked heparan sulfate (HS) chains attached via a tetrasaccharide linker at specific Ser residues

(Bülow & Hobert 2006); **Fig. 3.10a**). Prior studies on the role of HSPGs in other developmental pathways indicate that both the identity of the HSPG core proteins and the heterogeneity of their HS chains modified by epimerization and sulfations (Bülow & Hobert 2006) contribute to the specificity of the interactions between particular HSPGs and the proteins that they bind (Bülow & Hobert 2006, Van Vactor et al 2006, Xu & Esko 2014).

To address the importance of the HS chains linked to LON-2/glypican during axon guidance, we tested whether a mutated form of LON-2/glypican lacking its HS chains could still function in axon guidance. For this experiment, the three Ser residues serving as HS chain attachment sites were mutated to Ala residues, generating the mutant LON-2ΔGAG (Taneja-Bageshwar & Gumienny 2012). Western blot analysis confirmed that LON-2ΔGAG severely reduced HS chains associated with LON-2, in both worms and S2 cells (**Fig. 3.10b** and **Fig. 3.11**). We then expressed LON-2ΔGAG under the P*lon-2* endogenous promoter, and found that the AVM guidance defects of *lon-2 slt-1* double mutants were rescued back to the level of *slt-1* single mutants (**Fig. 3.10c**). Similarly, the DTC migration defects of *lon-2*/glypican mutants were rescued by LON-2ΔGAG expression (**Fig. 3.10d, Table 3.7**). Our results indicate that LON-2/glypican devoid of its HS-chain attachment sites can function in *unc-6*/netrin-mediated guidance, suggesting that the core protein is the critical part of LON-2/glypican for its function in *unc-6*/netrin-mediated guidance of cell and axon migrations.

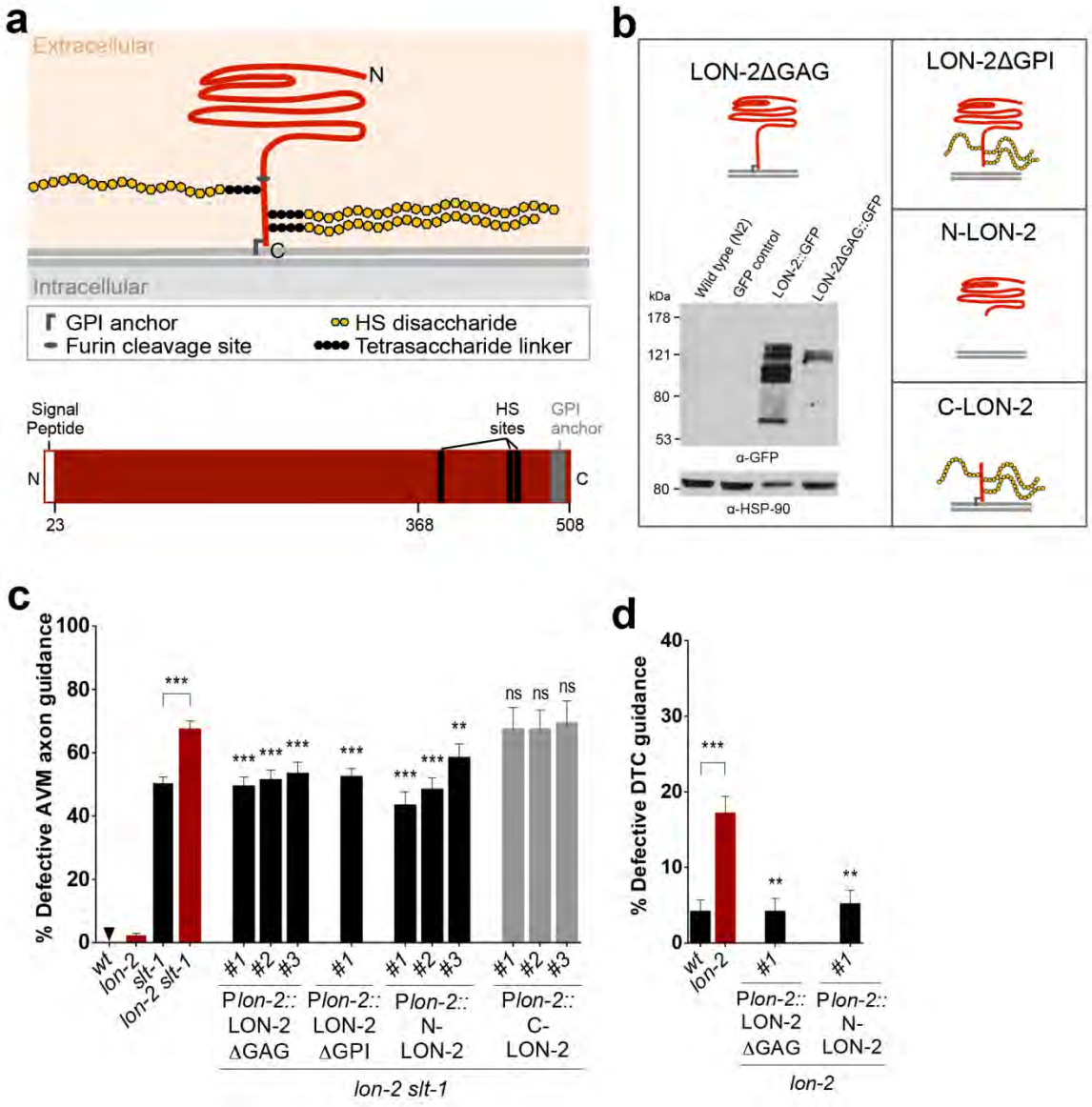
a
Extracellular
N
C
Intracellular
GPI anchor
Furin cleavage site
HS disaccharide
Tetrasaccharide linker
Signal Peptide
HS sites
GPI anchor
N
C
23
368
508
b
LON-2ΔGAG
LON-2ΔGPI
N-LON-2
C-LON-2
Wild type (N2)
GFP control
LON-2::GFP
LON-2ΔGAG::GFP
kDa
178
121
80
53
α-GFP
80
α-HSP-90
c
% Defective AVM axon guidance
wt
lon-2
slt-1
lon-2 slt-1
#1 #2 #3
Plon-2:: LON-2 ΔGAG
Plon-2:: LON-2 ΔGPI
Plon-2:: N-LON-2
Plon-2:: C-LON-2
lon-2 slt-1
ns
d
% Defective DTC guidance
wt
lon-2
Plon-2:: LON-2 ΔGAG
Plon-2:: N-LON-2
lon-2

**Figure 3.10. A secreted form of LON-2/glypican that lacks the heparan sulfate chain attachments is functional in axon guidance. (a)** The HSPG LON-2/glypican is composed of a core protein and three HS chains. The core protein is predicted to fold into a globular domain on its N-terminal region and to be GPI-anchored. **(b)** Schematics of the engineered forms of LON-2 that we used: LON-2ΔGAG, where the HS chain attachment sites are mutated; LON-2ΔGPI, where the GPI anchor is deleted; N-LON-2, where the C-terminus is deleted; and C-LON-2, where the N-terminal globular domain is deleted. Western blot analysis of protein extracts of worms expressing LON-2::GFP or LON-2ΔGAG::GFP confirms that deleting the HS attachment sites on LON-2 affects HS addition on LON-2. Protein extracts from wild type (N2) and an unrelated GFP strain (*lqIs4*) are negative controls. **(c)** A form of LON-2/glypican lacking HS chain attachment sites (LON-2ΔGAG) functions in axon guidance. LON-2ΔGAG rescues the AVM guidance defects of double mutants *lon-2 slt-1* back to the level of *slt-1* single mutants. Secreted globular LON-2/glypican is functional in axon guidance. LON-2/glypican was engineered to be secreted by deleting its GPI anchor (LON-2ΔGPI), or by deleting the C-terminus, thus lacking the GPI anchor and the HS attachment sites (N-LON-2). Both LON-2ΔGPI and N-LON-2 function in axon guidance, as assayed by their ability to rescue axon guidance defects of *lon-2 slt-1* back down to the level of *slt-1* single mutants. In contrast, a form of LON-2/glypican containing its C-terminus including the three HS attachment sites, but lacking its N-terminal globular domain (C-LON-2), is not functional (see **Tables 3.6 and 3.5**), indicating that the N-terminal globular domain of the core protein is key to the function of LON-2/glypican in axon guidance. For each rescued transgenic line, transgenic animals were compared to non-transgenic sibling controls (see **Tables 3.6 and 3.5**). Data for wild type, *lon-2, slt-1,* and *lon-2 slt-1* are the same as in Fig. 3.1b,c. **(d)** A form of LON-2/glypican lacking HS chain attachment sites is functional in DTC guidance. The DTC migration of *lon-2* mutants carrying the transgene P*lon-2::*LON-2ΔGAG is rescued back to wild-type levels. Secreted N-terminus globular LON-2/glypican (N-LON-2) is functional in DTC guidance, as DTC guidance defects of *lon-2* mutants are rescued by N-LON-2. Transgenic animals were compared to non-transgenic sibling controls (see **Table 3.7**). Data for wild type and *lon-2* the same as in Fig. 3.5b. Error bars are standard error of the proportion. Asterisks denote significant difference: *** $P \leq 0.001$, ** $P \leq 0.01$ (z-tests, P values were corrected by multiplying by the number of comparisons).

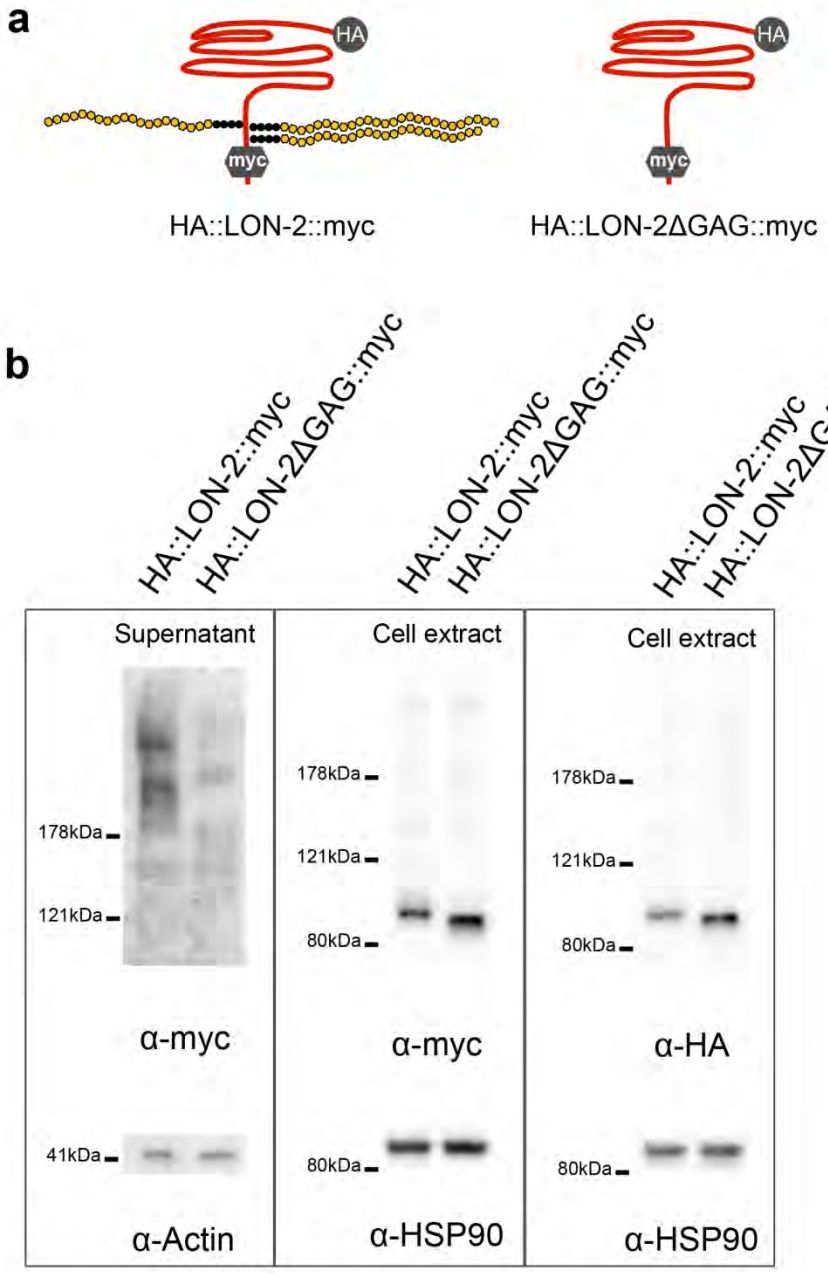
a
HA
myc
HA::LON-2::myc
HA
myc
HA::LON-2ΔGAG::myc
b
HA::LON-2::myc
HA::LON-2ΔGAG::myc
HA::LON-2::myc
HA::LON-2ΔGAG::myc
HA::LON-2::myc
HA::LON-2ΔGAG::myc
Supernatant
178kDa
121kDa
α-myc
41kDa
α-Actin
Cell extract
178kDa
121kDa
80kDa
α-myc
80kDa
α-HSP90
Cell extract
178kDa
121kDa
80kDa
α-HA
80kDa
α-HSP90

**Figure 3.11. Detection of LON-2 and LON-2ΔGAG in the supernatant and cell extracts of S2 cell cultures by western blot analysis.** (a) Diagram of LON-2/glypican variants expressed in S2 cells, HA::LON-2::myc and HA::LON-2ΔGAG::myc, in which the three HS attachment sites were mutated from Ser to Ala residues. The core protein of LON-2/glypican is red, and the heparan sulfate chains (HS) are yellow. (b) In the supernatant of cells expressing HA::LON-2::myc, high molecular weight species were detected with the anti-myc antibody, which likely corresponds to full length HA::LON-2::myc with HS chains attached. In contrast, the species detected in the supernatant of HA::LON-2ΔGAG::myc-expressing cells are smaller and fainter, indicating that HA::LON-2ΔGAG::myc indeed affects the synthesis of HS chains onto the LON-2/glypican core protein. No signal was detected with the anti-HA antibody in the supernatants, likely due to technical limitations. In the cell extracts from HA::LON-2::myc-expressing cells, the main species runs at ~90 kDa, and it is detected with both the anti-myc and anti-HA antibodies, suggesting that it is full length. This signal likely corresponds to the LON-2/glypican core protein devoid of HS chains, as it runs as a tight band. The slight mobility shift in cell extracts of HA::LON-2ΔGAG::myc-expressing cells compared to HA::LON-2::myc might correspond to a difference of mass and isoelectric point between HA::LON-2::myc and HA::LON-2ΔGAG::myc. Anti-actin and anti-HSP90 antibodies were used as loading controls. Representative blots of more than four independent repeats.

## LON-2/glypican associates with cells expressing UNC-40/DCC

Our above observations provide evidence that the HSPG *lon-2*/glypican functions in the same genetic pathway as *unc-6*/netrin to guide migrating axons. It has been shown in several models that HSPGs play multifaceted roles across various signaling pathways, such as facilitating ligand-receptor interactions, transporting morphogens, as well as localizing and stabilizing ligands (Lander & Selleck 2000, Yan & Lin 2009). We asked if the LON-2/glypican molecules might interact with either UNC-6/netrin or its receptor UNC-40/DCC, suggesting a potential mechanism of action for LON-2/glypican in *unc-6*/netrin-mediated guidance. To test these interactions, we generated epitope-tagged versions of LON-2/glypican, UNC-6/netrin, and UNC-40/DCC proteins, with HA, superfolder-GFP (SfGFP), and FLAG, respectively (**Fig. 3.12a**) and used cell-mixing experiments. We

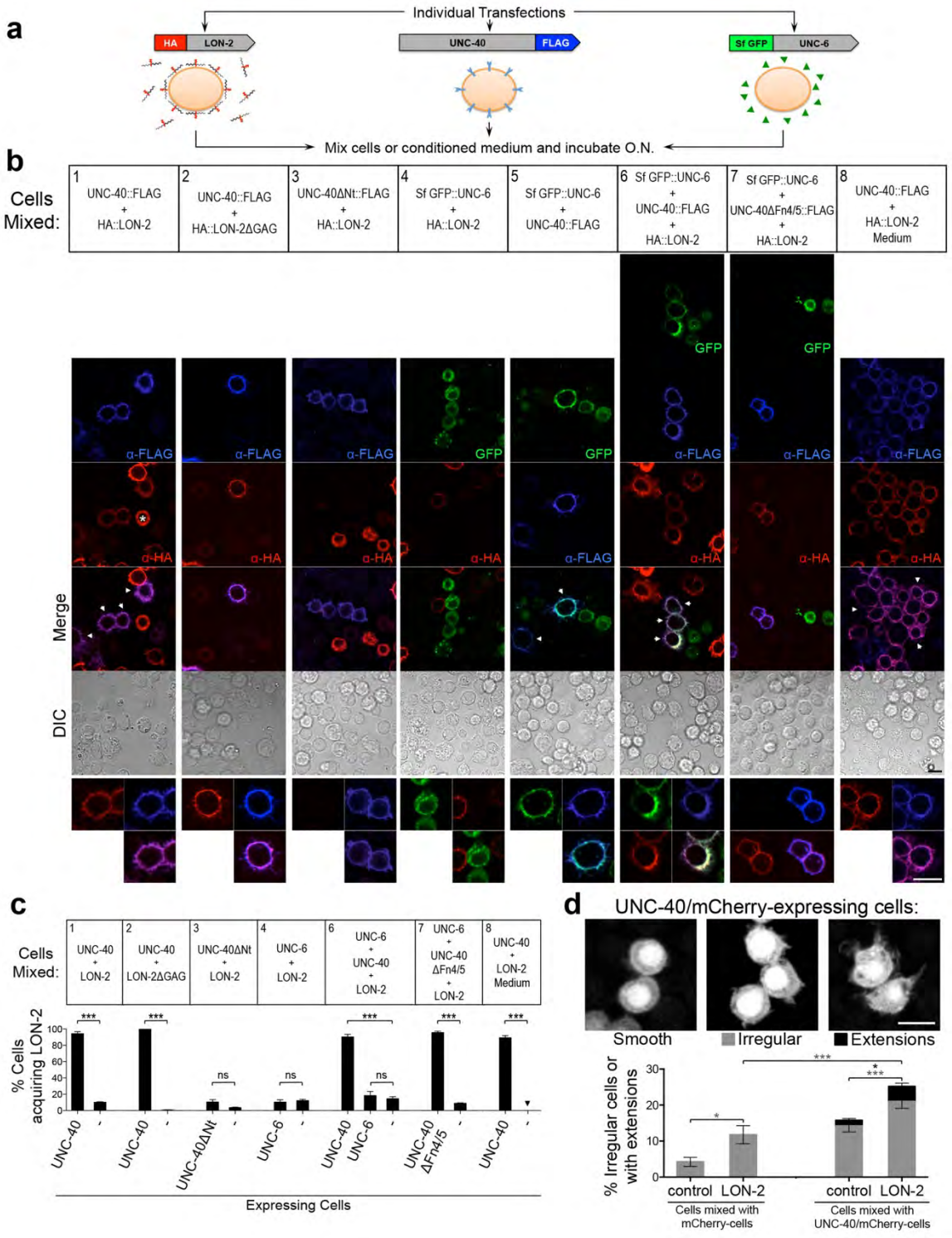
a
Individual Transfections
HA
LON-2
UNC-40
FLAG
Sf GFP
UNC-6
Mix cells or conditioned medium and incubate O.N.
b
Cells Mixed:
1 UNC-40::FLAG + HA::LON-2
2 UNC-40::FLAG + HA::LON-2ΔGAG
3 UNC-40ΔNt::FLAG + HA::LON-2
4 Sf GFP::UNC-6 + HA::LON-2
5 Sf GFP::UNC-6 + UNC-40::FLAG
6 Sf GFP::UNC-6 + UNC-40::FLAG + HA::LON-2
7 Sf GFP::UNC-6 + UNC-40ΔFn4/5::FLAG + HA::LON-2
8 UNC-40::FLAG + HA::LON-2 Medium
α-FLAG
α-HA
GFP
Merge
DIC
c
Cells Mixed:
1 UNC-40 + LON-2
2 UNC-40 + LON-2ΔGAG
3 UNC-40ΔNt + LON-2
4 UNC-6 + LON-2
6 UNC-6 + UNC-40 + LON-2
7 UNC-6 + UNC-40 ΔFn4/5 + LON-2
8 UNC-40 + LON-2 Medium
% Cells acquiring LON-2
***
ns
UNC-40
UNC-40ΔNt
UNC-6
UNC-40 UNC-6
UNC-40 ΔFn4/5
Expressing Cells
d
UNC-40/mCherry-expressing cells:
Smooth
Irregular
Extensions
% Irregular cells or with extensions
control
LON-2
Cells mixed with mCherry-cells
Cells mixed with UNC-40/mCherry-cells

**Figure 3.12. LON-2/glypican associates with UNC-40/DCC-expressing cells.**
**(a)** Experimental design. Each construct was individually and transiently transfected in S2 cells. After 2 days, cells from independent single transfections were mixed and incubated overnight, and then immunostained for the corresponding tags. HA::LON-2-conditioned medium was mixed with UNC-40::FLAG expressing cells. **(b)** HA::LON-2 is released from cells that produce it and associates with UNC-40-expressing cells. HA::LON-2 fills the cytoplasm of the cells that produce it (indicated by an asterisk, see also **Fig. 3.14**). Notably, HA::LON-2 is observed decorating the outline of UNC-40::FLAG expressing cells (experiments 1,6,7,8). HA::LON-2ΔGAG also associates with UNC-40::FLAG expressing cells (experiment 2). Cells expressing UNC-40ΔNt::FLAG that lacks the extracellular domain do not have HA::LON-2 signal, indicating that the association of LON-2 with UNC-40-expressing cells requires the extracellular domain of UNC-40 (experiment 3). HA::LON-2 conditioned medium contains HA::LON-2 that associates with UNC-40::FLAG expressing cells, indicating that HA::LON-2 is released from the cells that produce into a diffusible form that interacts with UNC-40::FLAG cells (experiment 8). HA::LON-2 does not associate with cells expressing SfGFP::UNC-6 (experiments 4,6,7), or with untransfected cells. UNC-40-FLAG expressing cells can simultaneously associate with HA::LON-2 and SfGFP::UNC-6 (experiment 6). HA::LON-2 associates with cells expressing a mutant form of UNC-40/DCC that is unable bind SfGFP::UNC-6, as it lacks the Fn4/5 UNC-6 binding domains (UNC-40ΔFn4/5::FLAG; experiment 7). Scale bars, 10 μm. **(c)** Quantification of the association of HA::LON-2 (from expressing cells, from medium of expressing cells, or from cells expressing HA::LON-2ΔGAG) with cells expressing UNC-40::FLAG, UNC-40ΔNt::FLAG, SfGFP::UNC-6, or UNC-40ΔFn4/5::FLAG, and untransfected. Ten different optical fields containing ~300 cells from three independent experiments were quantified and averaged. **(d)** Cells expressing UNC-40::FLAG can display irregular morphology, which is enhanced by the presence of HA::LON-2. Images of the different morphologies displayed by UNC-40::FLAG-expressing cells: with a smooth edge, with an irregular edge, or with membrane extensions. The morphology of S2 cells expressing mCherry alone or co-expressing UNC-40::FLAG and mCherry, that were mixed with control untransfected cells or with HA::LON-2-expressing cells, were quantified for irregular edges (grey bars) or membrane extensions (black bars). A higher percentage of UNC-40::FLAG expressing cells show membrane extensions or irregular edges when mixed with HA::LON-2-expressing cells, as compared to when they are mixed with control mCherry cells.
Error bars are standard error of the mean. Asterisks denote significant difference: *** $P \leq 0.001$, * $P \leq 0.05$. ns, not significant. In **(d)**, significant differences in irregular cell shape are indicated by grey asterisks, and significant difference in membrane extensions is indicated by the black asterisk.

independently expressed each of these labeled proteins in separate populations of *Drosophila* S2 cells for 2 days, then co-cultured them overnight, and detected the tagged proteins by western blot analysis (see **Figure 3.13**) and by immunostaining (**Fig. 3.12a**).

We observed that the HA::LON-2 signal filled the cytoplasm of HA::LON-2 producing cells (indicated by white asterisks in **Fig. 3.12b** experiment 1 and **Fig. 3.14**). Notably, HA::LON-2 was also found decorating the outline of UNC-40::FLAG expressing cells (**Fig. 3.12b,c** experiments 1,6,7,8). This observation suggests that LON-2/glypican is released from the cells that produce it, diffuses in the extracellular medium, and associates with UNC-40/DCC expressing cells. In contrast, HA::LON-2/glypican did not bind to cells expressing SfGFP::UNC-6 (**Fig. 3.12b,c** experiments 4,6,7), nor to cells expressing an unrelated type I transmembrane receptor, Evi (see **Fig. 3.15**), nor to untransfected cells (**Fig. 3.12b,c** experiments 1-8). Furthermore, we found that another HSPG, SDN-1/syndecan, did not bind UNC-40-expressing cells (see **Fig. 3.15**). These findings provide evidence for a specific interaction between LON-2/glypican and UNC-40-expressing cells.

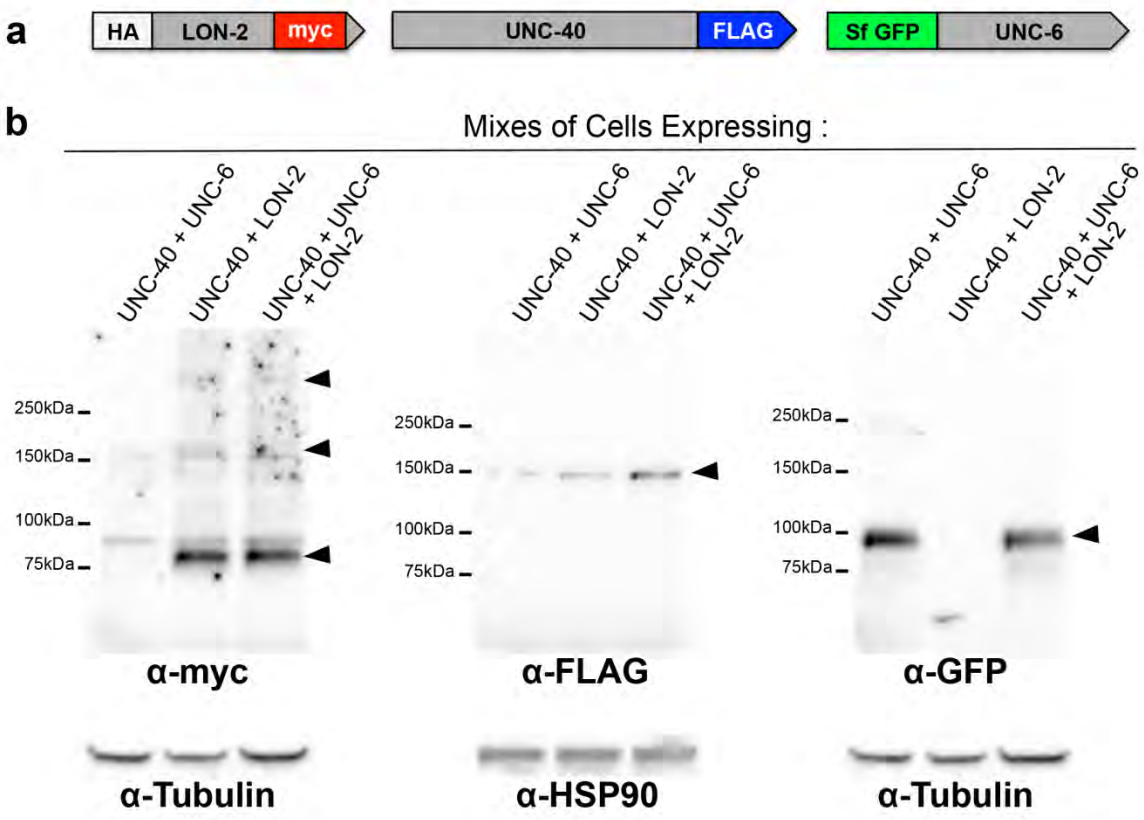


**Figure 3.13. Detection of LON-2, UNC-40 and UNC-6 expression in S2 cells by Western blot analysis.** (a) Diagram of constructs used to express these proteins in S2 cells, showing the tags used to detect them. (b) Western blots for detection of HA::LON-2::myc, UNC-40::FLAG and SfGFP::UNC-6. Constructs were individually and transiently transfected in S2 cells. Two days later, cells from single transfections were mixed and incubated overnight. Cells were harvested and combined with their corresponding supernatant from each of these cell mixes. Samples of each cell mix were split into 3 to run 3 parallel western blots and detect the proteins. As shown in Figure 3.11, a main species (~90 kDa, bottom arrow) and high molecular weight species (top arrows) are detected with the anti-myc antibody against HA::LON-2::myc. UNC-40::FLAG and SfGFP::UNC-6 run at ~156 kDa and ~99 kDa as expected, respectively. Representative blots of more than four independent repeats.

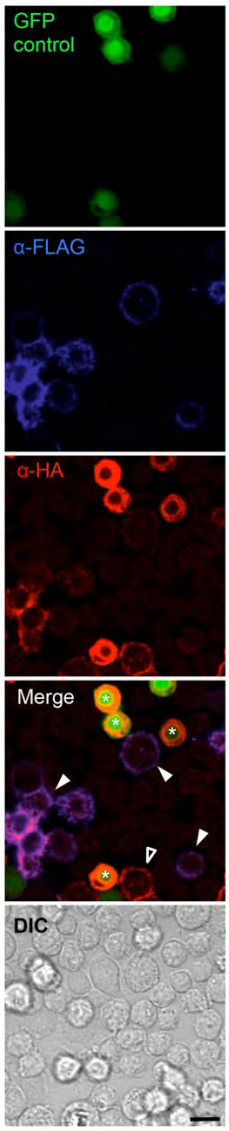


**Figure 3.14. HA::LON-2 is released from cells (co-transfected with GFP) and associates with cells expressing UNC-40::FLAG.** In order to distinguish HA::LON-2-*producing* cells from HA::LON-2-*acquiring* cells, two separate populations of cells were transfected. One population of S2 cells was transfected with UNC-40::FLAG. A second population of S2 cells was simultaneously transfected with both GFP and HA::LON-2. Two days later, the two populations of cells were mixed, incubated overnight, and immunostained with anti-HA and anti-FLAG antibodies, as described for Fig. 3.12. In GFP expressing cells (indicated by white asterisks), which had also been transfected with HA::LON-2, the HA::LON-2 signal was observed filling the cytoplasm. HA::LON-2 was also observed decorating the outline of UNC-40-expressing cells (indicated by white triangles, see Fig. 3.12), supporting that LON-2/glypican associates with UNC-40-expressing cells. Occasionally, HA::LON-2 was observed on cells in which no UNC-40::FLAG was detected (indicated by the empty triangle). Scale bar 10 μm.

We tested whether the HS chains of LON-2/glypican were necessary for its association with UNC-40-expressing cells. We used a mutated form of LON-2/glypican lacking its three HS chain attachment sites, HA::LON-2ΔGAG (Taneja-Bageshwar & Gumienny 2012), see **Fig. 3.11**). Western blot analysis confirmed that LON-2ΔGAG severely reduced HS chains associated with LON-2/glypican (**Fig. 3.11**). We found that LON-2ΔGAG associated with UNC-40/DCC-expressing cells (**Fig. 3.12b,c** experiment 2), suggesting that the association of LON-2/glypican with UNC-40/DCC-expressing cells is HS-chains independent.

The HA::LON-2 signal outlined the UNC-40/DCC expressing cells (**Fig. 3.12b**, experiments 1,6,7,8) suggesting a potential interaction at the cell surface. To further support this idea, we asked whether LON-2/glypican would associate with cells expressing a mutated form of UNC-40/DCC that lacks the extracellular domain, and contains only the intracellular and transmembrane domains (UNC-40ΔNt::FLAG). We found that HA::LON-2 did not associate with cells expressing the UNC-40ΔNt::FLAG (**Fig. 3.12b,c** experiment 3), indicating that the extracellular domain of UNC-40/DCC is required for LON-2/glypican to associate,

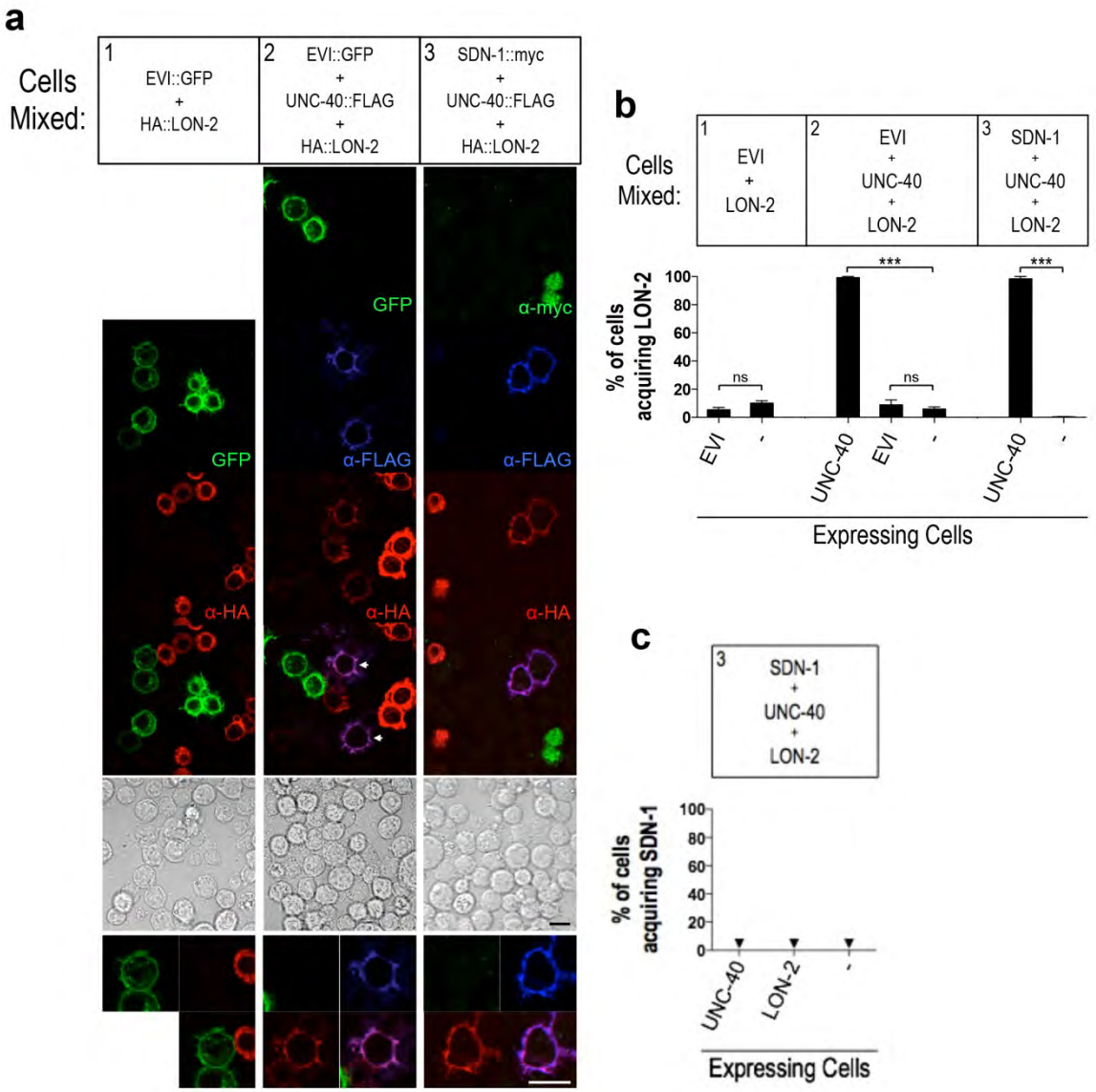
a
Cells Mixed:
1 EVI::GFP + HA::LON-2
2 EVI::GFP + UNC-40::FLAG + HA::LON-2
3 SDN-1::myc + UNC-40::FLAG + HA::LON-2
GFP
α-myc
GFP
α-FLAG
α-FLAG
α-HA
α-HA
α-HA
b
Cells Mixed:
1 EVI + LON-2
2 EVI + UNC-40 + LON-2
3 SDN-1 + UNC-40 + LON-2
% of cells acquiring LON-2
100
80
60
40
20
0
***
***
ns
ns
EVI
-
UNC-40
EVI
-
UNC-40
-
Expressing Cells
c
3 SDN-1 + UNC-40 + LON-2
% of cells acquiring SDN-1
100
80
60
40
20
0
UNC-40
LON-2
-
Expressing Cells

**Figure 3.15. Controls for the specificity of the association of LON-2/glypican with UNC-40-expressing cells.** (a) Experiments 1 and 2 show that HA::LON-2 does not associate with cells expressing the unrelated *Drosophila* type I transmembrane receptor Evi. Evi-expressing cells were mixed with cells expressing LON-2/glypican and/or UNC-40/DCC. As shown in experiment 2 and Fig. 3.12b,c, while LON-2/glypican associates with cells expressing UNC-40/DCC, LON-2/glypican does not associate with cells expressing Evi::GFP (experiments 1,2). Experiment 3 shows that SDN-1::myc/syndecan, another heparan sulfate proteoglycan, does not associate with UNC-40/DCC expressing cells. This SDN-1::myc was engineered to be secreted as it lacks its transmembrane and intracellular C-terminal domains. These results indicate that the association of LON-2/glypican with UNC-40/DCC expressing cells is specific, and not a general feature of any HSPG. (b) Quantification of the association of HA::LON-2 with cells expressing UNC-40::FLAG, Evi::GFP, and untransfected cells. Ten different optical fields containing ~300 cells from three independent experiments were quantified and averaged. Error bars are standard error of the mean. Asterisks denote significant difference: *** $P \leq 0.001$ (*t*-test versus untransfected cells). ns, not significant. (c) Quantification of the association of SDN-1::myc with cells expressing UNC-40::FLAG, HA::LON-2, and untransfected cells. Ten different optical fields containing ~300 cells from three independent experiments were quantified.

as would be predicted if LON-2/glypican and UNC-40/DCC interact, directly or indirectly, at the cell surface.

Interestingly, HA::LON-2 was absent from cells expressing SfGFP::UNC-6 (**Fig. 3.12b,c** experiments 4,6,7), indicating that while LON-2/glypican interacts with cells expressing UNC-40/DCC, it does not bind to UNC-6/netrin-expressing cells in this assay. Moreover, the presence of SfGFP::UNC-6 did not reduce the ability of HA::LON-2 to associate with UNC-40/DCC-expressing cells in experiments where the three singly-transfected cell populations were mixed (**Fig. 3.12b,c** experiment 6). These results suggest that if LON-2/glypican interacted directly or indirectly with UNC-40/DCC, then the interactions of LON-2/glypican and UNC-6/netrin would occur with different regions of UNC-40/DCC. Consistent with this

possibility, we found that LON-2/glypican still associated with cells expressing UNC-40ΔFn4/5::FLAG, a mutated form of UNC-40/DCC that lacks the UNC-6/netrin-binding sites (FnIII domains 4 and 5) ((Wang et al 2014, Xu et al 2014); **Fig. 3.12b,c** experiment 7). Our results indicate that for LON-2/glypican to associate with UNC-40/DCC-expressing cells, the FnIII domains 4 and 5 of UNC-40/DCC are dispensable and UNC-6/netrin does not need to be bound to UNC-40/DCC.

**LON-2/glypican increases membrane outgrowths triggered by UNC-40/DCC**

Previous work has suggested that overexpression of DCC in cells overactivates DCC downstream signaling pathways, leading to cytoskeletal rearrangements that result in increased membrane extensions and cell surface area (Shekarabi & Kennedy 2002). Similarly, expression of UNC-40/DCC leads to changes in cellular morphology in our cell assays (**Fig. 3.12d**). To test whether the association of LON-2/glypican with UNC-40/DCC-expressing cells results in an activation of signaling downstream of UNC-40/DCC, we examined the impact of LON-2/glypican on the morphology of UNC-40/DCC-expressing cells. For these experiments, we mixed mCherry expressing cells with either untransfected control cells or LON-2/glypican-expressing cells, and we also mixed UNC-40/mCherry-expressing cells with either untransfected control cells or LON-2/glypican-expressing cells. Examination of the morphology of these cells one day after mixing revealed that UNC-40/mCherry-expressing cells mixed with

LON-2/glypican exhibited an increased frequency of irregular shapes and membrane extensions, compared to UNC-40/mCherry cells mixed with control cells (**Fig. 3.12d**). Thus, consistent with a model in which LON-2/glypican functions in the UNC-6/netrin signaling pathway to guide developing axons, the association of LON-2/glypican with UNC-40/DCC-expressing cells leads to increased membrane extensions, suggestive of increased signaling downstream of the UNC-40/DCC receptor.

**LON-2/glypican is released extracellularly and its N-terminal domain is functional**

While LON-2/glypican possesses a signature GPI anchor that mediates its attachment to plasma membranes (**Fig. 3.10a**), our experiments indicate that LON-2/glypican is released into the extracellular milieu through cleavage where it can diffuse to associate with UNC-40/DCC-expressing cells. This is consistent with prior work demonstrating that many glypicans are shed or cleaved into a soluble form (Bernfield et al 1999). To verify that LON-2/glypican is indeed released into the extracellular medium, we collected cell-free media from HA::LON-2 cultures (HA::LON-2-conditioned medium) and added it to cells expressing UNC-40::FLAG. We found that HA::LON-2-conditioned medium contained HA::LON-2 that associated with UNC-40::FLAG-expressing cells. As above, this interaction was specific, as no HA::LON-2 signal was found on adjacent untransfected cells (**Fig. 3.12b,c** experiment 8). This result provides

compelling evidence that LON-2/glypican can be released from the membrane of LON-2/glypican-expressing cells, diffuses, and associates with UNC-40/DCC-expressing cells. We propose that using a similar mechanism, LON-2/glypican may be shed from epidermal cells and may interact with migrating axons that express UNC-40/DCC. This is consistent with our finding that LON-2/glypican is produced by the hypodermis to function non-autonomously in *unc-6*/netrin-mediated AVM axon guidance.

To provide evidence for the model that LON-2/glypican can function in axon guidance when detached from the plasma membrane, we used a form of LON-2/glypican lacking the GPI anchor, LON-2ΔGPI, which should be directly secreted into the extracellular milieu (Taneja-Bageshwar & Gumienny 2012). LON-2ΔGPI rescued the AVM guidance defects of *lon-2 slt-1* double mutants back to the level of *slt-1* single mutants (**Fig. 3.10c**). We also used a truncated form of LON-2/glypican (N-LON-2) containing the N-terminal globular domain, but lacking the C-terminal region, thus removing the three HS attachment sites and the GPI membrane anchor. N-LON-2 also rescued the AVM guidance defects of *lon-2 slt-1* double mutants back to the level of *slt-1* single mutants (**Fig. 3.10c**). In contrast, a reciprocal construct containing only the C-terminus with the three HS attachment sites and the GPI anchor (C-LON-2) did not rescue the AVM axon guidance defects of *lon-2 slt-1*, consistent with the model that the N-terminal globular domain of LON-2/glypican is the key functional domain during guidance

(**Fig. 3.10c**). A secreted form of LON-2/glypican is also functional in DTC guidance, as we found that DTC guidance defects of *lon-2*/glypican mutants could be rescued by expression of N-LON-2, containing only the N-terminal globular domain (**Fig. 3.10d**). These findings also support the hypothesis that LON-2/glypican may normally be released from the hypodermis to interact with the *unc-6*/netrin pathway to direct the migrating growth cone during development (**Fig. 3.16**).

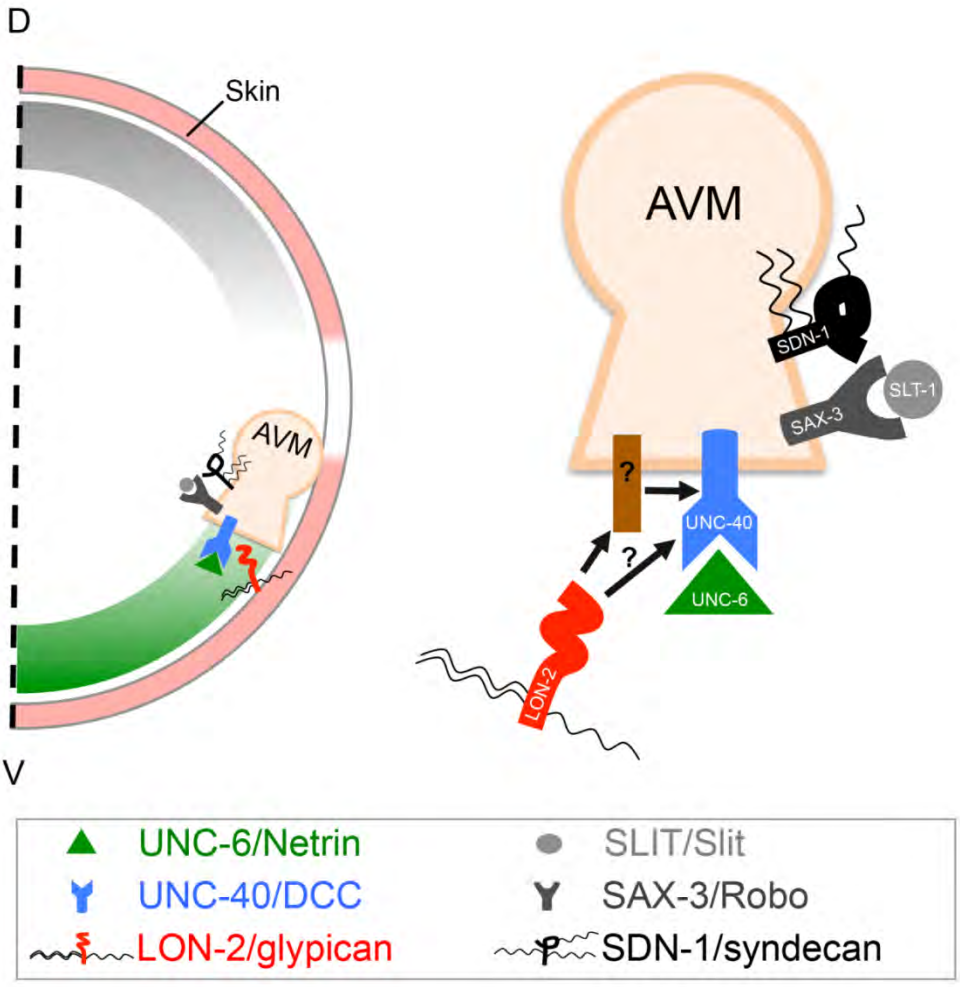

**Figure 3.16. A model for the role of LON-2/glypican in UNC-6/netrin-UNC-40/DCC-mediated axon guidance.** HSPG LON-2/glypican (red) is expressed from the hyp7 epidermal cells (pink) underlying the migrating growth cone of the AVM neuron (tan). LON-2/glypican is released from the hypodermal cell surface and may associate with the developing axon expressing the receptor UNC-40/DCC (blue), directly or indirectly interacting with UNC-40/DCC, to modulate UNC-6/netrin (green) signaling. A second HSPG, SDN-1/syndecan (black), acts in the SLT-1/Slit-SAX-3/Robo (grey) axon guidance pathway.

## DISCUSSION

Growth cone responses to guidance cues require precise regulation as developing axons traverse complex extracellular environments in order to reach their targets. The mechanisms by which guidance cue signals are regulated in the extracellular milieu are still poorly understood (Lai Wing Sun et al 2011). Here, we demonstrate that the *unc-6*/netrin-*unc-40*/DCC guidance system is modulated by the HSPG *lon-2*/glypican.

### *lon-2*/glypican is a component of the *unc-6*/netrin signaling pathways

Our studies identify the HSPG LON-2/glypican as a component of the *unc-6*/netrin attractive and repulsive signaling pathways that guide axons during development. We show that LON-2/glypican specifically acts on *unc-6*/netrin signaling independently of *slt-1*/Slit. We demonstrate that *lon-2*/glypican functions from the hypodermis, the epidermal cells that secrete the substrate along which growth cones extend (Hedgecock et al 1987), and that a secreted form of LON-2/glypican, containing only its N-terminal globular region and lacking its HS chains, guides cells and axons *in vivo*. In addition, we provide evidence that

LON-2/glypican is released from cells producing it and associates with cells expressing UNC-40/DCC receptors. Taken together, our observations support a hypothetical model where GPI-linked LON-2/glypican is produced by substrate epidermal cells, is released into the extracellular milieu, and binds growth cones expressing UNC-40/DCC receptors to regulate attractive and repulsive responses of the growth cone to UNC-6/netrin.

The impact of *lon-2*/glypican on the *unc-6*/netrin signaling pathway is highly specific. First, loss of *lon-2*/glypican, but not of *sdn-1*/syndecan, suppresses the guidance phenotypes elicited by the gain-of-function condition in which *unc-5*/UNC5 was misexpressed. Second, the complete loss of *lon-2*/glypican does not enhance the guidance defects observed in null mutants for *unc-6*/netrin or its receptors *unc-40*/DCC and *unc-5*/UNC5, whereas it does enhance the defects of several other axon guidance mutants, including *sdn-1*/syndecan, *slt-1*/Slit, misexpressed *slt-1*/Slit (P*myo-3::slt-1*), *sax-3*/Robo, and *sqv-5*, suggesting that *lon-2*/glypican functions specifically in the *unc-6*/netrin pathway. Third, *sdn-1*/syndecan, cannot replace *lon-2*/glypican function, highlighting a requirement for *lon-2*/glypican that cannot be achieved by any HSPG. Given that the core protein of LON-2/glypican, devoid of its HS chains, is fully functional in guidance, the specificity of action of LON-2/glypican in netrin-mediated guidance appears to reside in the core protein itself. As a note, whereas *lon-2*/glypican mutants are defective in DTC migration, the *lon-2*/glypican mutant by itself does not show

drastic alterations in AVM axon guidance as is observed with other modulators (Lander & Selleck 2000). It is possible that in the absence of *lon-2*/glypican, another HSPG may provide compensation, or that our scoring of strong alterations in pathfinding did not include more subtle phenotypes, as could be expected from a modulator of the signal (Lander & Selleck 2000).

**The core protein of LON-2/glypican is functional in UNC-6/netrin-mediated guidance**

We show that the LON-2/glypican core protein, devoid of HS attachment sites, is able to associate with UNC-40-expressing cells and is functional in *unc-6*/netrin-mediated guidance. Thus, the core protein is the critical region of LON-2/glypican for netrin-mediated axon guidance. This is in line with previous studies showing a contextual dependence of HS chains for glypican function. For instance, the core protein of *C. elegans* LON-2/glypican and of *Drosophila* glypican Dally do not require HS chains to function in the TGFβ pathway (Kirkpatrick et al 2006, Taneja-Bageshwar & Gumienny 2012). Similarly, *Drosophila* glypican Dally-like interacts with Wg and Hh through their protein core in a HS-independent manner (Williams et al 2010, Yan & Lin 2009, Yan et al 2010), and mammalian Glypican-3 does not require HS chains for its role in Wnt and Hh signaling (Capurro et al 2005, Capurro et al 2008, Gonzalez et al 1998, Song et al 2005). While the HS chains are not critical for the role of LON-2/glypican in guidance, a contribution of HS chains to modulate functionality, as observed for other glypicans in the

context of BMP4, Wnt3, Wg, and Hh signaling (Capurro et al 2005, Kirkpatrick et al 2006, Yan & Lin 2009, Yan et al 2010) cannot be ruled out. For instance, it is conceivable that the normal endogenous HS chains of LON-2/glypican may impact its trafficking, levels, release from the membrane, recruitment of binding partners, or recycling.

**LON-2/glypican is released from the cell surface to guide axons**

LON-2/glypican is predicted to localize at the cell surface via its GPI anchor (Taneja-Bageshwar & Gumienny 2012). However, in our cell culture studies we demonstrate that LON-2/glypican can be released as a soluble molecule from producing cells. We also show that two truncated forms of LON-2/glypican, LON-2ΔGPI and N-LON-2, which are no longer associated with the plasma membrane and are secreted into the extracellular milieu, can function to guide axons *in vivo*. This indicates that LON-2/glypican is likely released from the epidermal cells to reach the growth cone to modulate its guidance. This finding raises the question of how LON-2/glypican is released from the cell membrane and how this process might be regulated during development. The release of LON-2/glypican from the surface of cells could involve phospholipases that cleave the GPI anchor and/or proteases that cleave its extracellular domain, such as at a predicted furin-cleavage site (Taneja-Bageshwar & Gumienny 2012); **Fig. 3.10a**).

Glypican cleavage by lipases and proteases has been demonstrated to occur and to be functionally important in other contexts, such as in regulating FGF and Wnt signaling during morphogenesis (Bernfield et al 1999, Matsuo & Kimura-Yoshida 2013). For instance, the *Drosophila* glypican Dally-like protein is cleaved at the GPI anchor by the lipase Notum, to negatively regulate Wnts (Giraldez et al 2002). Similarly, several mammalian glypicans, including glypican-3, are cleaved by Notum (Traister et al 2008). The functional importance of glypican proteolytic cleavage is illustrated by the processing of glypican-3 by a furin-like convertase to modulate Wnt signaling in zebrafish (De Cat et al 2003). In addition, glypican-1 and glypican-4 are proteolytically cleaved to stimulate long-range FGF signaling in the *Xenopus* embryo (Hou et al 2007), and increase the efficiency of myogenic differentiation in the presence of FGF in mammalian cells (Velleman et al 2013), respectively. Our studies show that glypican processing also functions during axon guidance.

**LON-2/glypican associates with the surface of UNC-40/DCC-expressing cells**

We demonstrate that LON-2/glypican is secreted into the extracellular medium and decorates the outline of UNC-40/DCC-expressing cells. Deleting the extracellular domain of UNC-40 (UNC-40ΔNt) abrogated the association of LON-2/glypican with UNC-40/DCC expressing cells, indicating that LON-2/glypican may interact with UNC-40/DCC at the cell surface. The association of LON-

2/glypican with UNC-40/DCC may be direct, or indirect through interactions with other molecules (**Fig. 3.16**). Our experiments demonstrate that UNC-6/netrin binding to UNC-40/DCC was undisturbed by the association of UNC-40/DCC with LON-2/glypican, suggesting that the possible interaction of LON-2/glypican with UNC-40/DCC likely involves a region of UNC-40/DCC other than the netrin binding sites. Indeed, we found that LON-2/glypican associates with UNC-40/DCC-expressing cells even when the UNC-40/DCC receptors lack the UNC-6/netrin binding domains.

We found that LON-2/glypican leads to increased irregular morphology of UNC-40/DCC-expressing cells. Ectopic expression of DCC in mammalian cells activates downstream signaling via Cdc42 and Rac1, producing cytoskeletal rearrangements that lead to filopodia outgrowth and cell surface extensions (Shekarabi & Kennedy 2002). Our finding that the presence of LON-2/glypican enhances the UNC-40/DCC-induced irregular cell morphology and filopodia-like extensions, suggests that the association of LON-2/glypican with UNC-40/DCC-expressing cells may increase signaling downstream of UNC-40/DCC. Consistent with this notion, we show that *lon-2*/glypican functions in the same signaling pathway as the UNC-40/DCC downstream mediator *unc-34*/enabled during axon guidance.

Our results suggest a possible regulatory mechanism in the extracellular space in which secreted LON-2/glypican modulates the activity of the receptor UNC-40/DCC. LON-2/glypican may directly bind UNC-40/DCC, or alternatively, LON-2/glypican may instead interact with other molecules to impact UNC-40/DCC to modulate its stability, distribution, or activity. Alternatively, LON-2/glypican could potentially function as a co-receptor for UNC-6/netrin, where it may facilitate the formation of UNC-6/netrin-UNC-40/DCC-LON-2/glypican signaling complexes, similar to the situation in FGF signaling (Bülow & Hobert 2006). It is also conceivable that LON-2/glypican could bind UNC-6/netrin directly as well, even if undetected in our assays, as netrin has been found to bind heparin *in vitro* (Kappler et al 2000, Kennedy et al 1994, Shipp & Hsieh-Wilson 2007). Previous studies have also documented the binding of DCC to heparin *in vitro* (Bennett et al 1997, Geisbrecht et al 2003), and while we have found that the core protein is the critical portion of LON-2/glypican in netrin-mediated axon guidance, it remains possible that the endogenous HS chains contribute to the function of LON-2/glypican in axon guidance.

In summary, our studies uncover a novel mechanism by which UNC-6/netrin signaling through its UNC-40/DCC receptor is modulated by the HSPG LON-2/glypican during axon pathfinding. Given the evolutionary conservation of the UNC-6/netrin pathway components (UNC-6/netrin and its receptors UNC-40/DCC and UNC-5/UNC5), and of glypicans (LON-2 is most similar to

mammalian glypican-3), and that synthesis of HS chains is required for mammalian axons to respond to netrin-1 *in vitro* (Matsumoto et al 2007, Ogata-Iwao et al 2011), glypicans are likely to play a role in netrin-mediated axon pathfinding in mammals as well. Our findings provide a general mechanism for the extracellular regulation of growth cone responses to netrin during the development of nervous systems.

## MATERIALS AND METHODS

### Nematode strains and genetics

Nematode cultures were maintained at 20$^{o}$C on NGM plates seeded with OP50 bacteria as described (Brenner 1974). Strains were constructed using standard genetic procedures and are all listed in **Table 3.8**. Genotypes were confirmed by genotyping PCR or by sequencing when needed, using primers listed in **Table 3.9**.

### S2 cell culture, transfection, mixing, and immunostaining

S2 cells were maintained in SFX Insect Media (HyClone) containing 10% Fetal Bovine Serum (HyClone) and Penicillin-Streptomycin (50 units-50 µg/mL) (Sigma). 70-90% confluent S2 cells were transfected with 500 ng of each construct using Effectene® (Qiagen) according to manufacturer's protocol. 48 hr after transfection, old culture media was removed and new media was added to

resuspend the cells. Equal volumes of resuspended cells that had been transfected with individual constructs were plated onto coverslips and co-cultured overnight. Cells were then fixed with 4% paraformaldehyde and immunostained with rabbit anti-HA (Life Technologies #715500) and mouse anti-FLAG (Sigma #F3165) primary antibodies, and Alexa594 donkey anti-rabbit (Life Technologies #R37119) and Alexa647 goat anti-mouse (Life Technologies #A21235) secondary antibodies. Confocal analysis was performed on a Zeiss LSM 5 Pascal confocal microscope. Confocal images were processed using ImageJ. Each experiment was repeated at least three times.

For the experiment in which we use HA::LON-2-conditioned medium (supernatant) of cells expressing HA::LON-2, the culture media was also changed 48 hr after transfection, fresh media was added, and the cells were incubated for another 48 hr. This media was collected and centrifuged at 1500 rpm to remove cells and debris. This supernatant was added onto cells expressing UNC-40::FLAG, incubated overnight, and as above, fixed, stained, and imaged.

**RT-PCR for *gpn-1* alleles**

Total RNA was extracted from worm samples using Trizol (Invitrogen) according to manufacturer's instructions. 500 ng RNA was used to reverse transcribe using the High Capacity cDNA Reverse Transcription Kit (Applied Biosystems) and random primers. PCR reactions were carried out with 1$^{st}$ strand cDNA template

and primers oCB834 (ATCAAGACCGAGTGATAGTG) and oCB1321 (TGGCGAGTATTCCCGTTTAG) were used for *gpn-1* cDNA amplification, and primers oCB992 (TCGCTTCAAATCAGTTCAGC) and oCB993 (GCGAGCATTGAACAGTGAAG) were used for the control gene Y45F10D.4 (Hoogewijs et al 2008) cDNA amplification.

**Neuroanatomical and distal tip cell observations**

Animals were mounted on agarose pads, anaesthetized with 100 mM sodium azide, and examined under a Zeiss Axio Scope.A1 or a Zeiss Axioskop 2 Plus. *AVM and PVM axon guidance analysis.* Axons of neurons AVM and PVM were examined in L4 larvae and adult animals using *zdIs5,* an integrated P*mec-4::gfp* reporter (Clark & Chiu 2003). Animals with the cell body of AVM posterior to the vulva (cell migration defect) were excluded from axon guidance analysis. *AVM analysis:* Worms were counted as mutant for AVM ventral axon guidance if: **a)** AVM failed to send an axon ventrally and instead projected laterally to the anterior; or **b)** the AVM axon projected laterally, in the anterior or the posterior direction, for at least ~15 µm (>3 AVM cell body lengths) before projecting to the ventral side. The angle between the anterior/posterior axon projection and the ventral axon projection had to be >45° to be counted as mutant therefore excluding animals with a slight curve in the ventral axon of AVM from the mutant count. Values reported in **Table 3.6**.

*PVM analysis criteria:* Worms were counted as having their PVM axon misoriented dorsally if the axon of PVM was projecting to the dorsal side of the animal. The vulva was used as a reference for the ventral side. Worms whose *zdIs5* labeled neurons were too misplaced to be identified were excluded from analysis.

*Distal tip cell guidance analysis:* The path of migration of the distal tip cells (DTC) brings about the shape of the mature gonad arms (**Fig. 3.5a**, (Hedgecock et al, 1987)). In the wild type, the DTC migrates away from the vulva location along the antero-posterior axis of the animal. The DTC then turns dorsally to reach the dorsal side of the animal, where it then migrates towards the vulva along the antero-posterior axis of the animal. To infer the path of DTC migration, gonad arms were examined in late L4 and young adult animals using DIC microscopy. Animals were counted as having abnormal gonad arm shapes when a) the distal arm of the gonad was located ventrally instead of dorsally, indicating a failure of the DTC to migrate dorsally; b) the proximal gonad arm was too short, resulting from a premature turn of the DTC towards the dorsal side; or c) the gonad arm was twisted over itself.

*GABAergic motorneuron axon analysis:* Commissures of the GABAergic motorneurons were analyzed in L4 larvae and adults using *ufIs34*, an integrated P*unc-47::mCherry* reporter (Petrash et al 2013). For each animal, all GABAergic commissures (except DD1 and VD2) were counted and categorized as either reaching the dorsal cord, or failing to reach the dorsal cord. The fraction of

commissures failing to reach the dorsal cord among all the commissures extending from the ventral cord was determined for each animal, averaged for the genotype, and expressed as percentage.

### *C. elegans* constructs and microinjections to generate transgenic animals

All inserts of finalized clones were verified by sequencing.

**P*lon-2::lon-2* (PCR product):** Primers oCB1070 (CATGATAAGCTTTTCAAATTGGCGGTTAACTG) and oCB1124 (ATCATGGGGCCCTAAGCTGAATTCCCATAAC) were used to amplify a PCR product out of N2 genomic DNA containing bases 13,104 of cosmid C39E6 to 26,408 of cosmid F55D10 of the *lon-2* locus.

**P*dpy-7::lon-2* (pCB268):** Vector P*dpy-7* was cut with *Xma*I and *Apa*I and ligated with insert of *lon-2* cDNA digested out of pCB251 (P*mec-7::lon-2*) with *Xma*I and *Apa*I.

**P*elt-3::lon-2* (pCB304):** Vector P*dpy-7::lon*-2 (pCB268) was digested with *Hind*III and *Xma*I to release P*dpy-7* and ligated with insert of P*elt-3* 2-kb promoter (coordinates on cosmid K02B9: 16,117 to 18,081) amplified out of N2 genomic DNA (modeled after (Maduzia et al., 2002)) using primers oCB1063 (CATGATAAGCTTTGTGACACGTTGTTTCACG) and oCB1064 (ATCATGCCCGGGGAAGTTTGAAATACCAGGTAG) to add on *Hind*III and *Xma*I sites.

**P*grd-10::lon-2* (pCB266):** Vector P*grd-10::GFP* (in pPD95.75 backbone) was digested with *Kpn*I and *Eco*RI to release GFP and ligated with insert of *lon-2* cDNA (yk1346g07) amplified with primers oCB1034 (CATGATGGTACCATGGTCTTCCGGTGGCTCATTC) and oCB1035 (ATCATGGAATTCTCAAAAAAGTTTAATAACTGC) to add on *Kpn*I and *Eco*RI sites.

**P*mec-7::lon-2* (pCB251):** Vector pPD96.41 was digested with *Xma*I and *Nhe*I and ligated with insert of *lon-2* cDNA (yk1346g07) amplified by primers oCB963 (CATGATCCCGGGATGGTCTTCCGGTGGCTCATTC) and oCB964 (ATCATGGCTAGCTCAAAAAAGTTTAATAACTGC) to add on *Xma*I and *Nhe*I sites.

**P*elt-2::lon-2* (pCB218):** Vector P*dpy-7::lon-*2 (pCB268) was digested with *Hind*III and *Xma*I to release P*dpy-7* and ligated with insert of P*elt-2* 1-kb promoter (coordinates on cosmid C33D3: 2933 - 3875) amplified out of N2 genomic DNA (modeled after (Maduzia et al 2002)) using primers oCB1059 (CATGATAAGCTTTTGATTTTGTTTCACTCTGTG) and oCB1060 (ATCATGCCCGGGTATAATCTATTTTCTAGTTTC) to add on *Hind*III and *Xma*I sites.

**P*myo-3::lon-2* (pCB332):** Vector pCB268 (P*dpy-7::lon-2*) was digested with *Hind*III and *Xba*I to release P*dpy-7*, and was ligated with insert of P*myo-3* digested out of vector pPD95.86 with *Hind*III and *Xba*I.

**P*lon-2::lon-2* (pCB246):** Vector P*dpy-7::lon*-2 (pCB268) was digested with *Hind*III and *Xma*I to release P*dpy-7* and ligated with insert of *lon-2* 3-kb promoter (coordinates on cosmid C39E6: 13,104 - 10,105) amplified out of N2 genomic DNA (modeled after (Gumienny et al 2007)) using primers oCB1070 (CATGATAAGCTTTTCAAATTGGCGGTTAACTG) and oCB1069 (ATCATGCCCGGGTCTGAAATTTTGAATATGTAAGC) to add on *Hind*III and *Xma*I sites.

**P*lon-2*::LON-2ΔGPI (pCB269):** Vector pCB246 (P*lon-2::lon-2*) was digested with *Xma*I and *Eco*RI to release the *lon-2* cDNA and ligated with insert of *lon-2* cDNA (yk1346g07) amplified with primers oCB963 (CATGATCCCGGGATGGTCTTCCGGTGGCTCATTC) and oCB1074 (ATCATGCTCGAGTCAATCCGGCTGAATTTCTTTTTCC) to add on *Xma*I and *Eco*RI sites and generate a truncated form of LON-2 after amino acid 488 to remove the GPI anchor (modeled after (Taneja-Bageshwar & Gumienny 2012)).

**P*lon-2::*N-LON-2 (pCB270):** Vector pCB268 (P*dpy-7::lon-2*) was digested with *Xma*I and *Eco*RI to release the *lon-2* cDNA and was ligated with insert of *lon-2* cDNA (yk1346g07) amplified by primers oCB963 (CATGATCCCGGGATGGTCTTCCGGTGGCTCATTC) and oCB1075 (ATCATGGAATTCTCACCTTCCGAGTCGGTCCCACG), to add on *Xma*I and *Eco*RI sites and generate a truncated form of LON-2 after amino acid 368, ie, containing amino acids 1-368 (modeled after (Gumienny et al 2007)).

**P*lon-2*::C-LON-2 (pCB311):** Vector pCB246 (P*lon-2::lon-2*) was digested with *Xma*I and *Nhe*I to release *lon-2* cDNA and was ligated with insert of *lon-2* cDNA amplified by primers oCB964 (ATCATGGCTAGCTCAAAAAAGTTTAATAACTGC) and 1) oCB1253 (TCCGTCCTACCTGCAGAAGAAGTGAAAATCTGTGATCACTCG) 2) oCB1254 (ATTCTTTTTGTATTGCTCTACCGGTCCGTCCTACCTGCAGAAG) and 3) oCB1255 (CATGATCCCGGGATGGTCTTCCGGTGGCTCATTCTTTTTGTATTGCTCTACC) to add on *Xma*I and *Nhe*I sites, to add on the 22 amino acid *lon-2* signal peptide sequence, and to truncate LON-2 to begin at amino acid 369. Thus, this construct codes for 22 amino acid residues of the signal peptide of LON-2, followed by residues 369 – 508.

**P*mec-7::sdn-1* (pCB242):** Vector pPD96.41 was digested with *Xma*I and *Xho*I, and ligated with insert of *sdn-1* cDNA (yk139f3) amplified with primers oCB903 (CATGATCCCGGGATGATTCTGAAACTCAATTTC) and oCB904 (ATCATGCTCGAGTTACGCGTAAAATTCTTTTG) to add on *Xma*I and *Xho*I sites.

**P*lon-2::sdn-1* (pCB312):** Vector pCB246 (P*lon-2::lon-2*) was digested with *Xma*I and *Eco*RI to release *lon-2*, and was ligated with an insert of *sdn-1* cDNA digested out of pCB242 (P*mec-7::sdn-1*) with *Xma*I and *Eco*RI.

Transgenic animals were generated by standard microinjection techniques (Mello & Fire 1995). Each construct or PCR amplicon was injected at 1, 5, 10, or 25 ng/µL with one or two coinjection markers which included pRF4 (125-150 ng/µL), P*ttx-3::mCherry* (50 ng/µL), P*ceh-22::gfp* (50-75 ng/µL), and/or P*unc-122::rfp* (50-75 ng/µL). pBSK+ (90-100 ng/µL) used to increase total DNA concentration if needed. For details on specific coinjection marker(s) used for each rescued transgenic line, see **Table 3.8**.

**Western blot analysis of LON-2::GFP and LON-2ΔGAG::GFP expressed in worms**

Mixed-stage wild-type (N2), GFP control (*lqIs4*), LON-2::GFP (TLG257), and LON-2ΔGAG::GFP (TLG199) worms were collected in buffer and protease inhibitors (Roche). Worm pellets were subjected to repeated freeze-thaw cycles. Protein concentration was measured using the Pierce 660 nm Protein Assay on a Nanodrop. 70 µg of samples mixed with 2x Laemmli sample buffer (Bio-Rad) were boiled, separated by SDS-PAGE on a 4-20% Mini-Protean TGX gel (Bio-Rad), and transferred to PVDF membrane. Membranes were incubated in 1:3000 anti-GFP primary antibody (Millipore #AB3080) and 1:9000 goat anti-rabbit HRP secondary antibody (Bio-Rad #166-2408EDU). For the loading control, membranes were incubated in 1:5000 anti-HSP90 antibody (CST #4874) and 1:10000 goat anti-rabbit HRP secondary antibody (Bio-Rad #166-2408EDU).

Signal was revealed using Clarity Western ECL Substrate (Bio-Rad), and imaged using film (LabScientific).

**Constructs to express variants of LON-2, UNC-40, UNC-6, SDN-1 and Evi in S2 cells**

All inserts of finalized clones were verified by sequencing.

**HA::LON-2 (pCB285):** The *C. elegans lon-2* full length cDNA (yk1346g07) was amplified by PCR with primers adding the *Eco*RI and *Apa*I restriction enzyme sites and cloned into pBlueScript II (Life Technologies). HA::LON-2 was made by synthesizing a DNA fragment, carrying the restriction sites *Eco*RI and *Hinc*II, and containing the 5' end of the *lon-2* cDNA with the HA tag added after the signal peptide sequence (at cDNA position 61) and cloned into pBlueScript/*lon-2*. The HA::LON-2 *Eco*RI/*Apa*I fragment was then cloned into the pActin5.1/V5-His vector (Life Technologies).

**HA::LON-2::myc (pCB313):** The HA::LON-2::myc construct was made by synthesizing the 3' end of the *lon-2* cDNA (bases 739-1527) with the myc tag DNA sequence before the GPI anchor domain sequence (at cDNA position 1375) and an *Apa*I restriction site at the 3' end. The *Pml*I/*Apa*I synthesized fragment was then cloned into the *pActin5.1*/HA::LON-2 (pCB285) construct cut with the same restriction enzymes.

**HA::LON-2ΔGAG (pCB295):** The LON-2ΔGAG construct was made by replacing the *Xho*I/*Bsm*I fragment (bases 803-1340 of the *lon-2* cDNA) in the

pBlueScript/HA::*lon-2* plasmid with synthesized fragment where the *lon-2* sequence is mutated at the three predicted heparan sulfate chain attachment sites (S374A, S442A and S444A) modeled after (Taneja-Bageshwar & Gumienny 2012). Similar to the wild type version of *lon-2*, the HA::LON-2ΔGAG *Eco*RI/*Apa*I fragment was then cloned into the pActin5.1/V5-His vector (Life Technologies).

**HA::LON-2ΔGAG::myc (pCB330):** The double tagged HA::LON-2ΔGAG::myc construct was made by replacing the *Bsm*I/*Apa*I fragment (bases 1340-1527 of the *lon-2* cDNA) in the pBlueScript/HA::LON-2ΔGAG plasmid with a synthesized fragment containing the myc tag DNA sequence before the GPI anchor domain sequence (at cDNA position 1375) and an *Apa*I restriction site at the 3' end. The HA::LON-2ΔGAG::myc *Eco*RI/*Apa*I fragment was then cloned into the pActin5.1/V5-His vector (Life Technologies).

**SfGFP::UNC-6 (pCB292):** The *C. elegans unc-6* full length cDNA (yk603d12) was amplified by PCR with primers adding the *Eco*RI and *Apa*I restriction enzyme sites and cloned into pBlueScript II. The superfolder-GFP::UNC-6 construct was made by synthesizing a DNA fragment, carrying the restriction sites *Eco*RI and *Hinc*II, and containing the 5' end of the *unc-6* cDNA with the superfolder-GFP sequence after the signal peptide sequence (cDNA position 70) and cloned into pBlueScript/*unc-6*. The superfolder-GFP::UNC-6 *Eco*RI/*Apa*I fragment was then cloned into the pActin5.1/V5-His vector.

**UNC-40::FLAG (pCB301):** The *C. elegans* full length *unc-40* cDNA (yk449d8) was amplified by two sequential PCR reactions that added the *Xho*I

and *Apa*I restriction enzyme sites, as well as the FLAG tag at the 3' end before the stop codon (adding the FLAG tag at the C-terminus of UNC-40 after the intracellular domain). This UNC-40::FLAG cDNA was then cloned into the pActin5.1/V5-His vector.

**UNC-40ΔNt::FLAG (pCB310):** The *unc-40* intracellular fragment (cDNA bases 3022-4245 that include the coding sequence for the transmembrane and intracellular domains of UNC-40), along with the FLAG tag, was amplified by PCR using the UNC-40::FLAG cDNA as template and primers carrying the *Eco*RI and *Apa*I sites. A start codon (ATG) was added to the forward primer. The UNC-40ΔNt::FLAG fragment was then cloned into the pActin5.1/V5-His vector.

**UNC-40ΔFn4/5::FLAG (pCB334):** The UNC-40ΔFn4/5 construct was made by PCR amplifying a 2-kb DNA fragment from genomic DNA from the strain NK821 *qyIs155* containing a deletion of fibronectin III domains 4 and 5 of the *unc-40* cDNA using nested primers ((Wang et al., 2014)). The nested PCR added the FLAG tag to the 3' end of the UNC-40ΔFn4/5 cDNA fragment. This final fragment was cloned into the pActin5.1/*unc-40* vector using *Dra*III and *Apa*I restriction enzymes, thus generating an *unc-40* full length cDNA with a deletion of the fibronectin III domains 4 and 5.

**SDN-1::myc (pCB336):** The *C. elegans sdn-1* cDNA, excluding the coding region for the transmembrane and intracellular C-terminal tail (cDNA bases 1-678), was amplified by two sequential PCR reactions adding the *Eco*RI and *Apa*I restriction sites and the myc tag sequence at the 3' end before the stop

codon. The *sdn-1*::myc *Eco*RI/*Apa*I fragment was then cloned into the pActin5.1/V5-His vector (Life Technologies).

The pAc/Evi::EGFP (Bartscherer et al., 2006) and pAc/GFP constructs were a gift from V. Budnik (University of Massachusetts Medical School).

**Western blot analysis of HA::LON-2::myc and HA::LON-2ΔGAG::myc expressed in S2 cells**

S2 cells were transfected with HA::LON-2::myc (pCB313) and HA::LON-2ΔGAG::myc (pCB330) constructs. Cells were washed once with 1X Phosphate Buffered Saline and lysed for 30 min at 4°C in 1X Phosphate Buffered Saline, 0.5% Triton X-100 and 1X Protease Inhibitor Cocktail (Roche). Samples of supernatant and cell lysates were each mixed with 2X Laemmli sample buffer (BioRad). Proteins were separated by SDS-PAGE and transferred to PVDF membrane. Membranes were incubated with rabbit anti-HA (Life Technologies #715500) and rabbit anti-myc (Santa Cruz #sc-789) primary antibodies and HRP-linked goat anti-rabbit (Bio-Rad #166-2408EDU) secondary antibody. Signals were revealed by chemiluminescence with Clarity™ Western ECL Substrate (BioRad) and imaged using the ChemiDoc™ System (BioRad).

**Western blot analysis of HA::LON-2::myc, UNC-40::FLAG and SfGFP::UNC-6 expressed in S2 cells**

S2 cells were independently transfected with HA::LON-2::myc (pCB313), UNC-40::FLAG (pCB301) or SfGFP::UNC-6 (pCB292) constructs. 48 hr after transfection, old culture media was removed and new media was added to resuspend the cells. Equal volumes of resuspended cells that had been transfected with individual constructs were mixed and co-cultured overnight. Cells were harvested, centrifuged, and combined with their corresponding supernatant from each of these cell mixes. 100 µL of supernatant of each mixture was saved and kept on ice. Cell pellets were washed once with 1X Phosphate Buffered Saline and lysed for 30 min at 4°C in 100 µL of ice-cold RIPA buffer (50 mM Tris HCl pH 7.5, 150 mM NaCl, 1% Triton-X100, 0.5% sodium deoxycholate, 0.1% SDS, 1mM EDTA pH 8.0) supplemented with Protease Inhibitor Cocktail (Roche) and PMSF. Cell lysates were combined with their corresponding supernatant and mixed with 2X Laemmli sample buffer (BioRad). Each sample was split into 3 to run 3 protein gels in parallel. Proteins were separated by SDS-PAGE and transferred to PVDF membrane. Membranes were incubated with rabbit anti-myc (Santa Cruz #sc-789), mouse anti-FLAG (Sigma #F3165) and rabbit anti-GFP (Millipore AB3080) primary antibodies as well as HRP-linked goat anti-rabbit (Bio-Rad #166-2408EDU) and HRP-linked horse anti-mouse (Vector Labs PI-2000) secondary antibodies. Signals were revealed by chemiluminescence with Clarity™ Western ECL Substrate (BioRad) and imaged using the ChemiDoc™ System (BioRad).

**Analysis of the shape of UNC-40-expressing cells**

Independent populations of S2 cells were transfected with (1) 450 ng of pActin5.1::mCherry alone, (2) 50 ng of the UNC-40::FLAG construct plus 450 ng of the co-transfection marker pActin5.1::mCherry, or (3) 500 ng of HA::LON-2. The media was changed and cells were mixed 48 hr after transfection. Control mCherry expressing cells were mixed with untransfected cells, or with HA::LON-2 expressing cells. Similarly, UNC-40::FLAG/mCherry expressing cells were mixed with untransfected cells or with HA::LON-2 expressing cells. To maintain the total number of cells constant in our different mixes, one volume of UNC-40::FLAG/mCherry cells was mixed with either (a) one volume of control/untransfected cells, or (b) one volume of LON-2-transfected cells. Cell mixes were co-cultured overnight. Cells were then fixed with 4% paraformaldehyde and examined under a Zeiss LSM 5 Pascal confocal microscope. Control mCherry expressing cells or UNC-40::FLAG/mCherry expressing cells were identified by the co-transfection marker mCherry. 20 fields of ~300 cells each per mix per were photographed for each of 3 independent experiments. Cells were categorized as having the typical S2 cell round and smooth shape, irregular edges, and/or extensions protruding from the cell.

**ACKNOWLEDGEMENTS**

We are deeply grateful to Carlos Lois and Vivian Budnik for insightful discussions, help with the manuscript, and reagents; to Mark Alkema, Mike Francis, Michele Lemons, and Maria Doitsidou for discussions and editing the manuscript; to Marc Freeman for insights and equipment; to Yihang Li and Catalina Ruiz-Cañada for help with S2 cells and biochemistry. We thank Bénard lab members Catherine Harwood, Gillian Carella, Avery Fisher, Mark Broadwin, Lauren Goodale and James Ritch for help with building strains. We thank the Culotti (*evIs25*), Bargmann (*kyIs209*), Hengartner (*opIs171*), Sherwood (*qyIs155*), Mitani (*agr-1(tm2051)* and *gpn-1(tm595)* alleles) labs for strains, Dr. T. Gumienny for strains (*texEx164* and *texEx144*) and plasmid pSBL3SG006, Dr. H. Bülow for a plasmid containing P*grd-10*, Dr. A. Fire and Dr. Y. Kohara for clones, and the CGC funded by NIH Office of Research Infrastructure Programs (P40 OD010440) for strains. This work was supported by the R01 grant AG041870-01A1 from the NIH to C.Y.B..

## TABLES

**Table 3.1**. List of mutant alleles used.

| Gene | Allele | Nature of allele | Reference |
|---|---|---|---|
| *unc-52* | *e444* | Early stop in exon 18. Partial loss of function. | (Rogalski et al 1995) |
| *agr-1* | *tm2051* | 423 bp deletion, deleting exons 26 and 27 resulting in an in frame loss of 42 amino acids. | (Hrus et al 2007) |
| *gpn-1* | *ok377* | 1194 bp deletion, deletes most of exon 3, and introduces early Stop codons. Likely null. (see Figure S2) | (Hudson et al 2006) This study |
| *gpn-1* | *tm595* | 1411 bp deletion, deletes part of exon 2, exon 3, and introduces early Stop codons. Likely null. (see Figure S2) | (Hudson et al 2006) This study |
| *lon-2* | *e678* | ~9 kb deletion. Null. | (Gumienny et al 2007) |
| *sdn-1* | *zh20* | 1258 bp deletion. Null. | (Rhiner et al 2005) |
| *sdn-1* | *ok449* | 483 bp in-frame deletion. Produces truncated SDN-1. | (Minniti et al 2004) |
| *unc-6* | *ev400* | Early stop Q78*. Null. | (Wadsworth et al 1996) |
| *unc-6* | *e78* | C410Y. Partial loss of function. | (Lim & Wadsworth 2002) |
| *unc-40* | *e271* | Early stop R824*. Null. | (Stavoe et al 2012) |
| *unc-40* | *e1430* | Early stop R157*. Likely null. | (Colon-Ramos et al 2007) |
| *slt-1* | *eh15* | Duplication of locus and deletions. First copy contains a 1900 bp deletion. Both copies have a 100 bp deletion. First copy produces no mRNA while second copy produces mRNA with a frameshift. | (Hao et al 2001) |
| *sax-3* | *ky123* | Deletion of signal peptide and first exon. | (Zallen et al 1998) |
| *unc-34* | *e566* | A likely null mutation. | (Bloom 1993) (Fleming et al 2010) |
| *sqv-5* | *k172* | G663E. Partial loss of function. | (Suzuki et al 2006) |

**Table 3.2.** Distal tip cell guidance defects in strains examined.

| Genotype | N | % Defective distal tip cell guidance | s.e.p. |
|---|---|---|---|
| *uflS34; vsIs48* | 140 | **4** | 1.7 |
| *lon-2(e678); uflS34* | 251 | **17** | 2.4 |
| *unc-6(ev400); zdIs5* | 172 | **62** | 3.7 |
| *lon-2(e678) unc-6(ev400); zdIs5* | 160 | **65** | 3.8 |
| *unc-40(e271); uflS34; vsIs48* | 122 | **25** | 3.9 |
| *lon-2(e678); unc-40(e271); uflS34* | 136 | **22** | 3.6 |
| *unc-5(e53); vsIs48; uflS34* | 134 | **46** | 4.3 |
| *lon-2(e678); unc-5(e53); uflS34* | 138 | **49** | 4.3 |

**Table 3.3**. Motorneuron axon dorsal guidance defects in strains examined.

| Genotype | N | % GABA commissures failing to reach dorsal cord | s.e.p. |
|---|---|---|---|
| *uflS34; vsIs48* | 104 | **0.1** | 0.3 |
| *lon-2(e678); uflS34* | 86 | **0.2** | 0.5 |
| *unc-40(e271); uflS34; vsIs48* | 73 | **55** | 5.8 |
| *lon-2(e678); unc-40(e271); uflS34* | 67 | **50** | 6.1 |

**Table 3.4.** PVM dorsal guidance defects quantified in wild-type and mutant strains with or without misexpression of *unc-5* in the PVM neuron using transgene *evIs25* P*mec-7::unc-5*.

| Genotype | N | % Dorsal PVM axon ^ | s.e.p. |
|---|---|---|---|
| **PVM controls** | | | |
| *zdIs5* | 52 | **0** | 0.0 |
| *unc-6(ev400); zdIs5* | 44 | **0** | 0.0 |
| *unc-40(e271) zdIs5* | 30 | **0** | 0.0 |
| *unc-34(e566); zdIs5* | 73 | **0** | 0.0 |
| *lon-2(e678) unc-6(ev400); zdIs5* | 65 | **0** | 0.0 |
| *slt-1(eh15); zdIs5* | 60 | **0** | 0.0 |
| *sax-3(ky123); zdIs5* | 41 | **0** | 0.0 |
| *lon-2(e678); zdIs5* | 54 | **0** | 0.0 |
| *sdn-1(zh20); zdIs5* | 58 | **0** | 0.0 |
| *lon-2(e678) sdn-1(zh20); zdIs5* | 44 | **0** | 0.0 |
| **Strains with *evIs25* P*mec-7::unc-5*** | | | |
| *evIs25; zdIs5* | 228 | **66** | 3.1 |
| *unc-6(ev400) evIs25; zdIs5* | 41 | **0** | 0.0 |
| *unc-40(e271) zdIs5; evIs25* | 191 | **18** | 2.8 |
| *unc-34(e566); evIs25; zdIs5* | 159 | **13** | 2.7 |
| *unc-6(ev400) lon-2(e678) evIs25*; *zdIs5* | 62 | **0** | 0.0 |
| *unc-40(e271) zdIs5; lon-2(e678) evIs25* | 249 | **25** | 2.7 |
| *slt-1(eh15) evIs25*; *zdIs5* | 212 | **63** | 3.3 |
| *unc-34(e566); lon-2(e678) evIs25; zdIs5* | 207 | **8** | 1.9 |
| *sax-3(ky123) evIs25*; *zdIs5* | 201 | **66** | 3.3 |
| *lon-2(e678) evIs25; zdIs5* | 330 | **48** | 2.8 |
| *sdn-1(zh20) evIs25; zdIs5* | 259 | **64** | 3.0 |
| *lon-2(e678) sdn-1(zh20) evIs25; zdIs5* | 343 | **42** | 2.7 |

N, number of AVM axons examined. s.e.p., standard error of the proportion.
^ PVM axons normally never extend dorsally, not even in the complete absence of the *slt-1*/slit and the *unc-6*/netrin guidance pathways in *unc-6 slt-1* double null mutants, where axons defective in guidance extend *anteriorly*. Dorsal axon extension is only observed with *unc-5*/UNC5 ectopic expression, which overpowers the endogenous signaling mechanism within PVM and thus forces its axon to extend dorsally. This highlights the power of this ectopic-*unc-5*-expression system to uncover molecules specifically involved in *unc-6*/netrin signaling through the *unc-5*/UNC5 receptor, independently of other endogenous signals.

**Table 3.5**. Transgenic rescue of *lon-2* function in AVM guidance.
We assayed rescue of the AVM guidance defects in *lon-2 slt-1* double mutants back to *slt-1* single mutant levels. Underlined indicates “rescued”. Non-transgenic sibling controls of rescued transgenic lines were examined to ascertain that the rescue was transgene-dependent.

| **Genotype** | **Transgene** | | **Transgenic** | | | **Non-transgenic controls** | | |
|---|---|---|---|---|---|---|---|---|
| | | | **N** | **% Mut.** | **s.e.p** | **N** | **% Mut.** | **s.e.p** |
| *lon-2 slt-1; qvEx107* | P*lon-2::lon-2(+)* (14kb *lon-2* locus) | line #1 | 184 | **52** | 3.7 | 221 | **71** | 3.1 |
| *lon-2 slt-1; qvEx110* | P*lon-2::lon-2(+)* (P*lon-2::lon-2* cDNA) | line #2 | 263 | **51** | 3.1 | 223 | **68** | 3.1 |
| *lon-2 slt-1; qvEx108* | P*lon-2::lon-2(+)* (P*lon-2::lon-2* cDNA) | line #3 | 223 | **55** | 3.3 | 190 | **65** | 3.5 |
| *lon-2 slt-1; qvEx113* | P*elt-3::lon-2(+)* | line #1 | 116 | **47** | 4.6 | 71 | **75** | 5.1 |
| *lon-2 slt-1; qvEx116* | P*elt-3::lon-2(+)* | line #2 | 248 | **52** | 3.2 | 231 | **68** | 3.1 |
| *lon-2 slt-1; qvEx112* | P*dpy-7::lon-2(+)* | line #1 | 260 | **52** | 3.1 | 381 | **65** | 2.4 |
| *lon-2 slt-1; qvEx117* | P*dpy-7::lon-2(+)* | line #2 | 592 | **54** | 2.0 | 281 | **65** | 2.8 |
| *lon-2 slt-1; qvEx118* | P*dpy-7::lon-2(+)* | line #3 | 450 | **54** | 2.3 | 269 | **64** | 2.9 |
| *lon-2 slt-1; qvEx184* | P*grd-10::lon-2(+)* | line #1 | 83 | **63** | 5.3 | | n.d. | |
| *lon-2 slt-1; qvEx185* | P*grd-10::lon-2(+)* | line #2 | 99 | **65** | 4.8 | | n.d. | |
| *lon-2 slt-1; qvEx186* | P*grd-10::lon-2(+)* | line #3 | 80 | **70** | 5.1 | | n.d. | |
| *lon-2 slt-1; qvEx187* | P*mec-7::lon-2(+)* | line #1 | 81 | **62** | 5.4 | | n.d. | |
| *lon-2 slt-1; qvEx188* | P*mec-7::lon-2(+)* | line #2 | 76 | **63** | 5.5 | | n.d. | |
| *lon-2 slt-1; qvEx189* | P*mec-7::lon-2(+)* | line #3 | 99 | **70** | 4.6 | | n.d. | |
| *lon-2 slt-1; qvEx190* | P*elt-2::lon-2(+)* | line #1 | 55 | **62** | 6.5 | | n.d. | |
| *lon-2 slt-1;* | P*elt-2::lon-* | line | 49 | **67** | 6.7 | | n.d. | |

| | | | | | | | | |
|---|---|---|---|---|---|---|---|---|
| *qvEx191* | *2(+)* | #2 | | | | | | |
| *lon-2 slt-1; qvEx192* | P*elt-2::lon-2(+)* | line #3 | 65 | **68** | 5.8 | | n.d. | |
| *lon-2 slt-1; qvEx193* | P*myo-3::lon-2(+)* | line #1 | 52 | **63** | 6.7 | | n.d. | |
| *lon-2 slt-1; qvEx194* | P*myo-3::lon-2(+)* | line #2 | 44 | **70** | 6.9 | | n.d. | |
| *lon-2 slt-1; qvEx195* | P*myo-3::lon-2(+)* | line #3 | 54 | **78** | 5.6 | | n.d. | |
| *lon-2 slt-1; qvEx204* | P*lon-2::sdn-1(+)* | line #1 | 51 | **65** | 6.7 | | n.d. | |
| *lon-2 slt-1; qvEx205* | P*lon-2::sdn-1(+)* | line #2 | 37 | **65** | 7.8 | | n.d. | |
| *lon-2 slt-1; qvEx206* | P*lon-2::sdn-1(+)* | line #3 | 47 | **83** | 5.5 | | n.d. | |
| *lon-2 slt-1; qvEx207* | P*mec-7::sdn-1(+)* | line #1 | 42 | **74** | 6.8 | | n.d. | |
| *lon-2 slt-1; qvEx208* | P*mec-7::sdn-1(+)* | line #2 | 37 | **78** | 6.8 | | n.d. | |
| *lon-2 slt-1; qvEx209* | P*mec-7::sdn-1(+)* | line #3 | 39 | **82** | 6.2 | | n.d. | |
| *lon-2 slt-1; qvEx121* | P*lon-2::*LON-2ΔGAG | line #1 | 233 | **49** | 3.3 | 184 | 70 | 3.4 |
| *lon-2 slt-1; qvEx122* | P*lon-2::*LON-2ΔGAG | line #2 | 204 | **51** | 3.5 | 193 | 74 | 3.2 |
| *lon-2 slt-1; qvEx196* | P*lon-2::*LON-2ΔGAG | line #3 | 158 | **53** | 4 | 215 | 71 | 3.1 |
| *lon-2 slt-1; qvEx111* | P*lon-2::*LON-2ΔGPI | line #1 | 275 | **52** | 3.0 | 130 | **75** | 3.8 |
| *lon-2 slt-1; qvEx199* | P*lon-2::*N-LON-2 | line #1 | 111 | **43** | 4.7 | 83 | **71** | 5.0 |
| *lon-2 slt-1; qvEx173* | P*lon-2::*N-LON-2 | line #2 | 147 | **48** | 4.1 | 67 | **75** | 5.3 |
| *lon-2 slt-1; qvEx174* | P*lon-2::*N-LON-2 | line #3 | 116 | **58** | 4.8 | 145 | **74** | 3.6 |
| *lon-2 slt-1; qvEx176* | P*lon-2::*C-LON-2 | line #1 | 42 | **67** | 7.3 | | n.d. | |
| *lon-2 slt-1; qvEx177* | P*lon-2::*C-LON-2 | line #2 | 52 | **67** | 6.5 | | n.d. | |
| *lon-2 slt-1; qvEx178* | P*lon-2::*C-LON-2 | line #3 | 39 | **69** | 7.4 | | n.d. | |

N, number of AVM axons examined. s.e.p, standard error of the proportion. n.d., not determined.

**Table 3.6**. AVM ventral guidance defects in strains examined, including transgenic lines to rescue *sdn-1*.

| Genotype | N | % Defective | s.e.p. |
|---|---|---|---|
| *zdIs5* | 391 | **0** | 0.0 |
| **HSPG mutants** | | | |
| *lon-2(e678); zdIs5* | 238 | **2** | 0.9 |
| *sdn-1(zh20); zdIs5* | 506 | **12** | 1.4 |
| *sdn-1(ok449); zdIs5* | 205 | **13** | 2.3 |
| *gpn-1(ok377); zdIs5* | 58 | **0** | 0.0 |
| *gpn-1(tm595); zdIs5* | 129 | **0** | 0.0 |
| *unc-52(e444); zdIs5* | 190 | **2** | 1.0 |
| *agr-1(tm2051); zdIs5* | 107 | **1** | 1.0 |
| *lon-2(e678) gpn-1(ok377); zdIs5* | 110 | **1** | 0.9 |
| *lon-2(e678) gpn-1(tm595); zdIs5* | 181 | **2** | 1.0 |
| *sdn-1(zh20) gpn-1(ok377); zdIs5* | 222 | **13** | 2.3 |
| *sdn-1(zh20) gpn-1(tm595); zdIs5* | 197 | **16** | 2.6 |
| *lon-2(e678) sdn-1(zh20); zdIs5* | 283 | **33** | 2.8 |
| *lon-2(e678) sdn-1(ok449); zdIs5* | 264 | **25** | 2.7 |
| *unc-52(e444); sdn-1(zh20); zdIs5* | 131 | **12** | 2.8 |
| *unc-52(e444) agr-1(tm2051); zdIs5* | 97 | **1** | 1.0 |
| *lon-2(e678) gpn-1(ok377) sdn-1(zh20); zdIs5* | 218 | **41** | 3.3 |
| *lon-2(e678) gpn-1(tm595) sdn-1(zh20); zdIs5* | 271 | **29** | 2.8 |
| **Strains with *unc-6* and *unc-40*** | | | |
| *unc-6(ev400); zdIs5* | 199 | **43** | 3.5 |
| *unc-6(e78); zdIs5* | 199 | **32** | 3.3 |
| *unc-40(e1430) zdIs5* | 237 | **15** | 2.3 |
| *unc-40(e271) zdIs5* | 190 | **18** | 2.8 |
| *unc-40(e271) zdIs5; unc-6(ev400)* | 290 | **36** | 2.8 |
| *lon-2(e678) unc-6(ev400); zdIs5* | 205 | **45** | 3.5 |
| *lon-2(e678) unc-6(e78); zdIs5* | 262 | **28** | 2.8 |
| *unc-40(e271) zdIs5; lon-2(e678)* | 246 | **18** | 2.4 |
| *unc-40(e1430) zdIs5; lon-2(e678)* | 205 | **18** | 2.7 |
| *unc-40(e271) zdIs5; sdn-1(zh20)* | 94 | **84** | 3.8 |
| *unc-6(ev400) slt-1(eh15); zdIs5* | 188 | **91** | 2.1 |
| **Strains with *slt-1* and *sax-3*** | | | |
| *slt-1(eh15); zdIs5* | 465 | **50** | 2.3 |
| *sax-3(ky123); zdIs5* | 380 | **44** | 2.5 |
| *sax-3(ky123) slt-1(eh15); zdIs5* | 220 | **51** | 3.4 |
| *lon-2(e678) slt-1(eh15); zdIs5* | 233 | **67** | 3.1 |
| *sax-3(ky123) lon-2(e678); zdIs5* | 493 | **53** | 2.2 |

| | | | | |
|---|---|---|---|---|
| *sdn-1(zh20) slt-1(eh15); zdIs5* | | 378 | **41** | 2.5 |
| *sax-3(ky123) sdn-1(zh20); zdIs5* | | 137 | **45** | 4.3 |
| *kyIs209; zdIs5* | | 835 | **19** | 1.4 |
| *lon-2(e678) kyIs209; zdIs5* | | 783 | **25** | 1.5 |
| **Strains with *sqv-5*** | | | | |
| *sqv-5(k172)* | | 235 | **9** | 1.9 |
| *lon-2(e678); sqv-5(k172)* | | 189 | **23** | 3.1 |
| **Transgenic strains used to rescue *sdn-1* function in AVM guidance in *lon-2 sdn-1; zdIs5*^** | | | | |
| | **Transgene** | | | |
| *lon-2(e678) sdn-1(zh20); zdIs5; qvEx114* | P*mec-7::sdn-1(+)* line #1 | 129 | **14** | 3.1 |
| *lon-2(e678) sdn-1(zh20); zdIs5; qvEx115* | P*mec-7::sdn-1(+)* line #2 | 136 | **15** | 3.1 |
| *lon-2(e678) sdn-1(zh20); zdIs5; qvEx100* | P*mec-7::sdn-1(+)* line #3 | 99 | **14** | 3.5 |

N, number of AVM axons examined. s.e.p., standard error of the proportion.

^ We assayed rescue of *sdn-1* function using the double mutants *lon-2 sdn-1* since it is easier to rescue defects that are 33% penetrant (as in the double *lon-2(e678) sdn-1(zh20*)) than to rescue defects that are 12% penetrant (as in the single mutant *sdn-1(zh20)*).

**Table 3.7.** Transgenic rescue of *lon-2* function in distal tip cell guidance.

| **Genotype** | **Transgene** | **Transgenic** | | | **Non-transgenic sibling controls** | | |
|---|---|---|---|---|---|---|---|
| | | **N** | **% Defective** | **s.e.p** | **N** | **% Defective** | **s.e.p** |
| *lon-2(e678);ufIs34; qvEx200* | P*lon-2::lon-2(+)* (P*lon-2::lon-2* cDNA) | 182 | **5** | 1.6 | 100 | **18** | 3.8 |
| *lon-2(e678); texEx164* | P*lon-2::lon-2(+)* | 236 | **7** | 1.7 | 248 | **13** | 2.2 |
| *lon-2(e678); texEx144* | P*lon-2::*LON-2ΔGAG | 108 | **4** | 1.9 | 122 | **18** | 3.5 |
| *lon-2(e678);ufIs34; qvEx210* | P*lon-2::* N-LON-2 | 124 | **5** | 2.0 | 126 | **16** | 3.3 |

**Table 3.8. List of strains used.**

| Strain | Genotype | Transgene | Reference |
|---|---|---|---|
| **Inserted transgenes** | | | |
| N2 | | | (Brenner 1974) |
| MT4005 | *zdIs5 I* | P*mec-4::gfp; lin-15(+)* | (Clark & Chiu 2003) |
| VQ412 | *kyIs209 X* derived from CX5374 | P*myo-3::slt-1* | (Yu et al 2002) |
| NW767 | *evIs25 X* | P*mec-7::unc-5;* P*mec-7::lac-Z* | (Hamelin et al 1993) |
| WS3404 | *opIs171* | P*sdn-1::sdn-1::gfp; lin-15(+)* | (Rhiner et al 2005) |
| LE311 | *lqIs4* | P*ceh-10::gfp* | (Tsalik et al 2003) |
| VQ84 | *vsIs48 X; ufIs34* derived from LX949 and IZ829 | P*unc-17::gfp;* P*unc-47::mCherry* | (Chase et al 2004) (Petrash et al 2013) |
| **HSPG mutants** | | | |
| VQ398 | *lon-2(e678) X; zdIs5 I* | | This study |
| VQ423 | *sdn-1(zh20) X; zdIs5 I* | | This study |
| VQ584 | *sdn-1(ok449) X; zdIs5 I* | | This study |
| VQ400 | *gpn-1(ok377) X; zdIs5 I* | | This study |
| VQ728 | *gpn-1(tm595) X; zdIs5 I* | | This study |
| VQ411 | *unc-52(e444) II; zdIs5 I* | | This study |
| VQ419 | *agr-1(tm2051) II; zdIs5 I* | | This study |
| VQ458 | *lon-2(e678) gpn-1(ok377) X; zdIs5 I* | | This study |
| VQ730 | *lon-2(e678) gpn-1(tm595) X; zdIs5 I* | | This study |
| VQ460 | *sdn-1(zh20) gpn-1(ok377) X; zdIs5 I* | | This study |
| VQ737 | *sdn-1(zh20) gpn-1(tm595) X; zdIs5 I* | | This study |
| VQ461 | *lon-2(e678) sdn-1(zh20) X; zdIs5 I* | | This study |
| VQ587 | *lon-2(e678) sdn-1(ok449) X; zdIs5 I* | | This study |
| VQ474 | *unc-52(e444) II; sdn-1(zh20) X; zdIs5 I* | | This study |
| VQ483 | *unc-52(e444) agr-1(tm2051) II; zdIs5 I* | | This study |
| VQ486 | *lon-2(e678) gpn-1(ok377) sdn-1(zh20) X; zdIs5 I* | | This study |
| VQ740 | *lon-2(e678) gpn-1(tm595) sdn-1(zh20) X; zdIs5 I* | | This study |
| VQ693 | *lon-2(e678) X; ufIs34* | | This study |
| **Strains with *unc-6*, *unc-40, unc-34, and unc-5*** | | | |

| | | |
|---|---|---|
| VQ396 | *unc-6(ev400) X; zdIs5 I* | This study |
| VQ395 | *unc-6(e78) X; zdIs5 I* | This study |
| VQ470 | *unc-40(e271) zdIs5 I* | This study |
| VQ565 | *unc-40(e1430) zdIs5 I* | This study |
| VQ529 | *unc-40(e271) zdIs5 I; unc-6(ev400) X* | This study |
| VQ469 | *lon-2(e678) unc-6(ev400) X; zdIs5 I* | This study |
| VQ567 | *lon-2(e678) unc-6(e78) X; zdIs5 I* | This study |
| VQ522 | *unc-40(e271) zdIs5 I; lon-2(e678) X* | This study |
| VQ581 | *unc-40(e1430) zdIs5 I; lon-2(e678) X* | This study |
| VQ738 | *unc-40(e271) zdIs5 I; sdn-1(zh20) X* | This study |
| VQ481 | *unc-6(ev400) slt-1(eh15) X; zdIs5 I* | This study |
| VQ686 | *unc-40(e271) I; vsIs48 X; ufIs34* | This study |
| VQ727 | *unc-40(e271) I; lon-2(e678) X; ufIs34* | This study |
| VQ722 | *unc-34(e566) V; zdIs5 I* | This study |
| VQ724 | *unc-5(e53) IV; vsIs48 X; ufIs34* | This study |
| VQ723 | *unc-5(e53) IV; lon-2(e678) X; ufIs34* | This study |
| **Strains with *slt-1* and *sax-3*** | | |
| VQ401 | *slt-1(eh15) X; zdIs5 I* | This study |
| VQ473 | *sax-3(ky123) X; zdIs5 I* | This study |
| VQ578 | *sax-3(ky123) slt-1(eh15) X; zdIs5 I* | This study |
| VQ482 | *lon-2(e678) slt-1(eh15) X; zdIs5 I* | This study |
| VQ501 | *sax-3(ky123) lon-2(e678) X; zdIs5 I* | This study |
| VQ432 | *sdn-1(zh20) slt-1(eh15) X; zdIs5 I* | This study |
| VQ526 | *sax-3(ky123) sdn-1(zh20) X; zdIs5 I* | This study |
| VQ427 | *kyIs209 X; zdIs5 I* | This study |
| VQ582 | *lon-2(e678) kyIs209 X; zdIs5 I* | This study |
| **Strains with *evIs25*** | | |
| VQ536 | *evIs25 X; zdIs5 I* | This study |
| VQ538 | *unc-6(ev400) evIs25 X; zdIs5 I* | This study |

| | | | |
|---|---|---|---|
| VQ540 | *unc-40(e271) zdIs5 I; evIs25 X* | | This study |
| VQ555 | *unc-6(ev400) lon-2(e678) evIs25 X*; *zdIs5 I* | | This study |
| VQ645 | *unc-40(e271) zdIs5 I; lon-2(e678) evIs25 X* | | This study |
| VQ556 | *slt-1(eh15) evIs25 X*; *zdIs5 I* | | This study |
| VQ557 | *sax-3(ky123) evIs25 X*; *zdIs5 I* | | This study |
| VQ541 | *lon-2(e678) evIs25 X; zdIs5 I* | | This study |
| VQ572 | *sdn-1(zh20) evIs25 X; zdIs5 I* | | This study |
| VQ772 | *unc-34(e566) V; evIs25 X; zdIs5 I* | | This study |
| VQ773 | *unc-34(e566) V; evIs25 lon-2(e678) X; zdIs5 I* | | This study |
| VQ542 | *lon-2(e678) sdn-1(zh20) evIs25 X; zdIs5 I* | | This study |
| **Strains with *sqv-5*** | | | |
| VQ523 | *sqv-5(k172) zdIs5 I* | | This study |
| VQ530 | *lon-2(e678) X; sqv-5(k172) zdIs5 I* | | This study |
| **Transgenic Lines** | | | |
| VQ776 | *lon-2(e678) X; ufIs34; qvEx200* | pCB246 (P*lon-2::lon-2(+)*), P*ceh-22::gfp,* P*unc-122::rfp*. Line #1 | This study |
| TLG257 | *lon-2(e678) X; texEx164* | Plasmid HW483 (P*lon-2::lon-2::gfp),* P*ttx-3::mCherry*. Line #2 | This study |
| TLG199 | *lon-2(e678) X; texEx144* | pSBL3SG006 (P*lon-2::*LON-2ΔGAG::*gfp*), P*ttx-3::mCherry*. Line #1 | This study |
| VQ795 | *lon-2(e678) X; qvEx210* | pCB270 (P*lon-2::*N-LON-2), pBSK+, P*ceh-22::gfp*, P*unc122::rfp*. Line #1 | This study |
| VQ596 | *lon-2(e678) slt-1(eh15) X; zdIs5 I; qvEx107* | PCR product of bases 13,104 of cosmid C39E6 to 26,408 of F55D10, P*ceh-22::gfp,* P*unc-122::rfp.* Line #1 | This study |
| VQ612 | *lon-2(e678) slt-1(eh15) X; zdIs5 I; qvEx110* | pCB246 (P*lon-2::lon-2*), P*ceh-22::gfp,* P*unc-122::rfp*, pBSK+. Line #2 | This study |
| VQ597 | *lon-2(e678) slt-1(eh15) X; zdIs5 I; qvEx108* | pCB246 (P*lon-2::lon-2*), P*ceh-22::gfp,* P*unc-122::rfp,* pBSK+. Line #3 | This study |
| VQ615 | *lon-2(e678) slt-1(eh15) X; zdIs5 I; qvEx113* | pCB218 (P*elt-3::lon-2*), P*ceh-22::gfp,* P*unc-122::rfp,* pBSK+. Line *#1* | This study |

| | | | |
|---|---|---|---|
| VQ623 | *lon-2(e678) slt-1(eh15) X; zdIs5 I; qvEx116* | pCB218 (P*elt-3::lon-2*), P*ceh-22::gfp,* P*unc-122::rfp,* pBSK+. Line *#2* | This study |
| VQ614 | *lon-2(e678) slt-1(eh15) X; zdIs5 I; qvEx112* | pCB268 (P*dpy-7::lon-2),* P*ceh-22::gfp,* P*unc-122::rfp;* pBSK+. Line #1 | This study |
| VQ624 | *lon-2(e678) slt-1(eh15) X; zdIs5 I; qvEx117* | pCB268 (P*dpy-7::lon-2),* P*ceh-22::gfp,* P*unc-122::rfp,* pBSK+. Line #2 | This study |
| VQ625 | *lon-2(e678) slt-1(eh15) X; zdIs5 I; qvEx118* | pCB268 (P*dpy-7::lon-2),* P*ceh-22::gfp,* P*unc-122::rfp,* pBSK+. Line #3 | This study |
| VQ746 | *lon-2(e678) slt-1(eh15) X; zdIs5 I; qvEx184* | pCB266 (P*grd-10::lon-2*), P*ceh-22:gfp,* P*unc-122::rfp,* pBSK+. Line #1 | This study |
| VQ747 | *lon-2(e678) slt-1(eh15) X; zdIs5 I; qvEx185* | pCB266 (P*grd-10::lon-2*), P*ceh-22:gfp,* P*unc-122::rfp,* pBSK+. Line #2 | This study |
| VQ748 | *lon-2(e678) slt-1(eh15) X; zdIs5 I; qvEx186* | pCB266 (P*grd-10::lon-2*), P*ceh-22:gfp,* P*unc-122::rfp,* pBSK+. Line #3 | This study |
| VQ749 | *lon-2(e678) slt-1(eh15) X; zdIs5 I; qvEx187* | pCB251 (P*mec-7::lon-2*), P*ceh-22:gfp,* P*unc-122::rfp,* pBSK+. Line #1 | This study |
| VQ750 | *lon-2(e678) slt-1(eh15) X; zdIs5 I; qvEx188* | pCB251 (P*mec-7::lon-2*), P*ceh-22:gfp,* P*unc-122::rfp,* pBSK+. Line #2 | This study |
| VQ751 | *lon-2(e678) slt-1(eh15) X; zdIs5 I; qvEx189* | pCB251(P*mec-7::lon-2*), P*ceh-22:gfp,* P*unc-122::rfp,* pBSK+. Line #3 | This study |
| VQ752 | *lon-2(e678) slt-1(eh15) X; zdIs5 I; qvEx190* | pCB308 (P*elt-2::lon-2*), P*ceh-22:gfp,* P*unc-122::rfp,* pBSK+. Line #1 | This study |
| VQ753 | *lon-2(e678) slt-1(eh15) X; zdIs5 I; qvEx191* | pCB308 (P*elt-2::lon-2*), P*ceh-22:gfp,* P*unc-122::rfp,* pBSK+. Line #2 | This study |
| VQ754 | *lon-2(e678) slt-1(eh15) X; zdIs5 I; qvEx192* | pCB308 (P*elt-2::lon-2*), P*ceh-22:gfp,* P*unc-122::rfp,* pBSK+. Line #3 | This study |
| VQ755 | *lon-2(e678) slt-1(eh15) X; zdIs5 I; qvEx193* | pCB332 (P*myo-3::lon-2*), P*ceh-22:gfp,* P*unc-122::rfp,* pBSK+. Line #1 | This study |
| VQ756 | *lon-2(e678) slt-1(eh15) X; zdIs5 I; qvEx194* | pCB332 (P*myo-3::lon-2*), P*ceh-22:gfp,* P*unc-122::rfp,* pBSK+. Line #2 | This study |
| VQ757 | *lon-2(e678) slt-1(eh15) X; zdIs5 I; qvEx195* | pCB332 (P*myo-3::lon-2*), P*ceh-22:gfp,* P*unc-122::rfp,* pBSK+. Line #3 | This study |
| VQ621 | *lon-2(e678) sdn-1(zh20) X; zdIs5 I; qvEx114* | pCB242 (P*mec-7::sdn-1*), pRF4, P*ttx-3::mCherry.* Line #1 | This study |
| VQ622 | *lon-2(e678) sdn-* | pCB242 (P*mec-7::sdn-1*), | This study |

| | | | |
|---|---|---|---|
| | *1(zh20) X; zdIs5 I; qvEx115* | pRF4, P*ttx-3::mCherry*. Line #2 | |
| VQ507 | *lon-2(e678) sdn-1(zh20); zdIs5 I; qvEx100* | pCB242 (P*mec-7::sdn-1*), pRF4, P*ttx-3::mCherry*. Line #3 | This study |
| VQ781 | *lon-2(e678) slt-1(eh15) X; zdIs5 I; qvEx204* | pCB312 (P*lon-2::sdn-1*), P*ceh-22::gfp*, P*unc-122::rfp*, pBSK+. Line #1 | This study |
| VQ782 | *lon-2(e678) slt-1(eh15) X; zdIs5 I; qvEx205* | pCB312 (P*lon-2::sdn-1*), P*ceh-22::gfp*, P*unc-122::rfp*, pBSK+. Line #2 | This study |
| VQ783 | *lon-2(e678) slt-1(eh15) X; zdIs5 I; qvEx206* | pCB312 (P*lon-2::sdn-1*), P*ceh-22::gfp*, P*unc-122::rfp*, pBSK+. Line #3 | This study |
| VQ784 | *lon-2(e678) slt-1(eh15) X; zdIs5 I; qvEx207* | pCB242 (P*mec-7::sdn-1*), P*ceh-22::gfp*, P*unc-122::rfp*, pBSK+. Line #1 | This study |
| VQ785 | *lon-2(e678) slt-1(eh15) X; zdIs5 I; qvEx208* | pCB242 (P*mec-7::sdn-1*), P*ceh-22::gfp*, P*unc-122::rfp*, pBSK+. Line #2 | This study |
| VQ786 | *lon-2(e678) slt-1(eh15) X; zdIs5 I; qvEx209* | pCB242 (P*mec-7::sdn-1*), P*ceh-22::gfp*, P*unc-122::rfp*, pBSK+. Line #3 | This study |
| VQ646 | *lon-2(e678) slt-1(eh15) X; zdIs5 I; qvEx121* | pSBL3SG006 (P*lon-2*::LON-2ΔGAG::*gfp*), P*ceh-22::gfp*, P*unc-122::rfp,* pBSK+. Line #1 | This study |
| VQ647 | *lon-2(e678) slt-1(eh15) X; zdIs5 I; qvEx122* | pSBL3SG006 (P*lon-2*::LON-2ΔGAG::*gfp*), P*ceh-22::gfp*, P*unc-122::rfp,* pBSK+. Line #2 | This study |
| VQ758 | *lon-2(e678) slt-1(eh15) X; zdIs5 I; qvEx196* | pSBL35G006 (P*lon-2*::LON-2ΔGAG::*gfp*), P*ceh-22::gfp*, P*unc-122::rfp,* pBSK+. Line #3 | This study |
| VQ613 | *lon-2(e678) slt-1(eh15) X; zdIs5 I; qvEx111* | pCB269 (P*lon-2::* LON-*2*ΔGPI), P*ceh-22::gfp,* P*unc-122::rfp,* pBSK+. Line #1 | This study |
| VQ761 | *lon-2(e678) slt-1(eh15) X; zdIs5 I; qvEx199* | pCB270 (P*lon-2*::N-LON-2), P*ceh-22::gfp*, P*unc-122::rfp,* pBSK+. Line #1 | This study |
| VQ762 | *lon-2(e678) slt-1(eh15) X; zdIs5 I; qvEx173* | pCB270 (P*lon-2*::N-LON-2), P*ceh-22::gfp*, P*unc-122::rfp,* pBSK+. Line #2 | This study |
| VQ763 | *lon-2(e678) slt-1(eh15) X; zdIs5 I; qvEx174* | pCB270 (P*lon-2*::N-LON-2), P*ceh-22::gfp*, P*unc-122::rfp,* pBSK+. Line #3 | This study |
| VQ766 | *lon-2(e678) slt-1(eh15) X; zdIs5 I; qvEx176* | pCB311 (P*lon-2*::C-LON-2), P*ceh-22::gfp*, P*unc-122::rfp,* pBSK+. Line #1 | This study |
| VQ767 | *lon-2(e678) slt-1(eh15) X; zdIs5 I;* | pCB311 (P*lon-2*::C-LON-2), P*ceh-22::gfp*, P*unc-122::rfp,* | This study |

| | | | |
|---|---|---|---|
| | *qvEx177* | pBSK+. Line #2 | |
| VQ768 | *lon-2(e678) slt-1(eh15) X; zdIs5 I; qvEx178* | pCB311 (P*lon-2::*C-LON-2), P*ceh-22::gfp*, P*unc-122::rfp,* pBSK+. Line #3 | This study |

Note: Plasmid pSBL3SG006 (P*lon-2::lon-2(ΔGAG)*) is from (Taneja-Bageshwar & Gumienny 2012) In this plasmid, all 3 GAG attachment sites of *lon-2* are mutated.

**Table 3.9.** List of primers used for building strains.

| Gene | Primer | Sequence | PCR product (bp) |
|---|---|---|---|
| ***sdn-1(zh20)*** | | | |
| Mutant | oCB837 | aaagagatgccggtcaggtg | 410 |
| | oCB842 | aatggacgggatgagtgtcc | |
| Wild-type | oCB837 | aaagagatgccggtcaggtg | 293 |
| | oCB876 | cttcagattcgagcctgctttgc | |
| ***sdn-1(ok449)*** | | | |
| Mutant | oCB1114 | ttctgcctgtcgacttactc | 297 |
| | oCB1125 | aagattgcggtaaaacacatc | |
| Wild-type | oCB1114 | ttctgcctgtcgacttactc | 478 |
| | oCB1115 | ttcgtcgtcggttgggtagc | |
| ***gpn-1(ok377)*** | | | |
| Mutant | oCB834 | atcaagaccgagtgatagtg | 501 |
| | oCB843 | aatcatcagcatcgggaggg | |
| Wild-type | oCB834 | atcaagaccgagtgatagtg | 412 |
| | oCB832 | ttttttgagggatatcatcg | |
| ***gpn-1(tm595)*** | | | |
| Mutant | oCB1309 | agtcgattgcaaacgaatacg | 468 |
| | oCB1310 | tcacacagtacgcttggcacg | |
| Wild-type | oCB1309 | agtcgattgcaaacgaatacg | 393 |
| | oCB1311 | aagctttccatgcatactcgc | |
| ***agr-1(tm2051)*** | | | |
| Mutant | oCB891 | cgaaaaatcgagagcaaaagg | 362 |
| | oCB893 | tcagattcttgacacatccc | |
| Wild-type | oCB890 | tttgaactcttggacgaacc | 1210 |
| | oCB891 | cgaaaaatcgagagcaaaagg | |
| ***slt-1(eh15)*** | | | |
| Mutant | oCB919 | tatgacgtgttccggaaacc | 467 |
| | oCB920 | atttctctaatacgggtagc | |
| Wild-type | oCB922 | tctcaattctaacatccatgtc | 339 |
| | oCB920 | atttctctaatacgggtagc | |
| ***kyIs209:*** **Detection of insertion P*myo-3::slt-1*** | | | |
| | oCB945 | tcattcgggatattttgtgg | 592 |
| | oCB950 | aagaagaagcatgcttctgg | |

| | | | |
|---|---|---|---|
| ***sax-3(ky123)*** | | | |
| Mutant | oCB1038 | agaatgtggctctctagtcc | ~330 |
| | oCB1039 | tcgtttccgcgcattcagtc | |
| Wild-type | oCB1038 | agaatgtggctctctagtcc | 527 |
| | oCB1042 | agcttcggattactgcttgc | |
| ***evIs25:*** **Detection of insertion P*mec-7::unc-5*** | | | |
| | oCB933 | ttgtcagtcgagcctcaagg | ~631 |
| | oCB966 | tccactgtctgataatctgg | |
| ***unc-40(e271)*** **sequencing** | | | |
| | oCB1077 | aattcgtgtaactgcttcc | 577 |
| | oCB1076 | ttgaatatttcggaggttgc | |
| ***unc-40(e1430)*** **sequencing** | | | |
| | oCB1079 | atcaatgcgctgtacatgtg | 366 |
| | oCB1078 | agagaccagggagttacagg | |

# Chapter IV

## LON-1, a conserved CAP superfamily protein and TGF-β pathway target, functions with SAX-7/L1CAM to maintain nervous system architecture

Cassandra R. Blanchette, Devyn Oliver, Andrea Thackeray, James Ritch, Avery Fisher, Claire Y. Bénard

Department of Neurobiology, UMass Medical School

364 Plantation Street, Worcester, MA 01605, USA

**Contribution summary:** C.R.B., J.R., and C.Y.B. designed experiments. C.R.B. carried out all experiments, except D.O. (PVD and PVQ analysis), J.R. (suppressor screen, identification of *qv10,* and initial *qv10* rescue), A.T. (suppressor screen and heat shocks), and A.F. (suppressor screen and *qv10* outcross). C.R.B. wrote the manuscript, with editing help from C.Y.B.

**ABSTRACT**

After embryonic development of the nervous system, neuronal architecture needs to be maintained in the face of further growth, maturation, and the physical stress of body movements. *sax-7*/L1CAM is a key neuronal maintenance molecule that functions to maintain neuronal architecture after its initial establishment. Through a forward genetic screen using *C. elegans,* we have identified *lon-1* as a novel suppressor of the *sax-7*/L1CAM mutant defects in the maintenance of nervous system architecture. Although *lon-1* has been characterized as a downstream target of the TGF-β pathway to regulate body length, our results indicate that the *lon-1*-mediated suppression of *sax-7* mutant defects is independent of both body length and the TGF-β signaling pathway. We find that an interaction with *sax-7*/L1CAM is not a general feature of other CAP superfamily molecules, highlighting its specificity of action. We found that to function with *sax-7* in maintaining head ganglia organization, *lon-1* acts in neurons and the hypodermis. Using a heat shock-inducible expression system as well as temporally controlled RNAi knockdown, we found that both *lon-1* and *sax-7* function post-embryonically to maintain the architecture of the nervous system. We show that *lon-1*-mediated suppression of *sax-7* defects is context dependent, as loss of *lon-1* does not lead to the suppression all of *sax-7* defects. Our findings reveal a novel interaction between *lon-1* and *sax-7*, and provide insight into the molecular pathways that actively maintain structures of the nervous system.

## INTRODUCTION

A critical but poorly understood aspect of neurobiology is how the integrity and function of an embryonically-established nervous system is protected throughout life, despite post-embryonic body growth, movement, and the incorporation of new neurons into existing neural circuits (Benard & Hobert 2009). Dedicated mechanisms must be in place to actively protect the nervous system in spite of these stresses. Research in *C. elegans* has identified a handful of molecules that function to maintain specific structures of the nervous system after their initial establishment, such as the precise positioning of axons within fascicles, the organization of neuronal soma and axons within ganglia, and the distribution and density of synapses. (Aurelio et al 2002, Barsi-Rhyne et al 2013, Benard et al 2009, Benard et al 2006, Bülow et al 2004, Cherra & Jin 2016, Hammarlund et al 2007, Johnson & Kramer 2012, Pocock et al 2008, Sasakura et al 2005, Shao et al 2013, Wang et al 2005, Woo et al 2008, Zallen et al 1999).

One of these molecules, SAX-7, is the conserved *C. elegans* homologue of the L1 cell adhesion molecule (L1CAM) family, and functions in neurons to maintain the position of neuronal soma and axons (Chen et al 2001, Pocock et al 2008, Sasakura et al 2005, Wang et al 2005, Zallen et al 1999). SAX-7/L1CAM is a transmembrane protein of the immunoglobulin superfamily with roles as a cell adhesion molecule (Chen et al 2001, Pocock et al 2008, Sasakura et al 2005, Wang et al 2005). Both long (SAX-7L) and short (SAX-7S) isoforms of SAX-7 are

expressed in *C. elegans.* SAX-7L contains six extracellular Ig-like domains while SAX-7S contains four, and both contain five extracellular fibronectin type III domains, a transmembrane domain, and a cytoplasmic tail containing FERM, ankyrin, and PDZ binding motifs (Chen et al 2001, Pocock et al 2008, Sasakura et al 2005, Wang et al 2005, Zhou et al 2008); **Fig. 4.1**). Despite their normal initial development, a subset of embryonically developed axons of the ventral nerve cord become defasciculated during the first larval stage in *sax-7* mutant animals, and specific neuronal soma and axons within ganglia become progressively disorganized in later larval and adult stages of *sax-7* mutant animals (Pocock et al 2008, Sasakura et al 2005, Wang et al 2005, Zallen et al 1999).

In vertebrates, L1CAM carries out developmental roles in migration and fasciculation, and in humans, mutations in L1CAM lead to neurodevelopmental disorders (reviewed in (Hortsch et al 2014)). Moreover, mammalian L1 family members L1CAM, CHL1, NrCAM, and Neurofascin (Hortsch 2000) play roles in the adult vertebrate brain, as conditional knockouts in the adult nervous system lead to changes in synaptic transmission, alterations to the axon initial segment, and behavioral deficits (Amor et al 2014, Kolata et al 2008, Kriebel et al 2011, Law et al 2003, Zonta et al 2011). These results highlight that both *C. elegans* SAX-7 and vertebrate L1 family members have continued importance in the adult nervous system to actively promote its integrity and functionality.

Despite the identification of molecules that function to maintain the architecture of the nervous system, our mechanistic understanding of how these molecules carry out these functions remains limited. To elucidate the molecular mechanisms by which SAX-7 functions to maintain the nervous system, and identify conserved neuronal protection molecules, we have carried out a forward genetic screen for suppressors of the *sax-7* defective maintenance of head ganglia organization. Through this screen, we have identified *lon-1* as a potent suppressor of the *sax-7* defect in the maintenance of the relative positioning between the ASH/ASI soma and the nerve ring. We show that *lon-1*-mediated suppression of *sax-7* defects is both independent of the TGF-β signaling pathway and also separate from body length. We find that *lon-1*, rather than being a general suppressor of *sax-7* defects, acts in a context-dependent manner, as *sax-7* defects in ventral cord maintenance and in dendritic arbor development are not altered by loss of *lon-1*. We demonstrate that *lon-1* functions in the nervous system and hypodermis to maintain nervous system architecture, and provide evidence that both *lon-1* and *sax-7* function post-embryonically to maintain head ganglia organization. Our results point to a novel, post-embryonic interaction between *sax-7* and *lon-1*, which highlights a newly uncovered role for *lon-1* outside of body length regulation, in the maintenance of nervous system architecture.

## RESULTS

### Identification of *qv24*, a new allele of *sax-7*/L1CAM

While studying two members of the ZIG family of two-Ig domain proteins and their role in the maintenance of neuronal architecture (Benard et al 2012), we uncovered a novel and spontaneous *sax-7* background mutation in one of our strains, which we named *sax-7(qv24)*. Following PCR amplification and Sanger sequencing of all *sax-7* exons and splice sites we identified that *sax-7(qv24)* is a G to A mutation that changes the splice donor site at intron four of the short isoform and at intron seven of the long isoform of *sax-7*, potentially affecting both the long and short isoforms of *sax-7* (**Fig. 4.1A**). *sax-7(qv24)* does not appear to be a null allele, as our RT-PCR analysis reveals that *sax-7* transcripts are present in *sax-7(qv24)* (**Fig. 4.1B**). Similarly, *sax-7(nj48)* is a strong loss-of-function deletion mutant that affects both the long and short isoforms of *sax-7* (Sasakura et al 2005), but *sax-7* transcripts are detected in our RT-PCR analysis (**Fig. 4.1A,B**). These results, along with previous work, indicate that no null mutant of *sax-7* currently exists (Wang et al 2005, Zhou et al 2008) (**Fig. 4.1B**), and those available are instead, strong loss-of-function alleles.

Prior work has shown that *sax-7* mutants exhibit a post-developmental failure to maintain the organization of neuronal structures including head ganglia and axonal fascicles (Pocock et al 2008, Sasakura et al 2005, Wang et al 2005, Zallen et al 1999). We therefore characterized the phenotype of *sax-7(qv24)*

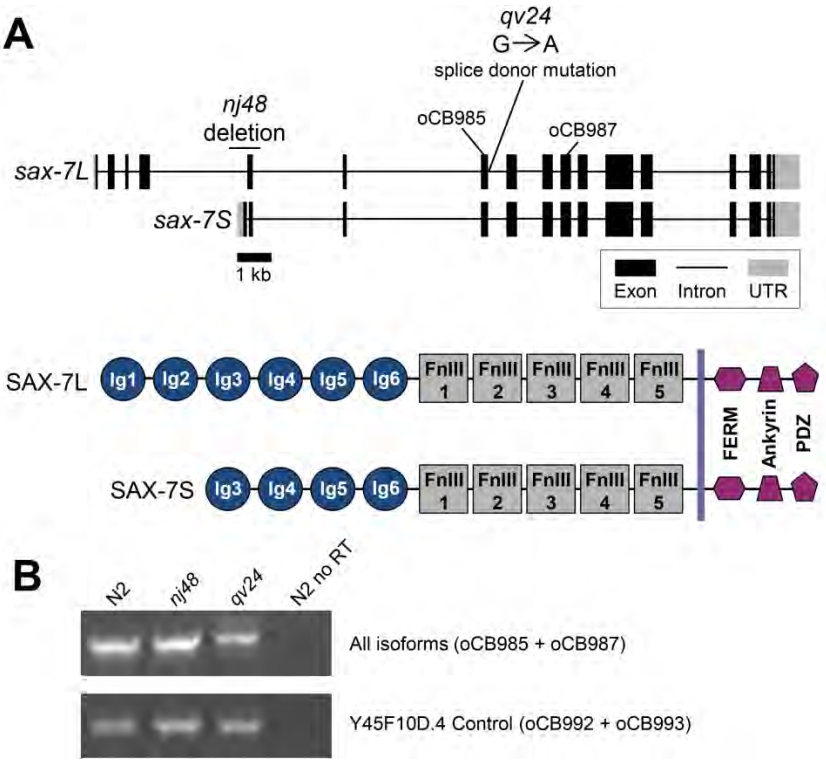


**Figure 4.1. *sax-7(nj48)* and *sax-7(qv24)* are not null alleles.**
A. Diagram of the *sax-7* locus depicting the gene structure of both the short (C18F3.2a) and long (C18F3.2b) *sax-7* isoforms. Exons (black boxes), introns (black lines), and UTRs (gray boxes) are to scale. *nj48* (Sasakura et al 2005) and *qv24* alleles used in this study are deletion and splice donor mutation alleles, respectively. Scale bar, 1 kb. Corresponding protein structure of SAX-7L and SAX-7S below.
B. RT-PCR using primers oCB985 and oCB987 to detect all *sax-7* isoforms yields products similar in size to N2 in both the *sax-7(nj48)* deletion mutant and the *sax-7(qv24)* splice donor site mutant worms. Y45F10D.4 is a housekeeping gene used as an RT-PCR control (Hoogewijs et al 2008). Primers used for RT-PCR of *sax-7* depicted in 4.1A. Neither *sax-7(nj48)* or *sax-7(qv24)* appear to be null.

mutants using the integrated *oyIs14* (P*sra-6::gfp*) transgene (Sarafi-Reinach et al 2001) which labels the ASH, ASI, and PVQ neurons and compared it to the phenotype of *sax-7(nj48)* mutants. We analyzed the maintenance of the relative positioning between the ASH/ASI soma and the nerve ring in wild type, *sax-7(nj48)*, and *sax-7(qv24)* animals across the first through fourth larval stages and

into adulthood. Initially, in the first larval stage, both *sax-7(nj48)* and *sax-7(qv24)* appear identical to wild type with regards to the relative positioning between the ASH/ASI soma and the nerve ring (**Fig. 4.2**). However, by the third larval stage, both *sax-7(nj48)* and *sax-7(qv24)* mutants begin to display defects in this relative positioning between the ASH/ASI soma and the nerve ring, and this progressively worsens as the animals go through the fourth larval stage and reach adulthood (**Fig. 4.2**). This suggests that the positioning of the ASH/ASI neurons and the nerve ring is initially properly established in *sax-7* mutants, but that they subsequently fail to maintain the relative positioning between the ASH/ASI soma and the nerve ring (Benard et al 2012, Pocock et al 2008). Despite the molecular differences between the *sax-7(nj48)* deletion and the *sax-7(qv24)* splice donor mutation, these mutants exhibit a very similar onset and severity in their failure to maintain the relative positioning between the ASH/ASI soma and the nerve ring.

We confirmed that the defects displayed by *sax-7(qv24)* mutants are indeed the result of the loss of *sax*-7 function, by introducing wild-type copies of *sax-7(+)* in *sax-7(qv24)* mutants and assaying for rescue. Previous work has shown that *sax-7S* is the adhesive isoform and the active form in the maintenance of head ganglia organization (Pocock et al 2008, Sasakura et al 2005) and that *sax-7* functions in the nervous system to maintain the relative positioning between the ASH/ASI soma and the nerve ring (Pocock et al 2008). Thus, we expressed *sax-*

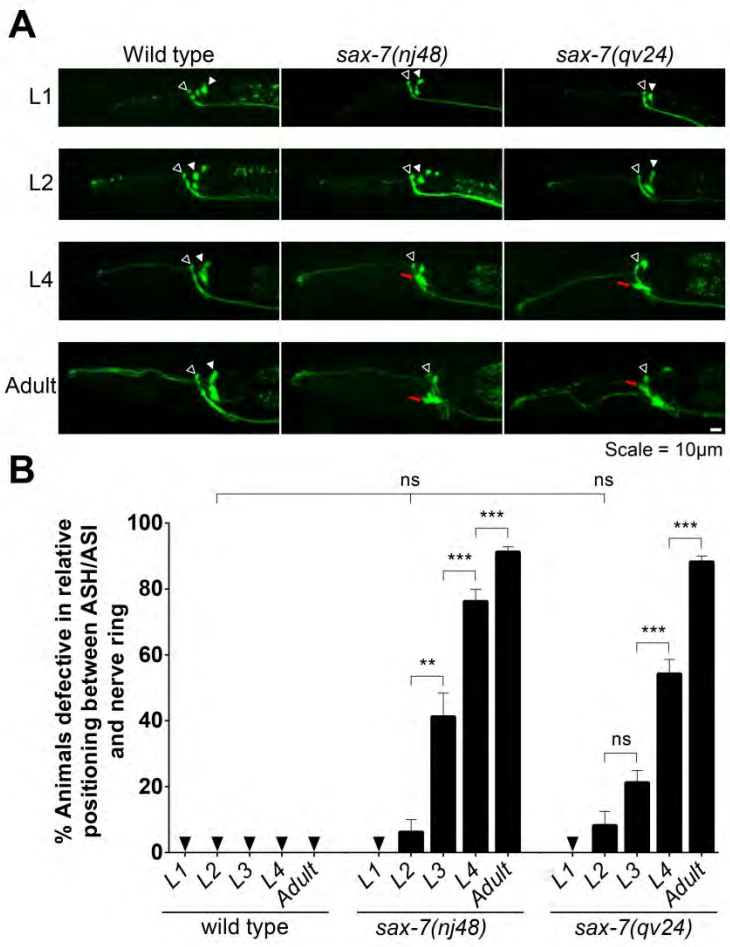


**Figure 4.2. *sax-7* mutants exhibit a progressive decline in the maintenance of head ganglia organization.**

A. Images of the ASH/ASI soma and the nerve ring visualized using *oyIs14* (P*sra-6::gfp*) in wild type, *sax-7(nj48),* and *sax-7(qv24)* mutants in the first (L1), second (L2), and fourth (L4) larval stages, and adulthood (Adult). In wild-type animals through adulthood, and *sax- 7* mutants until L2, the ASH/ASI soma (closed white arrowhead) are maintained posterior relative to the position of the nerve ring (open white arrowhead). In *sax-7* mutants, this relative positioning is disrupted (closed red arrow) in later larval stages and adults. Scale bar, 10 µm.

B. Quantification of animals defective for the relative positioning between the ASH/ASI soma and the nerve ring in wild type, *sax-7(nj48)* mutants, and *sax-7(qv24)* mutants from L1 through adulthood. Error bars are standard error of the proportion. ** P ≤ 0.01, *** P ≤ 0.001. (z-tests, P values were corrected by multiplying by the number of comparisons). ns, not significant.

*7S(+)* pan-neuronally under the control of the heterologous promoter P*unc-14* and found that expression of *sax-7S(+)* in the nervous system was sufficient to fully rescue the *sax-7(qv24)* defects (**Fig. 4.3**). This result indicates that disruption of the function of *sax-7* by the *qv24* mutation results in post-developmental defects in head ganglia organization. Our identification and analysis of the *sax-7(qv24)* mutation further confirms the functional importance of *sax-7* in maintaining neuronal architecture during post-embryonic development.

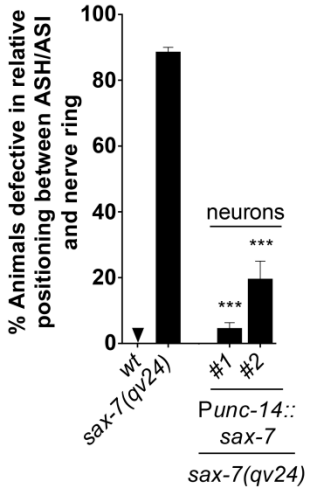


**Figure 4.3. *sax-7(qv24)* mutants are rescued by neuronal *sax-7S(+)* expression.**
*sax-7(qv24)* mutant defects are rescued by expression of *sax-7S(+)* in the nervous system using the heterologous promoter P*unc-14*. Error bars are standard error of the proportion. Asterisks denote significant difference: *** P ≤ 0.001. (z-tests, P values were corrected by multiplying by the number of comparisons).

## Expression of *sax-7S(+)* after establishment of head ganglia organization is sufficient for function

*sax-7* mutants display defects in the organization of the ASH/ASI neurons with respect to the nerve ring starting at the third larval stage and progressively worsening into adulthood. The appearance of these defects could be the result of either (1) an active role for *sax-7* during larval and adult stages, or (2) a

secondary consequence of undetectable developmental defects during embryogenesis that get amplified as the animal grows and moves. To distinguish between these possibilities, we induced transgenic expression of *sax-7S(+)* in *sax-7(nj48)* mutants at different time points and assayed for rescue of the sax-7 mutants' defects. For this, we expressed the rescuing *sax-7S(+)* cDNA under the control of P*hsp-16.2,* a heat shock inducible promoter that expresses in neurons and other tissues (Fire et al 1990, Jones et al 1986, Stringham et al 1992), in *sax-7(nj48)* mutant worms. As a control, *sax-7(nj48)* transgenic animals carrying P*hsp-16.2::sax-7S* were not rescued for the head ganglia defects when grown at 15°C and without heat shock. They were as defective as our reference *sax-7(nj48)* mutant strain and as their non-transgenic siblings under the same conditions (**Fig. 4.4**). These controls indicate that in the absence of heat shock, SAX-7S is not expressed from P*hsp-16.2::sax-7S(+)*.

We heat shocked *sax-7(nj48)* mutants carrying P*hsp-16.2::sax-7S* as freshly hatched first larval stage animals, kept the animals at 15°C at all times except during heat shock, and examined them as 1-day old adults. The *sax-7(nj48)* transgenic worms that were heat shocked in the first larval stage showed a significant rescue of the relative positioning between the ASH/ASI soma and the nerve ring compared to their non-transgenic control siblings that were also heat shocked (**Fig. 4.4**). Thus, *sax-7(nj48)* mutants can undergo embryogenesis and hatch lacking normal *sax-7* function and be rescued when provided with

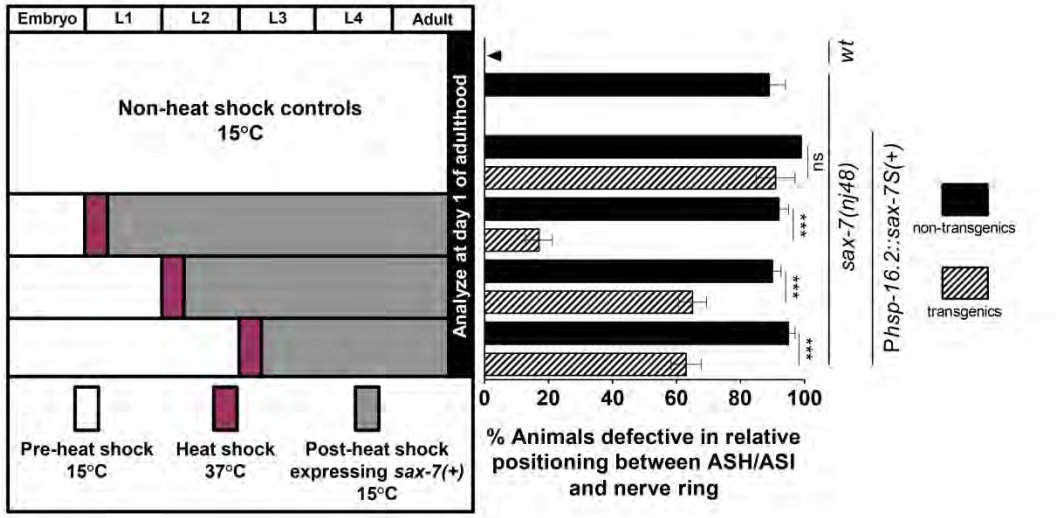


**Figure 4.4. Onset of *sax-7S(+)* expression in larval stages is sufficient for rescue of *sax-7(nj48)* mutants' defects.**
The top four lanes on the histogram correspond to non-heat shock controls of wild type, *sax-7(nj48)* mutants, transgenic *sax-7(nj48)* mutants carrying P*hsp-16.2::sax-7S(+)* (hatched bar), and non-transgenic controls (black bar). All were grown at 15°C and analyzed. The six bottom bars of the histogram correspond to heat-shocked animals, P*hsp-16.2::sax-7S(+)* transgenic (hatched bars), and non-transgenic controls (black bars). These heat-shocked animals were maintained at 15°C at all times except during heat shock at 37°C (pink box), which was done at the first, second, or third larval stage. All conditions tested showed a significant rescue of the *sax-7(nj48)* mutant defects with larval heat-shock induced *sax-7S(+)* expression, as compared to non-transgenic controls. Error bars are standard error of the proportion. Asterisks denote significant difference: *** $P \leq 0.001$. (z-tests, P values were corrected by multiplying by the number of comparisons). ns, not significant.

wild-type copies of *sax-7S(+)* post-hatch, indicating that post-embryonic *sax-7S* is sufficient for the maintenance of neuronal organization.

To determine when during larval development *sax-7* function is required for the maintenance of neuronal organization, we heat shocked transgenic *sax-7(nj48)* mutants carrying P*hsp-16.2::sax-7S* at the second and third larval stages.

Transgenic P*hsp-16.2::sax-7S* animals heat shocked in either the second or third larval stages showed a partial but significant rescue of the relative positioning between the ASH/ASI soma and the nerve ring compared to heat-shocked non-transgenic sibling controls (**Fig. 4.4**). By the third larval stage these *sax-7* mutant animals have been moving and growing for up to 42 hours without normal *sax-7* function, and roughly 40% already exhibit defects in head ganglia organization (**Fig. 4.2)**. Despite these factors, *sax-7S* expression starting in the third larval stage can rescue, which suggests these structures have not been irreparably damaged by the stresses they've encountered, and can still be protected by the presence of *sax-7S*.

### ***lon-1* identified as a novel suppressor of *sax-7* maintenance defects**

To gain understanding of the mechanism of action of *sax-7* we set out to identify molecules that function with *sax-7* to maintain the architecture of the nervous system. For this, we carried out an F2 clonal forward genetic screen to find suppressors of the *sax-7* mutant defect in the maintenance of head ganglia organization. We mutagenized $P_0$ *sax-7(qv24); oyIs14* worms with EMS and screened F3s to find broods of adults that maintained the ASH/ASI soma posterior to the nerve ring, despite harboring the *sax-7(qv24)* mutation (**Fig. 4.5**). Potential suppressors with impaired locomotion were not analyzed further, as paralysis is known to suppress *sax-7* defects in head ganglia organization (Benard et al 2012, Pocock et al 2008, Sasakura et al 2005). We isolated ten

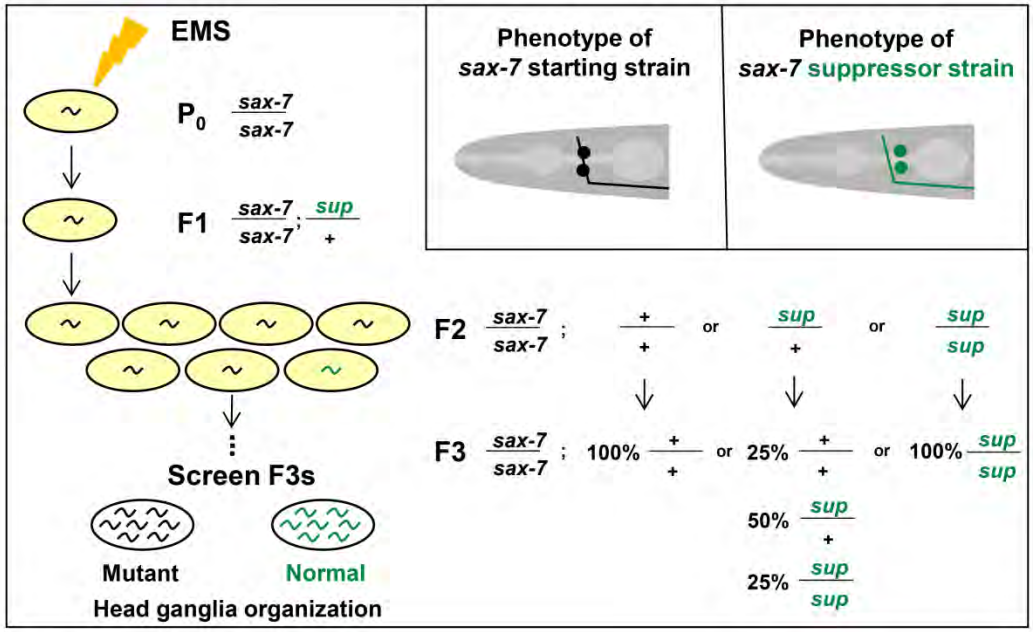


**Figure 4.5. A forward genetic screen to find suppressors of *sax-7*.**
Schematic of the EMS forward genetic screen carried out to find suppressors of the *sax-7* mutant defect in the maintenance of head ganglia organization. $P_0$ *sax-7(qv24)* worms were mutagenized with EMS. F1 progeny of the mutagenized $P_0$s were singled, those containing a suppressor mutation would be heterozygous. Seven F2s were singled from each F1 brood. If F1 was heterozygous for a suppressor mutation, expect one quarter of F2 broods to be homozygous for suppressor mutation (green worms). Adult F3s were screened to find broods of adults with properly maintained head ganglia organization.

suppressors, including *qv10* which displays profound suppression of the *sax-7* defects. We outcrossed this suppressor four times.

Next we set out to determine the molecular identity of the *qv10* suppressor mutation. Over the course of four outcrosses, we observed that the *qv10* worms were also longer than wild-type worms, and this Lon phenotype could not be segregated away from the suppression of the *sax-7* mutant phenotype. This

suggested that either the suppression was due to a *lon* mutation, or the suppressor mutation was tightly linked to one of the *lon* loci. We tested whether a mutation in one of the *lon* genes could suppress the *sax-7* neuronal maintenance defect. We built strains mutant for both *sax-7(nj48)* and *lon* mutants *lon-1(e185)* (Maduzia et al 2002, Morita et al 2002), *lon-2(e678)* (Gumienny et al 2007), *lon-3(e2175)* (Nystrom et al 2002, Suzuki et al 2002), and *lon-8(hu187)* (Soete et al 2007) and analyzed the relative positioning between the ASH/ASI soma and the nerve ring. We found that loss of function of *lon-1* in the *sax-7(nj48)* background suppressed the failure to maintain neuronal organization to a similar degree as our *qv10* suppressor. The other *lon* mutants showed either minimal or no suppression of the *sax-7* neuronal maintenance phenotype (**Fig. 4.6**). This finding suggested that *qv10* is an allele of *lon-1.* To directly test whether *qv10* harbors a mutation in the gene *lon-1*, we PCR amplified and Sanger sequenced all exons and splice sites of the *lon-1* locus in our *qv10* suppressor strain. We found that the *qv10* worms contain a G to A mutation at position 33,209 on cosmid F48E8, which converts a tryptophan residue to an early STOP at position 197 within the protein LON-1 (**Fig. 4.7**). To determine the impact of this allele on *lon-1* expression, we carried out RT-PCR which revealed that neither *qv10* nor *e185* are null, as *lon-1* transcripts are present in both mutant alleles (**Fig. 4.7**), indicating that *lon-1(qv10)* and *lon-1(e185)* are partial loss-of-function alleles.

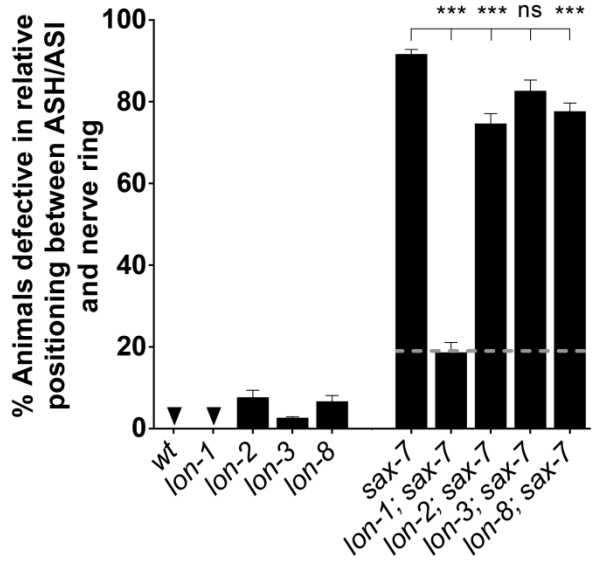


**Figure 4.6. Investigation of Lon mutants and their effect on the *sax-7* mutant phenotype.**
Isolated suppressor *qv10* was Lon. Analysis of head ganglia organization of double mutants between *lon-1,-2,-3,-8* with *sax-7(nj48)* revealed *lon-1* as the candidate with the highest degree of suppression. Gray dashed line indicates degree of suppression of *sax-7* mutant defects by loss of *lon-1*. Error bars are standard error of the proportion. Asterisks denote significant difference: *** P ≤ 0.001. (z-tests, P values were corrected by multiplying by the number of comparisons).

To test whether the suppression of the *sax-7(qv24)* neuronal maintenance defects by loss of *lon-1(qv10)* was allele-specific, we built and analyzed double mutants between two alleles of *lon-1* (*qv10* and *e185*) with two alleles of *sax-7* (*qv24* and *nj48*). We found that all four combinations of these alleles as double mutants between *lon-1* and *sax-7* produced a similar suppression of the *sax-7* mutant defects in maintaining the positioning of ASH/ASI soma with respect to the nerve ring (**Fig. 4.8**).

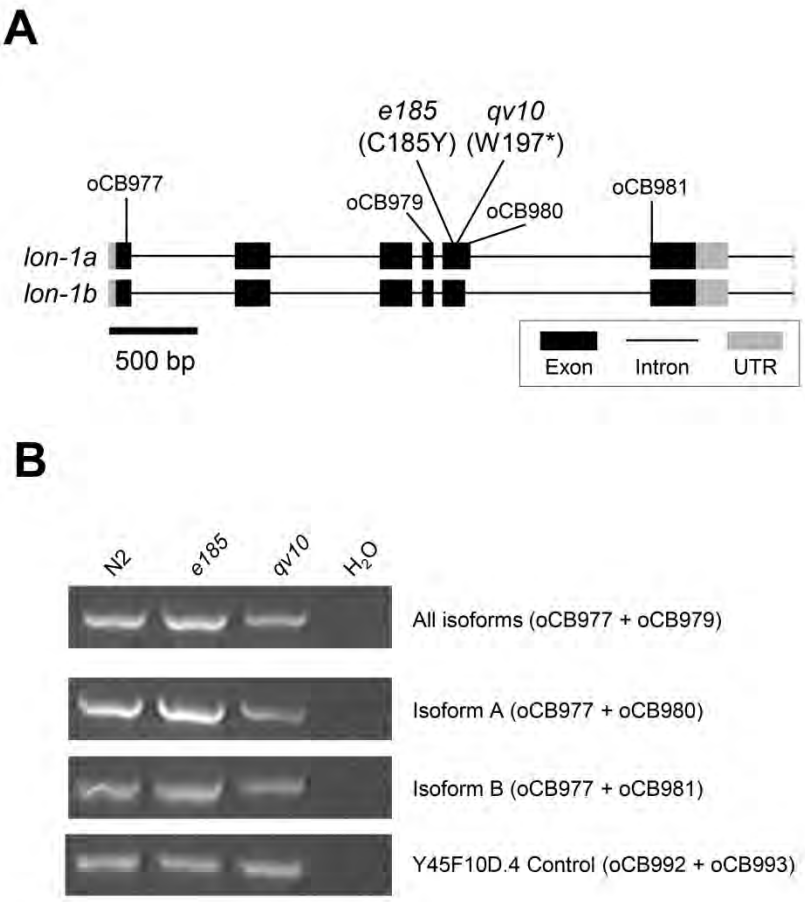


**Figure 4.7. *qv10* and *e185* are partial loss-of-function *lon-1* alleles.**
A. Diagram of the *lon-1* locus depicting the *lon-1a* and *lon-1b* isoforms. Exons (black boxes), introns (black lines), and UTRs (gray boxes) are to scale. *qv10* creates an early stop (*) at W197. *e185* is a missense mutation converting a cysteine residue at position 185 to a tyrosine residue (C185Y) (Maduzia et al 2002, Morita et al 2002). Scale bar, 500 bp.
B. RT-PCR using primers oCB977 and oCB979 to detect all *lon-1* isoforms yields a similar size product in N2, *lon-1(qv10),* and *lon-1(e185)*. Primers specific to *lon-1a* (primers oCB977 and oCB980) and *lon-1b* (primers oCB977 and oCB981) also yield products of similar size in N2, *lon-1(qv10),* and *lon-1(e185)*. Y45F10D.4 is a housekeeping gene used as an RT-PCR control (Hoogewijs et al 2008). Primers used for RT-PCR of *lon-1* depicted in 4.7A on top of gene diagram. Neither *lon-1(qv10)* nor *lon-1(e185)* appear to be null.

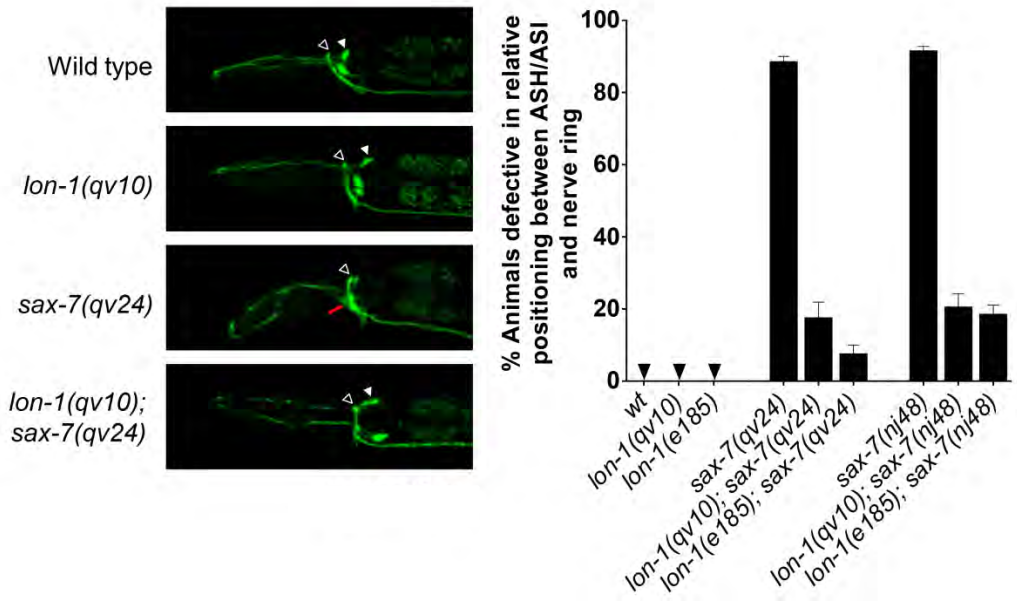


**Figure 4.8. Loss of *lon-1* suppresses the *sax-7* mutant defects in maintenance of head ganglia organization.**
Images of wild type, *lon-1(qv10)*, *sax-7(qv24)*, and *lon-1(qv10); sax-7(qv24)* double mutants expressing *oyIs14* (P*sra-6::gfp*) to label head neurons ASH/ASI and the nerve ring. The nerve ring (closed white arrowhead) is maintained anterior to the ASH/ASI soma (open white arrowhead) in wild type, *lon-1,* and *lon-1; sax-7* double mutants, while *sax-7* mutants exhibit a failure to maintain this relative positioning (closed red arrow). Quantification (on the right) of animals defective in the maintenance of this relative positioning indicates that loss of *lon-1(qv10)* or *lon-1(e185)* is able to suppress the *sax-7(qv24)* or *sax-7(nj48)* mutant defects in the maintenance of head ganglia organization. Error bars are standard error of the proportion.

To directly determine if the suppression of the *sax-7* neuronal maintenance defects is due to loss of *lon-1* function, we carried out rescue assays for *lon-1*. We introduced wild-type copies of *lon-1(+)* driven by its endogenous promoter including P*lon-1::lon-1(+)* genomic in the *lon-1; sax-7* double mutant background, and reasoned that if the suppression of *sax-7* defects was dependent on the loss of *lon-1* function, then the *sax-7* mutant phenotype would resurface in transgenic animals rescued for *lon-1*. Indeed, upon introduction of wild-type copies *lon-1(+)*

DNA in the *lon-1; sax-7* double mutant background, we found that the *sax-7* mutant phenotype reappeared (**Fig. 4.9A**). This indicates that loss of *lon-1* indeed suppresses the maintenance defects of *sax-7* mutants and identifies *lon-1* as a novel suppressor of the *sax-7* mutant defects in maintenance of neuronal architecture. As a control, we also overexpressed the same P*lon-1::lon-1(+)* genomic rescuing construct in the *lon-1* single mutants (without a *sax-7* mutation) and analyzed the relative positioning between the ASH/ASI soma and the nerve ring. We found that overexpression of *lon-1(+)* in the *lon-1* mutant background did not lead to neuronal defects (**Fig. 4.9B**), further confirming that the reappearance of neuronal maintenance defects in the *lon-1; sax-7* double mutants expressing *lon-1(+)* was indeed due to rescue of *lon-1* and not overexpression-induced defects. Taken together, these results indicate that loss of function of *lon-1* is able to suppress the *sax-7* mutant defect in the maintenance of the relative positioning between the ASH/ASI soma and the nerve ring.

LON-1 comes as two major isoforms, the a (313 aa) and b (302 aa) isoforms (**Fig. 4.7)**. To determine which isoform is functional in maintaining neuronal architecture, we carried out *lon-1* rescue assays with each isoform individually. We found that expression of either *lon-1a(+)* cDNA or *lon-1b(+)* cDNA under the endogenous promoter in the *lon-1; sax-7* double mutant could rescue the loss of

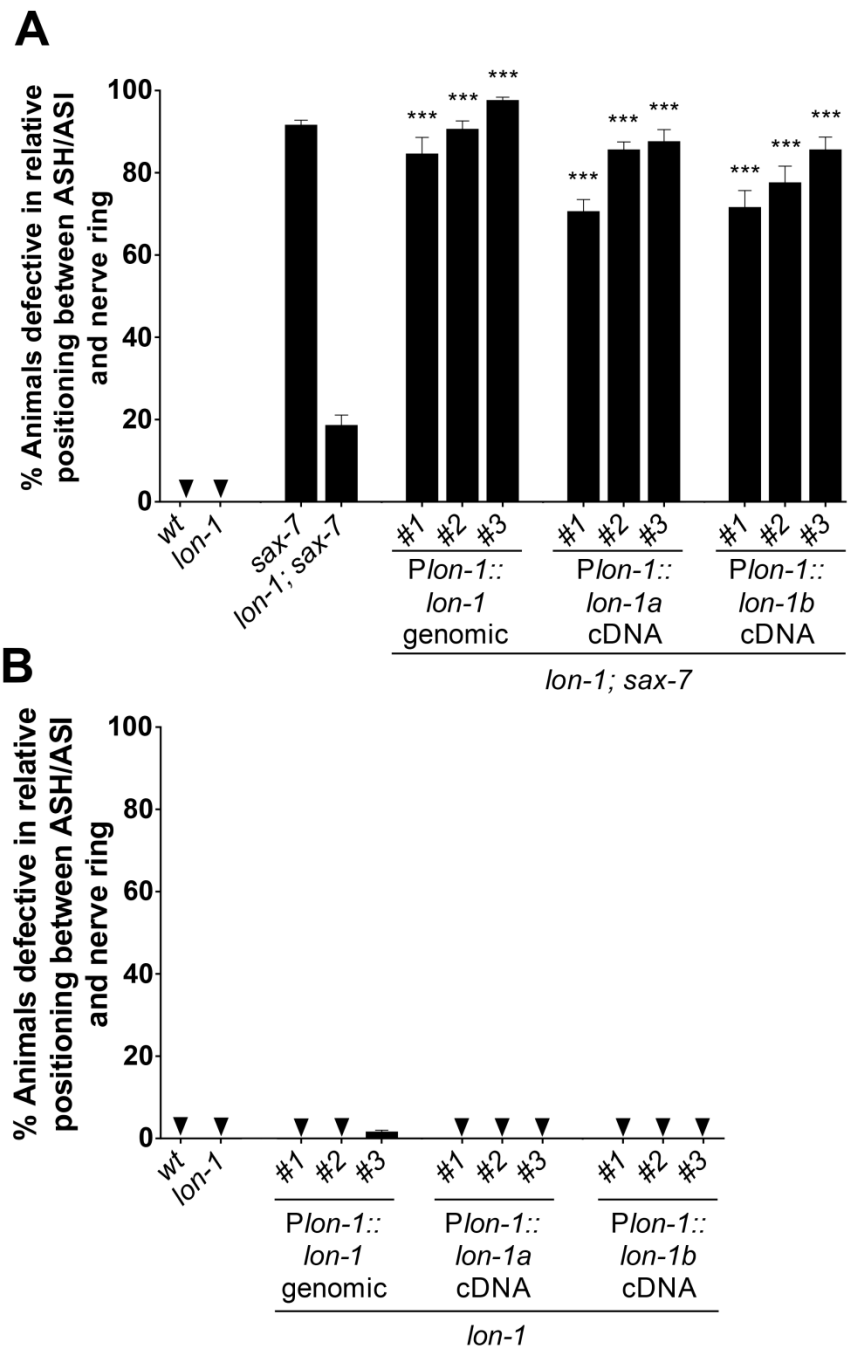
A
% Animals defective in relative positioning between ASH/ASI and nerve ring
100
80
60
40
20
0
***
wt
lon-1
sax-7
lon-1; sax-7
#1
#2
#3
Plon-1:: lon-1 genomic
Plon-1:: lon-1a cDNA
Plon-1:: lon-1b cDNA
lon-1; sax-7
B
% Animals defective in relative positioning between ASH/ASI and nerve ring
lon-1

**Figure 4.9. Rescue of *lon-1*-mediated suppression of *sax-7* by *lon-1(+)* expression.**
A. Loss of *lon-1* in the *sax-7* mutant background suppresses the *sax-7* defects in maintaining head ganglia organization. Expression of wild type copies of *lon-1(+)* under its endogenous promoter in *lon-1(e185); sax-7(nj48)* double mutants brings back the *sax-7* mutant phenotype and therefore rescues this *lon-1*-mediated suppression. Transgenic animals were compared to non-transgenic sibling controls.
B. Wild type copies of *lon-1(+)* under its endogenous promoter were expressed in *lon-1(qv10)* mutants. These animals exhibited no defects in the maintenance of the organization of the head ganglia. Therefore, the rescue observed in 4.9A is not due to the creation of an overexpression-induced phenotype.
Error bars are standard error of the proportion. Asterisks denote significant difference: *** P ≤ 0.001. (z-tests, P values were corrected by multiplying by the number of comparisons).

*lon-1* function and bring back the *sax-7* mutant defects. Additionally, we found that overexpression of either *lon-1a*(+) or *lon-1b*(+) in the *lon-1* mutant background did not lead to neuronal defects (**Fig. 4.9B**). These results indicate that both isoforms, LON-1a and LON-1b, are active in the maintenance of neuronal architecture.

## Loss of *lon-1* specifically suppresses head ganglia maintenance defects of *sax-7*

Having identified *lon-1* as a novel suppressor of the head ganglia maintenance defects of *sax-7*, we wondered if *lon-1* also participates in other functions of *sax-7*, such as in the maintenance of neuronal architecture in other areas of the nervous system or during neuronal development. For instance, *sax-7* mutants fail to maintain the precise positioning of axons along the ventral nerve cord, including the PVQ axons (Pocock et al 2008). In wild-type animals, the axon of the PVQ neurons is located ipsilaterally along the left or the right fascicle of the ventral nerve cord. However, in *sax-7* mutants, although in early first larval stage

worms the PVQ axons appear indistinguishable from wild type, by the late first larval stage the PVQ axons are not maintained within their specific fascicle along the ventral nerve cord and instead flip over to the opposite side (Pocock et al 2008). To determine whether loss of *lon-1* could suppress this *sax-7* defect in maintaining the PVQ axons within their appropriate fascicle, we analyzed the maintenance of the positioning of the PVQ axons in *lon-1; sax-7* double mutants compared to the single mutants. We found that the PVQ axons of *lon-1* appeared identical to wild type, and that *lon-1; sax-7* double mutants had a similar penetrance of PVQ axon flipover defects as *sax-7* single mutants (**Fig. 4.10A**). This result indicates that loss of *lon-1* did not suppress the *sax-7* defects in the maintenance of the axon positioning within their proper fascicle in the ventral nerve cord. This specificity suggests that loss of *lon-1* suppressing *sax-7* defects in the maintenance of neuronal architecture is context-dependent rather than *lon-1* acting as a general suppressor of *sax-7* maintenance defects.

In addition to defects in the maintenance of neuronal architecture, *sax-7* mutants also exhibit other neuronal phenotypes that are developmental in origin, including a defect in the development of the dendritic branches of the PVD neurons (Dong et al 2013, Salzberg et al 2013). In wild-type animals the PVD neurons are born postembryonically in the second larval stage (Sulston & Horvitz 1977) and extend their primary, secondary, tertiary, and quaternary dendritic branches that together have a menorah-like appearance during the second through fourth larval

stages (Oren-Suissa et al 2010, Smith et al 2010). *sax-7* mutants fail to develop this structure properly, as their PVD dendrites are highly disorganized (Dong et al 2013, Salzberg et al 2013). To address whether loss of *lon-1* could suppress developmental *sax-7* mutant phenotypes, we analyzed the development of the PVD dendrites in *lon-1; sax-7* double mutants compared to the single mutants, using the integrated transgene *wdIs52* (Smith et al 2010, Watson et al 2008). Whereas the dendritic structures between the secondary and tertiary PVD branches in *lon-1* mutants were indistinguishable from the wild type (T-shaped), we observed that they were severely disrupted in *sax-7* mutants, as previously reported (Dong et al 2013, Salzberg et al 2013) (**Fig. 4.10B**). We found that the PVD dendritic defects in *lon-1; sax-7* double mutants were as severely defective as in *sax-7* single mutants (**Fig. 4.10B**), indicating *sax-7* mutant defects in PVD dendrite development could not be suppressed by loss of *lon-1*. This observation supports the notion that *lon-1*, rather than functioning as a general suppressor of *sax-7*, may act in specific contexts depending on the cell types and/or the timing of action.

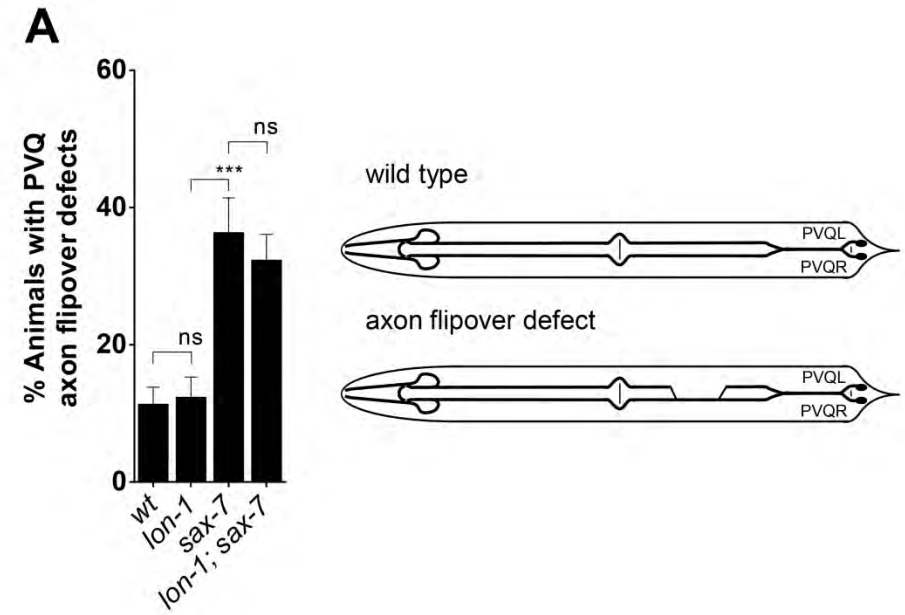
A
% Animals with PVQ axon flipover defects
60
40
20
0
ns
***
ns
wt
lon-1
sax-7
lon-1; sax-7
wild type
PVQL
PVQR
axon flipover defect
PVQL
PVQR

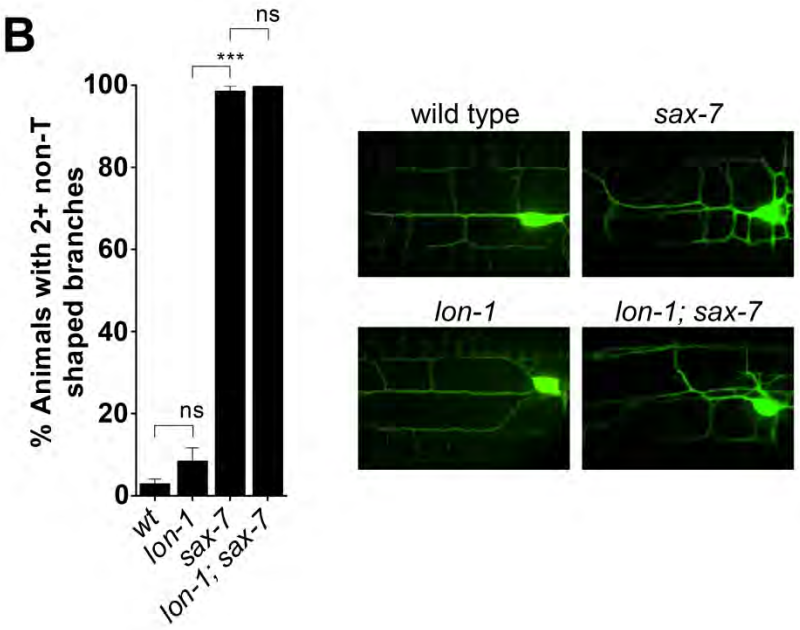
B
% Animals with 2+ non-T shaped branches
100
80
60
40
20
0
ns
***
ns
wt
lon-1
sax-7
lon-1; sax-7
wild type
sax-7
lon-1
lon-1; sax-7

**Figure 4.10. Loss of *lon-1* does not suppress other *sax-7* mutant defects.**
A. The positioning of the PVQ axons along the ventral nerve cord is maintained in wild type animals and *lon-1(e185)* mutants, but is not in *sax-7(nj48)* mutants. Similar to *sax-7(nj48)* mutants alone, *lon-1(e185); sax-7(nj48)* double mutants exhibit defects in PVQ axon maintenance.
B. Wild type and *lon-1(e185)* mutants exhibit normal PVD dendritic branch development, whereas *sax-7(nj48)* mutants and *lon-1(e185); sax-7(nj48)* double mutants exhibit defects in the development of the PVD dendritic branches.
Error bars are standard error of the proportion. Asterisks denote significant difference: *** P ≤ 0.001. (z-tests, P values were corrected by multiplying by the number of comparisons). ns, not significant.

## Suppression of *sax-7* defects by loss of *lon-1* is independent of the TGF-β signaling pathway

*lon-1* is a downstream target of the Sma/Mab TGF-β signaling pathway and regulates body length in a dose-dependent manner (**Fig. 4.11**). To gain mechanistic insight into how loss of function of *lon-1* might suppress the *sax-7* mutant defects in the maintenance of head ganglia organization, we investigated the role of the TGF-β signaling pathway and the impact of body length on the maintenance of neuronal architecture. We first determined the importance of TGF-β signaling in the maintenance of the neuronal architecture by analyzing the relative positioning between the ASH/ASI soma and the nerve ring in null or severe loss-of-function mutants for genes functioning in the TGF-β signaling pathway. This included mutants for a TGF-β ligand *dbl-1(nk3)* (Morita et al 1999), a type I TGF-β receptor *sma-6(wk7)* (Krishna et al 1999), the R-Smads *sma-2(e502)* and *sma-3(e491)*, the Co-Smad *sma-4(e729)* (Savage et al 1996), the extracellular TGF-β regulators *lon-2(e678)* (Gumienny et al 2007), *sma-10(ok2224)* (Gumienny et al 2010), *crm-1(tm2218)* (Fung et al 2007), *adt-*

*2(wk156)* (Fernando et al 2011), and *drag-1(tm3773)* (Tian et al 2010), and other associated genes related by homology, namely *unc-129(tm5461)* (Colavita et al 1998) and *tig-2(ok3416)* (Patterson & Padgett 2000). We found that loss of any of these TGF-β pathway components did not affect the maintenance of the relative positioning between the ASH/ASI soma and the nerve ring (**Fig. 4.12A**). Although loss of these TGF-β pathway components alone, including loss of *lon-1*, did not disrupt the maintenance of head ganglia organization, we addressed whether loss of these TGF-β pathway components could affect the *sax-7* mutant phenotype, as the loss of *lon-1* does. For this, we created double mutants between *sax-7(nj48)* and null/severe mutants for each of these TGF-β pathway components. Loss of four TGF-β pathway components other than *lon-1*, namely *lon-2*, *sma-10, sma-2,* and *adt-2,* reduced the penetrance of the *sax-7(nj48)* mutant defects but to a much lesser extent than the suppression elicited by loss of *lon-1* (**Fig. 4.12B**). Importantly, loss of the other eight TGF-β pathway components tested did not suppress the *sax-7(nj48)* neuronal maintenance mutant defects at all (**Fig. 4.12B**). Taken together, our results indicate that suppression of *sax-7* defects by loss of *lon-1* is independent of the TGF-β signaling pathway.

Other than loss of *lon-1*, the next best suppression of the *sax-7(nj48)* mutant defects by TGF-β components was by loss of *sma-2*. Since *sma-2* functions as a

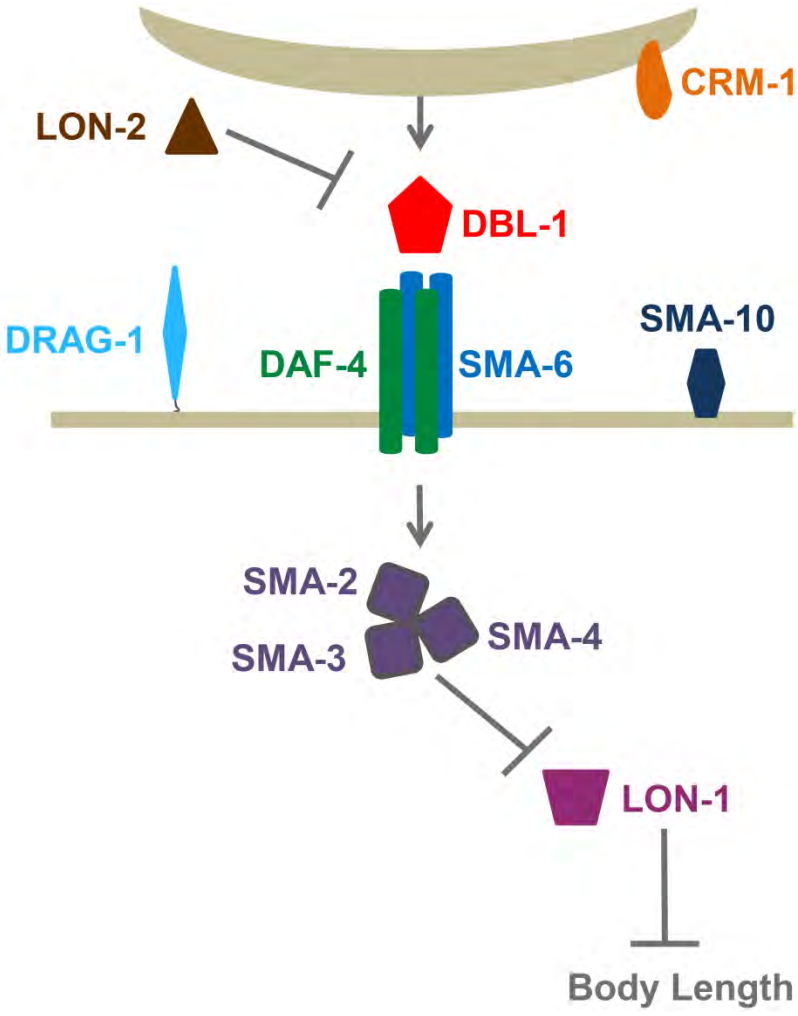


**Figure 4.11. Sma/Mab branch of the TGF-β signaling pathway.** One function of the Sma/Mab branch of the TGF-β signaling pathway is to regulate body length. TGF- β ligand (DBL-1) signals through a heteromeric complex of two type I (SMA-6) and two type II (DAF-4) receptor subunits. This is regulated by extracellular modulators including LON-2, CRM-1, DRAG-1, and SMA-10. Smads (SMA-2, SMA-3, and SMA-4) along with transcription factors regulate downstream targets, such as LON-1, to control body length. Diagram modeled after (Gumienny & Savage-Dunn 2013, Morck & Pilon 2006).

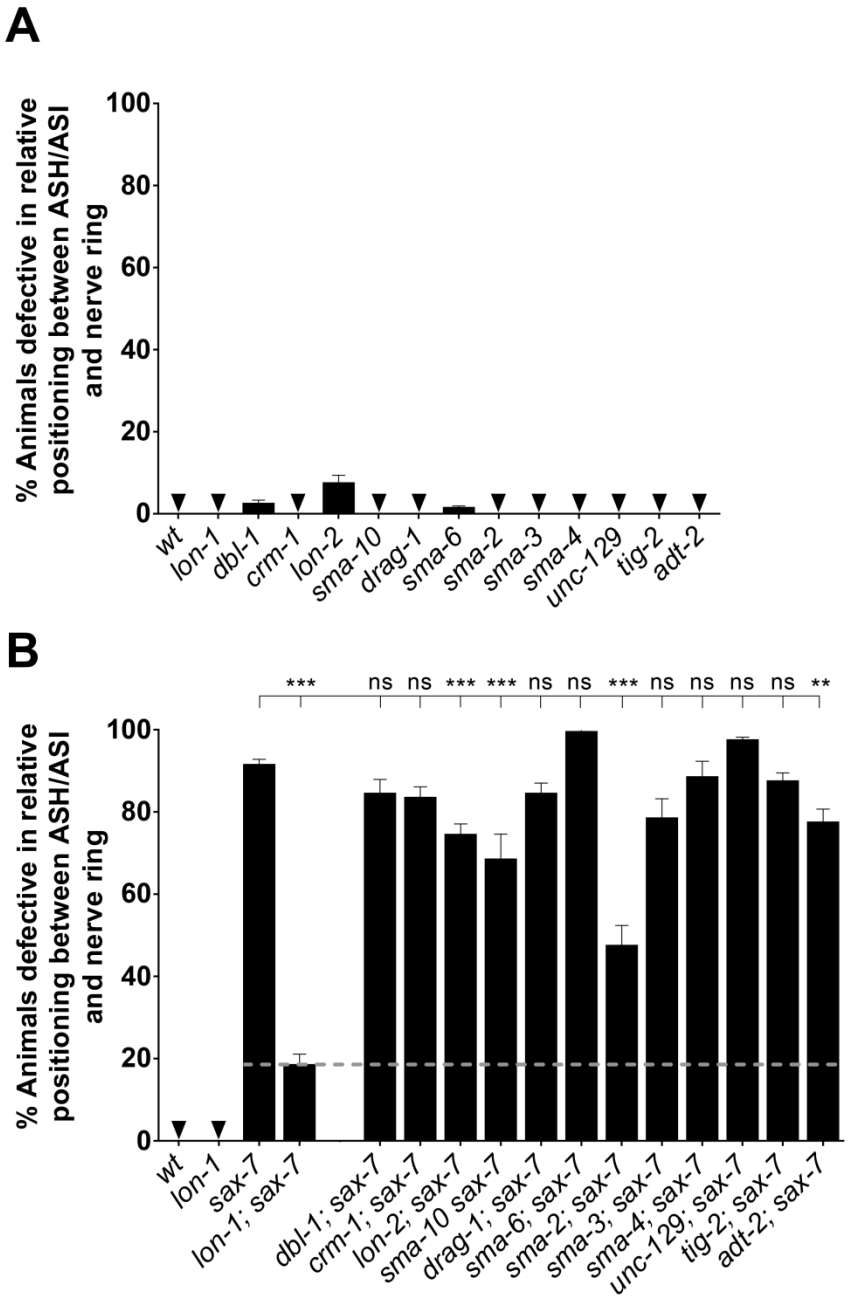
A
% Animals defective in relative positioning between ASH/ASI and nerve ring
100
80
60
40
20
0
wt
lon-1
dbl-1
crm-1
lon-2
sma-10
drag-1
sma-6
sma-2
sma-3
sma-4
unc-129
tig-2
adt-2
B
% Animals defective in relative positioning between ASH/ASI and nerve ring
*** ns ns *** *** ns ns *** ns ns ns ns **
100
80
60
40
20
0
wt
lon-1
sax-7
lon-1; sax-7
dbl-1; sax-7
crm-1; sax-7
lon-2; sax-7
sma-10 sax-7
drag-1; sax-7
sma-6; sax-7
sma-2; sax-7
sma-3; sax-7
sma-4; sax-7
unc-129; sax-7
tig-2; sax-7
adt-2; sax-7

**Figure 4.12. Maintenance of head ganglia organization is independent of TGF-β signaling.**
A. Loss of TGF-β signaling does not affect maintenance of head ganglia organization. ASH/ASI were visualized using *oyIs14* (P*sra-6::gfp)* in mutants for TGF-β pathway components including TGF-β ligand *dbl-1(nk3)*, type I TGF-β receptor *sma-6(wk7)*, the R-smads *sma-2(e502)* and *sma-3(e491)*, the Co-Smad *sma-4(e729)*, the extracellular TGF-β regulators *lon-2(e678)*, *sma-10(ok2224)*, *crm-1(tm2218)*, *adt-2(wk156)*, and *drag-1(tm3773)*, and genes related by homology including *unc-129(tm5461)* and *tig-2(ok3416)*. Animals mutant for these TGF-β signaling pathway components are able to maintain the relative positioning between the ASH/ASI soma and the nerve ring, similar to wild type.
B. Loss of TGF-β signaling in *sax-7* mutants does not suppress defects in head ganglia organization to the same degree as loss of *lon-1*. ASH/ASI were visualized using *oyIs14* (P*sra-6::gfp)* in double mutants between *sax-7(nj48)* and the TGF-β components listed in A. Gray dashed line indicates level of suppression of *sax-7* defects elicited by loss of *lon-1*. Error bars are standard error of the proportion. Asterisks denote significant difference: ** P ≤ 0.01, *** P ≤ 0.001. (z-tests, P values were corrected by multiplying by the number of comparisons). ns, not significant.

transcription factor to regulate gene expression in a pathway that normally inhibits *lon-1* expression (Savage et al 1996), perhaps the suppression of *sax-7* by *sma-2* is due to an upregulation of *lon-1* in the absence of *sma-2*. To test this, we overexpressed the *lon-1(+)* genomic sequence under its endogenous promoter (using P*lon-1::lon-1(+)* genomic) in the *sax-7(nj48)* mutant background. We analyzed the relative positioning between the ASH/ASI soma and the nerve ring in our transgenic animals compared to *sax-7(nj48)* single mutants at the fourth larval stage, and found that overexpression of *lon-1* in the *sax-7(nj48)* background did not significantly alter the *sax-7* mutant phenotype (**Fig. 4.13**). This suggests that loss of *sma-2* suppressing the *sax-7* mutant defects is unlikely simply due to increase in expression of *lon-1*. Alternatively, loss of *sma-2* may result in changes in the expression of other target genes, which could in turn

affect the *sax-7* mutant phenotype. Overall these results suggest that the TGF-β pathway per se does not regulate the maintenance of neuronal architecture.

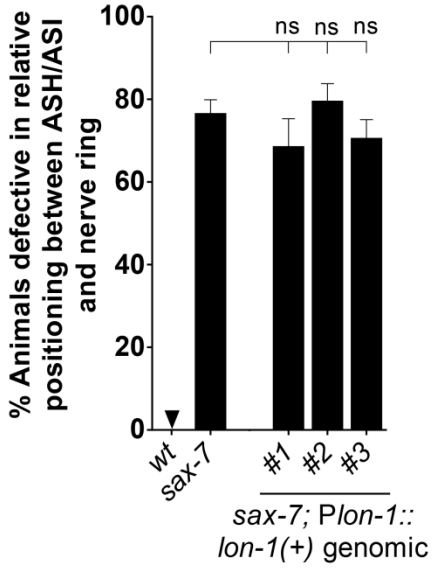


**Figure 4.13. Overexpression of *lon-1(+)* does not alter the *sax-7* mutant phenotype.**
*sax-7(nj48)* mutants overexpressing *lon-1(+)* show no significant difference compared to *sax-7(nj48)* alone in the maintenance of head ganglia organization. Animals were analyzed in the fourth larval stage when *sax-7(nj48)* mutant defects are not yet fully penetrant, to allow the detection of a potential enhancement of the defects. Error bars are standard error of the proportion. (z-tests, P values were corrected by multiplying by the number of comparisons). ns, not significant.

### *lon-1*-mediated suppression of the neuronal maintenance defects of *sax-7* mutants is independent of body length

While our results suggest that the *lon-1*-mediated suppression of the *sax-7* defects is independent of TGF-β signaling, the possibility remained that the mechanism of *lon-1*-mediated suppression of *sax-7* defects was dependent upon body length. Therefore, we investigated whether the suppression of *sax-7* mutant defects by loss of *lon-1* is due to the increased body length of the animals. As previously mentioned, our results show that loss of *lon-2(e678)*, *lon-3(e2175)*, and *lon-8(hu187)* did not suppress the *sax-7* defects to the same degree as *lon-1*, which suggests that this *lon-1*–mediated suppression is independent of body

length (**Fig. 4.6**). One caveat is that *lon-2, lon-3,* and *lon-8* mutants, while also Lon, are not as long as *lon-1(e185)* or *lon-1(qv10)* mutants (Nystrom et al 2002, Soete et al 2007). To directly test whether the Lon phenotype suppresses the *sax-7* mutant defects, we used an alternative approach to increase body length. Overexpression of the TGF-β ligand *dbl-1* using the integrated transgene *ctIs40* (Suzuki et al 1999) increases body length due to a downregulation of *lon-1* (Morita et al 1999, Suzuki et al 1999). Overexpression of *dbl-1* reduces *lon-1* expression but does not eliminate it completely (Maduzia et al 2002, Morita et al 2002) and also increases body length to a similar degree as *lon-1* mutants (Morita et al 1999). Therefore, we wondered if an increase in body length due to the overexpression of *dbl-1* in *sax-7(nj48)* mutants would lead to a suppression of the defects in the maintenance of the relative positioning between the ASH/ASI soma and the nerve ring. We found that *sax-7(nj48)* mutants overexpressing *dbl-1* in the *sax-7; ctIs40* strain did not exhibit a difference in phenotype compared to *sax-7(nj48)* mutants alone (**Fig. 4.14A**). This result suggests that an increase in body length is not responsible for the suppression, and that a greater reduction in *lon-1* expression than that triggered by overexpression of *dbl-1* is required to suppress the *sax-7* mutant defects.

To further address the relationship between body length and the *lon-1*-mediated suppression of defective maintenance of head ganglia organization, we examined whether loss of *lon-1* could suppress the defects of *dig-1,* another neuronal maintenance mutant unrelated to *sax-7*. *dig-1* encodes a large,

secreted protein required for proper basement membrane structure and maintenance of neuronal architecture (Benard et al 2006). Loss of function of *dig-1* leads to a failure to maintain head ganglia organization, similar to *sax-7(nj48)* mutants (**Fig. 4.14B**) (Benard et al 2006). We analyzed the relative positioning between the ASH/ASI soma and the nerve ring in *dig-1(ky188)* single mutants as compared to *lon-1(e185) dig-1(ky188)* double mutants and found that loss of *lon-1* did not suppress the *dig-1(ky188)* mutant defects (**Fig. 4.14B**). This finding indicates that the suppression of the head ganglia maintenance defect in *sax-7* mutants by loss of *lon-1* is highly specific, as the same defect in another mutant, *dig-1*, cannot be suppressed by loss of *lon-1*. Moreover, this result further corroborates that the increase in body size does not suppress defects in the maintenance of the relative positioning between the ASH/ASI soma and the nerve ring. Taken together, our results indicate that the mechanism by which *lon-1* impacts the *sax-7*-mediated maintenance of head ganglia organization is not via the TGF-β pathway and is not due to its effect on body size.

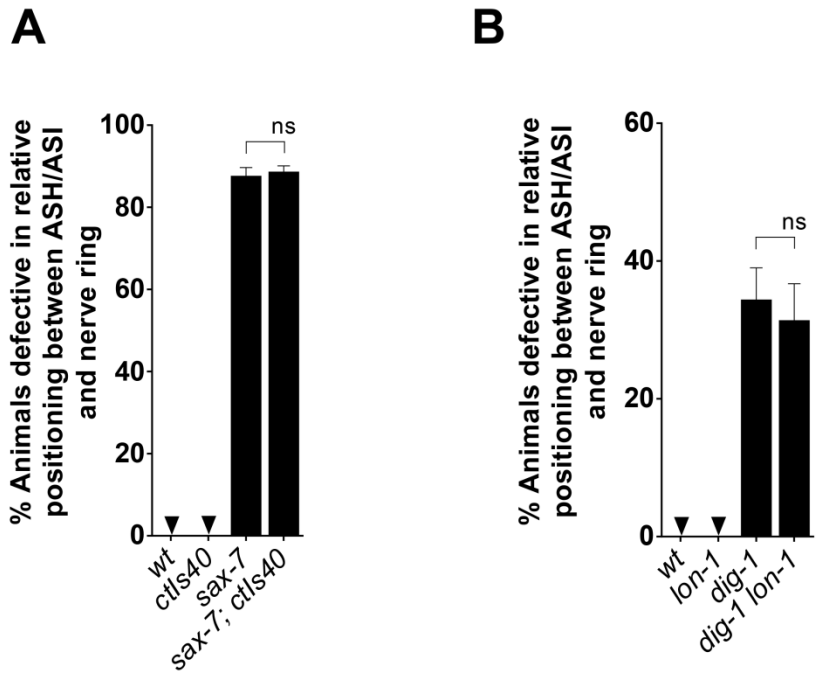


**Figure 4.14. *lon-1*-mediated suppression of *sax-7* defects is independent of body length.**

A. Increased body length cannot suppress *sax-7(nj48)* mutant defects. Animals overexpressing TGF-β ligand *dbl-1* (transgene *ctIs40*) are longer than wild type due to a decrease in *lon-1* expression (Morita et al 1999, Suzuki et al 1999), and maintain head ganglia organization similar to wild type. *sax-7(nj48); ctIs40* animals that overexpress *dbl-1* are long, yet do not display a significant difference compared to *sax-7(nj48)* mutants alone in the maintenance of head ganglia organization. This indicates increased body length alone cannot suppress *sax-7(nj48)* mutant defects.

B. *dig-1(ky188)* mutants, like *sax-7* mutants, exhibit a defective maintenance of the relative positioning between the ASH/ASI soma and the nerve ring (Bénard et al., 2006). Double mutant *lon-1(e185) dig-1(ky188)* exhibits defects in the maintenance of head ganglia organization that are not significantly different than *dig-1(ky188)* mutants alone. This suggests specificity of loss of *lon-1* in suppressing head ganglia organization defects resulting from loss of *sax-7*. Analysis done with two-day adults.

Error bars are standard error of the proportion. (z-tests, P values were corrected by multiplying by the number of comparisons). ns, not significant.

**Suppression of *sax-7* unlikely to be a general feature of CAP superfamily**

LON-1 is a member of the diverse CAP (cysteine-rich secretory proteins, antigen 5, and pathogenesis-related 1) superfamily (Maduzia et al 2002), which contains 28 members in *C. elegans*, 33 in mice, and 31 in humans (Gibbs et al 2008). This designation is based on LON-1 containing a cysteine-rich domain with homology to other CAP superfamily members which spans from approximately aa 78 to aa 217 of LON-1. Both the *lon-1(e185)* and *lon-1(qv10)* mutations fall within this conserved region ((Maduzia et al 2002); **Fig. 4.7)**, highlighting the functional importance of this sequence. CAP superfamily molecules are often secreted or associated with the membrane via a GPI-anchor (Gibbs et al 2008) and LON-1 contains a signal peptide sequence at the N-terminus (Maduzia et al 2002). We wondered whether the *lon-1*-mediated suppression of *sax-7* neuronal maintenance defects could be related to the presence of a CAP domain in LON-1 and if loss of other members of the CAP superfamily in *C. elegans* could suppress the *sax-7* mutant defects. We built double mutants between *sax-7(nj48)* and the three available CAP superfamily mutants, *vap-1(ok392)* (Cantacessi et al 2009, Hawdon et al 1999), *scl-1(ok1185)* (Ookuma et al 2003), and *scl-9(ok1138)* (Ashrafi et al 2003). Loss of any of these molecules did not lead to neuronal defects (**Fig. 4.15)**. We found that loss of *scl-1* or *scl-9* did not significantly alter the *sax-7(nj48)* mutant phenotype (**Fig 4.15)**. While loss of *vap-1* in the *sax-7(nj48)* mutant background decreases the defects compared to *sax-7(nj48)* single mutants, this suppression

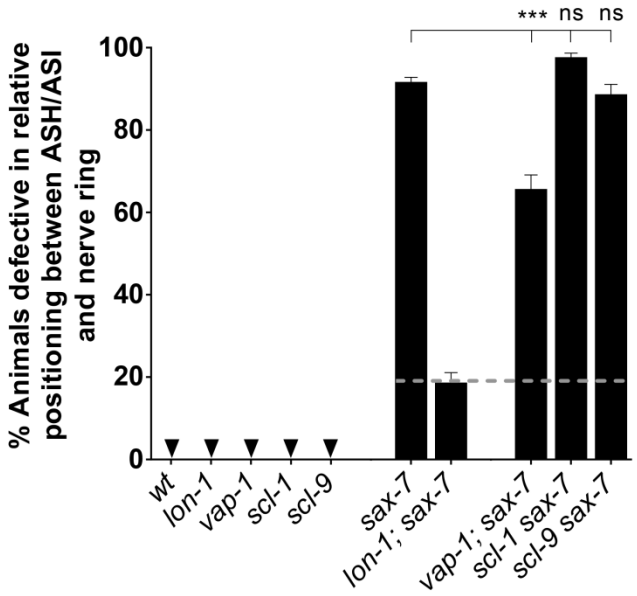


**4.15. CAP superfamily mutants are unable to suppress *sax-7* mutant defects to the same degree as *lon-1*.**
LON-1 is a member of the CAP superfamily. Mutants for other CAP superfamily members such as *vap-1(ok392), scl-1(ok1185),* and *scl-9(ok1138)* are able to maintain the relative positioning between the ASH/ASI soma and the nerve ring like wild-type and *lon-1* mutant animals. Loss of *scl-1(ok1185)* or *scl-9(ok1138)* does not alter the *sax-7(nj48)* mutant phenotype. While loss of *vap-1(ok392)* in the *sax-7(nj48)* mutant background does significantly decrease the phenotype compared to *sax-7(nj48)* alone, this is not to the same degree as seen with loss of *lon-1*. Gray dashed line indicates the degree of suppression of *sax-7* mutant defects by loss of *lon-1*. Error bars are standard error of the proportion. Asterisks denote significant difference: *** P ≤ 0.001. (z-tests, P values were corrected by multiplying by the number of comparisons). ns, not significant.

is far from that seen with loss of *lon-1* (**Fig. 4.15).** While we cannot rule out a role for other untested CAP superfamily molecules, these results suggest that the *lon-1*-mediated suppression of *sax-7* defects does not reflect a general function of CAP superfamily members in the maintenance of neuronal architecture.

## LON-1 functions in neurons and hypodermis to maintain neuronal architecture

To gain insight into the function of *lon-1* in neuronal maintenance, we characterized the focus of action of *lon-1*. *lon-1* is expressed in hypodermal cells and in the intestine and has been shown to function in the hypodermis for its role in the regulation of body length (Maduzia et al 2002, Morita et al 2002). To determine where *lon-1* functions to suppress the *sax-7* mutant defects, we expressed *lon-1a(+)* cDNA pan-neuronally (under the heterologous promoter P*unc-14*), in hypodermal cells (under the heterologous promoter P*elt-3*), in the intestine (under the heterologous promoter P*elt-2*), and in body wall muscles (under the heterologous promoter P*myo-3)* in *lon-1; sax-7* double mutants. We assayed for rescue of *lon-1* in these *lon-1; sax-7* double mutants by looking for a restoration of the *sax-7* mutant phenotype. We observed that the *sax-7* mutant phenotype resurfaced in *lon-1; sax-7* double mutants when *lon-1(+)* was expressed from either the nervous system or the hypodermis (**Fig. 4.16A**), suggesting that *lon-1* can function from the nervous system or the hypodermis for its role in the suppression of the *sax-7* mutant defects. Rescue was not observed upon expression of *lon-1* from the intestine or the body wall muscles (**Fig. 4.16A**). As a control, we ensured that this *lon-1*-induced reappearance of head ganglia disorganization in *lon-1; sax-7* double mutants was not due to an artefactual *lon-1(+)*-overexpression phenotype. For this, we expressed *lon-1(+)* in neurons, hypodermis, intestine, or muscles in *lon-1* mutants and analyzed the relative positioning between the ASH/ASI soma and the nerve ring.

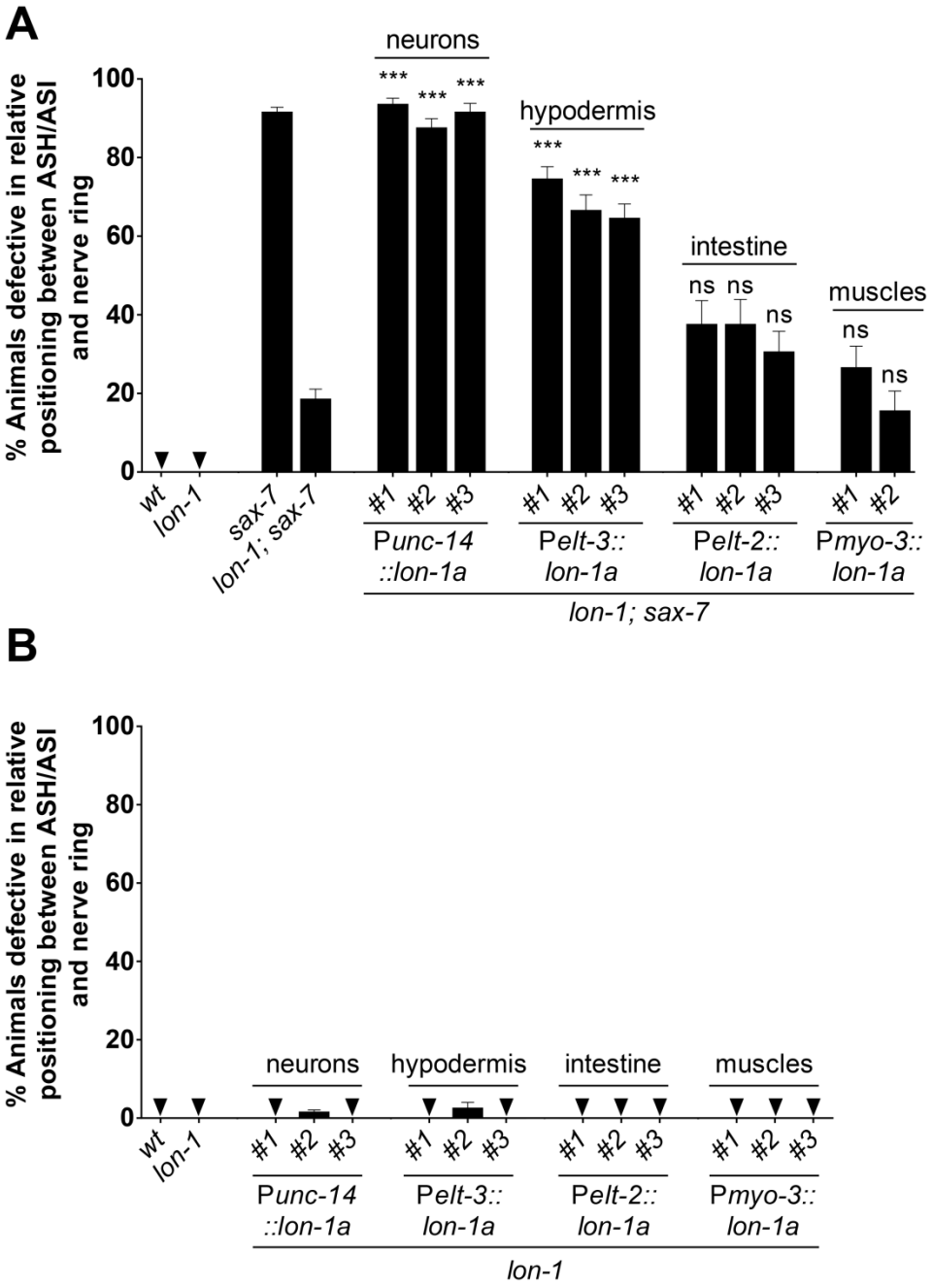
A
% Animals defective in relative positioning between ASH/ASI and nerve ring
100
80
60
40
20
0
neurons
hypodermis
intestine
muscles
***
ns
wt
lon-1
sax-7
lon-1; sax-7
#1
#2
#3
Punc-14 ::lon-1a
Pelt-3:: lon-1a
Pelt-2:: lon-1a
Pmyo-3:: lon-1a
lon-1; sax-7
B
% Animals defective in relative positioning between ASH/ASI and nerve ring
100
80
60
40
20
0
neurons
hypodermis
intestine
muscles
wt
lon-1
#1
#2
#3
Punc-14 ::lon-1a
Pelt-3:: lon-1a
Pelt-2:: lon-1a
Pmyo-3:: lon-1a
lon-1

**Figure 4.16. *lon-1* functions in the nervous system and hypodermis to maintain head ganglia organization.**
A. Expression of *lon-1(+)* in the nervous system (under the heterologous promoter P*unc-14*) or the hypodermis (under the heterologous promoter P*elt-3*), brings back the *sax-7(nj48)* mutant phenotype in the *lon-1(e185); sax-7(nj48)* double mutant, indicating LON-1 functions in the nervous system or hypodermis to maintain head ganglia organization. Expression of *lon-1(+)* in the intestine (under the heterologous promoter P*elt-2*), or muscles (under the heterologous promoter P*myo-3*), could not rescue. Transgenic animals were compared to non-transgenic sibling controls.
B. Overexpression of *lon-1(+)* in *lon-1(qv10)* mutants in the nervous system (using the heterologous promoter P*unc-14*), the hypodermis (using the heterologous promoter P*elt-3*), the intestine (using the heterologous promoter P*elt-2*), or the muscles (using the heterologous promoter P*myo-3*), did not affect the maintenance of head ganglia organization. This indicates the resurfaced mutant phenotype in 4.16A is due to rescue and not due to a *lon-1(+)* overexpression phenotype.
Error bars are standard error of the proportion. Asterisks denote significant difference: *** P ≤ 0.001. (z-tests, P values were corrected by multiplying by the number of comparisons). ns, not significant.

Overexpression of *lon-1(+)* from all tissues tested had no effect on head ganglia organization (**Fig. 4.16B**). This result confirms that the mutant defects seen in *lon-1; sax-7* double mutants upon expression of *lon-1(+)* in neurons or hypodermis reflects the rescue of the *lon-1*-mediated suppression of *sax-7*, and suggests that for neuronal maintenance of head ganglia organization, *lon-1* functions from neurons or hypodermis.

## SAX-7 functions in multiple adjacent neurons to maintain nervous system architecture

*sax-7* functions in the nervous system to maintain the relative positioning between the ASH/ASI soma and the nerve ring ((Pocock et al 2008); **Fig. 4.3**). To learn more about how *sax-7* functions to maintain the architecture of the nervous system and how it might interact with *lon-1*, we investigated whether

*sax-7* could function cell-autonomously or whether multi-neuron expression was required to maintain the relative positioning between the ASH/ASI soma and the nerve ring. To test this, we expressed *sax-7S* in *sax-7(nj48)* mutants under the heterologous promoter P*sra-6*, which restricts expression to the head neurons ASH and ASI, and to tail neurons PVQ. This restricted expression did not rescue the *sax-7(nj48)* mutant defects, suggesting that *sax-7* cannot function cell-autonomously in this context and is instead required from multiple neurons. To test this, we used the heterologous promoter P*osm-6*, to drive *sax-7S* in the ciliated sensory neurons, including ASH and ASI, in *sax-7(nj48)* mutants (this expression is much more restricted than the pan-neuronal P*unc-14* promoter that had previously conferred robust rescue of the *sax-7* mutant defects ((Pocock et al 2008); **Fig. 4.3**). Expression of *sax-7S* in the ciliated sensory neurons was sufficient to rescue the *sax-7(nj48)* defects in the maintenance of the relative positioning between the ASH/ASI soma and the nerve ring (**Fig. 4.17**). Our results indicate that *sax-7S* needs to be expressed from multiple neurons in close proximity to ASH/ASI, suggesting that homophilic interactions between SAX-7S molecules across neurons are required to maintain the relative positioning of the ASH/ASI soma with respect to the nerve ring, as has been observed in other contexts (Pocock et al 2008, Sasakura et al 2005).

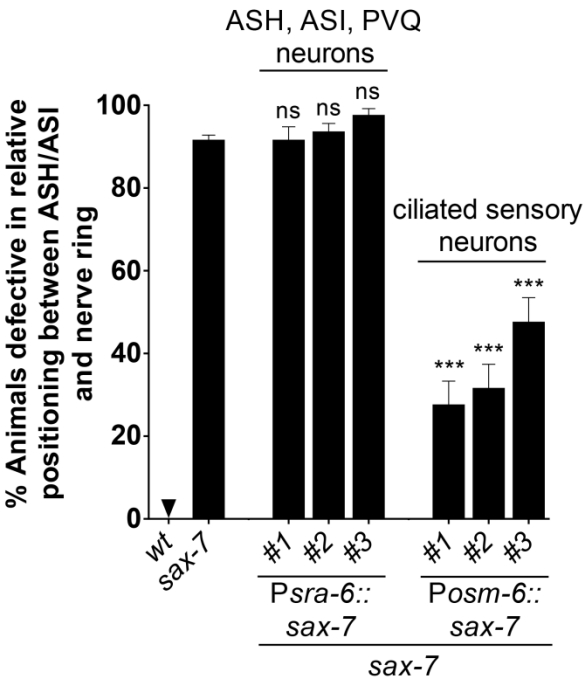


**4.17. *sax-7* functions in multiple neurons to maintain head ganglia organization.**
Expression of wild-type copies of *sax-7(+)* in the ASH/ASI head neurons and PVQ tail neurons (using the heterologous promoter P*sra-6*) is not sufficient to rescue the *sax-7(nj48)* mutant defects in head ganglia organization. Expression of wild-type copies of *sax-7(+)* in all ciliated sensory neurons (using the heterologous promoter P*osm-6*) is sufficient to rescue the *sax-7(nj48)* mutant defects. This indicates *sax-7* does not function cell autonomously but rather in multiple neurons to maintain head ganglia organization. Error bars are standard error of the proportion. Asterisks denote significant difference: *** P ≤ 0.001. (z-tests, P values were corrected by multiplying by the number of comparisons). ns, not significant.

**Post-embryonic loss of *lon-1* is sufficient to suppress *sax-7* mutant defects**

To help understand the function of *lon-1* in neuronal maintenance, we studied the timing of action of *lon-1*. Since we uncovered a post-embryonic role for *sax-7* in maintaining head ganglia organization (**Fig. 4.4**), we speculated that loss of *lon-1* function post-embryonically might be sufficient to suppress this *sax-7* mutant defect. To test this, we knocked down *lon-1* function at different times of larval development using RNAi against *lon-1* in *sax-7(nj48)* mutants. We used three different timing strategies (**Fig. 4.18A**). First, we verified that chronic *lon-1*(RNAi)

phenocopied the suppression of *sax-7* by *lon-1* mutations. $P_0$ *sax-7(nj48)* mutants were allowed to lay progeny on *lon-1(*RNAi), and these F1 progeny were maintained under *lon-1*(RNAi) conditions until they were 1-day old adults, when their neuroanatomy was examined (**Fig. 4.18A**). In this chronic *lon-1*(RNAi) condition, we found that *sax-7(nj48)* mutants grown on *lon-1(*RNAi) were significantly suppressed for head ganglia defects compared to the empty vector RNAi controls (**Fig. 4.18B**), indicating that *lon-1*(RNAi) phenocopied the *lon-1* loss-of-function mutations in suppressing *sax-7* defects.

Second, we addressed whether knock down of *lon-1* function post-embryonically would be sufficient to suppress *sax-7* head ganglia disorganization. For this, we collected freshly hatched first larval stage *sax-7(nj48)* mutants and raised them on *lon-1(*RNAi) bacteria until they were 1-day old adults, when we completed the analysis (**Fig. 4.18A**). Despite developing and hatching as a *sax-7* mutant and with wild-type *lon-1(+)*, the worms subjected to post-embryonic knock down of *lon-1* by *lon-1(*RNAi) displayed a significant reduction in the penetrance of defects as compared to empty vector RNAi controls (**Fig. 4.18B**). This result suggests that loss of *lon-1* function from the first larval stage onwards, well after the development of the head ganglia and of the nerve ring had been completed during embryogenesis, is sufficient to suppress the *sax-7* defects in head ganglia maintenance. These observations point to a post-embryonic role of *lon-1* in neuronal maintenance.

Third, we knocked down *lon-1* function from the second larval stage onwards and asked whether this could suppress *sax-7* head ganglia disorganization. For this, we collected second larval stage *sax-7(nj48)* mutants and raised them on *lon-1(*RNAi) until they were 1-day old adults, when we completed the analysis (**Fig. 4.18A**). We found that *sax-7* mutants on *lon-1(*RNAi) from the second larval stage onwards did not exhibit a significant difference from the control RNAi worms (**Fig. 4.18B**), indicating that loss of *lon-1* during and after the second larval stage is not sufficient to suppress these *sax-7* defects. This suggests that for the *sax-7* mutant defects to be suppressed the function of *lon-1* must be lost from the first larval stage; alternatively, *lon-1* might function during later larval stages as well, but the *lon-1* RNAi knockdown might be less efficient when started at the second larval stage. Nonetheless, these results indicate that *sax-7* mutants that undergo embryonic development and hatch lacking *sax-7* function can still become phenotypically wild type in adulthood through a post-embryonic intervention such as the loss of *lon-1* via RNAi.

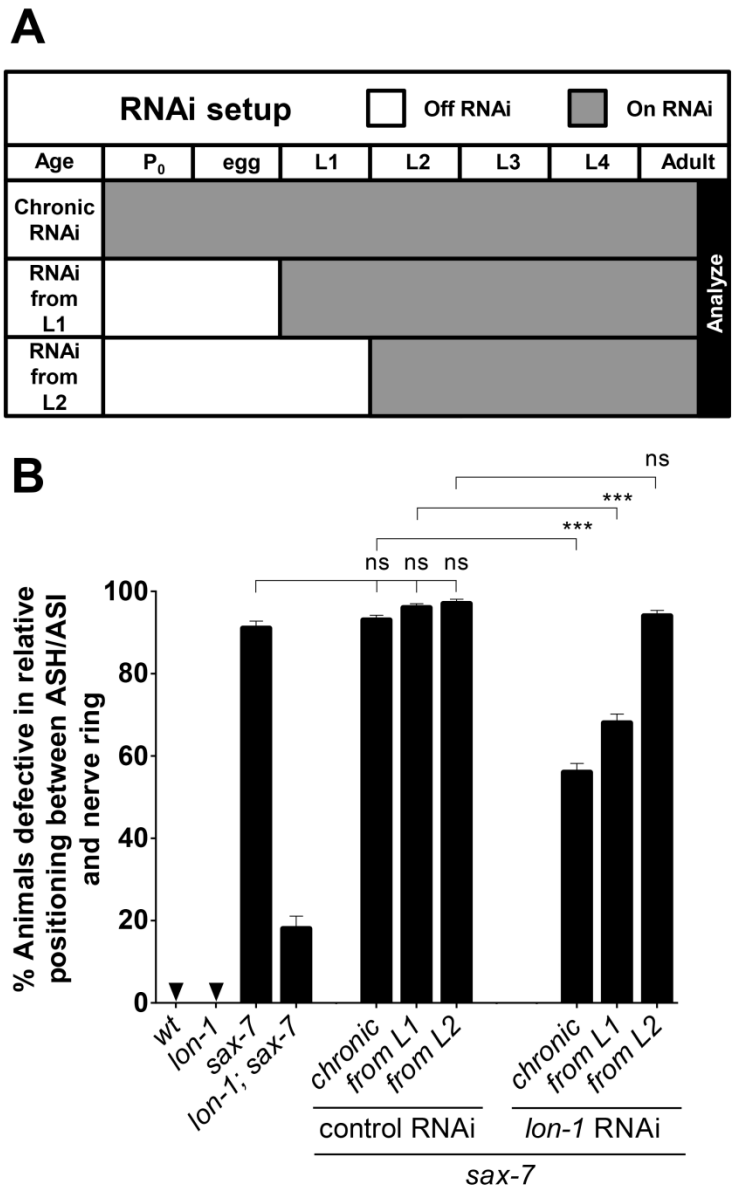
A
RNAi setup
Off RNAi
On RNAi
Age
P0
egg
L1
L2
L3
L4
Adult
Chronic RNAi
RNAi from L1
RNAi from L2
Analyze
B
ns
***
***
ns ns ns
% Animals defective in relative positioning between ASH/ASI and nerve ring
100
80
60
40
20
0
wt
lon-1
sax-7
lon-1; sax-7
chronic
from L1
from L2
chronic
from L1
from L2
control RNAi
lon-1 RNAi
sax-7

**4.18. Post-embryonic loss of *lon-1* is sufficient to suppress *sax-7* mutant defects.**
A. Diagram showing experimental set up of chronic RNAi, RNAi from L1, and RNAi from L2. *sax-7(nj48)* mutants were either on RNAi (gray bars) starting at $P_0$, L1, or L2 (ages on top), or off RNAi (white bars), and analyzed as adults (black vertical bar).
B. *sax-7(nj48)* mutants subjected to either chronic *lon-1* RNAi or *lon-1* RNAi from L1 exhibit a significant suppression of *sax-7(nj48)* mutant defects in the maintenance of head ganglia organization compared to control RNAi, while knockdown of *lon-1* from L2 in *sax-7(nj48)* mutants did not significantly alter the phenotype compared to control RNAi. This indicates that loss of *lon-1* function post-embryonically is sufficient to suppress *sax-7(nj48)* mutant defects. Error bars are standard error of proportion. Asterisks denote significant difference: *** $P \leq 0.001$. (z-tests, P values were corrected by multiplying by the number of comparisons). ns, not significant.

## DISCUSSION

Although a handful of molecules that maintain the architecture of the nervous system have been identified, the mechanisms by which they function remain poorly understood. In this study we have identified a conserved, novel neuronal maintenance factor, *lon-1*, and determined that it functions from the neurons themselves or the nearby hypodermis during larval development, to somehow impact the maintenance factor *sax-7* in maintaining nervous system architecture.

### Novel and specific interaction between *lon-1* and *sax-7* mediates the maintenance of head ganglia organization

Our study has identified *lon-1* as a suppressor of the *sax-7* defects in the maintenance of head ganglia organization. The *lon-1*-mediated suppression of *sax-7* defects is context dependent, as loss of *lon-1* does not impact all defects in neuronal architecture resulting from the disruption of *sax-7*. Although loss of *lon-1* powerfully suppresses the head ganglia disorganization defects of *sax-7*

mutants, loss of *lon-1* does not modify the defective maintenance of axon positioning in the ventral nerve cord, or the abnormal development of PVD dendrites of *sax-7* mutants (**Fig. 4.10)**.

Several factors may contribute to the specificity of action of *lon-1* in neuronal maintenance. One factor may be the timing of action of *lon-1*. *sax-7* is required to maintain aspects of neuronal architecture at different time points during larval and adult stages, and defects resulting from the loss of *sax-7* manifest at different ages. For instance, it is during the first larval stage that axons of the ventral nerve cord lose their normal position and flip over into the opposite fascicle in *sax-7* mutants (Pocock et al 2008), as well as in other neuronal maintenance mutants (Aurelio et al 2002, Benard et al 2009, Benard et al 2006). On the other hand, head ganglia disorganization emerges in the third larval stage and progresses through adulthood in *sax-7* mutants ((Benard et al 2012); **Fig. 4.2B**). Perhaps *lon-1* functions at later larval stages, interacting with *sax-7* in a way that influences head ganglia organization at the third larval stage and onwards, but cannot impact the maintenance of the ventral nerve cord during the first larval stage.

Consistent with this possibility, we found that knock down of *lon-1* from post-hatch and throughout larval stages via RNAi is sufficient to suppress *sax-7* head ganglia defects (**Fig. 4.18)**, indicating that *lon-1* acts during larval stages. It is

unclear, however, how quickly *lon-1* actually gets knocked down via RNAi, precluding our conclusion about its role during the first larval stage. Perhaps onset of PVQ axon flipover defects in *sax-7* mutants during the first larval stage occurs at a time when *lon-1* is not normally functionally required. In agreement with this, *lon-1* appears to have very low expression in embryos and L1s, with peak expression in L2 and L3 (Celniker et al 2009), when the *sax-7* PVQ axon flipover events have already occurred (Pocock et al 2008). It is possible that other early-acting molecular components function to maintain this structure along with *sax-7*. As a note, *lon-1* function is also temporally restricted in the context of its role in body length regulation, as *lon-1* mutants are initially wild type and display their Lon phenotype only at later larval stages (Maduzia et al 2002, Morita et al 2002).

A second factor that may contribute to *lon-1* suppressing specific neuronal defects of *sax-7* mutants relates to the distinct cellular contexts in which the neuronal structures exist, and the associated molecular differences in the extracellular milieu and neighboring tissues. For instance, the soma of the ASI and ASH neurons are located in head ganglia, in close proximity with numerous other neurons, which are all ensheathed by a basement membrane that defines each of the ganglia (White et al 1986), and are located sandwiched between the pharynx on one side and the muscles and hypodermis on the other side. The axons of ASI and ASH are part of the nerve ring, which is composed of

numerous other axons and runs around the pharyngeal isthmus, and is also wrapped by cephalic sheath glia (Ware et al 1975, White et al 1986). On the other hand, the PVD neurons are located along the body wall on the sides of the animal, and are largely isolated from other neurons (White et al., 1986). The PVQ axons are yet in a different context, spanning the length of the ventral midline where they run along the fascicles of the ventral nerve cord, along with other axons, and in close proximity to the hypodermis (White et al 1986).

One possible level of molecular specificity could come from interactions with the underlying basement membrane. The basement membrane is a specialized form of extracellular matrix that covers the interior surfaces of muscles, gonad, intestine, hypodermis, and pharynx (White et al 1976), structures which the nervous system is in contact with. Diversity in composition and thickness of basement membranes can vary in a tissue and temporal-specific manner (reviewed (Clay & Sherwood 2015, Kramer 2005) and could play a key role in creating a diverse environment for cell-cell interactions required for the development and maintenance of specific neuronal structures. Consistent with this, the large secreted maintenance factor DIG-1 plays important roles in maintaining the structure of the basement membrane (Benard et al 2006). Further research into the effect these maintenance factors, including LON-1, have on basement membrane regulation may provide insight into how these molecules function in long-term maintenance of neuronal architecture.

A third factor that may contribute to the specificity of action of *lon-1* in suppressing some of the neuronal defects of the *sax-7* mutants is the different tissue requirements for *sax-7* function by a given neuronal structure. Consistent with this, SAX-7 functions in distinct tissues to mediate its developmental and maintenance roles. For example, SAX-7 functions within the nervous system *in trans* across different neurons in a non-cell-autonomous manner for maintaining head ganglia (Pocock et al 2008, Sasakura et al 2005), but functions in the hypodermis to guide developing PVD dendrites (Dong et al 2013, Salzberg et al 2013), and loss of *lon-1* could suppress the maintenance of head ganglia organization but not PVD development. Also, for a pair of neurons in the retrovesicular ganglion, AIY and AVK, expression of *sax-7S(+)* in both cells is required for maintaining proper cell contact (Pocock et al 2008). Likewise, we find that expression of *sax-7S(+)* in only the ASH/ASI and PVQ neurons is not sufficient for rescue, but rather that expression in multiple neurons within the head ganglia is required (**Fig. 4.3 and 4.17)**. This suggests that neuron-to-neuron interactions are an important aspect of the maintenance of head ganglia organization, which is distinct from the neuronal-hypodermal interaction which dictates the proper development of the PVD dendrites. Perhaps *lon-1* function is specifically important for certain neuron-to-neuron *sax-7*-mediated interactions, yet is dispensable for neuron-hypodermis *sax-7*-mediated interactions.

Specificity of action in neuronal maintenance has also been observed in other mutants defective for the maintenance of neuronal architecture. While *sax-7* and the large secreted maintenance factor *dig-1* are required to maintain both the organization of the head ganglia and PVQ axon positioning, the two-Ig domain molecules *zig-3* and *zig-4* and a specific isoform of the FGF receptor *egl-15* are required to maintain PVQ axon positioning but are dispensable for the maintenance of head ganglia organization (Aurelio et al 2002, Benard et al 2009, Benard et al 2006, Bülow et al 2004, Pocock et al 2008). This highlights that the maintenance of these different structures requires different molecular interactions, and our results indicate that *lon-1* likely provides a level of molecular specificity in the maintenance of nervous system architecture.

### *lon-1* specifically, and not other CAP superfamily molecules, functions to maintain nervous system architecture

LON-1 is a member of the highly conserved CAP superfamily of molecules (Gibbs et al 2008, Maduzia et al 2002, Morita et al 2002), which is characterized by signature sequence motifs (Gibbs et al 2008). The CAP superfamily contains 28 members in *C. elegans,* 33 in mice, and 31 in humans (Gibbs et al 2008). The functions of CAP superfamily molecules are not well understood, yet are implicated in a diverse set of functions (Gibbs et al 2008). In *C. elegans,* CAP superfamily molecules (reviewed in (Cantacessi et al 2009)) function to regulate body length (Maduzia et al 2002, Morita et al 2002), stress resistance, longevity

and aging (Patterson 2003), fat storage (Ashrafi et al 2003), as well as apoptosis and immune responses (Pinkston-Gosse & Kenyon 2007). In mammals, CAP superfamily proteins are implicated in the regulation of extracellular matrix, regulation of ion channels, cell-cell adhesion, and cancer (Gibbs et al 2008).

We found that loss of three other CAP superfamily molecules (*vap-1, scl-1,* and *scl-9*), unlike loss of *lon-1*, did not affect the *sax-7* mutant phenotype, highlighting the specificity of *lon-1* function (**Fig. 4.15**). It is possible that the function of LON-1 in neuronal maintenance involves its conserved CAP domain. In fact, both the *e185* and *qv10* mutations fall within this conserved domain ((Maduzia et al 2002, Morita et al 2002); **Fig. 4.7**), suggesting that this area of the protein is functionally important for neuronal maintenance. Future work will likely shed light on the relevance of this new function of *lon-1* to its characterization as a CAP superfamily molecule.

### *lon-1* functions to maintain nervous system architecture independent of body length and the TGF-β pathway

*lon-1* was first identified by its Lon phenotype (Brenner 1974) and was later characterized as a downstream target of the TGF-β signaling pathway to regulate body length (Maduzia et al 2002, Morita et al 2002). We find that the *lon-1*-mediated suppression of *sax-7* defects is independent of body length and the TGF-β signaling pathway (**Fig. 4.12, 4.14, 4.16)**. Through this analysis we found

that both Lon and Sma mutants, which have drastically different body lengths and diameters, are able to consistently maintain the organization of head ganglia (**Fig. 4.6, 4.12)**. Additionally, we have focused our attention on the Sma/Mab DBL-1 branch of the TGF-β pathway in which *lon-1* functions as a downstream target (Maduzia et al 2002, Morita et al 2002), as *lon-1* is not known to function in the other DAF-7/TGF-β branch of the pathway, which regulates dauer formation. DAF-7 functions from the ASI neurons to control dauer formation (Ren et al 1996, Schackwitz et al 1996), and the DAF-7 pathway regulates chemoreceptor expression in the ASH and ASI neurons (Lesch & Bargmann 2010, Nolan et al 2002). Therefore, we expect that future work investigating the impact of this branch of the pathway on the maintenance of nervous system architecture either alone or in a *sax-7*-dependent way might be informative.

### ***lon-1*** **functions from the neurons or the underlying hypodermis to maintain nervous system architecture**

LON-1 is expressed in the hypodermis and intestine, which overlaps with its transcriptional expression pattern (Maduzia et al 2002, Morita et al 2002). CAP superfamily molecules, like LON-1, are often either secreted or GPI-anchored (Gibbs et al 2008). The primary amino acid sequence of LON-1 contains an N-terminal signal peptide sequence (Maduzia et al 2002); therefore, it is possible that after being produced, LON-1 is secreted into the extracellular milieu. While it has been proposed that LON-1 could possibly function as a transmembrane

molecule, the data are lacking proper controls, and the hydrophobic sequence proposed to be the LON-1 transmembrane domain (Morita et al 2002) is instead where the signal peptide sequence and cleavage site reside (Maduzia et al 2002). Therefore, it seems likely that LON-1 functions as a secreted molecule. Our work finds that LON-1 must be expressed in the neurons or underlying hypodermis to function in the maintenance of head ganglia organization (**Fig. 4.16**). We found that expression from more distant tissues such as the body wall muscles or gut did not rescue. This suggests that if LON-1 is indeed a secreted molecule, it may function locally to maintain head ganglia organization. In support of LON-1 acting locally to its secretion site, LON-1 antibody staining reveals co-localization with adherens junction marker MH27 in hypodermal and seam cells (Morita et al 2002). This puts LON-1 in a position to function in close proximity to transmembrane SAX-7 molecules, which act in the nervous system to maintain head ganglia organization.

### ***lon-1*** **and** ***sax-7*** **function post-embryonically to maintain nervous system architecture**

Thus far, only a handful of molecules have been identified that function to maintain specific aspects of the nervous system. This likely is a reflection of the difficulty associated with determining an adult role for molecules that also play critical roles during development. Through the use of a heat-shock-induced expression system and temporally regulated gene knockdown by RNAi, we

determined that both *sax-7* and *lon-1* are actively required during larval development to maintain the organization of the head ganglia (ASH/ASI soma) and the nerve ring (**Fig. 4.4 and 4.18)**, which are structures that develop during embryogenesis. This finding ruled out the possibility that the neuronal maintenance defects of *sax-7* mutants were a result of an embryonic defect that was amplified by growth and movement of the animal. Instead, our finding is consistent with an active requirement for *sax-7* and *lon-1* post-embryonically to subsequently maintain the organization of an already established nervous system structure.

A post-embryonic neuronal role for *sax*-7, the *C. elegans* homologue of the mammalian L1CAM family, is a conserved property of this gene family. Indeed, loss of L1CAM specifically from the adult mouse brain led to an increase in basal excitatory synaptic transmission and behavioral alterations (Law et al 2003). In rats, post-developmental nervous system knockdown of Neurofascin severely compromised the already established composition of the axon initial segment and led to an onset of motor deficits (Kriebel et al 2011, Zonta et al 2011). Postnatal disruption of CHL1 in excitatory neurons of the forebrain affected the duration of working memory (Kolata et al 2008). Together these results highlight the continued importance of L1 family members in the adult nervous system for proper function, and also underscore the power of conditional loss of molecules to determine post-developmental roles. These results also point to a high degree

of functional conservation between *sax-7* and L1CAM and indicate that findings from our work in *C. elegans* will likely have broad implications in other organisms. Through this work, we have identified LON-1 as a novel maintenance factor that functions with SAX-7 post-embryonically to maintain the architecture of the nervous system. Future studies that identify and characterize the other isolated *sax-7* suppressor mutations from our screen might also shed light into the cellular and molecular basis of neuronal maintenance.

## MATERIALS AND METHODS

### Nematode strains and genetics

Nematode cultures were maintained at 20$^{o}$C (unless otherwise noted) on NGM plates seeded with OP50 bacteria as described (Brenner 1974). Alleles used listed in **Table 4.1**. Strains were constructed using standard genetic procedures and are all listed in **Table 4.2**. Genotypes were confirmed by genotyping PCR or sequencing when needed, using primers listed in **Table 4.3**, or by visible phenotypes for *lon-1(qv10)*, *lon-1(e185)*, *lon-2(e678), lon-3(e2175), lon-8(hu187), sma-6(wk7), sma-2(e502), sma-3(e491),* and *sma-4(e729)*. All mutant alleles and reporters were outcrossed at least three times prior to use for analysis or strain building.

### Neuroanatomical observations

Animals were mounted on agarose pads, anaesthetized with 100 mM sodium azide, and examined under a Zeiss Axio Scope.A1 or Zeiss Axioskop 2 Plus.

*Analysis of ASH/ASI cell body positioning with respect to the nerve ring*

Cell bodies of ASH/ASI and the nerve ring were visualized in adults using *oyIs14* (Sarafi-Reinach et al 2001), an integrated P*sra-6::gfp* reporter; *hdIs29* (Schmitz et al 2008), an integrated P*sra-6::DsRed2; Podr-2::gfp* reporter; or *hdIs26* (Hutter 2003), an independent integrated P*sra-6::DsRed2;* P*odr-2::gfp* reporter. Unless otherwise noted, animals were selected as L4s and analyzed as 1-day adults. Animals were only analyzed when in a lateral orientation. Normally, both the two ASH and also the two ASI soma are located posterior to the nerve ring. Animals were counted as mutant when at least one ASH or ASI soma was touching, on top of, or anterior to the nerve ring. Animals were counted as wild type when all ASH/ASI soma were positioned posterior to the nerve ring.

*Analysis of PVQ axon flipover defects*

PVQ axons were visualized in L4 animals using *oyIs14,* an integrated P*sra-6::gfp* reporter (Sarafi-Reinach et al 2001). The axon of the PVQL and the PVQR neurons are normally maintained within the left and right fascicle of the ventral nerve cord, respectively. Animals were counted as having an axon flipover defect when one of the PVQ axons was flipped to the opposite fascicle at any point along the ventral nerve cord.

*Analysis of PVD dendritic branch development*

PVD dendritic branches were visualized in L4 animals using *wdIs52,* an integrated *F49H12.4::gfp* reporter (Smith et al 2010, Watson et al 2008). The shape of the structure formed by the secondary and tertiary dendritic branches of PVD normally resembles a “T” shape, as described (Dong et al 2013, Smith et al 2010). For each genotype, this shape was analyzed for multiple branches within a region anterior to the PVD cell body and categorized as the normal “T” shape, or abnormal variations such as “L”, “I”, loop, closed “Y”, open “Y”, or diagonally shaped. Percentage of animals with two or more non-T shaped branches was calculated.

**Identification of *sax-7(qv24)***

Initially we were carrying out a *zig-5(ok1065) zig-8(ok561)* double mutant suppressor screen, as we were studying two members of the ZIG family of two-Ig domain proteins, *zig-5* and *zig-8*, and their role in the maintenance of neuronal architecture. Our *zig-5(ok1065) zig-8(ok561)* double mutant strain exhibited defects similar to *sax-7* mutants in the relative positioning between the ASH/ASI soma and the nerve ring (Benard et al 2012). We later found out, after the screen had been completed, that this neuronal maintenance defect in the *zig-5(ok1065) zig-8(ok561)* double mutant strain was in fact due to the presence of a spontaneous novel background mutation, which we have called *sax-7(qv24)*. Following the screen, we determined that the phenotypic defects observed in our *zig-5(ok1065) zig-8(ok561); sax-7(qv24)* strain were solely due to the presence

of the *sax-7(qv24)* mutation and that loss of *zig-5(ok1065)* and *zig-8(ok561)* was dispensable for this phenotype.

**EMS forward genetic screen**

We carried out our forward screen for suppressors of neuronal maintenance defects using VQ90 *sax-7(qv24); zig-5(ok1065) zig-8(ok561); glp-4(bn2ts); oyIs14*) as our screening strain. *glp-4(bn2ts)*, a temperature sensitive sterile mutation (Beanan & Strome 1992), was used to ease the analysis of populations of adult worms on a large scale, without being confused by their progeny. VQ90 worms were grown at 15°C, mutagenized with 25 µM EMS, and allowed to recover at 15°C. Following recovery, five $P_0$ mutagenized worms were plated onto five plates (25 $P_0$s in total) and put back at 15°C to lay broods. From $P_0$ broods, 250 F1s were singled at the L4 or young adult stage (approximately 50 F1s from each $P_0$ plate). From each of the 250 F1 plates, seven F2s were singled for a total of 1750 F2s per mutagenesis round. After two days, these F2 plates were shifted to 25°C to prevent the production of progeny. Once reaching at least day five of adulthood, animals were incubated on ice to temporarily immobilize them and screened using Zeiss M2 Discovery stereo fluorescence microscopes to find broods that exhibited a high frequency of animals with the ASH/ASI soma posterior to the nerve ring, compared with control plates.

Upon identification of a candidate suppressor, animals were re-singled from the corresponding F1 plate to re-isolate the suppressor and analyze the animals mounted on slides and quantify the degree of suppression using the Zeiss Axioskop 2 Plus.

**Outcrossing candidate suppressors**

Successfully re-isolated alleles were outcrossed with the strain VQ47 *sax-7(qv24); zig-5(ok1065) zig-8(ok561); hdIs29* to confirm candidates, clean background EMS-induced mutations, and get rid of the *glp-4(bn2ts)* mutant allele when possible. F3s were analyzed for re-isolation of the *sax-7* suppression using the Zeiss Axioskop 2 Plus microscope.

**Removing the *zig-5* and *zig-8* mutations from the background of all the *sax-7(qv24)* and *lon-1(qv10)* suppressor strains**

Due to the presence of *zig-5(ok1065)* and *zig-8(ok561)* mutations in our screening and outcrossing strains, all isolated suppressors and outcrossed suppressors also contained these mutations. For isolated *sax-7* suppressor *lon-1(qv10)*, we crossed *lon-1(qv10)* away from *zig-5(ok1065), zig-8(ok561), glp-4(bn2ts),* and *sax7(qv24)*, before rebuilding as a double mutant with *sax-7(qv24)* to generate the *lon-1(qv10); sax-7(qv24)* double mutant. We ensured that all strains constructed and used in this work are wild type for *zig-5(ok1065), zig-*

*8(ok561),* and *glp-4(bn2ts)* to be confident that our suppressor was not dependent upon the presence of these mutations.

***C. elegans* constructs and microinjections to generate transgenic animals**

All inserts of finalized clones were verified by sequencing.

**P*lon-1::lon-1a* cDNA (pCB315):** Vector P*rgef-1*::*lon-1*a (pCB254) was digested with *Pst*I and *Bam*HI to release P*rgef-1* and ligated with insert of P*lon-1* 3-kb promoter (coordinates on cosmid F48E8: 28,244 to 31,288) amplified out of N2 genomic DNA using nested primers oCB1266 (TTCAGCGTGTAAGAGTTGAG) and oCB1267 (TAGGTCTTCAAATACGAAGG) followed by oCB1268 (CATGATCTGCAGTTTGATGGCTTGTACCTTGG) and oCB1269 (ATCATGGGATCCTTTGCCATATGTCGTGACG) to add on *Pst*I and *Bam*HI sites.

**P*lon-1::lon-1b* cDNA (pCB316):** Vector P*rgef-1*::*lon*-1b (pCB255) was digested with *Pst*I and *Bam*HI to release P*rgef-1* and ligated with insert of P*lon-1* 3-kb promoter (coordinates on cosmid F48E8: 28,244 to 31,288) amplified out of N2 genomic DNA using nested primers oCB1266 (TTCAGCGTGTAAGAGTTGAG) and oCB1267 (TAGGTCTTCAAATACGAAGG) followed by oCB1268 (CATGATCTGCAGTTTGATGGCTTGTACCTTGG) and oCB1269 (ATCATGGGATCCTTTGCCATATGTCGTGACG) to add on *Pst*I and *Bam*HI sites.

**P*lon-1::lon-1* genomic (pCB317):** Vector P*lon-1*::*lon*-1a (pCB315) was digested with *Xma*I and *Nco*I to release *lon-1a* cDNA and ligated with insert of *lon-1* 3.3-kb genomic (coordinates on cosmid F48E8: 31,289 to 34,582) amplified out of N2 genomic DNA using nested primers oCB1270 (AGATACTCTCTTTCCACTGG) and oCB1271 (ATAAATGCAGCGGTATGCAC) followed by oCB957 (CATGATCCCGGGATGAATTATCTGTTGACTGC) and oCB958 (ATCATGCCATGGTTAAACTCTCATTCGGAACC) to add on *Xma*I and *Nco*I sites.

**P*unc-14::lon-1a* cDNA (pCB318):** Vector P*dpy-7::lon-1a* (pCB249) was digested with *Hind*III and *Xma*I to release P*dpy-7* and ligated with insert of P*unc-14* 1.4-kb promoter digested with *Hind*III and *Xma*I from P*unc-14::sax-7L* (pCB174).

**P*elt-2::lon-1a* cDNA (pCB320):** Vector P*dpy-7::lon-1a* (pCB249) was digested with *Hind*III and *Xma*I to release P*dpy-7* and ligated with insert of P*elt-2* 1-kb promoter (coordinates on cosmid C33D3: 2933 to 3875) amplified out of N2 genomic DNA using nested primers oCB1058 (ACTTTGTAGGGTAATTGAGG) and oCB1061 (TCGGCTCATAGTTATTTGTGC) followed by oCB1059 (CATGATAAGCTTTTGATTTTGTTTCACTCTGTG) and oCB1060 (ATCATGCCCGGGTATAATCTATTTTCTAGTTTC) to add *Hind*III and *Xma*I sites.

**P*elt-3::lon-1a* cDNA (pCB322):** Vector P*rgef-1*::*lon*-1a (pCB254) was digested with *Pst*I and *Bam*HI to release P*rgef-1* and ligated with insert of P*elt-3* 2-Kb promoter amplified out of P*elt-3::lon-2* (pCB218) using oCB1272 (CATGATCTGCAGTGTGACACGTTGTTTCACG) and oCB1273 (ATCATGGGATCCGAAGTTTGAAATACCAGGTAG) to add on *Pst*I and *Bam*HI sites.

***lon-1* RNAi (pCB328):** Vector L4440 was digested with *Xma*I and *Nco*I and ligated with insert of *lon-1* 3.3-kb genomic (coordinates on cosmid F48E8: 31,289 to 34,582) amplified out of N2 genomic DNA using nested primers oCB1270 (AGATACTCTCTTTCCACTGG) and oCB1271 (ATAAATGCAGCGGTATGCAC) followed by oCB957 (CATGATCCCGGGATGAATTATCTGTTGACTGC) and oCB958 (ATCATGCCATGGTTAAACTCTCATTCGGAACC) to add on *Xma*I and *Nco*I sites.

**P*sra-6:: sax-7S* (pCB329):** Vector P*sra-6* was digested with *Xho*I and *Apa*I and ligated with insert of *sax-7S* 4.2-kb cDNA amplified out of P*unc-14::sax-7S* (pRP100) using oCB924 (CATGATCTCGAGATGGGGTTACGAGAGACGATG) and oCB886 (ATCATGGGGCCCGTACGGCCGACTAGTAGG) to add *Xho*I and *Apa*I sites.

**P*myo-3::lon-1a* cDNA (pCB352):** Vector P*myo-3* was digested with *Xba*I and *Nco*I and ligated with insert of *lon-1a* 1-kb cDNA digested out of P*dpy-7::lon-1a* (pCB249) using *Xba*I and *Nco*I.

**P*osm-6::sax-7S* (pCB363):** Vector P*unc-14::sax-7s* (pRP100) was digested with *Hind*III and *Bam*HI to release P*unc-14* and ligated with P*osm-6* 2.1-kb promoter digested out of P*osm-6::gfp::unc-54 3' UTR* (in pPD95.75 backbone) using *Hind*III and *Bam*HI.

Transgenic animals were generated by standard microinjection techniques (Mello & Fire 1995). Each construct was injected at 1 ng/µL (pCB191), 5 ng/µL (pRP100, pCB317, pCB315, pCB316, pCB318, pCB322, pCB320, and pCB352), or 75 ng/µL (pCB329 and pCB363), with two coinjection markers P*ttx-3::mCherry* at 50 ng/µL and P*unc-122::rfp* at 50 ng/µL. pBSK+ (25-99 ng/µL) was used to increase total DNA concentration of the injection mixes to 200 ng/µL.

**RT-PCR for *sax-7* and *lon-1* alleles**

Total RNA was extracted from worm samples using Trizol (Invitrogen) according to manufacturer's instructions. 500 ng RNA was used to reverse transcribe using the High Capacity cDNA Reverse Transcription Kit (Applied Biosystems) and random primers. PCR reactions were carried out with 1$^{st}$ strand cDNA template and primers oCB985 (CGATTTGCAACTCAACAGGA) and oCB987 (GTGTCCCGAACTGATTCGAT) were used for *sax-7* cDNA amplification. Primers oCB977 (TCCCACATGGTTTTCTCACA) and oCB979 (CTGAACATAGTGACCGCAACA) were used for *lon-1* cDNA amplification of all isoforms, while primers oCB977 (TCCCACATGGTTTTCTCACA) and oCB980 (AAAGCTGTCCTCTCGCAGTG) were used specifically for *lon-1a* and primers

oCB977 (TCCCACATGGTTTTCTCACA) and oCB981 (CCAGGTGAAAGCTGGCATCGTA) were used specifically for *lon-1b*. Primers oCB992 (TCGCTTCAAATCAGTTCAGC) and oCB993 (GCGAGCATTGAACAGTGAAG) were used for the control gene Y45F10D.4 (Hoogewijs et al 2008) cDNA amplification.

**Heat-shock induced expression of *sax-7S(+)***

Worms were maintained at 15°C for at least two generations prior to analysis. To generate freshly hatched pools of L1s, plates were washed three times with M9 buffer to remove adults and larvae, leaving only embryos on the plates. These plates were put back at 15°C for three hours, after which freshly hatched L1s were pooled onto new plates. Animals were either heat shocked immediately as L1s, as L2s (~24 hours post-hatch), or as L3s (~42 hours post-hatch). Heat shock treatment consisted of 30 minutes at 37°C, 60 minutes recovery at 15°C, 30 minutes at 37°C, followed by 15°C until analysis as adults. All experiments were repeated twice. Animals were examined as 1-day-old adults.

***lon-1* RNAi knockdown**

RNAi by feeding was based on previous methods (Kamath et al 2000, Timmons & Fire 1998). NGM plates were prepared with Ampicillin (Amp, 50 µg/ml) and IPTG (6 mM) and then kept unseeded at 4°C for a one week prior to starting experiment. RNAi bacteria from -80°C was streaked onto LB Amp (50 µg/ml)

Tetracyclin (12.5 µg/ml) plates and grown overnight at 37°C. Single colonies from these plates were grown overnight in LB Amp (50 µg/ml) liquid culture, and pelleted the next day to concentrate the bacteria. This concentrated bacteria was seeded onto NGM Amp/IPTG plates (room temperature), and these were then allowed to dry and induce overnight.

*Chronic RNAi condition*. L4 *sax-7(nj48); oyIs14* worms were put onto RNAi plates (*lon-1*, L4440 empty vector control (Timmons & Fire 1998), and *pos-1* RNAi-positive control (*pos-1* RNAi control leads to embryonic lethality and serves as a control for effectiveness of RNAi technique (Tabara et al 1999)) and kept on these plates overnight. The next day, these worms were repeatedly transferred to fresh RNAi plates, and allowed to lay embryos for three hour windows before being transferred to a fresh plate. This was repeated to create multiple plates. Worms were maintained on freshly seeded RNAi plates, no more than three days old, until being analyzed as adults.

*RNAi from L1*. Freshly hatched *sax-7(nj48); oyIs14* L1s were maintained on freshly seeded RNAi plates, no more than three days old (as above) until being analyzed as adults.

*RNAi from L2*. *sax-7(nj48); oyIs14* L2s were maintained on freshly seeded RNAi plates, no more than three days old (as above) until being analyzed as adults.

**ACKNOWLEDGEMENTS**

We thank Dr. A. Fire and Dr. Y. Kohara for clones, CGC funded by NIH Office of Research Infrastructure Programs (P40 OD010440) for strains, Mitani lab for strains, screening team (Steven DeGroot, Catherine Harwood, Akif Qutab, Mitz Qutab, Rachael Mazzamurro, Matthew Stigliano and Laura Pothier), and Paola Perrat for support with RT-PCR analysis. This work was funded by the NIH (ROI grant AG041870-01A1) to C.Y.B, the Ellison Biomedical Foundation New Scholar in Aging Research Award to C.Y.B, and the American Federation for Aging Research Award to C.Y.B.

## TABLES

### Table 4.1 List of mutant alleles used

| Gene | Allele | Nature of allele | Reference |
|---|---|---|---|
| ***sax-7*** | *nj48* | 582 bp deletion, 12457-13038 on cosmid C18F3. | (Sasakura et al 2005) |
| ***sax-7*** | *qv24* | Splice donor mutation. Partial loss of function. | This study |
| ***lon-1*** | *e185* | C185Y. Partial loss of function. | (Maduzia et al 2002, Morita et al 2002) |
| ***lon-1*** | *qv10* | G to A at position 33,209 on cosmid F48E8, introducing an early STOP. Partial loss of function. | This study |
| ***lon-2*** | *e678* | ~9 kb deletion. | (Gumienny et al 2007) |
| ***lon-3*** | *e2175* | Deletion of -2001 bp to +388 bp in relation to the initiator ATG codon and insertion of part of the transposon Tc5 (1 bp to 2779 bp). DNA rearrangement in the *lon-3* locus by Southern blot. | (Nystrom et al 2002, Suzuki et al 2002) |
| ***lon-8*** | *hu187* | 360 bp deletion of the first exon and surrounding sequence corresponding to on 71710…72069 YAC Y59A8B. Short transcript still detected by Northern blot. | (Soete et al 2007) |
| ***dbl-1*** | *nk3* | 5595 bp deletion, including almost all exons. Null. | (Morita et al 1999) |
| ***crm-1*** | *tm2218* | 192 bp deletion and 1 bp insertion, with deletion corresponding to 38330…38521 on cosmid B0024. Makes two truncated mRNA species. Loss of function allele. | (Mitani lab at NBRP *C. elegans*; (Fung et al 2007)) |
| ***sma-10*** | *ok2224* | 906 bp deletion corresponding to 20922…21827 on cosmid T21D12. | (Consortium 2012) |
| ***drag-1*** | *tm3773* | 892 bp deletion corresponding to 41703…42594 on YAC Y71G12B. | (Mitani lab at NBRP *C. elegans*) |
| ***sma-6*** | *wk7* | Y72 changed to an early STOP. | (Krishna et al 1999) |
| ***sma-2*** | *e502* | G372D. | (Savage et al 1996) |
| ***sma-3*** | *e491* | G350R. | (Savage et al 1996) |
| ***sma-4*** | *e729* | Molecularly uncharacterized. | (Brenner 1974, Savage et al 1996) |
| ***unc-129*** | *tm5461* | 660 bp deletion corresponding to 8166…8825 on cosmid C53D6. | (Mitani lab at NBRP *C. elegans*) |

| | | | |
|---|---|---|---|
| ***tig-2*** | *ok3416* | ~800 bp deletion. | (Consortium 2012) |
| ***adt-2*** | *wk156* | G364S. Partial loss of function. | (Fernando et al 2011) |
| ***dig-1*** | *ky188* | Molecularly uncharacterized. | (Benard et al 2006, Zallen et al 1999) |
| ***vap-1*** | *ok392* | 576 bp deletion corresponding to 3013…3588 on cosmid F11C7. | (Consortium 2012) |
| ***scl-1*** | *ok1185* | ~1600 bp deletion. | (Consortium 2012) |
| ***scl-9*** | *ok1138* | 910 bp deletion corresponding to 18889…19798 on cosmid F49E11. | (Consortium 2012) |

**Table 4.2 List of strains used.**

| Strain | Genotype | Transgene | Reference |
|---|---|---|---|
| N2 | | | (Brenner 1974) |
| VQ51 | *oyIs14 V* | P*sra-6::gfp* | (Sarafi-Reinach et al 2001) |
| | *hdIs29 V* | P*sra-6::DsRed2;* P*odr-2::gfp* | (Schmitz et al 2008) |
| VH648 | *hdIs26* III | P*sra-6::DsRed2;* P*odr-2::gfp* | (Hutter 2003) |
| **Strains for EMS suppressor screen** | | | |
| VQ90 | *sax-7(qv24) IV; zig-5(ok1065) zig-8(ok561) III; glp-4(bn2ts) I; oyIs14 V* | | *This study* |
| VQ47 | *sax-7(qv24) IV; zig-5(ok1065) zig-8(ok561) III; hdIs29 V* | | *This study* |
| ***lon-1* and *sax-7* mutants as single and double mutants** | | | |
| VQ357 | *lon-1(e185) III; oyIs14 V* | | *This study* |
| VQ484 | *lon-1(qv10) III; oyIs14 V* | | *This study* |
| OH7984 | *sax-7(nj48) IV; oyIs14 V* | | (Benard et al 2012) |
| VQ307 | *sax-7(qv24) IV; oyIs14 V* | | *This study* |
| VQ397 | *sax-7(nj48) IV; hdIs29 V* | | *This study* |
| VQ348 | *lon-1(e185) III; sax-7(nj48) IV; oyIs14 V* | | *This study* |
| VQ905 | *lon-1(e185) III; sax-7(qv24) IV; oyIs14 V* | | *This study* |
| VQ909 | *lon-1(qv10) III; sax-7(nj48) IV; oyIs14 V* | | *This study* |
| VQ906 | *lon-1(qv10) III; sax-7(qv24) IV; oyIs14 V* | | *This study* |
| **Other *lon* mutants alone and with *sax-7(nj48)*** | | | |
| VQ179 | *lon-2(e678) X; oyIs14 V* | | *This study* |
| VQ619 | *lon-3(e2175) oyIs14 V* | | *This study* |
| VQ620 | *lon-8(hu187) oyIs14 V* | | *This study* |
| VQ358 | *lon-2(e678) X; sax-7(nj48) IV; oyIs14 V* | | *This study* |
| VQ849 | *sax-7(nj48) IV; lon-3(e2175) oyIs14 V* | | *This study* |
| VQ677 | *sax-7(nj48) IV; lon-8(hu187) oyIs14 V* | | *This study* |
| **PVD labeled strains** | | | |
| VQ787 | *wdIs52* | | *This study* |
| VQ788 | *lon-1(e185) III; wdIs52* | | *This study* |
| VQ789 | *sax-7(nj48) IV; wdIs52* | | |
| VQ790 | *lon-1(e185) III; sax-7(nj48) IV;* | | *This study* |

| | | |
|---|---|---|
| | *wdIs52* | |
| **TGF-β pathway mutants alone and with *sax-7(nj48)*** | | |
| VQ796 | *dbl-1(nk3) V; hdIs26 III* | *This study* |
| VQ821 | *crm-1(tm2218) oyIs14 V* | *This study* |
| VQ836 | *sma-10(ok2224) IV; oyIs14 V* | *This study* |
| VQ822 | *drag-1(tm3773) I; oyIs14 V* | *This study* |
| VQ811 | *sma-6(wk7) II; oyIs14 V* | *This study* |
| VQ833 | *sma-2(e502) III; oyIs14 V* | *This study* |
| VQ834 | *sma-3(e491) III; oyIs14 V* | *This study* |
| VQ835 | *sma-4(e729) III; oyIs14 V* | *This study* |
| VQ775 | *unc-129(tm5461) IV; oyIs14 V* | *This study* |
| VQ777 | *tig-2(ok3416) oyIs14 V* | *This study* |
| VQ812 | *adt-2(wk156) X; oyIs14 V* | *This study* |
| VQ802 | *dbl-1(nk3) V; sax-7(nj48) IV; hdIs26 III* | *This study* |
| VQ857 | *sax-7(nj48) IV; crm-1(tm2218) oyIs14 V* | *This study* |
| VQ902 | *sma-10(ok2224) sax-7(nj48) IV; oyIs14 V* | *This study* |
| VQ850 | *drag-1(tm3773) I; sax-7(nj48) IV; oyIs14 V* | *This study* |
| VQ877 | *sma-6(wk7) II; sax-7(nj48) IV; oyIs14 V* | *This study* |
| VQ842 | *sma-2(e502) III; sax-7(nj48) IV; oyIs14 V* | *This study* |
| VQ869 | *sma-3(e491) III; sax-7(nj48) IV; oyIs14 V* | *This study* |
| VQ870 | *sma-4(e729) III; sax-7(nj48) IV; oyIs14 V* | *This study* |
| VQ794 | *unc-129(tm5461) sax-7(nj48) IV; oyIs14 V* | *This study* |
| VQ803 | *sax-7(nj48) IV; tig-2(ok3416) oyIs14 V* | *This study* |
| VQ843 | *adt-2(wk156) X; sax-7(nj48) IV; oyIs14 V* | *This study* |
| **SCP domain mutant strains** | | |
| VQ863 | *vap-1(ok392) X; oyIs14* | *This study* |
| VQ882 | *vap-1(ok392) X; sax-7(nj48) IV; oyIs14 V* | *This study* |
| VQ871 | *scl-1(ok1185) IV; oyIs14 V* | *This study* |
| VQ884 | *scl-1(ok1185) sax-7(nj48) IV; oyIs14 V* | *This study* |
| VQ872 | *scl-9(ok1138) IV; oyIs14 V* | *This study* |
| VQ901 | *scl-9(ok1138) sax-7(nj48) IV; oyIs14 V* | *This study* |

| | | | |
|---|---|---|---|
| ***ctIs40* (*dbl-1*(+++)) strains** | | | |
| VQ618 | *ctIs40 X; hdIs29 V* | | *This study* |
| VQ617 | *ctIs40 X; sax-7(nj48) IV; hdIs29 V* | | *This study* |
| ***dig-1* mutant strains** | | | |
| OH3534 | *dig-1(ky188) III; oyIs14 V* | | *This study* |
| OH3455 | *dig-1(ky188) lon-1(e185) III; oyIs14 V* | | *This study* |
| **Balancer strains for injection** | | | |
| VQ683 | *lon-1(qv10)/dpy-17(e164) unc-32(e189) III; oyIs14 V* | | *This study* |
| VQ687 | *lon-1(e185)/dpy-17(e164) unc-32(e189) III; sax-7(nj48) IV; oyIs14 V* | | *This study* |
| **Transgenic Lines** | | | |
| VQ924 | *sax-7(qv24); oyIs14; qvEx235* | pRP100 (P*unc-14::sax-7S(+)*), P*ttx-3::mCherry,* P*unc-122::rfp*, pBSK+. Line #1 | *This study* |
| VQ925 | *sax-7(qv24); oyIs14; qvEx236* | pRP100 (P*unc-14::sax-7S(+)*), P*ttx-3::mCherry,* P*unc-122::rfp*, pBSK+. Line #2 | *This study* |
| VQ922 | *sax-7(nj48); oyIs14; qvEx234* | pCB191 (P*hsp-16.2::sax-7(+)*), P*ttx-3::mCherry,* P*unc-122::rfp*, pBSK+. Line #1 | *This study* |
| VQ926 | *lon-1(e185); sax-7(nj48); oyIs14; qvEx237* | pCB317 (P*lon-1::lon-1(+)* genomic), P*ttx-3::mCherry,* P*unc-122::rfp*, pBSK+. Line 1 | *This study* |
| VQ927 | *lon-1(e185); sax-7(nj48); oyIs14; qvEx238* | pCB317 (P*lon-1::lon-1(+)* genomic), P*ttx-3::mCherry,* P*unc-122::rfp*, pBSK+. Line 2 | *This study* |
| VQ920 | *lon-1(e185); sax-7(nj48); oyIs14; qvEx233* | pCB317 (P*lon-1::lon-1(+)* genomic), P*ttx-3::mCherry,* P*unc-122::rfp*, pBSK+. Line 3 | *This study* |
| VQ928 | *lon-1(e185); sax-7(nj48); oyIs14; qvEx239* | pCB315 (P*lon-1::lon-1a(+)* cDNA), P*ttx-3::mCherry,* P*unc-122::rfp*, pBSK+. Line 1 | *This study* |
| VQ701 | *lon-1(e185); sax-7(nj48); oyIs14; qvEx160* | pCB315 (P*lon-1::lon-1a(+)* cDNA), P*ttx-3::mCherry,* P*unc-122::rfp*, pBSK+. Line 2 | *This study* |
| VQ929 | *lon-1(e185); sax-7(nj48); oyIs14; qvEx240* | pCB315 (P*lon-1::lon-1a(+)* cDNA), P*ttx-3::mCherry,* P*unc-122::rfp*, pBSK+. Line 3 | *This study* |
| VQ848 | *lon-1(e185); sax-7(nj48); oyIs14; qvEx219* | pCB316 (P*lon-1::lon-1b(+)* cDNA), P*ttx-3::mCherry,* P*unc-122::rfp*, pBSK+. Line 1 | *This study* |
| VQ932 | *lon-1(e185); sax-7(nj48); oyIs14; qvEx243* | pCB316 (P*lon-1::lon-1b(+)* cDNA), P*ttx-3::mCherry,* P*unc-122::rfp*, pBSK+. Line 2 | *This study* |

| | | | |
|---|---|---|---|
| VQ933 | *lon-1(e185); sax-7(nj48); oyIs14; qvEx244* | pCB316 (P*lon-1::lon-1b(+)* cDNA), P*ttx-3::mCherry,* P*unc-122::rfp*, pBSK+. Line 3 | *This study* |
| VQ697 | *lon-1(qv10); oyIs14; qvEx156* | pCB317 (P*lon-1::lon-1(+)* genomic), P*ttx-3::mCherry,* P*unc-122::rfp*, pBSK+. Line 1 | *This study* |
| VQ930 | *lon-1(qv10); oyIs14; qvEx241* | pCB317 (P*lon-1::lon-1(+)* genomic), P*ttx-3::mCherry,* P*unc-122::rfp*, pBSK+. Line 2 | *This study* |
| VQ931 | *lon-1(qv10); oyIs14; qvEx242* | pCB317 (P*lon-1::lon-1(+)* genomic), P*ttx-3::mCherry,* P*unc-122::rfp*, pBSK+. Line 3 | *This study* |
| VQ934 | *lon-1(qv10); oyIs14; qvEx245* | pCB315 (P*lon-1::lon-1a(+)* cDNA), P*ttx-3::mCherry,* P*unc-122::rfp*, pBSK+. Line 1 | *This study* |
| VQ935 | *lon-1(qv10); oyIs14; qvEx246* | pCB315 (P*lon-1::lon-1a(+)* cDNA), P*ttx-3::mCherry,* P*unc-122::rfp*, pBSK+. Line 2 | *This study* |
| VQ936 | *lon-1(qv10); oyIs14; qvEx247* | pCB315 (P*lon-1::lon-1a(+)* cDNA), P*ttx-3::mCherry,* P*unc-122::rfp*, pBSK+. Line 3 | *This study* |
| VQ937 | *lon-1(qv10); oyIs14; qvEx248* | pCB316 (P*lon-1::lon-1b(+)* cDNA), P*ttx-3::mCherry,* P*unc-122::rfp*, pBSK+. Line 1 | *This study* |
| VQ938 | *lon-1(qv10); oyIs14; qvEx249* | pCB316 (P*lon-1::lon-1b(+)* cDNA), P*ttx-3::mCherry,* P*unc-122::rfp*, pBSK+. Line 2 | *This study* |
| VQ939 | *lon-1(qv10); oyIs14; qvEx250* | pCB316 (P*lon-1::lon-1b(+)* cDNA), P*ttx-3::mCherry,* P*unc-122::rfp*, pBSK+. Line 3 | *This study* |
| VQ940 | *sax-7(nj48); oyIs14; qvEx251* | pCB317 (P*lon-1::lon-1(+)* genomic), P*ttx-3::mCherry,* P*unc-122::rfp*, pBSK+. Line 1 | *This study* |
| VQ941 | *sax-7(nj48); oyIs14; qvEx252* | pCB317 (P*lon-1::lon-1(+)* genomic), P*ttx-3::mCherry,* P*unc-122::rfp*, pBSK+. Line 2 | *This study* |
| VQ942 | *sax-7(nj48); oyIs14; qvEx253* | pCB317 (P*lon-1::lon-1(+)* genomic), P*ttx-3::mCherry,* P*unc-122::rfp*, pBSK+. Line 3 | *This study* |
| VQ943 | *sax-7(nj48); oyIs14; qvEx254* | pCB363 (P*osm-6::sax-7S(+)*), P*ttx-3::mCherry,* P*unc-122::rfp*, pBSK+. Line 1 | *This study* |
| VQ944 | *sax-7(nj48); oyIs14; qvEx255* | pCB363 (P*osm-6::sax-7S(+)*), P*ttx-3::mCherry,* P*unc-122::rfp*, pBSK+. Line 2 | *This study* |
| VQ945 | *sax-7(nj48); oyIs14; qvEx256* | pCB363 (P*osm-6::sax-7S(+)*), P*ttx-3::mCherry,* P*unc-122::rfp*, pBSK+. Line 3 | *This study* |
| VQ946 | *sax-7(nj48); oyIs14; qvEx257* | pCB329 (P*sra-6::sax-7S(+)*), P*ttx-3::mCherry,* P*unc-122::rfp*, pBSK+. Line 1 | *This study* |
| VQ947 | *sax-7(nj48); oyIs14; qvEx258* | pCB329 (P*sra-6::sax-7S(+)*), | *This study* |

| | | | |
|---|---|---|---|
| | | P*ttx-3::mCherry,* P*unc-122::rfp*, pBSK+. Line 2 | |
| VQ948 | *sax-7(nj48); oyIs14; qvEx259* | pCB329 (P*sra-6::sax-7S(+)*), P*ttx-3::mCherry,* P*unc-122::rfp*, pBSK+. Line 3 | *This study* |
| VQ961 | *lon-1(e185); sax-7(nj48); oyIs14; qvEx272* | pCB318 (P*unc-14::lon-1a(+)* cDNA), P*ttx-3::mCherry,* P*unc-122::rfp*, pBSK+. Line 1 | *This study* |
| VQ700 | *lon-1(e185); sax-7(nj48); oyIs14; qvEx159* | pCB318 (P*unc-14::lon-1a(+)* cDNA), P*ttx-3::mCherry,* P*unc-122::rfp*, pBSK+. Line 2 | *This study* |
| VQ962 | *lon-1(e185); sax-7(nj48); oyIs14; qvEx273* | pCB318 (P*unc-14::lon-1a(+)* cDNA), P*ttx-3::mCherry,* P*unc-122::rfp*, pBSK+. Line 3 | *This study* |
| VQ919 | *lon-1(e185); sax-7(nj48); oyIs14; qvEx232* | pCB322 (P*elt-3::lon-1a(+)* cDNA), P*ttx-3::mCherry,* P*unc-122::rfp*, pBSK+. Line 1 | *This study* |
| VQ963 | *lon-1(e185); sax-7(nj48); oyIs14; qvEx274* | pCB322 (P*elt-3::lon-1a(+)* cDNA), P*ttx-3::mCherry,* P*unc-122::rfp*, pBSK+. Line 2 | *This study* |
| VQ964 | *lon-1(e185); sax-7(nj48); oyIs14; qvEx275* | pCB322 (P*elt-3::lon-1a(+)* cDNA), P*ttx-3::mCherry,* P*unc-122::rfp*, pBSK+. Line 3 | *This study* |
| VQ917 | *lon-1(e185); sax-7(nj48); oyIs14; qvEx230* | pCB320 (P*elt-2::lon-1a(+)* cDNA), P*ttx-3::mCherry,* P*unc-122::rfp*, pBSK+. Line 1 | *This study* |
| VQ965 | *lon-1(e185); sax-7(nj48); oyIs14; qvEx276* | pCB320 (P*elt-2::lon-1a(+)* cDNA), P*ttx-3::mCherry,* P*unc-122::rfp*, pBSK+. Line 2 | *This study* |
| VQ966 | *lon-1(e185); sax-7(nj48); oyIs14; qvEx277* | pCB320 (P*elt-2::lon-1a(+)* cDNA), P*ttx-3::mCherry,* P*unc-122::rfp*, pBSK+. Line 3 | *This study* |
| VQ918 | *lon-1(e185); sax-7(nj48); oyIs14; qvEx231* | pCB352 (P*myo-3::lon-1a(+)* cDNA), P*ttx-3::mCherry,* P*unc-122::rfp*, pBSK+. Line 1 | *This study* |
| VQ967 | *lon-1(e185); sax-7(nj48); oyIs14; qvEx278* | pCB352 (P*myo-3::lon-1a(+)* cDNA), P*ttx-3::mCherry,* P*unc-122::rfp*, pBSK+. Line 2 | *This study* |
| VQ949 | *lon-1(qv10); oyIs14; qvEx260* | pCB318 (P*unc-14::lon-1a(+)* cDNA), P*ttx-3::mCherry,* P*unc-122::rfp*, pBSK+. Line 1 | *This study* |
| VQ950 | *lon-1(qv10); oyIs14; qvEx261* | pCB318 (P*unc-14::lon-1a(+)* cDNA), P*ttx-3::mCherry,* P*unc-122::rfp*, pBSK+. Line 2 | *This study* |
| VQ951 | *lon-1(qv10); oyIs14; qvEx262* | pCB318 (P*unc-14::lon-1a(+)* cDNA), P*ttx-3::mCherry,* P*unc-122::rfp*, pBSK+. Line 3 | *This study* |
| VQ952 | *lon-1(qv10); oyIs14; qvEx263* | pCB322 (P*elt-3::lon-1a(+)* cDNA), P*ttx-3::mCherry,* P*unc-122::rfp*, pBSK+. Line 1 | *This study* |
| VQ953 | *lon-1(qv10); oyIs14; qvEx264* | pCB322 (P*elt-3::lon-1a(+)* cDNA), P*ttx-3::mCherry,* P*unc-* | *This study* |

| | | | |
|---|---|---|---|
| | | *122::rfp*, pBSK+. Line 2 | |
| VQ954 | *lon-1(qv10); oyIs14; qvEx265* | pCB322 (P*elt-3::lon-1a(+)* cDNA), P*ttx-3::mCherry,* P*unc-122::rfp*, pBSK+. Line 3 | *This study* |
| VQ955 | *lon-1(qv10); oyIs14; qvEx266* | pCB320 (P*elt-2::lon-1a(+)* cDNA), P*ttx-3::mCherry,* P*unc-122::rfp*, pBSK+. Line 1 | *This study* |
| VQ956 | *lon-1(qv10); oyIs14; qvEx267* | pCB320 (P*elt-2::lon-1a(+)* cDNA), P*ttx-3::mCherry,* P*unc-122::rfp*, pBSK+. Line 2 | *This study* |
| VQ957 | *lon-1(qv10); oyIs14; qvEx268* | pCB320 (P*elt-2::lon-1a(+)* cDNA), P*ttx-3::mCherry,* P*unc-122::rfp*, pBSK+. Line 3 | *This study* |
| VQ958 | *lon-1(qv10); oyIs14; qvEx269* | pCB352 (P*myo-3::lon-1a(+)* cDNA), P*ttx-3::mCherry,* P*unc-122::rfp*, pBSK+. Line 1 | *This study* |
| VQ959 | *lon-1(qv10); oyIs14; qvEx270* | pCB352 (P*myo-3::lon-1a(+)* cDNA), P*ttx-3::mCherry,* P*unc-122::rfp*, pBSK+. Line 1 | *This study* |
| VQ960 | *lon-1(qv10); oyIs14; qvEx271* | pCB352 (P*myo-3::lon-1a(+)* cDNA), P*ttx-3::mCherry,* P*unc-122::rfp*, pBSK+. Line 1 | *This study* |

## Table 4.3 Primers used for strain building

| Gene | Primer | Sequence | PCR product (bp) |
|---|---|---|---|
| ***sax-7(nj48)*** | | | |
| Mutant specific | oCB1022 | tggtggtagcgatggtgtag | 257 |
| | oCB208 | gagttattggggtattttagcg | |
| Wild-type specific | oCB212 | gaaatacacacaaatacgagtgc | 592 |
| | oCB723 | tagttgattaaaatgtttcaagattg | |
| ***sax-7(qv24)*** | dCAPS primers | | |
| Mutant specific | oCB916 | cgaacattcaatgttgtagtggcgg | 264 |
| | oCB917 | ccatttaaaaaattatattcgaccccaatatttcc | |
| Wild-type specific | oCB915 | ggatattgatcgaacattcaatgttgtagtccagg | 264 |
| | oCB917 | ccatttaaaaaattatattcgaccccaatatttcc | |
| PCR products digested to determine genotype. Mutant specific product digested with *Eci*I only cuts *qv24* sequence, wild-type specific product digested with *Bsa*JI only cuts wild type sequence. | | | |
| ***dbl-1(nk3)*** | | | |
| Mutant specific | oCB1336 | ttctgcatcgtatcagttcc | 633 |
| | oCB1338 | aaggatcagtgcatacagac | |
| Wild-type specific | oCB1336 | ttctgcatcgtatcagttcc | 307 |
| | oCB1337 | tttgacgatagacgaagagc | |
| ***crm-1(tm2218)*** | | | |
| Mutant specific | oCB1368 | atgcttgtggcactgatgg | 562 |
| | oCB1370 | agagacaaccacttgaaacc | |
| Wild-type specific | oCB1368 | atgcttgtggcactgatgg | 577 |
| | oCB1369 | tgcacttggatcggcatacc | |
| ***sma-10(ok2224)*** | | | |
| Mutant specific | oCB1393 | tattgctaaatgttcctacc | 533 |
| | oCB1395 | aatcagagaacgtcgtctgg | |
| Wild-type specific | oCB1393 | tattgctaaatgttcctacc | 651 |
| | oCB1394 | tcaaaataatggtgcgtcagc | |
| ***drag-1(tm3773)*** | | | |
| Mutant specific | oCB1390 | tatgagacggcactggaagg | 346 |
| | oCB1392 | ttctcacgagaacagtaacc | |
| Wild-type specific | oCB1390 | tatgagacggcactggaagg | 1028 |
| | oCB1391 | tgaaatagcatctggaacag | |
| ***unc-129(tm5461)*** | | | |
| Mutant specific | oCB1333 | agaaatgtaatgccactcacc | 538 |
| | oCB1335 | agatggtaatctggtacgtgc | |
| Wild-type specific | oCB1333 | agaaatgtaatgccactcacc | 517 |
| | oCB1334 | taatgatgttcgagttgtgc | |
| Mutant specific | oCB1341 | agtgtttccagacaggccac | 600 |
| | oCB1342 | gagttgtggaggcggatcta | |
| Wild-type specific | oCB1341 | agtgtttccagacaggccac | 588 |
| | oCB1345 | agtgtgaccatctatcgacc | |
| ***adt-2(wk156)*** | | | |
| | oCB1388 | ttaccagacaaccggtaggg | 553 |
| | oCB1389 | tgatgacatgatatgcttgg | |
| PCR product sent to sequence with oCB1388 to determine genotype. | | | |
| ***vap-1(ok392)*** | | | |
| Mutant specific | oCB1413 | agtaggtggtgcattcagc | 498 |
| | oCB1414 | aaaacgttgtggtagaatggc | |
| Wild-type specific | oCB1413 | agtaggtggtgcattcagc | 609 |
| | oCB1415 | ttagaaccgtaggacttacg | |

| | | | |
|---|---|---|---|
| ***scl-1(ok1185)*** | | | |
| Mutant specific | oCB1421 | atacctgtatacttttctcgg | 616 |
| | oCB1422 | agttccttttgccacgtagg | |
| Wild-type specific | oCB1421 | atacctgtatacttttctcgg | ~500 |
| | oCB1423 | accaattgctaggaggcagag | |
| ***scl-9(ok1138)*** | | | |
| Mutant specific | oCB1424 | tgacaagtataccgaagagc | 434 |
| | oCB1425 | agtcccatccattggtttcg | |
| Wild-type specific | oCB1424 | tgacaagtataccgaagagc | 396 |
| | oCB1426 | aaagtctgcctgacttgtcg | |

# Chapter V

# GENERAL DISCUSSION

**Part I: Heparan sulfate synthesis is required for guidance during development**

Heparan sulfate proteoglycans (HSPGs) have critical and diverse functions in development, owing in part to their interactions with receptors and ligands of numerous signaling pathways. While HSPGs were previously thought of as extracellular space-filling molecules, it has become clear that they play dedicated and specific roles in the modulation of signaling pathways to ensure proper development. One level of added complexity in the study of HSPGs is that functions attributed to specific HSPGs can be mediated by the core protein, the heparan sulfate (HS) chains, or a combination of both. Research focused on HS biosynthesis will likely improve our understanding of the regulation of HS chains on core proteins and how specifically the HS chains function to affect biological processes.

Although *C. elegans* is a strong model for the investigation of biological questions concerning HS biosynthesis, previously available mutants for the enzymes that synthesize HS chains in *C. elegans* were lethal (Franks et al 2006, Kitagawa et al 2007, Morio et al 2003). We have now isolated and identified viable mutations in the two subunits of the HS co-polymerase, *rib-1* and *rib-2*, that function together to synthesize HS chains onto core proteins to generate HSPGs. These mutants have allowed us to study the impact of impaired HS biosynthesis using *C. elegans* in a manner that was previously unavailable. My thesis work has

characterized the axon and cell guidance defects exhibited by our *rib-1* and *rib-2* mutants as a result of compromised HS biosynthesis. We have confirmed that HS biosynthesis is impaired in our *rib-1* and *rib-2* mutants, both in general and onto specific core proteins. We analyzed the expression pattern and localization of RIB-1 and found that it is expressed dynamically during development with continued expression through adulthood. Our work demonstrates that modified HS chains function with both the SLT-1/Slit and UNC-6/netrin signaling pathways in axon guidance. In addition, we have found that the coordinated expression of HS from multiple tissue types is required to properly guide axons. This work provides an avenue for the future use of the powerful model organism *C. elegans* to study HS biology and how it relates to many biological processes.

*Insights from the RIB-1 expression pattern and the requirement for coordinated expression of HSPGs in development*

HS chains are synthesized and modified in the Golgi to generate HSPGs which are subsequently transported to the membrane or secreted. Our analysis of the expression and localization of RIB-1, one of the enzymes that functions to polymerize HS chains, sheds light on the specific sites where HS biosynthesis takes place in *C. elegans*. In particular, we saw expression in a number of tissues including the pharynx, neurons, muscles of the digestive and reproductive system, and some hypodermal cells. This overlaps with known expression patterns of specific HSPG core proteins. For example, membrane bound SDN-

1/syndecan is expressed in neurons, hypodermis, and pharynx (Rhiner et al 2005), and GPI-linked LON-2/glypican shows expression in the intestine and hypodermis (Gumienny et al 2007). UNC-52/perlecan, a secreted HSPG, is expressed in body wall muscles, digestive system muscles, and pharynx (Mullen et al 1999, Rogalski et al 1993); Mullen et al., 1999). Overlap between expression of HS biosynthetic machinery, such as RIB-1, and the localization of specific HSPGs, suggests that HSPGs may remain near cells where HS synthesis occurs. This may have functional relevance, as glypicans in fibroblast cells were shown to be internalized through endocytosis, returned to the Golgi, and then transported back to the membrane with HS chains altered both in length and modification pattern (Edgren et al 1997, Fransson et al 1995). Whether an internal recycling of HSPGs back to the HS biosynthetic machinery in the Golgi occurs in *C. elegans*, or whether it has functional relevance to guidance, remains to be determined.

We demonstrated that HS synthesis is functionally required in multiple tissues, specifically the muscles, hypodermis, and neurons, for PVQ axon guidance. This suggests that a coordinated multi-tissue interaction between HSPGs drives PVQ axon guidance, and that likely the rescue is a result of restored HS synthesis onto core proteins that function in those tissues. Consistent with the idea that multiple HSPGs function together to guide the PVQ axons, double mutants lacking *lon*-2/glypican and *sdn-1*/syndecan exhibit a higher penetrance of PVQ

axon guidance defects than either single mutant alone (Diaz-Balzac et al 2014). It is likely that not only HS, but modified HS chains on specific core proteins are required to guide the PVQ axons, as loss of HS-modifying enzymes in different combinations leads to enhanced PVQ axon guidance defects compared to the single mutants alone (Bülow & Hobert 2004). This is not an isolated example, as we also found that *rib-1* is required either in the neuron itself, or in the underlying hypodermis for proper AVM axon guidance. We expect that analysis of our *rib-1* and *rib-2* mutants will provide insight into more examples where the coordinated interactions between HSPGs are required for cell and axon guidance during development.

*Continued post-embryonic requirement for HS and relevance to synapses*

Through our analysis of the expression and localization of *rib-1*, we found that *rib-1* continues to be expressed in adult worms, and in some tissues expression levels visibly increased with age. This is consistent with *C. elegans* expression profiling datasets which show continued expression of both *rib-1* and *rib-2* from the beginning of embryogenesis through adulthood (Celniker et al 2009). This hints that HS synthesis may not only be critical for early development, but also may have continued functions in adulthood as well. Indeed, there is evidence for a critical function of HS synthesis in the post-natal mouse brain. Conditional loss of EXT1 in postnatal excitatory neurons led to autism-like behavioral deficits as well as defects in excitatory synaptic transmission resulting from reduced surface

expression of glutamatergic receptors (Irie et al 2012). An association with autism has also been seen in humans with mutations in EXT1 (Li et al 2002).

Work from the conditional EXT1 knockout mouse suggests that HS plays important roles at the post-natal synapse (Irie et al 2012). Consistent with this, HSPGs have been shown to have synaptic functions, for example agrin and perlecan are involved in the clustering of acetylcholine receptors and acetylcholinesterase at the NMJ, respectively (Arikawa-Hirasawa et al 2002, Glass et al 1996, Godfrey et al 1984, Nitkin et al 1987, Peng et al 1999). Syndecan promotes mature dendritic spine formation in hippocampal neurons, while also being important for synaptic growth at *Drosophila* NMJs (Ethell & Yamaguchi 1999, Johnson et al 2006), and glypicans have implicated roles in synaptogenesis such as the formation of the active zone and the regulation of glutamatergic receptor clustering (Allen et al 2012, Johnson et al 2006). In some cases the HS chains on the core proteins were shown to be required for these functions (Allen et al 2012, Johnson et al 2006).

Despite the involvement of multiple HSPGs in different aspects of synapse biology, our understanding of the role that the HS chains play in synaptogenesis remains limited. While it is clear from the EXT1 conditional knockout mouse study that HS chains are important for receptor clustering and synaptic transmission (Irie et al 2012), there is still much more for us to learn about the

role of HS chains in the regulation of synapses. Our newly isolated, viable *rib-1* and *rib-2* mutants, as well as the knowledge that RIB-1 expression persists post-embryonically, provide an opportunity to study the impact of HS biosynthesis on synapses in *C. elegans*. This type of work could help to clarify the importance of the HSPG core protein versus the HS chains in these processes, and expand our knowledge on the role of HS in synaptogenesis and how that relates to the function of the nervous system.

*Parallels between rib-1/rib-2 mutants and hereditary multiple exostoses*

We characterized various guidance events in our *rib-1* and *rib-2* mutants to determine the impact of impaired HS biosynthesis, and found guidance defects in cells and axons that migrate both embryonically and post-hatch. During this analysis we also observed in multiple cases a tendency for overgrowth of material. For example, when analyzing AVM ventral axon guidance in our *rib-1* and *rib-2* mutants we observed AVM neurons with bipolar axon projections emanating from the cell body. We also saw instances in our *rib-1* and *rib-2* mutants where the HSN axon sent out two projections from the cell body, each projecting in opposite directions. This was not limited to the nervous system; when we analyzed the canals of the excretory cell which consists of four canals (two anterior and two posterior), we found examples of *rib-1* and *rib-2* mutant animals with five canals. These phenotypes suggested that somehow the loss of normal HS biosynthesis created an environment which favored extra growth.

RIB-1 and RIB-2 are homologous to the mammalian EXT1 and EXT2/EXTL3, respectively (Clines et al 1997, Kitagawa et al 2001). These phenotypes of overgrowth observed in the *rib-1* and *rib-2* mutants draw intriguing parallels with the disorder hereditary multiple exostoses (HME), which is an autosomal dominant disorder linked to mutations in human EXT1 and EXT2 (Cook et al 1993, Francannet et al 2001, Le Merrer et al 1994, Wu et al 1994, Wuyts & Van Hul 2000). HME is characterized by cartilaginous bone tumors known as osteochondromas which form at the growth plates of long bones and are often, but not always, benign (Schmale et al 1994, Solomon 1964). It remains unknown how loss of function of EXT1 or EXT2, or the consequent reduction in HS synthesis, can lead to HME. Our isolated hypomorphic *rib-1* and *rib-2* mutants provide us with the opportunity to use *C. elegans* as a model to decipher how loss of HS biosynthesis can lead to overgrowth of specific tissues.

**Part II: Glypican is a modulator of netrin-mediated guidance**

While many of the signaling molecules, receptors, and downstream cascades involved in wiring a complex nervous system have been identified, simply knowing the key players is not enough. The number of guidance decisions required to pattern a functional nervous system far outnumber the combinations of implicated signaling pathways involved in this process. Therefore, mechanisms must exist to precisely modulate in space and time how developing

axons respond to these cues. While some signaling pathways have been shown to be modulated in this manner, how the netrin signaling pathway is regulated extracellularly was unknown.

The *C. elegans* nervous system provided us with single cell resolution with which to study netrin-mediated axon guidance, and we used this system to provide insight into how the netrin signaling pathway is regulated by extracellular molecules. My thesis work identified that LON-2/glypican, a HSPG, modulates the netrin pathway that guides migrating axons and cells. This work sheds light on how UNC-6/netrin signals are modulated extracellularly to properly wire the nervous system. We provide evidence that LON-2/glypican functions both in the attractive and repulsive UNC-6/netrin-mediated guidance pathways. Our work demonstrates that the N-terminal globular region of LON-2/glypican, which lacks HS chains, is sufficient for its function in netrin-mediated guidance. We determined that LON-2/glypican functions non-autonomously in the hypodermis to exert its effects on migrating cells and axons. We broadened our genetic results by demonstrating that LON-2/glypican associates with UNC-40/DCC receptor-expressing cells. This work has identified a novel interaction between a HSPG core protein, LON-2/glypican, and the UNC-40/DCC netrin receptor, to modulate netrin-mediated guidance.

*Domains required for the interaction between LON-2/glypican and UNC-40/DCC in UNC-6/netrin-mediated guidance*

Our cellular assays investigated the interactions between LON-2/glypican, UNC-6/netrin, and the UNC-40/DCC receptor, and indicated that LON-2/glypican molecules were preferentially transferred from the LON-2/glypican-expressing cells to the UNC-40/DCC receptor-expressing cells. We found that the interaction between LON-2/glypican and the UNC-40/DCC-expressing cells required the extracellular portion of UNC-40/DCC, yet was independent of the fourth and fifth FnIII domains, which are required for UNC-6/netrin binding (Geisbrecht et al 2003, Kruger et al 2004). Therefore, an extracellular UNC-40/DCC domain or sequence motif, aside from the fourth and fifth FnIII domains, likely mediates this interaction with LON-2/glypican.

UNC-40/DCC is an immunoglobulin superfamily transmembrane receptor (Chan et al 1996) that consists of four Ig-like domains, six fibronectin type III domains (FnIII), a transmembrane domain, and a cytoplasmic tail which contains conserved sequence motifs P1, P2, and P3 (Keino-Masu et al 1996). It will be important to test which parts of the UNC-40/DCC receptor mediate this interaction with LON-2/glypican, by deleting parts of the UNC-40/DCC receptor and testing in our cellular assays to determine the critical sequences required for an interaction with LON-2/glypican. It would also be informative to test the interactions between LON-2/glypican and UNC-40/DCC in a pull-down assay, to

provide more direct evidence of a possible physical interaction, either directly or within a complex, between LON-2/glypican and the UNC-40/DCC receptor.

LON-2/glypican is a GPI-anchored HSPG that has an N-terminal globular head structured by cysteine disulfide bonds, and a C-terminal neck region where three HS chain attachment sites reside (Gumienny et al 2007, Taneja-Bageshwar & Gumienny 2012). We found that the N-terminal globular head of LON-2/glypican, independent of HS chains, was sufficient for function in netrin-mediated guidance. Future experiments addressing the sequences within this region of LON-2/glypican required for its function will complement the UNC-40/DCC domain analysis. Together these experiments have the potential to provide mechanistic insight into how LON-2/glypican and UNC-40/DCC function together either directly or within a complex to modulate netrin signaling.

*Possibility that LON-2/glypican interacts with UNC-6/netrin*

While we found that UNC-6/netrin and LON-2/glypican could both interact with UNC-40/DCC-expressing cells at the same time, we were unable to detect an interaction between UNC-6/netrin and LON-2/glypican in our cellular assays. We speculated this may be due to both molecules being secreted into the medium, and based on our results, we cannot rule out a possible interaction between the UNC-6/netrin and LON-2/glypican molecules. In the future it will be important to use an alternative assay, such as a pull-down, to possibly detect an interaction

between UNC-6/netrin and LON-2/glypican that was previously undetectable with our cellular assays, especially considering netrin has been shown to bind heparin *in vitro* (Kappler et al 2000, Kennedy et al 1994, Shipp & Hsieh-Wilson 2007). Determining whether LON-2/glypican molecules interact with UNC-40/DCC alone, or with both UNC-40/DCC and UNC-6/netrin, will provide mechanistic insight into how LON-2/glypican might function to regulate netrin signaling. For example, if LON-2/glypican interacts with both UNC-6/netrin and UNC-40/DCC, it could play a role in facilitating receptor-ligand interactions. Alternatively, if LON-2/glypican specifically interacts with UNC-40/DCC but not UNC-6/netrin, it may point to a modulation of netrin-mediated guidance through effects on the receptor alone.

*Potential for regulation of UNC-40/DCC receptor by LON-2/glypican*

We demonstrated that LON-2/glypican molecules are shed from the cell surface to then interact with UNC-40/DCC expressing cells. To elucidate the mechanism by which LON-2/glypican modulates UNC-6/netrin signaling, it is critical to determine the effect of this interaction between LON-2/glypican and UNC-40/DCC expressing cells. It has been shown in *C. elegans* that the UNC-40/DCC receptors ventrally cluster during ventral axon outgrowth of the HSN neurons, and that this is controlled by UNC-6/netrin (Adler et al 2006). We wondered if LON-2/glypican, like UNC-6/netrin, could play a role in clustering or organizing UNC-40/DCC receptors ventrally to mediate axon outgrowth. Our analysis of

UNC-40/DCC clustering in AVM was hindered by UNC-40::GFP being undetectable until after AVM axon outgrowth had occurred (data not shown). We were able to detect the ventral accumulation of UNC-40::GFP in the HSN soma at the time of axon outgrowth, and while we did see a disruption of this in *unc-6* mutants (Adler et al 2006), we did not detect a difference in this between wild type and *lon-2/*glypican mutants (data not shown).

While we did not detect any gross differences in UNC-40::GFP localization in the HSNs, this does not completely rule out a role for LON-2/glypican in directional UNC-40/DCC receptor clustering. For example, there could be subtle defects in timing of ventral clustering which our analysis did not pick up, that could have an impact on a temporally-controlled axon guidance event. In addition, our quantification was done in a binary fashion where either UNC-40::GFP was, or was not, ventrally localized at a specific time point. Future analysis of the levels of ventrally localized UNC-40::GFP between wild type and *lon-2/*glypican mutants may provide insight into the regulation of the UNC-40/DCC receptor localization and whether LON-2/glypican plays a role.

Alternatively, perhaps this negative result points to an interaction between LON-2/glypican and UNC-40/DCC that does not strictly affect localization of the UNC-40/DCC receptor. DCC dimerizes when bound to netrin (Stein et al 2001) and crystal structures of DCC bound to netrin-1 have revealed that in these dimerized

DCC molecules, netrin-1 bridges the two DCC molecules through interactions with the fourth fibronectin type III domain of one DCC molecule and the fifth fibronectin type III domain of the other (Finci et al 2015, Xu et al 2014). An interaction between HS and the dimerization of receptors has been shown for another signaling pathway critical for development, the fibroblast growth factor (FGF) pathway. Crystal structure analysis revealed that two fibroblast growth factor receptors (FGFRs) dimerize with two FGF molecules (Plotnikov et al 1999) and that HS is critically involved in forming, and likely stabilizing this dimerized structure (Pellegrini et al 2000, Schlessinger et al 2000). Perhaps LON-2/glypican could play a role in some aspect of the dimerization of UNC-40/DCC receptors, and impact UNC-6/netrin signaling through this type of mechanism.

Insight into this possibility comes from the crystal structure of Netrin-1 either bound to two DCC receptors to mediate attraction, or to one DCC and one UNC5A receptor to mediate repulsion (Finci et al 2015). This work uncovered that Netrin-1 has one binding site that is DCC specific, and another generic binding site which can bind either DCC or the repulsive netrin receptor, UNC5A (Finci et al 2015). However, it is unknown how the netrin-1 molecule switches between the DCC dimer alone, to the dimer of DCC with UNC5A. Finci et al., 2015 speculates that HSPGs could be the missing link in determining which receptor Netrin-1 will interact with. They propose that Netrin-1, bound to one

HSPG, could preferentially interact with DCC whereas when bound to a different HSPG could instead favor an interaction with UNC5A (Finci et al 2015).

In *C. elegans* UNC-40/DCC mediates attractive guidance towards UNC-6/netrin, while UNC-40/DCC with UNC-5/UNC5, or UNC-5/UNC5 alone mediates repulsive guidance away from UNC-6/netrin (Chan et al 1996, Hedgecock et al 1990, Leung-Hagesteijn et al 1992). We have shown that LON-2/glypican functions with UNC-6/netrin signaling to mediate both attractive and repulsive guidance processes, and that LON-2/glypican molecules interact with cells expressing the UNC-40/DCC receptor which is involved in both processes. Perhaps LON-2/glypican could function as the molecular switch which assists UNC-6/netrin molecules in determining which netrin receptor to associate with to carry out a given guidance process. It will be important to test with our cellular assays whether LON-2/glypican can interact with cells expressing the UNC-5/UNC5 receptor, as this would provide insight into whether the function of LON-2/glypican in netrin-mediated attractive and repulsive guidance is due to interactions with the UNC-40/DCC receptor alone, or whether it functions with both UNC-40/DCC and UNC-5/UNC5 in these processes.

It is possible that other HSPGs may function in netrin-mediated repulsive guidance, though specifically through interactions with the UNC-5/UNC5 receptor alone. For example, *sdn-1*/syndecan mutants exhibit defects in motorneuron

axon guidance (Gysi et al 2013, Rhiner et al 2005), a process driven by *unc-6*/netrin-mediated repulsive signaling (Hedgecock et al 1990, Hedgecock et al 1987). We demonstrate that for ventral axon guidance of AVM, *sdn-1*/syndecan functions with the repulsive *slt-1/*slit signaling pathway, and independently of *unc-40*/DCC. Furthermore, through our cellular assays we determined that SDN-1/syndecan molecules do not get transferred to UNC-40/DCC expressing cells. It would therefore be interesting to investigate using our cellular assays whether SDN-1/syndecan molecules interact with UNC-5/UNC5 receptor expressing cells, as perhaps SDN-1/syndecan functions in repulsive netrin-mediated guidance with the UNC-5/UNC5 receptor.

*Mode of action of LON-2/glypican on UNC-6/netrin signaling*

While our work provides novel insight into how netrin-mediated signals are modulated extracellularly, we still aim to determine the specific impact LON-2/glypican has on UNC-6/netrin signaling. Our results suggest that LON-2/glypican functions to enhance UNC-6/netrin signals. For example, we showed that loss of *lon-2/*glypican reduced the penetrance of netrin-dependent dorsalization of PVM upon expression of P*mec-7::unc-5*. This suggested that *unc-6*/netrin signaling was somehow compromised in the *lon-2/*glypican mutant background. In addition, we have evidence from our cellular assays that the presence of LON-2/glypican enhances UNC-6/netrin downstream signaling. Previous literature has shown that cells expressing DCC exhibited an increase in

membrane extensions due to an overactivation of DCC downstream signaling pathways (Shekarabi & Kennedy 2002). We also demonstrated in our cellular assays that the expression of UNC-40/DCC in cells led to an increase in membrane extensions, which was enhanced by the presence of LON-2/glypican. It will be important to directly test whether LON-2/glypican functions to enhance UNC-6/netrin signals, and there are hints from the literature that a HSPG, like LON-2/glypican, could function to amplify netrin signals.

When netrin was first purified, a second component termed “NSA” was present that potentiated the axon outgrowth activity of netrin. Its identity has remained a mystery, though its biochemical properties were consistent with the possibility of it being a HSPG (Kennedy et al 1994). Perhaps the function of LON-2/glypican, similar to what was seen with NSA, is to boost netrin signals. This could be useful in situations where increased netrin sensitivity is required for proper guidance, such as in situations where concentrations of netrin are low. We could test this using spinal cord explant assays which examine axon outgrowth in response to netrin. If LON-2/glypican does function to boost netrin signals, like NSA, we would expect to see an enhancement in netrin-mediated axon outgrowth in the presence of LON-2/glypican with netrin, as compared to netrin alone. This would provide direct evidence as to the role LON-2/glypican plays in modulating UNC-6/netrin signaling to mediate axon guidance, and perhaps may serve to identify that LON-2/glypican is the thus far unidentified NSA molecule.

**Part III: LON-1 functions with SAX-7/L1CAM to maintain nervous system architecture**

After the complex process of nervous system development, the challenge of how to preserve its structure and function begins. Although research using *C. elegans* has identified a handful of molecules with dedicated roles in the maintenance of neuronal architecture, our knowledge of the mechanisms by which these molecules function to preserve established nervous system structures remains limited. One molecule that functions to maintain nervous system architecture is SAX-7/L1CAM. In order to determine the molecular mechanisms by which SAX-7 functions to maintain the nervous system, and identify conserved neuronal protection molecules, we carried out a forward genetic screen for suppressors of the *sax-7* mutant defects in the maintenance of head ganglia organization.

Through this screen, we identified *lon-1* as a novel suppressor of the *sax-7* defects in the maintenance of head ganglia organization. Although the known function of *lon-1* resides in its function in body length regulation through the TGF-β signaling pathway, we determined that the *lon-1*-mediated suppression of *sax-7* defects is independent of body length and the TGF-β signaling pathway. We determined that *lon-1* is a context-dependent suppressor of *sax-7* as loss of *lon-1* is unable to suppress all *sax-7* defects. Expression of *lon-1* in the nervous system or hypodermis is sufficient for its function in the maintenance of neuronal architecture, and this overlaps with the requirement of *sax-7* in multiple adjacent

neurons for proper maintenance. We found that post-embryonic expression of *sax-7* or loss of *lon-1* was sufficient to maintain nervous system architecture in *sax-7* mutants, highlighting a post-embryonic role for both *sax-7* and *lon-1* in nervous system maintenance. My thesis work has identified *lon-1* as a novel maintenance factor that functions with *sax-7* to post-embryonically maintain the architecture of the nervous system.

*Manifestation of head ganglia disorganization*

While we know that the relative positioning between the ASH/ASI soma and the nerve ring fails to be maintained in *sax-7* mutants, yet is able to be maintained in *lon-1; sax-7* double mutants, whether this is a result of an effect on the nerve ring positioning, soma positioning, or both, remains to be determined. Two mutants that show this phenotype, *dig-1* and *sax-7*, were both initially identified as having a posterior displacement of nerve ring axons despite their initial wild-type position (Zallen et al 1999). A thorough analysis of this phenotype from the first larval stage through adulthood in wild type, *lon-1*, *sax-7*, and *lon-1; sax-7* mutant animals will provide insight into how the positioning and organization of these structures changes over time in these genotypes. This will also provide information as to how loss of *lon-1* might be able to suppress these defects in *sax-7* mutants.

*Molecular interactions that maintain nervous system architecture*

The function of SAX-7/L1CAM in the maintenance of neuronal architecture is closely tied to its adhesive properties. The two SAX-7 isoforms, SAX-7L and SAX-7S, differ not only in their extracellular domain structure (Chen et al 2001) but also in their adhesive and functional properties (Pocock et al 2008, Sasakura et al 2005). SAX-7S is the more adhesive isoform as it can induce cellular aggregation when expressed in cultured cells, and its expression can also force attachment between two neighboring neurons, which are properties not seen with SAX-7L (Sasakura et al 2005). Homophilic interactions between SAX-7S molecules are important for cell-cell adhesion. For instance, *sax-7* mutants exhibit a disruption of cell contact between the AIY and AVK neurons which can only be restored through expression of SAX-7S in both neurons (and not through expression of SAX-7L) (Pocock et al 2008). Our work demonstrates that expression of *sax-7S(+)* in multiple adjacent neurons is required to maintain head ganglia organization, highlighting the importance of SAX-7-mediated cell-cell adhesion in the maintenance of nervous system architecture.

In addition, intracellular interactions with the actin cytoskeleton are also important for cell-cell adhesion, and the maintenance of neuronal architecture. Prior work has shown that intracellularly, SAX-7 interacts with UNC-44/ankyrin through its C-terminal ankyrin binding motif, with STN-2/γ-syntrophin through its PDZ binding domain, and that DYS-1/dystrophin interacts with STN-2/γ-syntrophin.

These intracellular interactions link SAX-7 to the actin cytoskeleton to maintain the positioning of motorneurons (Zhou & Chen 2011, Zhou et al 2008). Vertebrate L1 family members also mediate cell-cell adhesion through ankyrin-mediated interactions with the actin cytoskeleton. For example, deletion of the ankyrin binding motif or the entire intracellular domain of L1 family member neurofascin reduced its cell-cell adhesion activity in aggregation assays (Tuvia et al 1997). Likewise, a version of SAX-7S with either the entire intracellular domain or the ankyrin binding motif deleted is no longer able to restore cell contact between the AIY and AVK neurons in *sax-7* mutants, indicating that loss of ankyrin binding renders the SAX-7 molecule less adhesive (Pocock et al 2008).

Our results demonstrate that in a *sax-7* mutant the loss of *lon-1,* even post-embryonically, is sufficient to restore the maintenance of relative positioning between the ASH/ASI soma and the nerve ring. Even in the absence of these critical SAX-7 extracellular and intracellular interactions, the organization of the head ganglia can be properly maintained upon loss of *lon-1,* which raises an important question. Which molecules are maintaining this structure in the *lon-1; sax-7* double mutant, which are not sufficient for maintenance in the *sax-7* mutant alone? Some potential candidates include molecules that SAX-7 is known to interact with intracellularly, such as UNC-44/ankyrin, STN-2/γ-syntrophin, and DYS-1/dystrophin (Zhou & Chen 2011, Zhou et al 2008). Other candidates include extracellular molecules that L1CAM heterophilically interacts with, such

as contactin (De Angelis et al 1999), which is homologous to RIG-6 in *C. elegans* (Katidou et al 2013). It is possible that upon loss of *sax-7* and *lon-1,* these molecules that might normally interact with SAX-7 to maintain nervous system architecture, instead interact with additional molecules to carry out this function. Perhaps loss of one of these molecules in the *lon-1; sax-7* double mutant would abolish the *lon-1*-mediated suppression of *sax-7* maintenance defects, thus providing insight into the molecular interactions maintaining head ganglia organization in the *lon-1; sax-7* double mutant.

*Possibility that LON-1 and SAX-7 molecules interact*

Our results indicate that the *sax-7* mutant defects in the maintenance of head ganglia organization are suppressed by loss of *lon-1*, which points to a novel interaction between *lon-1* and *sax-7* in neuronal maintenance. We speculated that perhaps the genetic interaction we uncovered between *lon-1* and *sax-7* could indicate a close association between the LON-1 and SAX-7 molecules. Expression of LON-1 and SAX-7 is required in nearby and overlapping tissues for each of their functions in the maintenance of neuronal architecture, and therefore, it is feasible that these molecules exist in close proximity and could possibly physically interact.

To test whether LON-1 and SAX-7 physically interact, we could carry out yeast two-hybrid assays, a technique which has successfully detected physical

intracellular interactions between SAX-7 and other proteins in the past (Zhou & Chen 2011, Zhou et al 2008). If we did detect a physical interaction between LON-1 and SAX-7, we could also test different parts of the SAX-7 protein to determine which domains are required for the interaction. Although this method has worked to detect intracellular interactions, we may need to use an alternative assay to test for extracellular interactions. It is also possible that LON-1 and SAX-7 physically function together, but in an indirect manner within a complex through interactions with other molecules. For this type of interaction, we could use a pull-down assay which would allow for the detection of an interaction that may occur within a complex.

One related question that would provide insight into how the SAX-7 and LON-1 molecules might function together is testing whether LON-1 indeed functions as a secreted protein, as has been previously predicted (Maduzia et al 2002). Based on its classification as a CAP superfamily member, and its N-terminal signal peptide sequence (Maduzia et al 2002), it is possible that LON-1 functions as a secreted molecule. We could test this by engineering a LON-1 molecule with a transmembrane domain and assaying whether this molecule is functional. Whether LON-1 functions as a secreted protein or as a membrane-associated protein could affect the ways it might potentially interact with SAX-7, or other molecules, to maintain neuronal architecture.

*Possible mechanisms of lon-1-mediated suppression of sax-7 defects*

Head neurons ASH and ASI do not exist in isolation and instead are located within a densely packed multi-tissue environment. The ASH and ASI soma are part of the lateral ganglion and are in contact with multiple other head neurons within this same region (White et al 1986). More than half of *C. elegans* neurons, including ASH and ASI, send projections into the nerve ring, which is a synapse-rich bundle of axons that encircles the isthmus of the pharynx and is ensheathed by glial cells (Ware et al 1975, White et al 1986). Head neurons, including ASH and ASI, are sandwiched between the pharynx on one side, and the hypodermis and muscles on the other (White et al 1986). In addition, these structures are all ensheathed with a specialized type of extracellular matrix called the basement membrane (Albertson & Thomson 1976, White et al 1976).

*sax-7* mutants were initially identified by their failure to maintain the positioning of the nerve ring, which became posteriorly displaced compared to wild type, while the position of the soma remained unchanged (Zallen et al 1999). While it deserves more careful analysis in the future, we have preliminarily observed that in the *lon-1; sax-7* double mutants, the ASH and ASI soma of adults are often more posteriorly positioned than we see in wild type or *sax-7* mutants alone. This favors the possibility that in the *lon-1; sax-7* double mutants a posterior displacement of the ASH/ASI soma may restore the relative positioning between the ASH/ASI soma and the nerve ring. However, this raises the question of how

structures such as the nerve ring or the ASH/ASI soma are able to become disorganized and displaced despite their densely packed environment filled with potential physical barriers to mobility.

One attractive possibility is that the basement membrane, surrounding the neuronal ganglion, nerve ring, pharynx, hypodermis, and muscles (Albertson & Thomson 1976, White et al 1976), could somehow be affected in the *lon-1; sax-7* double mutants to allow for the ASH/ASI soma to be displaced posteriorly. There is a precedent from research in *C. elegans* that molecules required to maintain the architecture of the nervous system could function to maintain basement membrane integrity. For instance, the large secreted maintenance factor DIG-1, is required for proper basement membrane maintenance as well as the maintenance of nervous system architecture (Benard et al 2006). Additionally, the F-spondin extracellular matrix protein, SPON-1, functions in part to maintain the precise positioning of axons within fascicles (Woo et al 2008). Furthermore, LON-1 is classified as a CAP superfamily protein (Cantacessi et al 2009, Maduzia et al 2002), a family which in vertebrates has implicated functions in processes such as the regulation of the extracellular matrix and how it relates to branching morphogenesis (Gibbs et al 2008).

We can gain insight into the possible role the extracellular matrix plays in the positioning of neuronal soma and axons and how this relates to the *lon-1-*

mediated suppression of *sax-7* defects through comparisons with the mechanism of cell motility. Motile cells require an optimum density of extracellular matrix and show a tendency to move from areas of low extracellular matrix concentration towards areas with a higher concentration. Though it is important to note that if the density is too low, cells will lack the adhesion necessary for movement, and conversely if the density is too high, cells may be stuck and unable to move ((Palecek et al 1997); reviewed in (Rozario & DeSimone 2010)). For example, T cells were found to be motile in regions with low densities of fibronectin and collagen, yet were less able to migrate in areas of higher density (Salmon et al 2012). In addition to changes to the extracellular matrix itself, cells can also reduce their degree of adhesion to the extracellular matrix to allow for increased mobility (Alford et al 1998). In the context of the maintenance of head ganglia organization, for a cell to be displaced from its normal position it seems feasible that either the basement membrane itself or the interaction of the cell with the basement membrane may be altered.

To investigate whether the *lon-1*-mediated suppression of *sax-7* defects in head ganglia organization is a result of a change to the basement membrane, we could analyze fluorescently tagged or immunostained molecules associated with the basement membrane, including LAM-1/laminin (Kao et al 2006), NID-1/nidogen (Kang & Kramer 2000), SPON-1/F-spondin (Woo et al 2008), CLE-1/collagen type XVIII (Ackley et al 2001, Ackley et al 2003), HSPGs such as

SDN-1/syndecan (Rhiner et al 2005) and LON-2/glypican (Gumienny et al 2007), as well as others, and assess whether their expression or localization is altered in our *lon-1; sax-7* double mutants compared to wild type or the single mutants alone. If it is too technically challenging to visualize changes in basement membrane composition or expression within the head ganglia environment of *C. elegans*, perhaps we could investigate the role of *lon-1* and *sax-7* in basement membrane regulation in the context of *C. elegans* anchor cell invasion, which is an established model of basement membrane regulation in *C. elegans* (Hagedorn et al 2014, Hagedorn et al 2009, Hagedorn et al 2013, Sherwood et al 2005, Sherwood & Sternberg 2003, Ziel et al 2009). A potential mechanism of *lon-1*-mediated suppression of *sax-7* that involves basement membrane regulation could have broader implications beyond the maintenance of nervous system architecture including the biology diseases such as fibrosis or cancer (Frantz et al 2010).

*Concluding remarks*

Nervous system development is a beautifully orchestrated and complex process, requiring precise regulation for proper execution. Once assembled, the structures of the nervous system must persist as they endure a lifetime of challenges. My thesis work provides contributions to both our understanding of nervous system development and also its subsequent long-term maintenance. In this work, we have shed light on the molecular mechanisms required for proper wiring of the

nervous system as well as its long-term maintenance. We specifically focused on the role of HS in cell and axon guidance, both the importance of HS chain synthesis as well as the role of specific HSPGs in guidance processes. We identified and characterized viable loss-of-function alleles in the HS co-polymerase enzymes and found that the coordinated expression of HS is required to properly guide axons. We identified that the HSPG LON-2/glypican functions to modulate netrin-mediated axon guidance and may do this through interactions with the UNC-40/DCC netrin receptor. After the proper establishment of the nervous system, molecules such as SAX-7/L1CAM function to actively preserve its integrity. Through a forward genetic screen we identified LON-1 as a novel maintenance factor that functions with SAX-7 to post-embryonically preserve the architecture of the nervous system. My thesis sheds light on the molecular interactions important for both the initial establishment and the long-term maintenance of the nervous system, and provides avenues for future investigation into these areas of research.

## BIBLIOGRAPHY

Ackley BD, Crew JR, Elamaa H, Pihlajaniemi T, Kuo CJ, Kramer JM. 2001. The NC1/Endostatin Domain of Caenorhabditis elegans Type XVIII Collagen Affects Cell Migration and Axon Guidance. *J Cell Biol* 152: 1219-32.

Ackley BD, Kang SH, Crew JR, Suh C, Jin Y, Kramer JM. 2003. The basement membrane components nidogen and type XVIII collagen regulate organization of neuromuscular junctions in Caenorhabditis elegans. *J Neurosci* 23: 3577-87

Adler CE, Fetter RD, Bargmann CI. 2006. UNC-6/Netrin induces neuronal asymmetry and defines the site of axon formation. *Nat Neurosci* 9: 511-8

Albertson DG, Thomson JN. 1976. The pharynx of Caenorhabditis elegans. *Philos Trans R Soc Lond B Biol Sci* 275: 299-325

Alford D, Baeckstrom D, Geyp M, Pitha P, Taylor-Papadimitriou J. 1998. Integrin-matrix interactions affect the form of the structures developing from human mammary epithelial cells in collagen or fibrin gels. *J Cell Sci* 111 ( Pt 4): 521-32

Allen NJ, Bennett ML, Foo LC, Wang GX, Chakraborty C, et al. 2012. Astrocyte glypicans 4 and 6 promote formation of excitatory synapses via GluA1 AMPA receptors. *Nature* 486: 410-4

Altun-Gultekin Z, Andachi Y, Tsalik EL, Pilgrim D, Kohara Y, Hobert O. 2001. A regulatory cascade of three homeobox genes, ceh-10, ttx-3 and ceh-23, controls cell fate specification of a defined interneuron class in C. elegans. *Development* 128: 1951-69.

Amor V, Feinberg K, Eshed-Eisenbach Y, Vainshtein A, Frechter S, et al. 2014. Long-term maintenance of Na+ channels at nodes of Ranvier depends on glial contact mediated by gliomedin and NrCAM. *J Neurosci* 34: 5089-98

Arikawa-Hirasawa E, Rossi SG, Rotundo RL, Yamada Y. 2002. Absence of acetylcholinesterase at the neuromuscular junctions of perlecan-null mice. *Nat Neurosci* 5: 119-23

Ashrafi K, Chang FY, Watts JL, Fraser AG, Kamath RS, et al. 2003. Genome-wide RNAi analysis of Caenorhabditis elegans fat regulatory genes. *Nature* 421: 268-72

Aurelio O, Hall DH, Hobert O. 2002. Immunoglobulin-domain proteins required for maintenance of ventral nerve cord organization. *Science* 295: 686-90

Azevedo FA, Carvalho LR, Grinberg LT, Farfel JM, Ferretti RE, et al. 2009. Equal numbers of neuronal and nonneuronal cells make the human brain an isometrically scaled-up primate brain. *The Journal of comparative neurology* 513: 532-41

Barsi-Rhyne BJ, Miller KM, Vargas CT, Thomas AB, Park J, et al. 2013. Kinesin-1 acts with netrin and DCC to maintain sensory neuron position in Caenorhabditis elegans. *Genetics* 194: 175-87

Beanan MJ, Strome S. 1992. Characterization of a germ-line proliferation mutation in C. elegans. *Development* 116: 755-66

Bellaiche Y, The I, Perrimon N. 1998. Tout-velu is a Drosophila homologue of the putative tumour suppressor EXT-1 and is needed for Hh diffusion. *Nature* 394: 85-8

Benard C, Hobert O. 2009. Looking beyond development: maintaining nervous system architecture. *Curr Top Dev Biol* 87: 175-94

Benard C, Tjoe N, Boulin T, Recio J, Hobert O. 2009. The small, secreted immunoglobulin protein ZIG-3 maintains axon position in Caenorhabditis elegans. *Genetics* 183: 917-27

Benard CY, Blanchette C, Recio J, Hobert O. 2012. The secreted immunoglobulin domain proteins ZIG-5 and ZIG-8 cooperate with L1CAM/SAX-7 to maintain nervous system integrity. *PLoS Genet* 8: e1002819

Benard CY, Boyanov A, Hall DH, Hobert O. 2006. DIG-1, a novel giant protein, non-autonomously mediates maintenance of nervous system architecture. *Development* 133: 3329-40

Benes FM, Turtle M, Khan Y, Farol P. 1994. Myelination of a key relay zone in the hippocampal formation occurs in the human brain during childhood, adolescence, and adulthood. *Arch Gen Psychiatry* 51: 477-84

Bennett KL, Bradshaw J, Youngman T, Rodgers J, Greenfield B, et al. 1997. Deleted in colorectal carcinoma (DCC) binds heparin via its fifth fibronectin type III domain. *J Biol Chem* 272: 26940-6

Bernfield M, Gotte M, Park PW, Reizes O, Fitzgerald ML, et al. 1999. Functions of cell surface heparan sulfate proteoglycans. *Annual review of biochemistry* 68: 729-77

Berry KL, Bulow HE, Hall DH, Hobert O. 2003. A C. elegans CLIC-like protein required for intracellular tube formation and maintenance. *Science* 302: 2134-7

Bishop JR, Schuksz M, Esko JD. 2007. Heparan sulphate proteoglycans fine-tune mammalian physiology. *Nature* 446: 1030-7

Blanchette CR, Perrat PN, Thackeray A, Benard CY. 2015. Glypican Is a Modulator of Netrin-Mediated Axon Guidance. *PLoS Biol* 13: e1002183

Bloom L. 1993. Genetic and molecular analysis of genes required for axon outgrowth in Caenorhabditis elegans. Massachusetts Institute of Technology; Cambridge

Blumenthal T, Evans D, Link CD, Guffanti A, Lawson D, et al. 2002. A global analysis of Caenorhabditis elegans operons. *Nature* 417: 851-4

Brenner S. 1974. The genetics of Caenorhabditis elegans. *Genetics* 77: 71-94

Brose K, Bland KS, Wang KH, Arnott D, Henzel W, et al. 1999. Slit proteins bind Robo receptors and have an evolutionarily conserved role in repulsive axon guidance. *Cell* 96: 795-806

Bülow HE, Berry KL, Topper LH, Peles E, Hobert O. 2002. Heparan sulfate proteoglycan-dependent induction of axon branching and axon misrouting by the Kallmann syndrome gene kal-1. *Proc Natl Acad Sci U S A* 99: 6346-51

Bülow HE, Boulin T, Hobert O. 2004. Differential functions of the C. elegans FGF receptor in axon outgrowth and maintenance of axon position. *Neuron* 42: 367-74

Bülow HE, Hobert O. 2004. Differential sulfations and epimerization define heparan sulfate specificity in nervous system development. *Neuron* 41: 723-36

Bülow HE, Hobert O. 2006. The Molecular Diversity of Glycosaminoglycans Shapes Animal Development. *Annu Rev Cell Dev Biol*

Bulow HE, Tjoe N, Townley RA, Didiano D, van Kuppevelt TH, Hobert O. 2008. Extracellular Sugar Modifications Provide Instructive and Cell-Specific Information for Axon-Guidance Choices. *Curr Biol* 18: 1978-85

Buss RR, Sun W, Oppenheim RW. 2006. Adaptive roles of programmed cell death during nervous system development. *Annu Rev Neurosci* 29: 1-35

Busse-Wicher M, Wicher KB, Kusche-Gullberg M. 2014. The exostosin family: proteins with many functions. *Matrix Biol* 35: 25-33

Cantacessi C, Campbell BE, Visser A, Geldhof P, Nolan MJ, et al. 2009. A portrait of the "SCP/TAPS" proteins of eukaryotes--developing a framework for fundamental research and biotechnological outcomes. *Biotechnol Adv* 27: 376-88

Capurro MI, Xiang YY, Lobe C, Filmus J. 2005. Glypican-3 promotes the growth of hepatocellular carcinoma by stimulating canonical Wnt signaling. *Cancer research* 65: 6245-54

Capurro MI, Xu P, Shi W, Li F, Jia A, Filmus J. 2008. Glypican-3 inhibits Hedgehog signaling during development by competing with patched for Hedgehog binding. *Dev Cell* 14: 700-11

Carleton A, Petreanu LT, Lansford R, Alvarez-Buylla A, Lledo PM. 2003. Becoming a new neuron in the adult olfactory bulb. *Nat Neurosci* 6: 507-18

Celniker SE, Dillon LA, Gerstein MB, Gunsalus KC, Henikoff S, et al. 2009. Unlocking the secrets of the genome. *Nature* 459: 927-30

Chan SS, Zheng H, Su MW, Wilk R, Killeen MT, et al. 1996. UNC-40, a C. elegans homolog of DCC (Deleted in Colorectal Cancer), is required in motile cells responding to UNC-6 netrin cues. *Cell* 87: 187-95

Chang C, Adler CE, Krause M, Clark SG, Gertler FB, et al. 2006. MIG-10/lamellipodin and AGE-1/PI3K promote axon guidance and outgrowth in response to slit and netrin. *Curr Biol* 16: 854-62

Chase DL, Pepper JS, Koelle MR. 2004. Mechanism of extrasynaptic dopamine signaling in Caenorhabditis elegans. *Nat Neurosci* 7: 1096-103

Chen L, Ong B, Bennett V. 2001. LAD-1, the Caenorhabditis elegans L1CAM homologue, participates in embryonic and gonadal morphogenesis and is a substrate for fibroblast growth factor receptor pathway-dependent phosphotyrosine-based signaling. *J Cell Biol* 154: 841-56.

Cherra SJ, 3rd, Jin Y. 2016. A Two-Immunoglobulin-Domain Transmembrane Protein Mediates an Epidermal-Neuronal Interaction to Maintain Synapse Density. *Neuron*

Clark SG, Chiu C. 2003. C. elegans ZAG-1, a Zn-finger-homeodomain protein, regulates axonal development and neuronal differentiation. *Development* 130: 3781-94

Clay MR, Sherwood DR. 2015. Basement Membranes in the Worm: A Dynamic Scaffolding that Instructs Cellular Behaviors and Shapes Tissues. *Curr Top Membr* 76: 337-71

Clines GA, Ashley JA, Shah S, Lovett M. 1997. The structure of the human multiple exostoses 2 gene and characterization of homologs in mouse and Caenorhabditis elegans. *Genome Res* 7: 359-67

Colavita A, Culotti JG. 1998. Suppressors of ectopic UNC-5 growth cone steering identify eight genes involved in axon guidance in Caenorhabditis elegans. *Dev Biol* 194: 72-85

Colavita A, Krishna S, Zheng H, Padgett RW, Culotti JG. 1998. Pioneer axon guidance by UNC-129, a C. elegans TGF-beta. *Science* 281: 706-9

Colon-Ramos DA, Margeta MA, Shen K. 2007. Glia promote local synaptogenesis through UNC-6 (netrin) signaling in C. elegans. *Science* 318: 103-6

Consortium CeDM. 2012. large-scale screening for targeted knockouts in the Caenorhabditis elegans genome. *G3 (Bethesda)* 2: 1415-25

Cook A, Raskind W, Blanton SH, Pauli RM, Gregg RG, et al. 1993. Genetic heterogeneity in families with hereditary multiple exostoses. *Am J Hum Genet* 53: 71-9

Curtis MA, Kam M, Nannmark U, Anderson MF, Axell MZ, et al. 2007. Human neuroblasts migrate to the olfactory bulb via a lateral ventricular extension. *Science* 315: 1243-9

David G, Bai XM, Van der Schueren B, Cassiman JJ, Van den Berghe H. 1992. Developmental changes in heparan sulfate expression: in situ detection with mAbs. *J Cell Biol* 119: 961-75

De Angelis E, MacFarlane J, Du JS, Yeo G, Hicks R, et al. 1999. Pathological missense mutations of neural cell adhesion molecule L1 affect homophilic and heterophilic binding activities. *EMBO J* 18: 4744-53

De Cat B, Muyldermans SY, Coomans C, Degeest G, Vanderschueren B, et al. 2003. Processing by proprotein convertases is required for glypican-3 modulation of cell survival, Wnt signaling, and gastrulation movements. *J Cell Biol* 163: 625-35

Dekaban AS. 1978. Changes in brain weights during the span of human life: relation of brain weights to body heights and body weights. *Ann Neurol* 4: 345-56

Demyanenko GP, Schachner M, Anton E, Schmid R, Feng G, et al. 2004. Close homolog of L1 modulates area-specific neuronal positioning and dendrite orientation in the cerebral cortex. *Neuron* 44: 423-37

Demyanenko GP, Shibata Y, Maness PF. 2001. Altered distribution of dopaminergic neurons in the brain of L1 null mice. *Brain Res Dev Brain Res* 126: 21-30

Diaz-Balzac CA, Lazaro-Pena MI, Tecle E, Gomez N, Bulow HE. 2014. Complex cooperative functions of heparan sulfate proteoglycans shape nervous system development in Caenorhabditis elegans. *G3 (Bethesda)* 4: 1859-70

Dobbing J, Sands J. 1973. Quantitative growth and development of human brain. *Arch Dis Child* 48: 757-67

Doitsidou M, Poole RJ, Sarin S, Bigelow H, Hobert O. 2010. C. elegans mutant identification with a one-step whole-genome-sequencing and SNP mapping strategy. *PLoS One* 5: e15435

Dong X, Liu OW, Howell AS, Shen K. 2013. An extracellular adhesion molecule complex patterns dendritic branching and morphogenesis. *Cell* 155: 296-307

Edgren G, Havsmark B, Jonsson M, Fransson LA. 1997. Glypican (heparan sulfate proteoglycan) is palmitoylated, deglycanated and reglycanated during recycling in skin fibroblasts. *Glycobiology* 7: 103-12

Edwards TJ, Hammarlund M. 2014. Syndecan promotes axon regeneration by stabilizing growth cone migration. *Cell Rep* 8: 272-83

Eriksson PS, Perfilieva E, Bjork-Eriksson T, Alborn AM, Nordborg C, et al. 1998. Neurogenesis in the adult human hippocampus. *Nat Med* 4: 1313-7

Esko JD, Selleck SB. 2002. Order out of chaos: assembly of ligand binding sites in heparan sulfate. *Annual review of biochemistry* 71: 435-71

Ethell IM, Yamaguchi Y. 1999. Cell surface heparan sulfate proteoglycan syndecan-2 induces the maturation of dendritic spines in rat hippocampal neurons. *J Cell Biol* 144: 575-86

Fernando T, Flibotte S, Xiong S, Yin J, Yzeiraj E, et al. 2011. C. elegans ADAMTS ADT-2 regulates body size by modulating TGFbeta signaling and cuticle collagen organization. *Dev Biol* 352: 92-103

Finci L, Zhang Y, Meijers R, Wang JH. 2015. Signaling mechanism of the netrin-1 receptor DCC in axon guidance. *Prog Biophys Mol Biol* 118: 153-60

Fire A, Harrison SW, Dixon D. 1990. A modular set of lacZ fusion vectors for studying gene expression in Caenorhabditis elegans. *Gene* 93: 189-98

Firnhaber C, Hammarlund M. 2013. Neuron-specific feeding RNAi in C. elegans and its use in a screen for essential genes required for GABA neuron function. *PLoS Genet* 9: e1003921

Flanagan JG, Vanderhaeghen P. 1998. The ephrins and Eph receptors in neural development. *Annu Rev Neurosci* 21: 309-45

Fleming T, Chien SC, Vanderzalm PJ, Dell M, Gavin MK, et al. 2010. The role of C. elegans Ena/VASP homolog UNC-34 in neuronal polarity and motility. *Dev Biol* 344: 94-106

Francannet C, Cohen-Tanugi A, Le Merrer M, Munnich A, Bonaventure J, Legeai-Mallet L. 2001. Genotype-phenotype correlation in hereditary multiple exostoses. *J Med Genet* 38: 430-4

Franks DM, Izumikawa T, Kitagawa H, Sugahara K, Okkema PG. 2006. C. elegans pharyngeal morphogenesis requires both de novo synthesis of pyrimidines and synthesis of heparan sulfate proteoglycans. *Dev Biol* 296: 409-20

Fransson LA, Edgren G, Havsmark B, Schmidtchen A. 1995. Recycling of a glycosylphosphatidylinositol-anchored heparan sulphate proteoglycan (glypican) in skin fibroblasts. *Glycobiology* 5: 407-15

Frantz C, Stewart KM, Weaver VM. 2010. The extracellular matrix at a glance. *J Cell Sci* 123: 4195-200

Friedland AE, Tzur YB, Esvelt KM, Colaiacovo MP, Church GM, Calarco JA. 2013. Heritable genome editing in C. elegans via a CRISPR-Cas9 system. *Nat Methods* 10: 741-3

Fung WY, Fat KF, Eng CK, Lau CK. 2007. crm-1 facilitates BMP signaling to control body size in Caenorhabditis elegans. *Dev Biol* 311: 95-105

Geisbrecht BV, Dowd KA, Barfield RW, Longo PA, Leahy DJ. 2003. Netrin Binds Discrete Subdomains of DCC and UNC5 and Mediates Interactions between DCC and Heparin. *J Biol Chem* 278: 32561-8

Gertler FB, Comer AR, Juang JL, Ahern SM, Clark MJ, et al. 1995. enabled, a dosage-sensitive suppressor of mutations in the Drosophila Abl tyrosine kinase, encodes an Abl substrate with SH3 domain-binding properties. *Genes Dev* 9: 521-33

Gertler FB, Doctor JS, Hoffmann FM. 1990. Genetic suppression of mutations in the Drosophila abl proto-oncogene homolog. *Science* 248: 857-60

Gibbs GM, Roelants K, O'Bryan MK. 2008. The CAP superfamily: cysteine-rich secretory proteins, antigen 5, and pathogenesis-related 1 proteins--roles in reproduction, cancer, and immune defense. *Endocr Rev* 29: 865-97

Giedd JN, Blumenthal J, Jeffries NO, Castellanos FX, Liu H, et al. 1999. Brain development during childhood and adolescence: a longitudinal MRI study. *Nat Neurosci* 2: 861-3

Giraldez AJ, Copley RR, Cohen SM. 2002. HSPG modification by the secreted enzyme Notum shapes the Wingless morphogen gradient. *Dev Cell* 2: 667-76

Gitai Z, Yu TW, Lundquist EA, Tessier-Lavigne M, Bargmann CI. 2003. The netrin receptor UNC-40/DCC stimulates axon attraction and outgrowth through enabled and, in parallel, Rac and UNC-115/AbLIM. *Neuron* 37: 53-65

Glass DJ, Bowen DC, Stitt TN, Radziejewski C, Bruno J, et al. 1996. Agrin acts via a MuSK receptor complex. *Cell* 85: 513-23

Godfrey EW, Nitkin RM, Wallace BG, Rubin LL, McMahan UJ. 1984. Components of Torpedo electric organ and muscle that cause aggregation of acetylcholine receptors on cultured muscle cells. *J Cell Biol* 99: 615-27

Gonzalez AD, Kaya M, Shi W, Song H, Testa JR, et al. 1998. OCI-5/GPC3, a glypican encoded by a gene that is mutated in the Simpson-Golabi-Behmel overgrowth syndrome, induces apoptosis in a cell line-specific manner. *J Cell Biol* 141: 1407-14

Gumienny TL, Macneil L, Zimmerman CM, Wang H, Chin L, et al. 2010. Caenorhabditis elegans SMA-10/LRIG is a conserved transmembrane protein that enhances bone morphogenetic protein signaling. *PLoS Genet* 6: e1000963

Gumienny TL, MacNeil LT, Wang H, de Bono M, Wrana JL, Padgett RW. 2007. Glypican LON-2 is a conserved negative regulator of BMP-like signaling in Caenorhabditis elegans. *Curr Biol* 17: 159-64

Gumienny TL, Savage-Dunn C. 2013. TGF-beta signaling in C. elegans. *WormBook*: 1-34

Gysi S, Rhiner C, Flibotte S, Moerman DG, Hengartner MO. 2013. A network of HSPG core proteins and HS modifying enzymes regulates netrin-dependent guidance of D-type motor neurons in Caenorhabditis elegans. *PLoS One* 8: e74908

Hagedorn EJ, Kelley LC, Naegeli KM, Wang Z, Chi Q, Sherwood DR. 2014. ADF/cofilin promotes invadopodial membrane recycling during cell invasion in vivo. *J Cell Biol* 204: 1209-18

Hagedorn EJ, Yashiro H, Ziel JW, Ihara S, Wang Z, Sherwood DR. 2009. Integrin acts upstream of netrin signaling to regulate formation of the anchor cell's invasive membrane in C. elegans. *Dev Cell* 17: 187-98

Hagedorn EJ, Ziel JW, Morrissey MA, Linden LM, Wang Z, et al. 2013. The netrin receptor DCC focuses invadopodia-driven basement membrane transmigration in vivo. *J Cell Biol* 201: 903-13

Hamelin M, Zhou Y, Su MW, Scott IM, Culotti JG. 1993. Expression of the UNC-5 guidance receptor in the touch neurons of C. elegans steers their axons dorsally. *Nature* 364: 327-30

Hammarlund M, Jorgensen EM, Bastiani MJ. 2007. Axons break in animals lacking beta-spectrin. *J Cell Biol* 176: 269-75

Han C, Belenkaya TY, Khodoun M, Tauchi M, Lin X, Lin X. 2004. Distinct and collaborative roles of Drosophila EXT family proteins in morphogen signalling and gradient formation. *Development* 131: 1563-75

Hao JC, Yu TW, Fujisawa K, Culotti JG, Gengyo-Ando K, et al. 2001. C. elegans Slit Acts in Midline, Dorsal-Ventral, and Anterior-Posterior Guidance via the SAX-3/Robo Receptor. *Neuron* 32: 25-38.

Harris J, Honigberg L, Robinson N, Kenyon C. 1996. Neuronal cell migration in C. elegans: regulation of Hox gene expression and cell position. *Development* 122: 3117-31.

Hawdon JM, Narasimhan S, Hotez PJ. 1999. Ancylostoma secreted protein 2: cloning and characterization of a second member of a family of nematode secreted proteins from Ancylostoma caninum. *Mol Biochem Parasitol* 99: 149-65

Hedgecock EM, Culotti JG, Hall DH. 1990. The unc-5, unc-6, and unc-40 genes guide circumferential migrations of pioneer axons and mesodermal cells on the epidermis in C. elegans. *Neuron* 4: 61-85

Hedgecock EM, Culotti JG, Hall DH, Stern BD. 1987. Genetics of cell and axon migrations in Caenorhabditis elegans. *Development* 100: 365-82

Hedgecock EM, Culotti JG, Thomson JN, Perkins LA. 1985. Axonal guidance mutants of Caenorhabditis elegans identified by filling sensory neurons with fluorescein dyes. *Dev Biol* 111: 158-70

Hekimi S, Boutis P, Lakowski B. 1995. Viable maternal-effect mutations that affect the development of the nematode Caenorhabditis elegans. *Genetics* 141: 1351-64

Holland BA, Haas DK, Norman D, Brant-Zawadzki M, Newton TH. 1986. MRI of normal brain maturation. *AJNR Am J Neuroradiol* 7: 201-8

Hong K, Hinck L, Nishiyama M, Poo MM, Tessier-Lavigne M, Stein E. 1999. A ligand-gated association between cytoplasmic domains of UNC5 and DCC family receptors converts netrin-induced growth cone attraction to repulsion. *Cell* 97: 927-41

Hoogewijs D, Houthoofd K, Matthijssens F, Vandesompele J, Vanfleteren JR. 2008. Selection and validation of a set of reliable reference genes for quantitative sod gene expression analysis in C. elegans. *BMC molecular biology* 9: 9

Hortsch M. 2000. Structural and functional evolution of the L1 family: are four adhesion molecules better than one? *Mol Cell Neurosci* 15: 1-10

Hortsch M, Nagaraj K, Mualla R. 2014. The L1 family of cell adhesion molecules: a sickening number of mutations and protein functions. *Adv Neurobiol* 8: 195-229

Hou S, Maccarana M, Min TH, Strate I, Pera EM. 2007. The secreted serine protease xHtrA1 stimulates long-range FGF signaling in the early Xenopus embryo. *Dev Cell* 13: 226-41

Hrus A, Lau G, Hutter H, Schenk S, Ferralli J, et al. 2007. C. elegans agrin is expressed in pharynx, IL1 neurons and distal tip cells and does not genetically interact with genes involved in synaptogenesis or muscle function. *PLoS One* 2: e731

Hudson ML, Kinnunen T, Cinar HN, Chisholm AD. 2006. C. elegans Kallmann syndrome protein KAL-1 interacts with syndecan and glypican to regulate neuronal cell migrations. *Dev Biol* 294: 352-65

Huttenlocher PR, Dabholkar AS. 1997. Regional differences in synaptogenesis in human cerebral cortex. *The Journal of comparative neurology* 387: 167-78

Huttenlocher PR, De Courten C, Garey LJ, Van der Loos H. 1982. Synaptic development in human cerebral cortex. *Int J Neurol* 16-17: 144-54

Hutter H. 2003. Extracellular cues and pioneers act together to guide axons in the ventral cord of C. elegans. *Development* 130: 5307-18

Hwang HY, Horvitz HR. 2002a. The Caenorhabditis elegans vulval morphogenesis gene sqv-4 encodes a UDP-glucose dehydrogenase that

is temporally and spatially regulated. *Proc Natl Acad Sci U S A* 99: 14224-9

Hwang HY, Horvitz HR. 2002b. The SQV-1 UDP-glucuronic acid decarboxylase and the SQV-7 nucleotide-sugar transporter may act in the Golgi apparatus to affect Caenorhabditis elegans vulval morphogenesis and embryonic development. *Proc Natl Acad Sci U S A* 99: 14218-23

Hwang HY, Olson SK, Brown JR, Esko JD, Horvitz HR. 2003a. The Caenorhabditis elegans genes sqv-2 and sqv-6, which are required for vulval morphogenesis, encode glycosaminoglycan galactosyltransferase II and xylosyltransferase. *J Biol Chem* 278: 11735-8

Hwang HY, Olson SK, Esko JD, Horvitz HR. 2003b. Caenorhabditis elegans early embryogenesis and vulval morphogenesis require chondroitin biosynthesis. *Nature* 423: 439-43

Irie F, Badie-Mahdavi H, Yamaguchi Y. 2012. Autism-like socio-communicative deficits and stereotypies in mice lacking heparan sulfate. *Proc Natl Acad Sci U S A* 109: 5052-6

Ishii N, Wadsworth WG, Stern BD, Culotti JG, Hedgecock EM. 1992. UNC-6, a laminin-related protein, guides cell and pioneer axon migrations in C. elegans. *Neuron* 9: 873-81

Jinek M, Chylinski K, Fonfara I, Hauer M, Doudna JA, Charpentier E. 2012. A programmable dual-RNA-guided DNA endonuclease in adaptive bacterial immunity. *Science* 337: 816-21

Johnson KG, Ghose A, Epstein E, Lincecum J, O'Connor MB, Van Vactor D. 2004. Axonal heparan sulfate proteoglycans regulate the distribution and efficiency of the repellent slit during midline axon guidance. *Curr Biol* 14: 499-504

Johnson KG, Tenney AP, Ghose A, Duckworth AM, Higashi ME, et al. 2006. The HSPGs Syndecan and Dallylike bind the receptor phosphatase LAR and exert distinct effects on synaptic development. *Neuron* 49: 517-31

Johnson RP, Kramer JM. 2012. Neural maintenance roles for the matrix receptor dystroglycan and the nuclear anchorage complex in Caenorhabditis elegans. *Genetics* 190: 1365-77

Jones D, Russnak RH, Kay RJ, Candido EP. 1986. Structure, expression, and evolution of a heat shock gene locus in Caenorhabditis elegans that is flanked by repetitive elements. *J Biol Chem* 261: 12006-15

Kamath RS, Martinez-Campos M, Zipperlen P, Fraser AG, Ahringer J. 2000. Effectiveness of specific RNA-mediated interference through ingested double-stranded RNA in Caenorhabditis elegans. *GenomeBiology.com* 2

Kang SH, Kramer JM. 2000. Nidogen is nonessential and not required for normal type IV collagen localization in Caenorhabditis elegans. *Mol Biol Cell* 11: 3911-23

Kao G, Huang CC, Hedgecock EM, Hall DH, Wadsworth WG. 2006. The role of the laminin beta subunit in laminin heterotrimer assembly and basement membrane function and development in C. elegans. *Dev Biol* 290: 211-9

Kappler J, Franken S, Junghans U, Hoffmann R, Linke T, et al. 2000. Glycosaminoglycan-binding properties and secondary structure of the C-terminus of netrin-1. *Biochem Biophys Res Commun* 271: 287-91

Katidou M, Tavernarakis N, Karagogeos D. 2013. The contactin RIG-6 mediates neuronal and non-neuronal cell migration in Caenorhabditis elegans. *Dev Biol* 373: 184-95

Keino-Masu K, Masu M, Hinck L, Leonardo ED, Chan SS, et al. 1996. Deleted in Colorectal Cancer (DCC) encodes a netrin receptor. *Cell* 87: 175-85

Keleman K, Dickson BJ. 2001. Short- and long-range repulsion by the Drosophila Unc5 netrin receptor. *Neuron* 32: 605-17

Kennedy TE, Serafini T, de la Torre JR, Tessier-Lavigne M. 1994. Netrins are diffusible chemotropic factors for commissural axons in the embryonic spinal cord. *Cell* 78: 425-35

Kidd T, Bland KS, Goodman CS. 1999. Slit is the midline repellent for the robo receptor in Drosophila. *Cell* 96: 785-94.

Kidd T, Brose K, Mitchell KJ, Fetter RD, Tessier-Lavigne M, et al. 1998a. Roundabout controls axon crossing of the CNS midline and defines a novel subfamily of evolutionarily conserved guidance receptors. *Cell* 92: 205-15.

Kidd T, Russell C, Goodman CS, Tear G. 1998b. Dosage-sensitive and complementary functions of roundabout and commissureless control axon crossing of the CNS midline. *Neuron* 20: 25-33.

Kimble J, Hirsh D. 1979. The postembryonic cell lineages of the hermaphrodite and male gonads in Caenorhabditis elegans. *Dev Biol* 70: 396-417

Kinnunen T, Huang Z, Townsend J, Gatdula MM, Brown JR, et al. 2005. Heparan 2-O-sulfotransferase, hst-2, is essential for normal cell migration in Caenorhabditis elegans. *Proc Natl Acad Sci U S A* 102: 1507-12

Kirkpatrick CA, Knox SM, Staatz WD, Fox B, Lercher DM, Selleck SB. 2006. The function of a Drosophila glypican does not depend entirely on heparan sulfate modification. *Dev Biol* 300: 570-82

Kitagawa H, Egusa N, Tamura JI, Kusche-Gullberg M, Lindahl U, Sugahara K. 2001. rib-2, a Caenorhabditis elegans homolog of the human tumor suppressor EXT genes encodes a novel alpha1,4-N-acetylglucosaminyltransferase involved in the biosynthetic initiation and elongation of heparan sulfate. *J Biol Chem* 276: 4834-8

Kitagawa H, Izumikawa T, Mizuguchi S, Dejima K, Nomura KH, et al. 2007. Expression of rib-1, a Caenorhabditis elegans homolog of the human tumor suppressor EXT genes, is indispensable for heparan sulfate synthesis and embryonic morphogenesis. *J Biol Chem* 282: 8533-44

Knickmeyer RC, Gouttard S, Kang C, Evans D, Wilber K, et al. 2008. A structural MRI study of human brain development from birth to 2 years. *J Neurosci* 28: 12176-82

Knight CG, Patel MN, Azevedo RB, Leroi AM. 2002. A novel mode of ecdysozoan growth in Caenorhabditis elegans. *Evol Dev* 4: 16-27

Kolata S, Wu J, Light K, Schachner M, Matzel LD. 2008. Impaired working memory duration but normal learning abilities found in mice that are conditionally deficient in the close homolog of L1. *J Neurosci* 28: 13505-10

Kolodkin AL, Matthes DJ, Goodman CS. 1993. The semaphorin genes encode a family of transmembrane and secreted growth cone guidance molecules. *Cell* 75: 1389-99

Kolodkin AL, Matthes DJ, O'Connor TP, Patel NH, Admon A, et al. 1992. Fasciclin IV: sequence, expression, and function during growth cone guidance in the grasshopper embryo. *Neuron* 9: 831-45

Kolodkin AL, Tessier-Lavigne M. 2011. Mechanisms and molecules of neuronal wiring: a primer. *Cold Spring Harbor perspectives in biology* 3

Kolodziej PA, Timpe LC, Mitchell KJ, Fried SR, Goodman CS, et al. 1996. frazzled encodes a Drosophila member of the DCC immunoglobulin subfamily and is required for CNS and motor axon guidance. *Cell* 87: 197-204

Kramer JM. 2005. Basement membranes In *WormBook*, ed. TCeR Community: WormBook, doi/10.1895/wormbook.1.7.1, http://www.wormbook.org.

Kriebel M, Metzger J, Trinks S, Chugh D, Harvey RJ, et al. 2011. The cell adhesion molecule neurofascin stabilizes axo-axonic GABAergic terminals at the axon initial segment. *J Biol Chem* 286: 24385-93

Krishna S, Maduzia LL, Padgett RW. 1999. Specificity of TGFbeta signaling is conferred by distinct type I receptors and their associated SMAD proteins in Caenorhabditis elegans. *Development* 126: 251-60

Kruger RP, Lee J, Li W, Guan KL. 2004. Mapping netrin receptor binding reveals domains of Unc5 regulating its tyrosine phosphorylation. *J Neurosci* 24: 10826-34

Lai Wing Sun K, Correia JP, Kennedy TE. 2011. Netrins: versatile extracellular cues with diverse functions. *Development* 138: 2153-69

Lander AD, Selleck SB. 2000. The elusive functions of proteoglycans: in vivo veritas. *J Cell Biol* 148: 227-32

Law JW, Lee AY, Sun M, Nikonenko AG, Chung SK, et al. 2003. Decreased anxiety, altered place learning, and increased CA1 basal excitatory synaptic transmission in mice with conditional ablation of the neural cell adhesion molecule L1. *J Neurosci* 23: 10419-32

Le Merrer M, Legeai-Mallet L, Jeannin PM, Horsthemke B, Schinzel A, et al. 1994. A gene for hereditary multiple exostoses maps to chromosome 19p. *Hum Mol Genet* 3: 717-22

Leonardo ED, Hinck L, Masu M, Keino-Masu K, Ackerman SL, Tessier-Lavigne M. 1997. Vertebrate homologues of C. elegans UNC-5 are candidate netrin receptors. *Nature* 386: 833-8

Lesch BJ, Bargmann CI. 2010. The homeodomain protein hmbx-1 maintains asymmetric gene expression in adult C. elegans olfactory neurons. *Genes Dev* 24: 1802-15

Leung-Hagesteijn C, Spence AM, Stern BD, Zhou Y, Su MW, et al. 1992. UNC-5, a transmembrane protein with immunoglobulin and thrombospondin type 1 domains, guides cell and pioneer axon migrations in C. elegans. *Cell* 71: 289-99

Li H, Yamagata T, Mori M, Momoi MY. 2002. Association of autism in two patients with hereditary multiple exostoses caused by novel deletion mutations of EXT1. *J Hum Genet* 47: 262-5

Li HS, Chen JH, Wu W, Fagaly T, Zhou L, et al. 1999. Vertebrate slit, a secreted ligand for the transmembrane protein roundabout, is a repellent for olfactory bulb axons. *Cell* 96: 807-18

Lim YS, Wadsworth WG. 2002. Identification of domains of netrin UNC-6 that mediate attractive and repulsive guidance and responses from cells and growth cones. *J Neurosci* 22: 7080-7

Lin X. 2004. Functions of heparan sulfate proteoglycans in cell signaling during development. *Development* 131: 6009-21

Maduzia LL, Gumienny TL, Zimmerman CM, Wang H, Shetgiri P, et al. 2002. lon-1 regulates Caenorhabditis elegans body size downstream of the dbl-1 TGF beta signaling pathway. *Dev Biol* 246: 418-28

Matsumoto Y, Irie F, Inatani M, Tessier-Lavigne M, Yamaguchi Y. 2007. Netrin-1/DCC signaling in commissural axon guidance requires cell-autonomous expression of heparan sulfate. *J Neurosci* 27: 4342-50

Matsuo I, Kimura-Yoshida C. 2013. Extracellular modulation of Fibroblast Growth Factor signaling through heparan sulfate proteoglycans in mammalian development. *Curr Opin Genet Dev* 23: 399-407

McKee AC, Cantu RC, Nowinski CJ, Hedley-Whyte ET, Gavett BE, et al. 2009. Chronic traumatic encephalopathy in athletes: progressive tauopathy after repetitive head injury. *J Neuropathol Exp Neurol* 68: 709-35

Mello C, Fire A. 1995. DNA transformation. *Methods Cell Biol* 48: 451-82

Merz DC, Alves G, Kawano T, Zheng H, Culotti JG. 2003. UNC-52/perlecan affects gonadal leader cell migrations in C. elegans hermaphrodites through alterations in growth factor signaling. *Dev Biol* 256: 173-86

Minevich G, Park DS, Blankenberg D, Poole RJ, Hobert O. 2012. CloudMap: a cloud-based pipeline for analysis of mutant genome sequences. *Genetics* 192: 1249-69

Minniti AN, Labarca M, Hurtado C, Brandan E. 2004. Caenorhabditis elegans syndecan (SDN-1) is required for normal egg laying and associates with the nervous system and the vulva. *J Cell Sci* 117: 5179-90

Mitchell KJ, Doyle JL, Serafini T, Kennedy TE, Tessier-Lavigne M, et al. 1996. Genetic analysis of Netrin genes in Drosophila: Netrins guide CNS commissural axons and peripheral motor axons. *Neuron* 17: 203-15.

Mizuguchi S, Uyama T, Kitagawa H, Nomura KH, Dejima K, et al. 2003. Chondroitin proteoglycans are involved in cell division of Caenorhabditis elegans. *Nature* 423: 443-8

Morck C, Pilon M. 2006. C. elegans feeding defective mutants have shorter body lengths and increased autophagy. *BMC Dev Biol* 6: 39

Morio H, Honda Y, Toyoda H, Nakajima M, Kurosawa H, Shirasawa T. 2003. EXT gene family member rib-2 is essential for embryonic development and heparan sulfate biosynthesis in Caenorhabditis elegans. *Biochem Biophys Res Commun* 301: 317-23

Morita K, Chow KL, Ueno N. 1999. Regulation of body length and male tail ray pattern formation of Caenorhabditis elegans by a member of TGF-beta family. *Development* 126: 1337-47

Morita K, Flemming AJ, Sugihara Y, Mochii M, Suzuki Y, et al. 2002. A Caenorhabditis elegans TGF-beta, DBL-1, controls the expression of LON-1, a PR-related protein, that regulates polyploidization and body length. *EMBO J* 21: 1063-73

Mueller MJ, Maluf KS. 2002. Tissue adaptation to physical stress: a proposed "Physical Stress Theory" to guide physical therapist practice, education, and research. *Phys Ther* 82: 383-403

Mullen GP, Rogalski TM, Bush JA, Gorji PR, Moerman DG. 1999. Complex patterns of alternative splicing mediate the spatial and temporal distribution of perlecan/UNC-52 in Caenorhabditis elegans. *Mol Biol Cell* 10: 3205-21

Nagai T, Ibata K, Park ES, Kubota M, Mikoshiba K, Miyawaki A. 2002. A variant of yellow fluorescent protein with fast and efficient maturation for cell-biological applications. *Nat Biotechnol* 20: 87-90

Nitkin RM, Smith MA, Magill C, Fallon JR, Yao YM, et al. 1987. Identification of agrin, a synaptic organizing protein from Torpedo electric organ. *J Cell Biol* 105: 2471-8

Nolan KM, Sarafi-Reinach TR, Horne JG, Saffer AM, Sengupta P. 2002. The DAF-7 TGF-beta signaling pathway regulates chemosensory receptor gene expression in C. elegans. *Genes Dev* 16: 3061-73

Nystrom J, Shen ZZ, Aili M, Flemming AJ, Leroi A, Tuck S. 2002. Increased or decreased levels of Caenorhabditis elegans lon-3, a gene encoding a collagen, cause reciprocal changes in body length. *Genetics* 161: 83-97

O'Donnell M, Chance RK, Bashaw GJ. 2009. Axon growth and guidance: receptor regulation and signal transduction. *Annu Rev Neurosci* 32: 383-412

Ogata-Iwao M, Inatani M, Iwao K, Takihara Y, Nakaishi-Fukuchi Y, et al. 2011. Heparan sulfate regulates intraretinal axon pathfinding by retinal ganglion cells. *Invest Ophthalmol Vis Sci* 52: 6671-9

Ookuma S, Fukuda M, Nishida E. 2003. Identification of a DAF-16 transcriptional target gene, scl-1, that regulates longevity and stress resistance in Caenorhabditis elegans. *Curr Biol* 13: 427-31

Oren-Suissa M, Hall DH, Treinin M, Shemer G, Podbilewicz B. 2010. The fusogen EFF-1 controls sculpting of mechanosensory dendrites. *Science* 328: 1285-8

Palecek SP, Loftus JC, Ginsberg MH, Lauffenburger DA, Horwitz AF. 1997. Integrin-ligand binding properties govern cell migration speed through cell-substratum adhesiveness. *Nature* 385: 537-40

Patterson GI. 2003. Aging: new targets, new functions. *Curr Biol* 13: R279-81

Patterson GI, Padgett RW. 2000. TGF beta-related pathways. Roles in Caenorhabditis elegans development. *Trends Genet* 16: 27-33

Pedersen ME, Snieckute G, Kagias K, Nehammer C, Multhaupt HA, et al. 2013. An epidermal microRNA regulates neuronal migration through control of the cellular glycosylation state. *Science* 341: 1404-8

Pellegrini L, Burke DF, von Delft F, Mulloy B, Blundell TL. 2000. Crystal structure of fibroblast growth factor receptor ectodomain bound to ligand and heparin. *Nature* 407: 1029-34

Peng HB, Xie H, Rossi SG, Rotundo RL. 1999. Acetylcholinesterase clustering at the neuromuscular junction involves perlecan and dystroglycan. *J Cell Biol* 145: 911-21

Petrash HA, Philbrook A, Haburcak M, Barbagallo B, Francis MM. 2013. ACR-12 ionotropic acetylcholine receptor complexes regulate inhibitory motor neuron activity in Caenorhabditis elegans. *J Neurosci* 33: 5524-32

Pinkston-Gosse J, Kenyon C. 2007. DAF-16/FOXO targets genes that regulate tumor growth in Caenorhabditis elegans. *Nat Genet* 39: 1403-9

Plotnikov AN, Schlessinger J, Hubbard SR, Mohammadi M. 1999. Structural basis for FGF receptor dimerization and activation. *Cell* 98: 641-50

Pocock R, Benard CY, Shapiro L, Hobert O. 2008. Functional dissection of the C. elegans cell adhesion molecule SAX-7, a homologue of human L1. *Mol Cell Neurosci* 37: 56-68

Quinn CC, Pfeil DS, Chen E, Stovall EL, Harden MV, et al. 2006. UNC-6/netrin and SLT-1/slit guidance cues orient axon outgrowth mediated by MIG-10/RIAM/lamellipodin. *Curr Biol* 16: 845-53

Quinn CC, Pfeil DS, Wadsworth WG. 2008. CED-10/Rac1 mediates axon guidance by regulating the asymmetric distribution of MIG-10/lamellipodin. *Curr Biol* 18: 808-13

Ramón y Cajal S. 1890a. Notas anatómicas. I. Sobre la aparición de las expansiones celulares en la médula embrionaria. *Gac. Sanit. Barc.* 12: 413–19.

Ramón y Cajal S. 1890b. A quelle époque apparaissent les expansions des cellules nerveuses de la moelle épinière du poulet. *Anat. Anz.* 5: 609–13

Ramón y Cajal S. 1892. La rétine des vertébrés. *La Cellule* 9: 121–255

Raper J, Mason C. 2010. Cellular strategies of axonal pathfinding. *Cold Spring Harbor perspectives in biology* 2: a001933

Ren P, Lim CS, Johnsen R, Albert PS, Pilgrim D, Riddle DL. 1996. Control of C. elegans larval development by neuronal expression of a TGF-beta homolog. *Science* 274: 1389-91

Rhiner C, Gysi S, Frohli E, Hengartner MO, Hajnal A. 2005. Syndecan regulates cell migration and axon guidance in C. elegans. *Development* 132: 4621-33

Rogalski TM, Gilchrist EJ, Mullen GP, Moerman DG. 1995. Mutations in the unc-52 gene responsible for body wall muscle defects in adult Caenorhabditis elegans are located in alternatively spliced exons. *Genetics* 139: 159-69

Rogalski TM, Williams BD, Mullen GP, Moerman DG. 1993. Products of the unc-52 gene in Caenorhabditis elegans are homologous to the core protein of the mammalian basement membrane heparan sulfate proteoglycan. *Genes Dev* 7: 1471-84

Rozario T, DeSimone DW. 2010. The extracellular matrix in development and morphogenesis: a dynamic view. *Dev Biol* 341: 126-40

Salmon H, Franciszkiewicz K, Damotte D, Dieu-Nosjean MC, Validire P, et al. 2012. Matrix architecture defines the preferential localization and migration of T cells into the stroma of human lung tumors. *J Clin Invest* 122: 899-910

Salzberg Y, Diaz-Balzac CA, Ramirez-Suarez NJ, Attreed M, Tecle E, et al. 2013. Skin-derived cues control arborization of sensory dendrites in Caenorhabditis elegans. *Cell* 155: 308-20

Sarafi-Reinach TR, Melkman T, Hobert O, Sengupta P. 2001. The lin-11 LIM homeobox gene specifies olfactory and chemosensory neuron fates in C. elegans. *Development* 128: 3269-81

Sasakura H, Inada H, Kuhara A, Fusaoka E, Takemoto D, et al. 2005. Maintenance of neuronal positions in organized ganglia by SAX-7, a Caenorhabditis elegans homologue of L1. *Embo J* 24: 1477-88

Savage C, Das P, Finelli AL, Townsend SR, Sun CY, et al. 1996. Caenorhabditis elegans genes sma-2, sma-3, and sma-4 define a conserved family of transforming growth factor beta pathway components. *Proc Natl Acad Sci U S A* 93: 790-4

Schackwitz WS, Inoue T, Thomas JH. 1996. Chemosensory neurons function in parallel to mediate a pheromone response in C. elegans. *Neuron* 17: 719-28

Schlessinger J, Plotnikov AN, Ibrahimi OA, Eliseenkova AV, Yeh BK, et al. 2000. Crystal structure of a ternary FGF-FGFR-heparin complex reveals a dual role for heparin in FGFR binding and dimerization. *Mol Cell* 6: 743-50

Schmale GA, Conrad EU, 3rd, Raskind WH. 1994. The natural history of hereditary multiple exostoses. *J Bone Joint Surg Am* 76: 986-92

Schmitz C, Wacker I, Hutter H. 2008. The Fat-like cadherin CDH-4 controls axon fasciculation, cell migration and hypodermis and pharynx development in Caenorhabditis elegans. *Dev Biol* 316: 249-59

Seeger M, Tear G, Ferres-Marco D, Goodman CS. 1993. Mutations affecting growth cone guidance in Drosophila: genes necessary for guidance toward or away from the midline. *Neuron* 10: 409-26

Serafini T, Kennedy TE, Galko MJ, Mirzayan C, Jessell TM, Tessier-Lavigne M. 1994. The netrins define a family of axon outgrowth-promoting proteins homologous to C. elegans UNC-6. *Cell* 78: 409-24

Shao Z, Watanabe S, Christensen R, Jorgensen EM, Colon-Ramos DA. 2013. Synapse location during growth depends on glia location. *Cell* 154: 337-50

Shekarabi M, Kennedy TE. 2002. The netrin-1 receptor DCC promotes filopodia formation and cell spreading by activating Cdc42 and Rac1. *Mol Cell Neurosci* 19: 1-17

Sherwood DR, Butler JA, Kramer JM, Sternberg PW. 2005. FOS-1 promotes basement-membrane removal during anchor-cell invasion in C. elegans. *Cell* 121: 951-62

Sherwood DR, Sternberg PW. 2003. Anchor cell invasion into the vulval epithelium in C. elegans. *Dev Cell* 5: 21-31

Shipp EL, Hsieh-Wilson LC. 2007. Profiling the sulfation specificities of glycosaminoglycan interactions with growth factors and chemotactic proteins using microarrays. *Chemistry & biology* 14: 195-208

Smith CJ, Watson JD, Spencer WC, O'Brien T, Cha B, et al. 2010. Time-lapse imaging and cell-specific expression profiling reveal dynamic branching and molecular determinants of a multi-dendritic nociceptor in C. elegans. *Dev Biol* 345: 18-33

Soete G, Betist MC, Korswagen HC. 2007. Regulation of Caenorhabditis elegans body size and male tail development by the novel gene lon-8. *BMC Dev Biol* 7: 20

Solomon L. 1964. Hereditary Multiple Exostosis. *Am J Hum Genet* 16: 351-63

Song HH, Shi W, Xiang YY, Filmus J. 2005. The loss of glypican-3 induces alterations in Wnt signaling. *J Biol Chem* 280: 2116-25

Stavoe AK, Nelson JC, Martinez-Velazquez LA, Klein M, Samuel AD, Colon-Ramos DA. 2012. Synaptic vesicle clustering requires a distinct MIG-10/Lamellipodin isoform and ABI-1 downstream from Netrin. *Genes Dev* 26: 2206-21

Steigemann P, Molitor A, Fellert S, Jackle H, Vorbruggen G. 2004. Heparan sulfate proteoglycan syndecan promotes axonal and myotube guidance by slit/robo signaling. *Curr Biol* 14: 225-30

Stein E, Zou Y, Poo M, Tessier-Lavigne M. 2001. Binding of DCC by netrin-1 to mediate axon guidance independent of adenosine A2B receptor activation. *Science* 291: 1976-82.

Stiles J, Jernigan TL. 2010. The basics of brain development. *Neuropsychol Rev* 20: 327-48

Stringham EG, Dixon DK, Jones D, Candido EP. 1992. Temporal and spatial expression patterns of the small heat shock (hsp16) genes in transgenic Caenorhabditis elegans. *Mol Biol Cell* 3: 221-33

Sugahara K, Kitagawa H. 2000. Recent advances in the study of the biosynthesis and functions of sulfated glycosaminoglycans. *Curr Opin Struct Biol* 10: 518-27

Sulston JE, Horvitz HR. 1977. Post-embryonic cell lineages of the nematode, Caenorhabditis elegans. *Dev Biol* 56: 110-56

Sulston JE, Schierenberg E, White JG, Thomson JN. 1983. The embryonic cell lineage of the nematode Caenorhabditis elegans. *Dev Biol* 100: 64-119

Suzuki N, Toyoda H, Sano M, Nishiwaki K. 2006. Chondroitin acts in the guidance of gonadal distal tip cells in C. elegans. *Dev Biol* 300: 635-46

Suzuki Y, Morris GA, Han M, Wood WB. 2002. A cuticle collagen encoded by the lon-3 gene may be a target of TGF-beta signaling in determining Caenorhabditis elegans body shape. *Genetics* 162: 1631-9

Suzuki Y, Yandell MD, Roy PJ, Krishna S, Savage-Dunn C, et al. 1999. A BMP homolog acts as a dose-dependent regulator of body size and male tail patterning in Caenorhabditis elegans. *Development* 126: 241-50

Tabara H, Sarkissian M, Kelly WG, Fleenor J, Grishok A, et al. 1999. The rde-1 gene, RNA interference, and transposon silencing in C. elegans. *Cell* 99: 123-32

Takagi S, Benard C, Pak J, Livingstone D, Hekimi S. 1997. Cellular and axonal migrations are misguided along both body axes in the maternal-effect mau-2 mutants of Caenorhabditis elegans. *Development* 124: 5115-26

Taneja-Bageshwar S, Gumienny TL. 2012. Two functional domains in C. elegans glypican LON-2 can independently inhibit BMP-like signaling. *Dev Biol* 371: 66-76

Tessier-Lavigne M, Goodman CS. 1996. The molecular biology of axon guidance. *Science* 274: 1123-33

The I, Bellaiche Y, Perrimon N. 1999. Hedgehog movement is regulated through tout velu-dependent synthesis of a heparan sulfate proteoglycan. *Mol Cell* 4: 633-9

Tian C, Sen D, Shi H, Foehr ML, Plavskin Y, et al. 2010. The RGM protein DRAG-1 positively regulates a BMP-like signaling pathway in Caenorhabditis elegans. *Development* 137: 2375-84

Timmons L, Fire A. 1998. Specific interference by ingested dsRNA [letter]. *Nature* 395: 854

Toga AW, Thompson PM, Sowell ER. 2006. Mapping brain maturation. *Trends in neurosciences* 29: 148-59

Topp KS, Boyd BS. 2006. Structure and biomechanics of peripheral nerves: nerve responses to physical stresses and implications for physical therapist practice. *Phys Ther* 86: 92-109

Townley RA, Bulow HE. 2011. Genetic analysis of the heparan modification network in Caenorhabditis elegans. *J Biol Chem* 286: 16824-31

Toyoda H, Kinoshita-Toyoda A, Selleck SB. 2000. Structural analysis of glycosaminoglycans in Drosophila and Caenorhabditis elegans and demonstration that tout-velu, a Drosophila gene related to EXT tumor suppressors, affects heparan sulfate in vivo. *J Biol Chem* 275: 2269-75

Traister A, Shi W, Filmus J. 2008. Mammalian Notum induces the release of glypicans and other GPI-anchored proteins from the cell surface. *Biochem J* 410: 503-11

Tsalik EL, Niacaris T, Wenick AS, Pau K, Avery L, Hobert O. 2003. LIM homeobox gene-dependent expression of biogenic amine receptors in restricted regions of the C. elegans nervous system. *Dev Biol* 263: 81-102

Tuvia S, Garver TD, Bennett V. 1997. The phosphorylation state of the FIGQY tyrosine of neurofascin determines ankyrin-binding activity and patterns of cell segregation. *Proc Natl Acad Sci U S A* 94: 12957-62

van Praag H, Schinder AF, Christie BR, Toni N, Palmer TD, Gage FH. 2002. Functional neurogenesis in the adult hippocampus. *Nature* 415: 1030-4

Van Vactor D, Wall DP, Johnson KG. 2006. Heparan sulfate proteoglycans and the emergence of neuronal connectivity. *Curr Opin Neurobiol* 16: 40-51

Velleman SG, Song Y, Shin J, McFarland DC. 2013. Modulation of turkey myogenic satellite cell differentiation through the shedding of glypican-1. *Comparative biochemistry and physiology. Part A, Molecular & integrative physiology* 164: 36-43

Wadsworth WG, Bhatt H, Hedgecock EM. 1996. Neuroglia and pioneer neurons express UNC-6 to provide global and local netrin cues for guiding migrations in C. elegans. *Neuron* 16: 35-46

Wang X, Kweon J, Larson S, Chen L. 2005. A role for the C. elegans L1CAM homologue lad-1/sax-7 in maintaining tissue attachment. *Dev Biol* 284: 273-91

Wang Z, Linden LM, Naegeli KM, Ziel JW, Chi Q, et al. 2014. UNC-6 (netrin) stabilizes oscillatory clustering of the UNC-40 (DCC) receptor to orient polarity. *J Cell Biol* 206: 619-33

Ware RW, Clark D, Crossland K, Russell RL. 1975. The nerve ring of the nematode Caenorhabditis elegans: sensory input and motor output. *J. Comp. Neurol* 162: 71-110

Watson JD, Wang S, Von Stetina SE, Spencer WC, Levy S, et al. 2008. Complementary RNA amplification methods enhance microarray identification of transcripts expressed in the C. elegans nervous system. *BMC Genomics* 9: 84

White JG, Southgate E, Thomson JN, Brenner S. 1976. The structure of the ventral nerve cord of Caenorhabditis elegans. *Philos Trans R Soc Lond B Biol Sci* 275: 327-48

White JG, Southgate E, Thomson JN, Brenner S. 1986. The structure of the nervous system of the nematode *Caenorhabditis elegans*. *Philosophical Transactions of the Royal Society of London B. Biological Sciences* 314: 1-340

Williams EH, Pappano WN, Saunders AM, Kim MS, Leahy DJ, Beachy PA. 2010. Dally-like core protein and its mammalian homologues mediate stimulatory and inhibitory effects on Hedgehog signal response. *Proc Natl Acad Sci U S A* 107: 5869-74

Woo WM, Berry EC, Hudson ML, Swale RE, Goncharov A, Chisholm AD. 2008. The C. elegans F-spondin family protein SPON-1 maintains cell adhesion in neural and non-neural tissues. *Development* 135: 2747-56

Wu YQ, Heutink P, de Vries BB, Sandkuijl LA, van den Ouweland AM, et al. 1994. Assignment of a second locus for multiple exostoses to the pericentromeric region of chromosome 11. *Hum Mol Genet* 3: 167-71

Wuyts W, Van Hul W. 2000. Molecular basis of multiple exostoses: mutations in the EXT1 and EXT2 genes. *Hum Mutat* 15: 220-7

Xu D, Esko JD. 2014. Demystifying heparan sulfate-protein interactions. *Annual review of biochemistry* 83: 129-57

Xu K, Wu Z, Renier N, Antipenko A, Tzvetkova-Robev D, et al. 2014. Neural migration. Structures of netrin-1 bound to two receptors provide insight into its axon guidance mechanism. *Science* 344: 1275-9

Yakovlev P, Lecours A. 1967. *The myelinogenetic cycles of regional maturation of the brain.* pp. 3-70. Boston, MA: Blackwell Scientific Publications Inc.

Yamada S, Van Die I, Van den Eijnden DH, Yokota A, Kitagawa H, Sugahara K. 1999. Demonstration of glycosaminoglycans in Caenorhabditis elegans. *FEBS Lett* 459: 327-31

Yan D, Lin X. 2009. Shaping morphogen gradients by proteoglycans. *Cold Spring Harbor perspectives in biology* 1: a002493

Yan D, Wu Y, Yang Y, Belenkaya TY, Tang X, Lin X. 2010. The cell-surface proteins Dally-like and Ihog differentially regulate Hedgehog signaling strength and range during development. *Development* 137: 2033-44

Yu TW, Hao JC, Lim W, Tessier-Lavigne M, Bargmann CI. 2002. Shared receptors in axon guidance: SAX-3/Robo signals via UNC-34/Enabled and a Netrin-independent UNC-40/DCC function. *Nat Neurosci* 5: 1147-54

Zallen JA, Kirch SA, Bargmann CI. 1999. Genes required for axon pathfinding and extension in the C. elegans nerve ring. *Development* 126: 3679-92

Zallen JA, Yi BA, Bargmann CI. 1998. The conserved immunoglobulin superfamily member SAX-3/Robo directs multiple aspects of axon guidance in C. elegans. *Cell* 92: 217-27

Zhou S, Chen L. 2011. Neural integrity is maintained by dystrophin in C. elegans. *J Cell Biol* 192: 349-63

Zhou S, Opperman K, Wang X, Chen L. 2008. unc-44 Ankyrin and stn-2 gamma-syntrophin regulate sax-7 L1CAM function in maintaining neuronal positioning in Caenorhabditis elegans. *Genetics* 180: 1429-43

Ziel JW, Hagedorn EJ, Audhya A, Sherwood DR. 2009. UNC-6 (netrin) orients the invasive membrane of the anchor cell in C. elegans. *Nat Cell Biol* 11: 183-9

Zonta B, Desmazieres A, Rinaldi A, Tait S, Sherman DL, et al. 2011. A critical role for Neurofascin in regulating action potential initiation through maintenance of the axon initial segment. *Neuron* 69: 945-56

Zuryn S, Le Gras S, Jamet K, Jarriault S. 2010. A strategy for direct mapping and identification of mutations by whole-genome sequencing. *Genetics* 186: 427-30